23 June 2006 | $10

Science

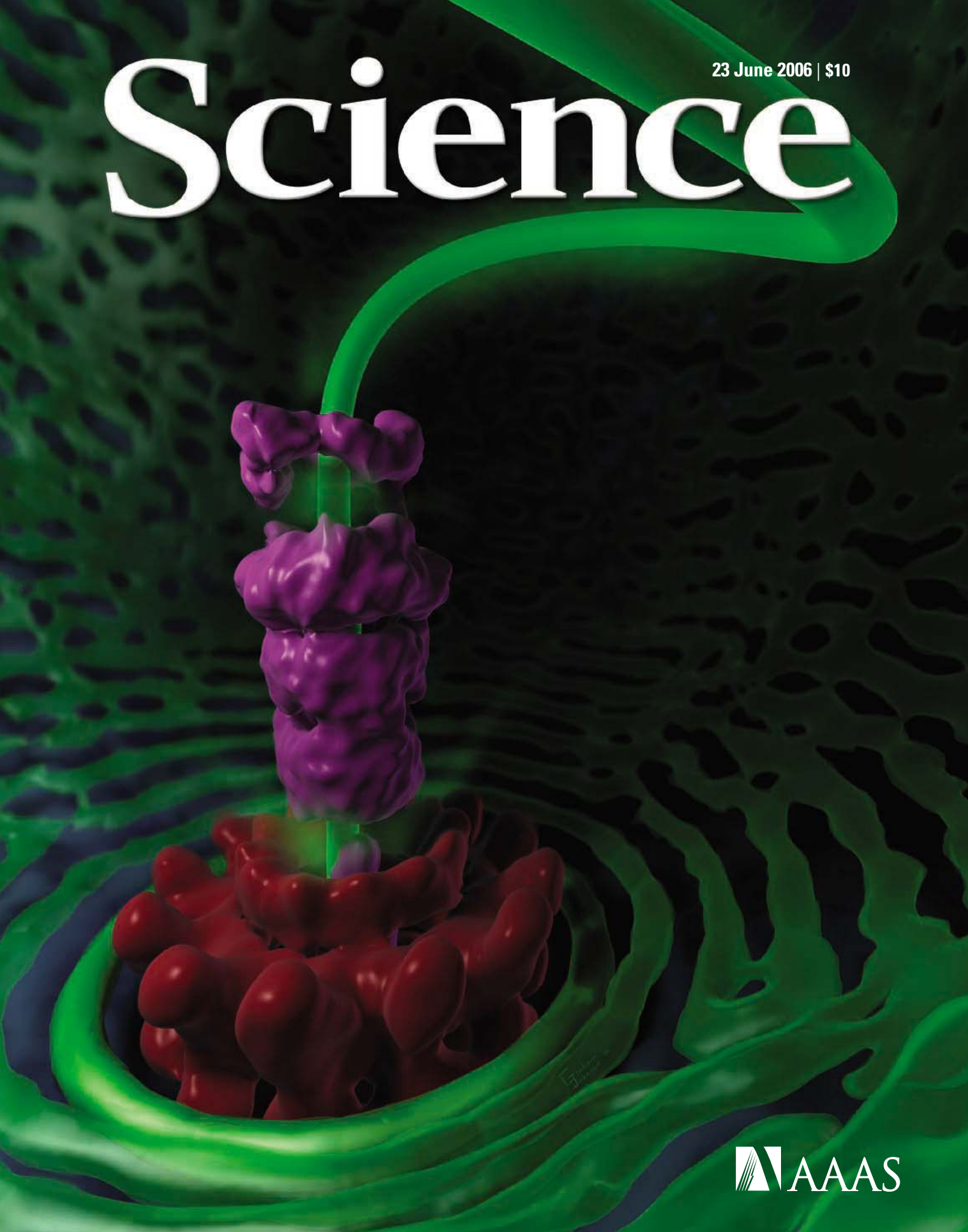

AAAS

Volume 312, Issue 5781

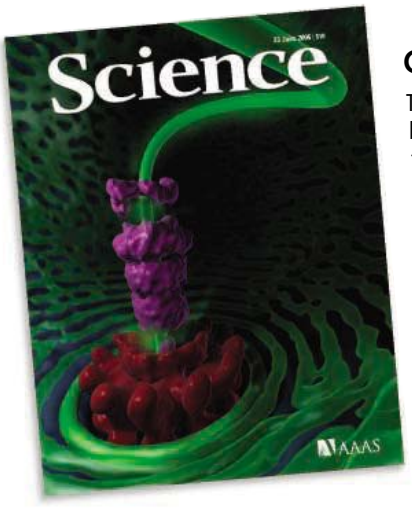

COVER

The pressure-sensing mechanism of bacteriophage P22 that signals when the phage head is full, viewed from the interior. The portal complex (red) is hypothesized to change conformation when the virus is full of DNA (green), which signals the packaging motors to stop. Such a sensor may serve as a drug target in human viruses. See page 1791.

Image: G. Johnson and G. Lander

DEPARTMENTS

1711 *Science* Online
1712 This Week in *Science*
1717 Editors' Choice
1720 Contact *Science*
1721 NetWatch
1723 Random Samples
1741 Newsmakers
1813 New Products
1814 *Science* Careers

EDITORIAL

1715 **Biodiversity Research Still Grounded**
by Iris E. Hendriks, Carlos M. Duarte, Carlo H. R. Heip
>> Policy Forum p. 1750; Report p. 1806

NEWS OF THE WEEK

Scientists Steal a Daring Look at Merapi's Explosive Potential 1724
What Came Before 1918? Archaeovirologist Offers a First Glimpse 1725
The Value of the Stick: Punishment Was a Driver of Altruism *>> Research Article p. 1767* 1727
SCIENCESCOPE 1727
China's Science Ministry Fires a Barrage of Measures at Misconduct 1728
House Panel Tells NSF to Keep Eye on the Prize 1728
Space Scientists Score a Modest Victory in House Spending Bill 1729
Spider Genes and Fossils Spin Tales of the Original Worldwide Web 1730
>> Brevia pp. 1761 and 1762
A 'Forever' Seed Bank Takes Root in the Arctic 1730
First Jewelry? Old Shell Beads Suggest Early Use of Symbols *>> Report p. 1785* 1731
The Strain Builds in Southern California 1732
E.U. Parliament Approves Funding for Human ES Cells 1732
House Panel Finds Fault With How NIH Handles Tissue Samples 1733

NEWS FOCUS

Social Animals Prove Their Smarts 1734
Man's Best Friend(s) Reveal the Possible Roots of Social Intelligence
A Rare Meeting of the Minds 1739
Paleoanthropology's Unsung Hero

LETTERS

Looking at Biofuels and Bioenergy *T. Dalgaard* et al.; *D. Connor and I. Mínguez; T. H. Deluca* 1743
Response *S. E. Koonin*
Measuring the Efficiency of Biomass Energy *K. R. Brower*
Response *B. H. Davison* et al.
Harvesting Our Meadows for Biofuel? *M. W. Palmer*
Response *M. Downing*
Energy Returns on Ethanol Production *C. J. Cleveland* et al.; *N. Hagens* et al.; *L. Lynd* et al.; *R. K. Kaufmann; T. W. Patzek.* **Response** *A. E. Farrell* et al.
Caution on Nominee to Head USGS *K. Wayland*

BOOKS *ET AL.*

Earthquake Nation The Cultural Politics of Japanese Seismicity 1868–1930 *G. Clancey, reviewed by I. Stewart* 1749

1749

POLICY FORUM

Coral Reefs and the Global Network of Marine Protected Areas 1750
C. Mora et al. *>> Editorial p. 1715*

PERSPECTIVES

Gene Expression Needs a Break to Unwind Before Carrying On 1752
J.-F. Haince et al. *>> Report p. 1798*
Our Local Astrophysical Laboratory 1753
J. A. Burns and J. N. Cuzzi
Threats to Water Supplies in the Tropical Andes 1755
R. S. Bradley et al.
A New Way to Burn Fat 1756
J. G. Neels and J. M. Olefsky *>> Research Article p. 1763*
A Direct Proxy for Oceanic Phosphorus? 1758
E. A. Boyle *>> Report p. 1788*
Very Energetic γ-Rays from Microquasars and Binary Pulsars 1759
I. F. Mirabel *>> Report p. 1771*

CONTENTS continued **>>**

Systems Biology — Proteins and Proteomics

Standardized solutions for proteins

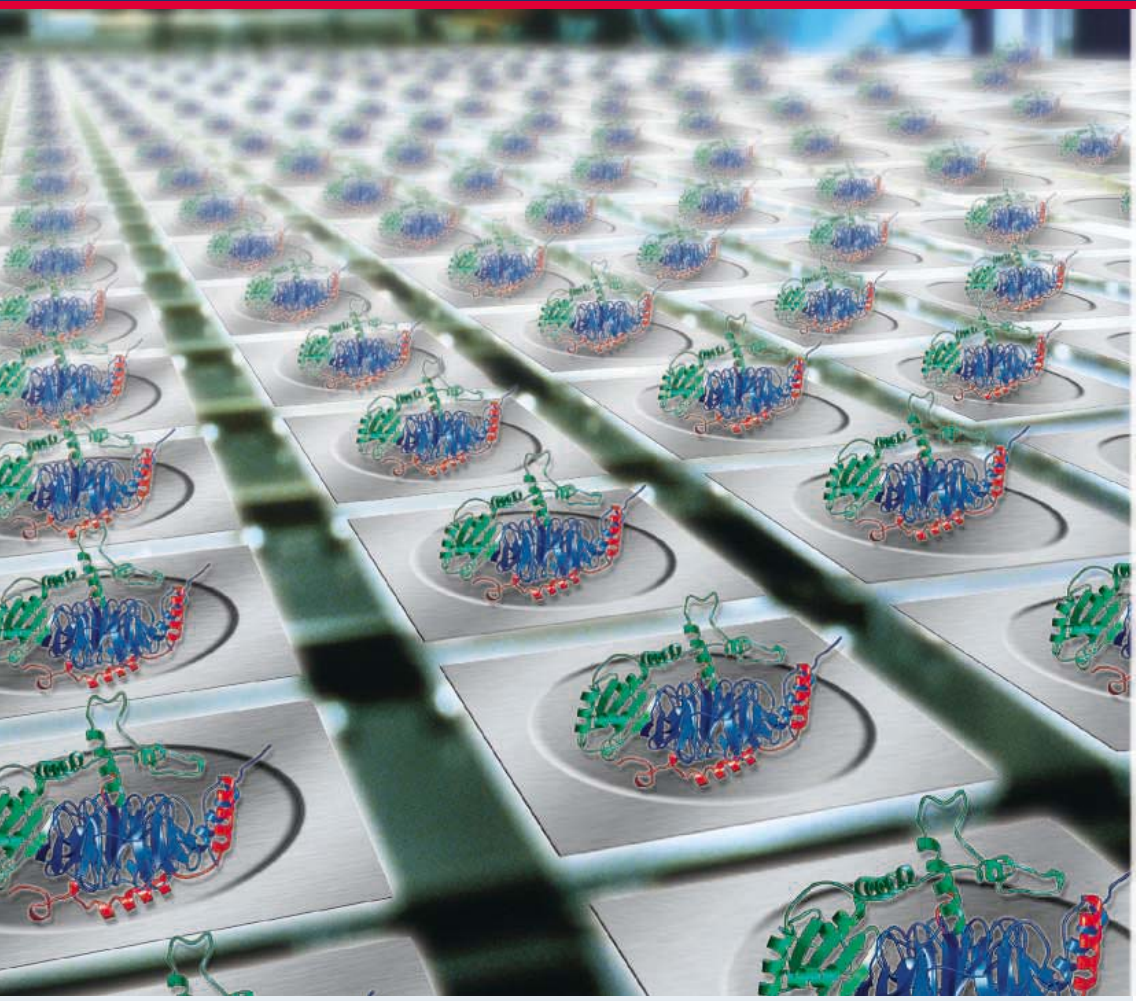

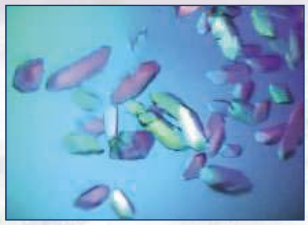

More reproducibility, streamlined crystallization*

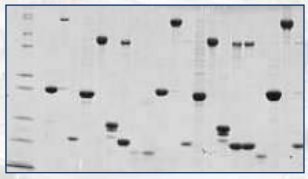

More proteins, purer, faster

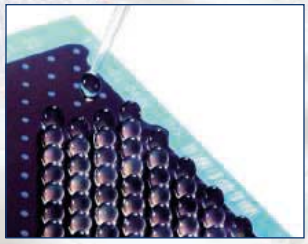

More peptide matches, more protein hits

Success with proteins — made possible by QIAGEN's expertise!

QIAGEN's comprehensive protein portfolio will help you rise to the challenge of working with proteins. QIAGEN provides easy-to-use, integrated solutions to help you succeed with:

- Expression
- Purification
- Detection
- Assay
- Crystallization
- MALDI sample prep
- Proteomics sample prep
- Automation
- Fractionation

Find a standardized solution for your protein challenge at www.qiagen.com/protein !

* Image shows *E. coli* gyrase A C-terminal domain crystals. Courtesy of Alex Ruthenburg from Prof. Verdine's laboratory, Harvard University, Boston, USA.

QIAGEN

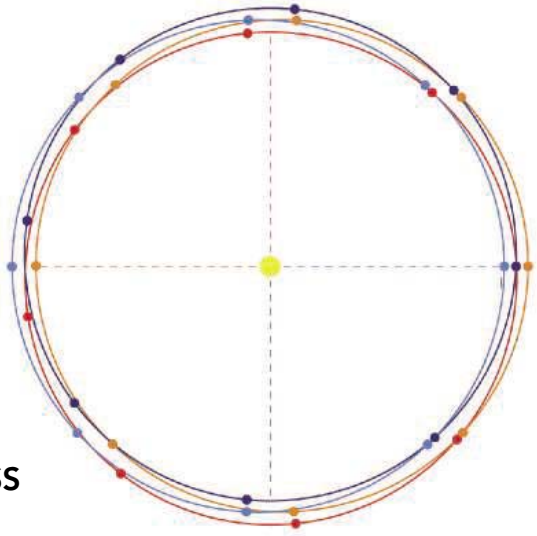

SCIENCE EXPRESS

www.sciencexpress.org

CLIMATE CHANGE

Early Pleistocene Glacial Cycles and the Integrated Summer Insolation Forcing

P. Huybers

Early glacial cycles may have had a 40,000-year cycle because glaciers are more sensitive to integrated summer solar heating than to the 23,000-year cycles in peak heating.

10.1126/science.1125249

CLIMATE CHANGE

Plio-Pleistocene Ice Volume, Antarctic Climate, and the Global $\delta^{18}O$ Record

M. E. Raymo, L. E. Lisiecki, K. H. Nisancioglu

Early glacial cycles appear to have a 40,000-year cycle because the opposing 23,000-year insolation cycles in the Northern and Southern hemispheres may have canceled one another.

10.1126/science.1123296

MEDICINE

α-Synuclein Blocks ER-Golgi Traffic and Rab1 Rescues Neuron Loss in Parkinson's Models

A. A. Cooper et al.

An abnormal protein that causes a defect in membrane trafficking may account for some of the pathology of Parkinson's disease.

10.1126/science.1129462

CELL BIOLOGY

Arginylation of Beta Actin Regulates Actin Cytoskeleton and Cell Motility

M. Karakozova et al.

Addition of an amino acid to actin modulates its properties, affecting (for example) its localization and the formation of lamella in motile cells.

10.1126/science.1129344

CELL BIOLOGY

A Clamping Mechanism Involved in SNARE-Dependent Exocytosis

C. G. Giraudo, W. S. Eng, T. J. Melia, J. E. Rothman

The protein complexin prevents synaptic vesicles from fusing until calcium is sensed by another protein, synaptotagmin, to initiate fusion.

10.1126/science.1129450

TECHNICAL COMMENT ABSTRACTS

OCEAN SCIENCE

Comment on "Nature of Phosphorus Limitation in the Ultraoligotrophic Eastern Mediterranean" 1748

M. S. Hale and R. B. Rivkin

full text at www.sciencemag.org/cgi/content/full/312/5781/1748c

Response to Comment on "Nature of Phosphorus Limitation in the Ultraoligotrophic Eastern Mediterranean"

T. F. Thingstad et al.

full text at www.sciencemag.org/cgi/content/full/312/5781/1748d

BREVIA

EVOLUTION

Early Cretaceous Spider Web with Its Prey 1761

E. Peñalver, D. A. Grimaldi, X. Delclòs

A spider web with entrapped wasps and a beetle within 110-million-year-old amber documents that web-spinning spiders had already evolved.

>> News story p. 1730

EVOLUTION

Silk Genes Support the Single Origin of Orb Webs 1762

J. E. Garb, T. DiMauro, V. Vo, C. Y. Hayashi

Sequence analyses of the genes for spider silk proteins show that orb-webs, which allow spiders to catch flying prey, have a single, ancient origin in the late Jurassic.

>> News story p. 1730

RESEARCH ARTICLES

CELL SIGNALING

TRB3 Links the E3 Ubiquitin Ligase COP1 to Lipid Metabolism 1763

L. Qi et al.

A protein that regulates the degradation of acetyl-CoA carboxylase, the rate-limiting enzyme in fatty acid synthesis, confers resistance to diet-induced obesity.

>> Perspective p. 1756

PSYCHOLOGY

Costly Punishment Across Human Societies 1767

J. Henrich et al.

People from 15 different cultures are all willing to punish others who exhibit selfish behavior that increases societal inequity, but the extent varies widely.

>> News story p. 1727

REPORTS

ASTRONOMY

Variable Very-High-Energy Gamma-Ray Emission from the Microquasar LS I +61 303 1771

J. Albert et al.

The motion of two co-orbiting stars modulates their emission of very-high-energy gamma rays such that the highest emissions occur when the stars are not closest together.

>> Perspective p. 1759

CONTENTS continued **>>**

www.roche-applied-science.com

NEW FuGENE® HD Transfection Reagent

Cover new ground

One reagent for superior results

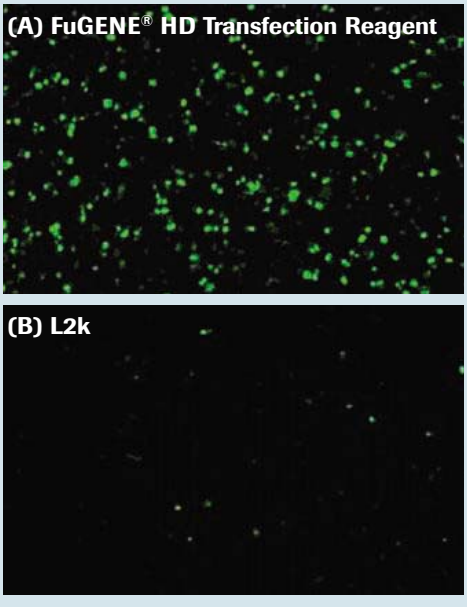

Figure 1: GFP expression in RAW 264.7 cells, 48 hours following transfection using (A) FuGENE® HD Transfection Reagent or (B) a transfection reagent (L2k) from another supplier.

Roche Applied Science set the standard for transfection with FuGENE® 6 Transfection Reagent. With the launch of **FuGENE® HD Transfection Reagent**, Roche again takes transfection to a higher level, enabling the results you need to move your research forward.

- **Achieve new levels of transfection efficiency** in cell lines not transfected well by other reagents (Figure 1).
- **Generate physiologically relevant data** you can trust by using a reagent that has exceptionally low cytotoxicity.
- **Produce higher levels of protein expression** over extended periods with scalability that other reagents cannot provide.
- **Accelerate the move to development** by using this unique non-liposomal reagent that is free of animal-derived components.

Cover new ground and move closer to new discovery.

For more information and a list of successfully transfected cell lines, visit ***www.roche-applied-science.com/fugene***

Roche Diagnostics

Roche Diagnostics GmbH
Roche Applied Science
68298 Mannheim
Germany

REPORTS *CONTINUED...*

ASTRONOMY

The Spiral Structure of the Outer Milky Way in Hydrogen 1773

E. S. Levine, L. Blitz, C. Heiles

Imaging the distribution and density of atomic hydrogen in the Milky Way shows that our Galaxy forms a multiarmed spiral that is not symmetric about its axis.

PHYSICS

Optical Conformal Mapping 1777

U. Leonhardt

In theory, the tunable dielectric and magnetic properties of metamaterials could be used in stealth technologies to pass light completely around an object and cloak it from view.

>> Report p. 1780

PHYSICS

Controlling Electromagnetic Fields 1780

J. B. Pendry et al.

The tunable dielectric and magnetic properties of metamaterials could be used in stealth technologies to cloak an object from view.

>> Report p. 1777

MATERIALS SCIENCE

Nanoassembly of a Fractal Polymer: A Molecular "Sierpinski Hexagonal Gasket" 1782

G. R. Newkome et al.

Ligands with twofold and threefold symmetry, joined by iron and ruthenium ions, self-assemble to form 10-nanometer hexagons that in turn assemble into increasingly larger hexagons.

ANTHROPOLOGY

Middle Paleolithic Shell Beads in Israel and Algeria 1785

M. Vanhaeren et al.

A few drilled sea shells from two inland sites imply that humans developed ornamentation, a form of symbolic behavior, by about 100,000 years ago.

>> News story p. 1731

OCEANOGRAPHY

Phosphorus in Cold-Water Corals as a Proxy for Seawater Nutrient Chemistry 1788

P. Montagna et al.

A cold-water coral takes up phosphorus in an amount proportional to its concentration in local seawater, making it a potential archive of past ocean productivity.

>> Perspective p. 1758

STRUCTURAL BIOLOGY

The Structure of an Infectious P22 Virion Shows the Signal for Headful DNA Packaging 1791

G. C. Lander et al.

During assembly of an infectious virus, DNA is packed into the viral head through a protein portal; when the head is full, pressure on the portal causes it to close.

1715 & 1806

VIROLOGY

Metagenomic Analysis of Coastal RNA Virus Communities 1795

A. I. Culley et al.

Previously unknown RNA viruses are abundant in coastal marine ecosystems; a few dominant species probably infect protists and plants.

MOLECULAR BIOLOGY

A Topoisomerase IIβ–Mediated dsDNA Break Required for Regulated Transcription 1798

B.-G. Ju

Estrogen-initiated gene transcription involves enzymatically driven DNA cleavage, repair, and local reconfiguration of chromatin.

>> Perspective p. 1752

NEUROSCIENCE

The Muscle Protein Dok-7 Is Essential for Neuromuscular Synaptogenesis 1802

K. Okada

A newly described protein is required for normal formation of the neuromuscular junction, where it binds to a signaling protein and causes receptor clustering.

ECOLOGY

Depletion, Degradation, and Recovery Potential of Estuaries and Coastal Seas 1806

H. K. Lotze

Historical data show that human impacts on coastal environments have been similar across the globe, even in quite different ecosystems.

>> Editorial p. 1715

CELL BIOLOGY

JETLAG Resets the *Drosophila* Circadian Clock by Promoting Light-Induced Degradation of TIMELESS 1809

K. Koh, X. Zheng, A. Sehgal

A light pulse changes the phase of the *Drosophila* circadian clock by activating a protein that marks a clock component for rapid degradation.

AAAS
ADVANCING SCIENCE, SERVING SOCIETY

SCIENCE (ISSN 0036-8075) is published weekly on Friday, except the last week in December, by the American Association for the Advancement of Science, 1200 New York Avenue, NW, Washington, DC 20005. Periodicals Mail postage (publication No. 484460) paid at Washington, DC, and additional mailing offices. Domestic individual membership and subscription (51 issues): $139 ($74 allocated to subscription). Domestic institutional subscription (51 issues): $650; Foreign postage extra: Mexico, Caribbean (surface mail) $55; other countries (air assist delivery) $85. First class, airmail, student, and emeritus rates on request. Canadian rates with GST available upon request, GST #1254 88122. Publications Mail Agreement Number 1069624. **Printed in the U.S.A.**

Change of address: Allow 4 weeks, giving old and new addresses and 8-digit account number. **Postmaster:** Send change of address to AAAS, P.O. Box 96178, Washington, DC 20090–6178. **Single-copy sales:** $10.00 current issue, $15.00 back issue prepaid includes surface postage; bulk rates on request. The identification code for *Science* is 0036-8075. *Science* is indexed in the *Reader's Guide to Periodical Literature* and in several specialized indexes.

CONTENTS continued **>>**

Western Blotting Systems and Reagents

The complete blotting solution is easy to spot.

The industry leader in innovative and powerful protein blotting equipment, Bio-Rad offers an extensive line of blotting kits, membranes, and reagents to meet all your blotting needs.

- An array of versatile electrophoretic transfer systems for efficient transfer of proteins from a broad range of gel sizes
- Microfiltration or dot-blotting devices for easy, reproducible binding of proteins and nucleic acids to membranes
- HRP- and AP-based chemiluminescent and colorimetric detection kits and substrates — for all western blotting applications
- High-quality blotting-grade reagents to simplify your blotting experience
- A wide range of precut membranes and membrane sandwiches in nitrocellulose, supported nitrocellulose, and PVDF formats

For more information on protein blotting equipment and reagents, contact your local Bio-Rad representative or visit us on the Web at **discover.bio-rad.com**

Visit us on the Web at **discover.bio-rad.com**
Call toll free at 1-800-4BIORAD (1-800-424-6723); outside the US, contact your local sales office.

BIO-RAD

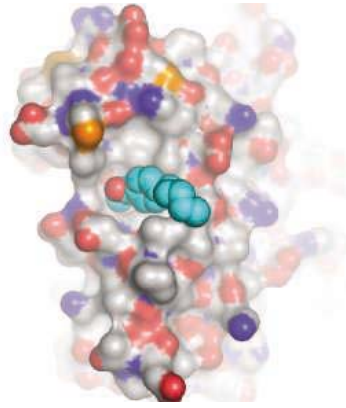

Thyroid receptor bound to L3, an inhibitor.

SCIENCE'S **STKE**

www.stke.org SIGNAL TRANSDUCTION KNOWLEDGE ENVIRONMENT

PROTOCOL: A High-Throughput Screening Method to Identify Small Molecule Inhibitors of Thyroid Hormone Receptor Coactivator Binding
L. A. Arnold et al.
A fluorescence polarization assay can be used for drug discovery.

DIRECTORY
Find collaborators and colleagues in this list of cell signaling researchers.

Rodents for aging-related research.

SCIENCE'S **SAGE KE**

www.sageke.org SCIENCE OF AGING KNOWLEDGE ENVIRONMENT

EXPERIMENTAL RODENT STRAINS
Check out the biological characteristics of inbred and hybrid strains used to study aging.

CLASSIC PAPERS
View historical (pre-1990) articles on aging-related topics.

SCIENCE**NOW**

www.sciencenow.org DAILY NEWS COVERAGE

Columbia Lab Issues Four Additional Retractions
First author implies cover-up.

Pandas Times Two
Genetic census technique doubles estimate of a key giant panda population.

Mind Reading Is Child's Play
Neurons that help us predict the actions of others start working after motor skills have developed.

Making your own luck beats the odds.

SCIENCE **CAREERS**

www.sciencecareers.org CAREER RESOURCES FOR SCIENTISTS

US: Getting Lucky
K. Flanagan
You might get lucky waiting for an offer, but chance favors the prepared mind.

UK: Researchers Learn the Business
T. J. Reynolds
New courses popping up across the U.K. teach researchers about science-related enterprise.

MISCINET: Educated Woman, Chapter 52—What, Me Write?
M. P. DeWhyse
In the throes of her dissertation, Micella has contracted a severe case of writer's block.

GRANTSNET: International Grants and Fellowship Index
A. Kotok
Find the latest funding opportunities from Europe, Asia, and the Americas.

SCIENCE**PODCAST**

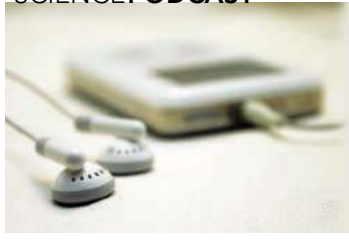

Listen to the 23 June edition of the *Science* Podcast to hear about a possible route to practical cloaking devices, new views on animal cognition, and early evidence of human jewelry making.
www.sciencemag.org/about/podcast.dtl

Separate individual or institutional subscriptions to these products may be required for full-text access.

EDITED BY STELLA HURTLEY AND PHIL SZUROMI

Extending the Art of Concealment

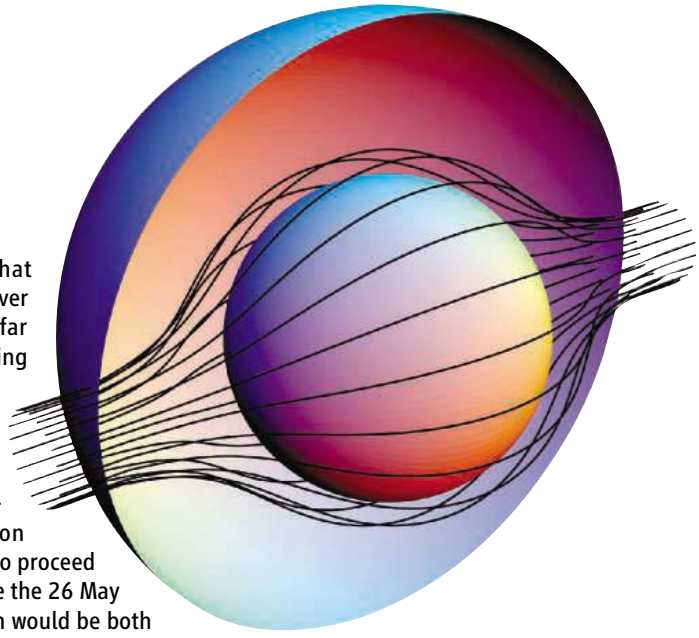

Stealth technology relies on impedance matching that absorbs impinging radiation, thereby denying the observer a back-reflected signal. However, an observer on the far side of the "hidden" object can still see a shadow. Using properties of metamaterials, artificial materials with tunable dielectric and magnetic properties, **Pendry *et al.*** (p. 1780, published online 25 May) and **Leonhardt** (p. 1777, published online 25 May) present theoretical studies proposing that such materials could be used to steer electromagnetic radiation around an object, subsequently allowing the radiation to proceed as if it had not been scattered from the object at all (see the 26 May news story by **Cho**). This sophisticated version of stealth would be both reflectionless and shadowless.

Energy Extreme

Microquasars are binary star systems with twin radio-emitting jets that resemble those of quasars, albeit on smaller scales. Radiation from these jets arises from particles moving at relativistic speeds in high magnetic fields, but little is known about the jets' composition or how they are formed. **Albert *et al.*** (p. 1771, published online 18 May; see the Perspective by **Mirabel**) have used the Major Atmospheric Gamma-ray Imaging Cherenkov (MAGIC) telescope to monitor monthly variations caused by very high energy gamma rays (>100 gigaelectron volts) from a microquasar. A comparison of the phases of the gamma-ray variability with those of radio waves and x-rays shows that the gamma-ray emission peak does not coincide with the time when the two stars are closest to one another, which suggests that there is a strong orbital modulation of the emission processes. Further analysis of the emission favors an underlying leptonic over a hadronic process.

Cold-Water Recorder

Phosphate ultimately limits biological productivity in the ocean, and much of what is understood about past productivity depends on knowing how phosphorus (P) was distributed in the sea. Unfortunately, reconstructions of ocean phosphate contents have always relied on indirect proxies that can be affected by other factors such as temperature, carbonate ion concentration, and incomplete preservation, and so their utility often is limited by their inherent uncertainties. **Montagna *et al.*** (p. 1788; see the Perspective by **Boyle**) present evidence that the cold-water coral *Desmophyllum dianthus* incorporates P into its skeleton in amounts proportional to the concentration of P in ambient seawater. Such a direct proxy would make robust reconstructions of long-term variations in ocean P content possible and allow changes in the residence times and the sources of deep-water masses to be detected.

Unmasking Spiral Arms

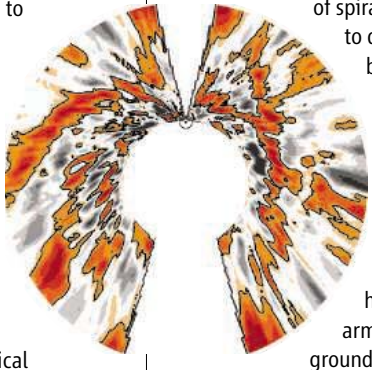

The Milky Way is a spiral galaxy, but its precise shape and even the number and extent of spiral arms has been difficult to discern. For example, the brightness of the 21-centimeter hyperfine transition of neutral atomic hydrogen (HI) falls off rapidly away from the Galaxy's center and fluctuates greatly over the sky, so it has been hard to pick out spiral arms against this background. **Levine *et al.*** (p. 1773, published online 1 June) applied a technique similar to "unsharp" masking to previous survey maps that essentially removes a coarse template of the large-scale emission and reveals finer details. The maps show spiral structures out to distances of 25 kiloparsecs from the Galactic center that fit a logarithmic spiral form.

Ancient Accessorizing

Art or other forms of symbolic expression are found in many early human sites that date to about 50,000 years ago, but earlier evidence of such modern cultural behavior has been sparse. **Vanhaeren *et al.*** (p. 1785; see the news story by **Balter**) now describe a few gastropod shells apparently modified for jewelry that were collected previously from two inland sites in western Asia and North Africa. Both sites date to older than 100,000 years ago, about 25,000 years earlier than similar but more abundant drilled shells found in South Africa. Examination shows that these shells were drilled by humans, presumably for threading and wear.

Phasing Out Fat

The protein known as TRB3 is a pseudokinase (a kinase-like protein that lacks kinase activity) synthesized in fasting animals. TRB3 modulates insulin signaling and is related to a *Drosophila* protein that coordinates mitosis and morphogenesis during development. **Qi *et al.*** (p. 1763; see the Perspective by **Neels and Olefsky**) find that overexpression of TRB3 in mice confers resistance to diet-induced obesity. This effect appears to be the result of decreased activity of acetyl–coenzyme A carboxylase (ACC) and consequent decreased synthesis of fatty acids. TRB3 directly interacts with ACC to promote its degradation via the E3 ubiquitin ligase constitutive photomorphogenic protein 1. Understanding the regulation of lipid metabolism may promote therapeutic strategies for the control of obesity.

CREDITS (TOP TO BOTTOM): IMAGE CREATED BY D. SCHURIG; LEVINE *ET AL.*

Limits on Cultural Variation

Behavior does not always agree with claimed intent—hence, "Do as I say, not as I do." In order to assess variations in the assessment of fairness and punishment across the breadth of humanity, **Henrich *et al.*** (p. 1767; see the news story by **Bhattacharjee**) have complemented existing evidence from questionnaire-based surveys by adapting three economic games—the ultimatum game, third party punishment, and the dictator game—and by sampling 15 small-scale societies distinctly dissimilar to the commonly used pool of students in industrialized countries. Individuals across populations become more willing to administer punishment (even when they must "pay to punish") as inequality increases, and this willingness co-varies with altruistic behavior.

Getting a Headful

Double-stranded DNA viruses pump their genome into preassembled procapsids until the particles are filled to capacity with internal pressures higher than corked champagne. How is this internal "headful" density signaled to the outside packaging machinery? Insight comes from a 17 angstrom resolution asymmetric reconstruction of the infectious P22 virion by **Lander *et al.*** (p. 1791, published online 18 May). DNA is tightly spooled around the P22 portal, which is in a different conformation from the isolated portal. The authors suggest that DNA tightens around the portal as packaging density increases. When the headful density is reached, a conformational switch signals the termination of packaging.

Flies and *jetlag*

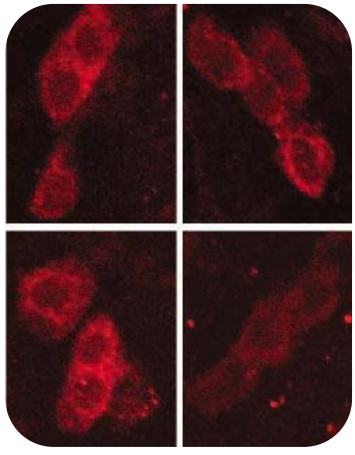

Circadian clocks can be reset to a new phase by a brief exposure to light, but the molecular details of this resetting are not clear. In *Drosophila*, a light-sensitive protein cryptochrome undergoes a conformational change in response to light and binds to a clock component, the protein TIMELESS (TIM). This interaction then triggers TIM degradation and effectively resetting the clock. By screening mutant flies that show reduced sensitivity to this light-induced resetting, **Koh *et al.*** (p. 1809) identify a gene, termed *jetlag*, that is necessary for degradation of TIM after the light pulse. JETLAG exists in a complex with TIM and increases its ubiquitination, a tag that marks the protein for degradation. Thus, JETLAG is an F-box protein that targets TIM for ubiquitination and consequent rapid degradation in response to light.

CREDIT: KOH *ET AL.*

TopoIIβ Gets to Work

DNA topoisomerases regulate conformational changes in DNA topology by catalyzing DNA strand breakage and rejoining. Topoisomerase IIβ (TopoIIβ) alters DNA conformation near gene promoters, and associates with sequence-specific transcription factors and chromatin modifying and remodeling factors. **Ju *et al.*** (p. 1798; see the Perspective by **Haince *et al.***) now show that DNA TopoIIβ generates double-strand breaks at transcriptional promoters when these genes are activated in a signal-dependent manner. Subsequently, DNA repair enzymes are activated, and there is a resultant exchange in histone composition and local chromatin structure.

Moving to the Seaside

Humans have settled by coasts since prehistoric times. Recent impacts of such settlement have been far better documented than historical and prehistorical effects. **Lotze *et al.*** (p. 1806) quantified detailed historical baselines for 12 estuarine and coastal ecosystems in North America, Europe, and Australia since the onset of human occupation. Patterns of change were surprisingly similar at all sites. Overexploitation and habitat loss alone explained ~95% of all species declines, extinctions, and consequent shifts in diversity and ecosystem functioning. Significant recovery in upper trophic levels was seen where those impacts were restrained, indicating that well-targeted management can reverse destructive trends.

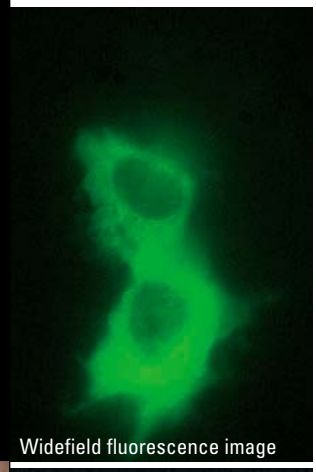

Widefield fluorescence image

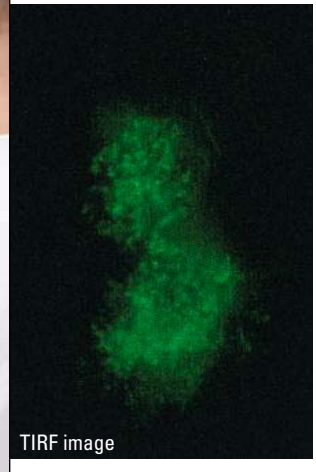

TIRF image

Visualize Life's Secrets with Complete, Automated TIRF

New! Complete, automated microscope system for precise TIRF. The Leica AM TIRF system gives accurate results for all research examinations of close-to-membrane specimen structures. Minimum light stress, high-sensitivity, and the most favorable signal-to-noise ratio combine to assure exact spatial resolution.

Leica's innovative auto-alignment functions automatically find the correlation between the penetration depths of the evanescent field and the TIRF angles. The system's dynamic scanner can be used to precisely position the laser beam and determine the exact penetration depth. Leica's TIRF objective offers maximum apochromatic correction for high-performance imaging.

www.leica-microsystems.com/AM_TIRF

Leica

MICROSYSTEMS

Iris E. Hendriks is an associated scientist at the University of the Balearic Islands, Spain, and management associate of the EU Network of Excellence MarBEF (Marine Biodiversity and Ecosystem Functioning). E-mail: iris.hendriks@uib.es

Carlos M. Duarte is Research Professor at the Spanish Council for Scientific Research, Spanish National Research Counsel (CSIC), Spain, and theme leader of the EU Network of Excellence MarBEF. E-mail: carlosduarte@imedea.uib.es

Carlo H. R. Heip is director of the Centre for Estuarine and Marine Ecology of the Netherlands Institute of Ecology in Yerseke, Netherlands, and coordinator of the EU Network of Excellence MarBEF. E-mail: c.heip@nioo.knaw.nl

Biodiversity Research Still Grounded

LAST WEEK, THE UNITED STATES DESIGNATED NEARLY 140,000 SQUARE MILES OF THE PACIFIC OCEAN northwest of Hawaii as the largest protected marine reserve in the world. This is good news, considering that earlier this year, 4000 delegates left the international Conference of the Parties to the Convention on Biological Diversity (held in March 2006 in Brazil) with mixed feelings. Portrayal of the conference as successful by the Executive Secretary was in stark contrast to the frustration expressed by environmentalist groups about the failure to progress toward creating large marine protected areas. Paradoxically, the fact that the oceans are the patrimony of all nations creates a legislation gap that is the major obstacle to increasing the percent of protected ocean to the 10% targeted by the convention. This obstacle is augmented by a lack of awareness by legislators and the general public about the role, status, and prospects of biological diversity in oceans relative to the land. Until a better understanding of the diversity of and threats to life in the oceans is achieved, there will be no progress in protecting marine biodiversity.

The vast richness of marine biodiversity remains to be discovered, particularly in remote habitats such as the deep ocean. There is a widespread misconception that extinction in the ocean is unlikely because of its huge biogeographical ranges and high connectivity of habitat. But recent surveys and molecular analyses of ocean samples have revealed marine invertebrates with biogeographical ranges as small as 4 km. Specialized communities in deep-sea habitats, such as hydrothermal vents and cold seeps, are isolated across thousands of kilometers. Marine diversity is much more extensive and vulnerable than previously thought. Moreover, much of this diversity is microbial and therefore generally unappealing to society. Indeed, more charismatic animals and plants receive most of the conservationists' attention. Scientific research must unveil the importance of ocean life diversity, test for declines in important taxa and ecosystems, elucidate the causes of these declines, and provide remedial options to change these perception biases.

Although research on biodiversity has increased, these efforts are dominated by studies on land. Between 1987 and 2004, only 9.8% of published research dealt with marine biodiversity. This severe imbalance percolates through international programs. For instance, only about 10% of the First Open Science Conference of the Diversitas Programme (November 2005 in Mexico) that dealt with biodiversity science addressed marine biodiversity.

This disproportionally small research effort on marine biodiversity is in sharp contrast to the large genomic diversity in the oceans as compared to that on land. Most branches of the evolutionary tree of life thrive in the oceans, whereas most terrestrial species are contained within only two branches, a result of the extended history of life in the oceans (3500 million years). The genomic richness of the ocean is an untapped resource for biotechnology, pharmacy, and food. The number of marine species brought into aquaculture exceeds, after only 30 years of development, the number of animal species domesticated over 10,000 years of husbandry on land. Realizing these opportunities requires progress to improve our present knowledge about sustainably managing marine resources.

The oceans have lost much of their fish biomass and megafauna to hunting, and key coastal habitats are lost globally at rates 2 to 10 times faster than those in tropical forests [also see the Report by Lotze *et al*. in this issue (p. 1806)]. Anthropogenic inputs to the ocean are causing hypoxia and widespread deterioration of water quality, and anthropogenic CO_2 emissions are causing ocean acidification, which is emerging as a global threat to calcifying marine organisms.

The concept of protected areas that emerged from studies of life on land cannot be readily extrapolated to the ocean. Until last week, the total protected marine area was 10 times smaller than that on land, and most marine protected areas are too small to be effective. Mounting evidence indicates that marine food webs are connected across oceanic scales, but the forces driving these connections are poorly understood. We must improve our understanding of how the global ocean ecosystem works in order to design networks of protected areas that effectively preserve biodiversity. Indeed, as Mora *et al*. point out in this issue (p. 1750), the present design of some marine protected areas may not be optimal. Further promoting marine biodiversity research requires a larger scientific community and more resources than currently exist. This can be achieved through increased international cooperative efforts and networking. We must do this before we face a future depleted of marine resources.

– Iris E. Hendriks, Carlos M. Duarte, Carlo H. R. Heip

10.1126/science.1128548

CREDIT: GETTY IMAGES

PIERCE

The Protein People

price

Precisely our point.

Precise™ Precast Protein Gels … get 20 for the price of 10.

(that's $4.95/gel!)*

- Requires unique Tris-HEPES Running Buffer for excellent separation and high-resolution protein bands (Product # 28398)
- Easy-to-load lanes with durable plastic dividers
- Long shelf life – 12-month guarantee ensures consistent performance
- Compatible with Laemmli sample buffer and standard mini-gel tanks

- Easy-to-open, no need for special tools
- Short run time – 45-minute run time provides results quickly
- 1 mm thick gels stain quickly and with high sensitivity using coomassie and silver stains
- Transfers quickly and efficiently to nitrocellulose and PVDF membranes for Western blotting

Ordering Information

Product #	Percent Acrylamide	# of Sample Wells	Sample Well Volume	Pkg. Size	U.S. Price
PIER25200	8%	10	50 µl	~~10~~ 20 gels	$ 99
PIER25201	10%	10	50 µl	~~10~~ 20 gels	$ 99
PIER25202	12%	10	50 µl	~~10~~ 20 gels	$ 99
PIER25203	8-16%	10	50 µl	~~10~~ 20 gels	$ 99
PIER25204	4-20%	10	50 µl	~~10~~ 20 gels	$ 99
PIER25220	8%	12	30 µl	~~10~~ 20 gels	$ 99
PIER25221	10%	12	30 µl	~~10~~ 20 gels	$ 99
PIER25222	12%	12	30 µl	~~10~~ 20 gels	$ 99
PIER25223	8-16%	12	30 µl	~~10~~ 20 gels	$ 99
PIER25224	4-20%	12	30 µl	~~10~~ 20 gels	$ 99

Product #	Percent Acrylamide	# of Sample Wells	Sample Well Volume	Pkg. Size	U.S. Price
PIER25240	8%	15	25 µl	~~10~~ 20 gels	$ 99
PIER25241	10%	15	25 µl	~~10~~ 20 gels	$ 99
PIER25242	12%	15	25 µl	~~10~~ 20 gels	$ 99
PIER25243	8-16%	15	25 µl	~~10~~ 20 gels	$ 99
PIER25244	4-20%	15	25 µl	~~10~~ 20 gels	$ 99
28398	BupH™ Tris-HEPES-SDS Running Buffer Each pack yields 500 ml of 100 mM Tris, 100 mM HEPES, 3 mM SDS, pH 8 ± 0.25 when dissolved in 500 ml distilled water (5 L total).			10 pack	$ 27

New low price!

*Purchase direct from Pierce or ask your Fisher or VWR sales representative about this special offer. Offer valid through August, 31, 2006, and only in North America. Void where prohibited. For a similar offer in Europe, please visit *www.perbio.com.*

www.piercenet.com/241gels

PIERCE

Tel: 815-968-0747 or 800-874-3723 • Fax: 815-968-7316
Customer Assistance E-mail: CS@piercenet.com

For distributors outside the U.S. and Europe, visit www.piercenet.com

For European offices and distributors, visit www.perbio.com

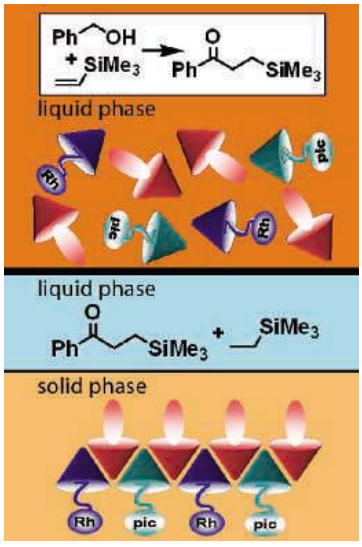

Self-assembly components during the reaction (above) and after cooling (below).

CHEMISTRY

Settling Down After It's All Over

Homogeneous catalysis maximizes the frequency and conformational flexibility of the collisions between catalyst and substrate, but a major shortcoming is the challenge of separating catalyst from product once the reaction is complete. Biphasic solvent systems can mitigate this problem, but often do so at the expense of reduced mixing efficiency.

Kim *et al.* demonstrate how to take advantage of molecular self-assembly in order to recover the catalyst in the dehydrogenative coupling of benzylic alcohols with olefins. The reaction is catalyzed by a phosphine-coordinated Rh complex and aminopyridine chelator (with one equivalent of olefin acting as the hydrogen acceptor). The phosphine and pyridine fragments are tethered to barbiturate derivatives that can assemble into a rigid network together with a third component—a triaminopyrimidine—by means of hydrogen bonding. When a dioxane suspension of the reagents and network-bound catalysts is heated to 150°C, the hydrogen bonds break, and a homogeneous solution forms. High yields are obtained in 2 hours, and cooling then regenerates the self-assembled network and precipitates the catalyst, allowing the product to be decanted. Catalysts were cycled eight times without significant loss in activity; moreover, switching substrates between cycles confirmed that none of the desired products partitioned into the solid phase. — JSY

Org. Lett. **8**, 10.1021/ol0608045 (2006).

APPLIED PHYSICS

Plasmons Go the Distance

The coupling of light with electronic surface excitations—specifically, surface plasmon polaritons—offers the opportunity to bridge the orders-of-magnitude difference in sizes between optical and electronic carriers. To develop schemes for coupling and transporting surface plasmons around a chip, the determination of their propagation lengths is particularly important. In this vein, van Wijngaarden *et al.* have excited surface plasmons using a focused beam of electrons and then detected the luminescence emitted as the plasmons decayed. Based on these cathodoluminescence intensity decay profiles, they could determine propagation lengths as a function of wavelength. Gold and silver thin films (on silicon and quartz substrates, respectively) were patterned with gratings to direct the emission, allowing the measurement of propagation lengths as short as several hundred nanometers. The resolution of the technique is limited by excitation volume and so should increase as film thickness decreases. The authors suggest that extensions to the characterization of more elaborate plasmonic nanostructures should also be possible. — ISO

Appl. Phys. Lett. **88**, 221111 (2006).

MOLECULAR BIOLOGY

Please Release Me

MicroRNAs (miRNAs) are small (20- to 22-nucleotide) RNAs that are encoded in the genomes of most plants and animals and that regulate gene expression by pairing with complementary sequences in the 3′ untranslated regions (UTRs) of target mRNAs. A perfect match between miRNA and target, as found in plants, generally results in cleavage and subsequent degradation of the target. An imperfect match, as often found in animals, generally results in repression of translation (of the mRNA into protein) and sequestration of the mRNA into cytoplasmic P bodies. Can such a repressed mRNA break free from its inhibitory miRNA and re-enter the pool of active mRNAs or is it doomed to stay silenced?

Bhattacharyya *et al.* investigate the dynamics of miRNA regulation by analyzing miR-122–directed repression of the human cationic amino acid transporter 1 (CAT-1). In Huh7 cells, CAT-1 translation is repressed by miR-122, and CAT-1 mRNA is found in P bodies. Stressing the cells by amino acid starvation results in the movement of CAT-1 mRNA from P bodies into actively translating ribosomes and in an increase of CAT-1 protein, brought about by the release of CAT-1 mRNA from the inhibitory action of miR-122. These effects are mediated by the interaction of the AU-rich element (ARE)–binding protein HuR with a segment of the CAT-1 3′ UTR that is rich in A and U residues. Thus, miRNA-based down-regulation in animals is not all or none, as in plants, and can be reversed in response to changing conditions. — GR

Cell **125**, 1111 (2006).

CELL BIOLOGY

The Hole Story

The actin cytoskeleton is responsible for controlling cell shape and function. Small Rho-type GTPases regulate actin dynamics and are often the target of bacterial virulence factors that commandeer actin and use it to promote bacterial invasion strategies. Boyer *et al.* describe how *Staphylococcus aureus* exploits this cellular machinery. *S. aureus* produces a protein known as EDIN (epidermal cell differentiation inhibitor), which induces large, transient, transcellular holes in endothelial cell layers. These macroapertures are large enough to allow the passage of bacteria across the endothelium basement membrane. It seems that EDIN acts by inhibiting RhoA; this results in the disruption of actin cables and promotes

Endothelial holes containing invasive bacteria (orange).

Continued on page 1719

CREDITS (TOP TO BOTTOM): DO-WON KIM *ET AL.*, *ORG. LETT.* **8** (2006); EMMANUEL LEMICHEZ

PathFinder

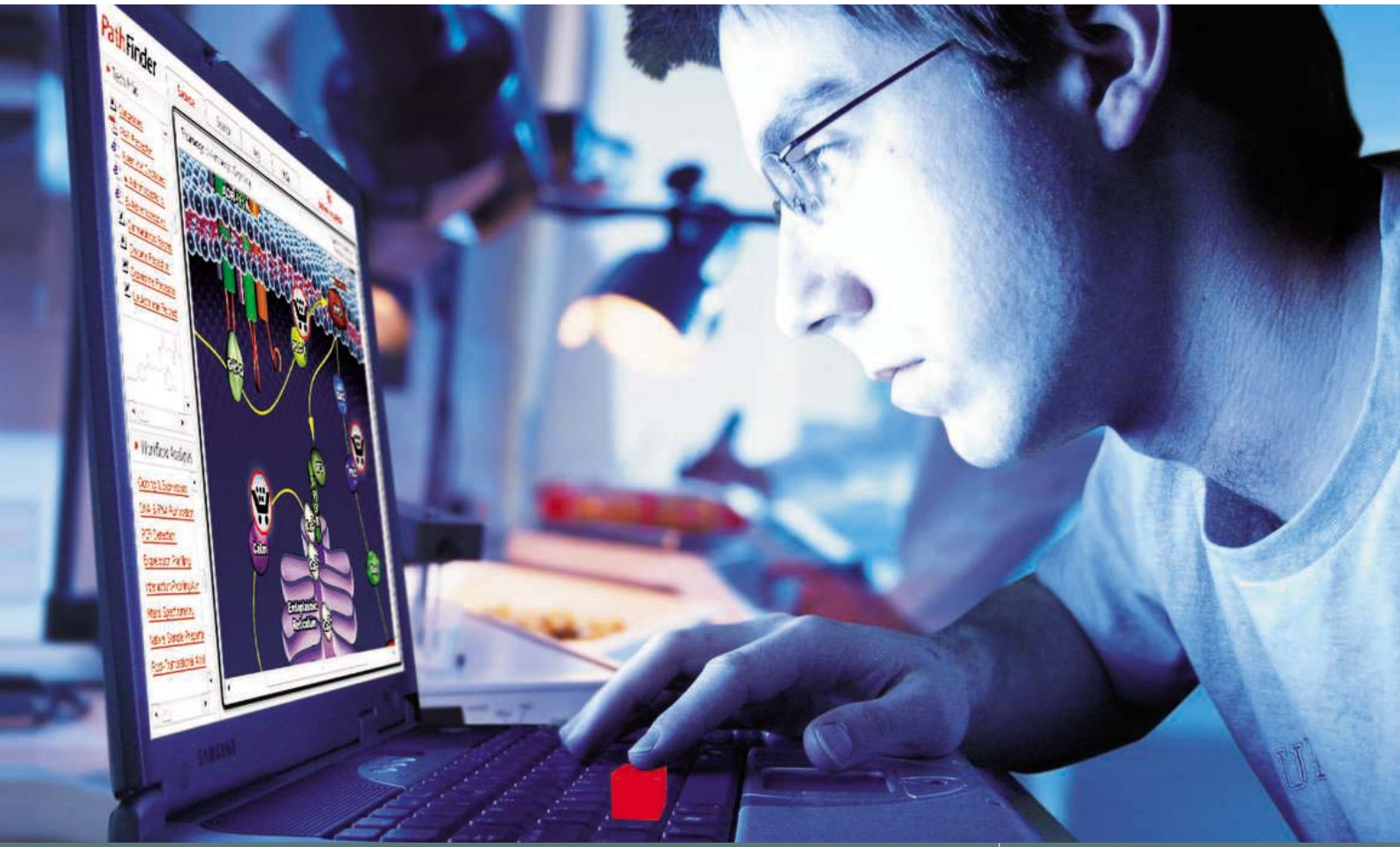

INNOVATION @ WORK

Discover Your Path to Innovation

On your path to innovation, Sigma is with you every step of the way. PathFinder is an online collection of interactive, interconnected maps showing biological signaling and metabolic pathways. For you to explore the relationships between different pathway elements, individual components are linked with related high-quality products.

You know your destination. PathFinder will get you there.

With Sigma's broad range of products, you will discover that we offer everything from small molecules to antibodies and enzymes. You will also be able to use PathFinder to locate qPCR components and siRNAs for gene knockdown. A valuable resource, PathFinder provides fast and accurate information on numerous levels, all in one place – and all linked to the important products that are key to the success of your research. In addition to products and services, you'll have immediate access to these helpful tools:

- Specific workflow analysis
- In-depth technical information
- Detailed product descriptions
- Relevant technical articles

Learn how PathFinder can help you discover your path to innovation by visiting us at:

sigma-aldrich.com/pathfinder

Accelerating Customers' success through Leadership in **Life Science, High Technology** and **Service**
SIGMA-ALDRICH CORPORATION • BOX 14508 • ST. LOUIS • MISSOURI 63178 • USA

SIGMA®

Continued from page 1717

the production of actin-rich membrane waves, which open up the holes. — SMH

J. Cell Biol. **173**, 809 (2006).

IMMUNOLOGY

Another Function for AID

Activation-induced cytidine deaminase (AID) plays a pivotal role in the immune system, controlling antibody class switching and generating diversity through somatic hypermutation of immunoglobulin genes. AID is also part of a larger group of deaminases, which include the antiretroviral APOBEC family members.

Gourzi *et al.* explored the possibility that AID might possess a similar capacity for protection against retroviruses and found that cells from mice lacking AID were indeed less able to cope with a replication-deficient form of the transforming Abelson murine leukemia virus (Ab-MLV). In response to infection, AID activity was induced in the bone marrow, extending its territory beyond the B cell germinal center. Furthermore, mice succumbed to transformed B cell tumors more rapidly if they lacked AID, and showed a corresponding failure to control cellular proliferation. AID activity induced phosphorylation of the cell cycle checkpoint kinase Chk1 and increased the sensitivity of host cells to killing by natural killer (NK) cells by up-regulating NK cell receptor ligands. These observations fit well with a model in which generalized DNA damage caused by widespread AID-induced mutations in transcribed genes prompts both checkpoint arrest and elimination by the immune system. It will now be interesting to see how broadly the scope for AID in protecting host from pathogen might extend. — SJS

Immunity **24**, 10.1016/j.immuni.2006.03.021 (2006).

BIOMEDICINE

Carbs Worth Remembering

The brains of patients with Alzheimer's disease (AD) show an aberrant buildup of oligomeric aggregates of amyloid β peptide (Aβ). These aggregates are neurotoxic and are believed by many researchers to be a central cause of the memory loss and cognitive decline that characterize the disease. Hence, interventions that inhibit Aβ oligomerization would be expected to slow or prevent disease progression.

McLaurin *et al.* test this hypothesis in a mouse model of AD by administering cyclohexanehexols, a group of small carbohydrate-like molecules that had been found in previous cell culture studies to stabilize Aβ in a conformation that precluded its assembly into oligomers. The treated mice showed improved cognitive function and reduced neuropathology, and they lived longer than control mice. The cyclohexanehexols were effective not only in a prevention setting but even when given to mice after the onset of symptoms. These results underscore the pathogenic role of Aβ oligomerization in AD and raise the possibility that derivatives of these compounds, which cross the blood/brain barrier and can be taken orally, may offer therapeutic benefit to patients with the disease. — PAK

Nat. Med. **12**, 10.1038/nm1423 (2006).

NANOTECHNOLOGY

All Wound Up

Nanohelices can be used in micro- and nanoelectromechanical systems as resonators, mech-anical components, or sensors. One route for the controlled fabrication of nanohelices is to grow strained heterofilms on a substrate and to etch and release the films, which then form coiled structures attached to the substrate at one end. Previously, Zhang *et al*. developed such a method for SiGe and SiGe/Cr films on single-crystalline Si(100) substrates that was limited to helical angles of 45° or more (the maximum orientation mismatch). They now report that as the width of the stripes is decreased below 1 μm, edge effects lead to tighter pitches and cause the handedness of the helices to reverse (from right to left, through a disordered transition regime); even concentric multiwall rings can be fabricated. Although the Cr layers are isotropic, they change the edge stresses and cause the onset of anomalous coiling (deviation from the preferred <100> scrolling direction) to occur at larger stripe widths. The authors map out the conditions for controlling helical angles to less than 10° and model the relaxation behavior of these films with finite-element simulations. — PDS

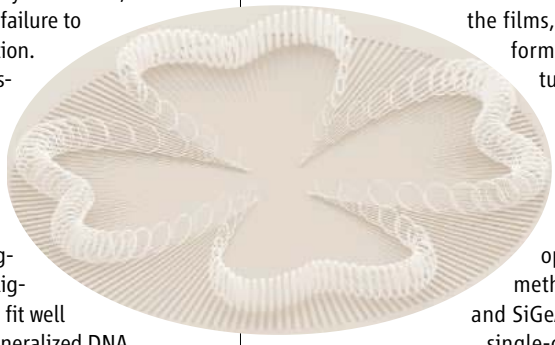

Scanning electron micrograph of Si/Cr bilayers; the similarity of coiling illustrates the dominant effect of the Cr layer over substrate direction.

CREDIT: LI ZHANG *ET AL.*, *NANO LETT.* 6 (2006)

Nano Lett. **6**, 10.1021/nl053240u (2006).

www.sciencemag.org

Science

1200 New York Avenue, NW
Washington, DC 20005
Editorial: 202-326-6550, FAX 202-289-7562
News: 202-326-6500, FAX 202-371-9227

Bateman House, 82-88 Hills Road
Cambridge, UK CB2 1LQ
+44 (0) 1223 326500, FAX +44 (0) 1223 326501

Subscription Services For change of address, missing issues, new orders and renewals, and payment questions: 866-434-AAAS (2227) or 202-326-6417, FAX 202-842-1065. Mailing addresses: AAAS, P.O. Box 96178, Washington, DC 20090-6178 or AAAS Member Services, 1200 New York Avenue, NW, Washington, DC 20005

Institutional Site Licenses please call 202-326-6755 for any questions or information

Reprints: Author Inquiries 800-635-7181
Commercial Inquiries 803-359-4578
Corrections 202-326-6501

Permissions 202-326-7074, FAX 202-682-0816

Member Benefits Bookstore: AAAS/BarnesandNoble.com bookstore www.aaas.org/bn; Car purchase discount: Subaru VIP Program 202-326-6417; Credit Card: MBNA 800-847-7378; Car Rentals: Hertz 800-654-2200 CDP#343457, Dollar 800-800-4000 #AA1115; AAAS Travels: Betchart Expeditions 800-252-4910; Life Insurance: Seabury & Smith 800-424-9883; Other Benefits: AAAS Member Services 202-326-6417 or www.aaasmember.org.

science_editors@aaas.org	(for general editorial queries)
science_letters@aaas.org	(for queries about letters)
science_reviews@aaas.org	(for returning manuscript reviews)
science_bookrevs@aaas.org	(for book review queries)

Published by the American Association for the Advancement of Science (AAAS), *Science* serves its readers as a forum for the presentation and discussion of important issues related to the advancement of science, including the presentation of minority or conflicting points of view, rather than by publishing only material on which a consensus has been reached. Accordingly, all articles published in *Science*—including editorials, news and comment, and book reviews—are signed and reflect the individual views of the authors and not official points of view adopted by the AAAS or the institutions with which the authors are affiliated.

AAAS was founded in 1848 and incorporated in 1874. Its mission is to advance science and innovation throughout the world for the benefit of all people. The goals of the association are to: foster communication among scientists, engineers and the public; enhance international cooperation in science and its applications; promote the responsible conduct and use of science and technology; foster education in science and technology for everyone; enhance the science and technology workforce and infrastructure; increase public understanding and appreciation of science and technology; and strengthen support for the science and technology enterprise.

Information for Contributors

See pages 102 and 103 of the 6 January 2006 issue or access www.sciencemag.org/feature/contribinfo/home.shtml

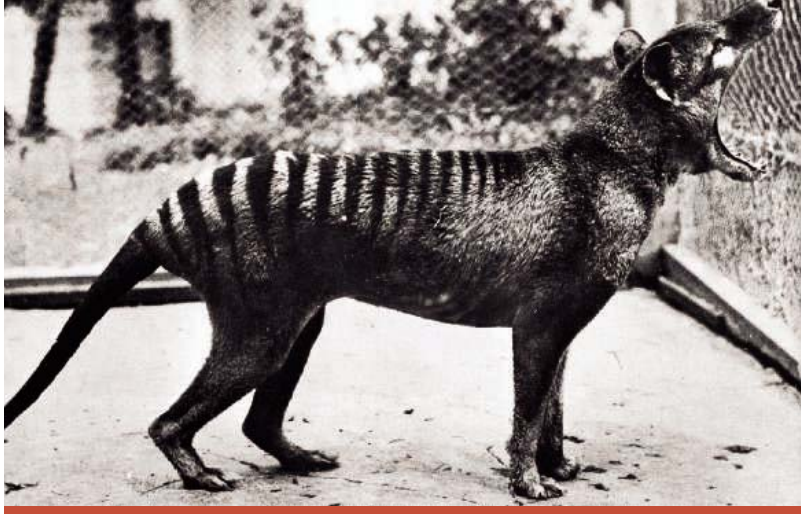

EXHIBITS

A POSSUM IN WOLF'S CLOTHING

The thylacine, or Tasmanian tiger (*Thylacinus cynocephalus*), had a tiger's stripes, a wolf's physique, and a kangaroo's pouch. The Thylacine Museum, curated by natural history enthusiast Cameron Campbell of Fort Worth, Texas, brims with data and lore about the carnivorous Australian marsupial, which most researchers think died out in the mid-1900s.

The animal comes alive in the film section, which features seven clips of captive animals. The thylacine has become a conservation symbol, and the site details human persecution of the species. Between 1888 and 1910, hunters seeking a government bounty slaughtered more than 2000 of the animals remaining in Tasmania, although disease might have spurred the species' collapse. No conclusive evidence of thylacines has turned up since the last zoo specimen (above) died in 1936. But some people, including Campbell, hold out hope that a few individuals hang on—or that the species can be resurrected. The museum recounts many unsuccessful expeditions that have searched for survivors and describes some of the difficulties facing an on-again, off-again project to clone thylacines using DNA from preserved specimens. >> www.naturalworlds.org/thylacine/index.htm

DATABASE

Bad Micromanagers

To control gene activity, cells sometimes deploy stumpy strands called microRNAs (miRNAs) that latch onto a corresponding sequence in a messenger RNA molecule and stall protein production. Mutations can foul up these matching sequences or form new ones in inappropriate locations, mistakes that might underlie some cases of Tourette syndrome (*Science*, 14 October 2005, p. 211) and other conditions. The new database Patrocles from the University of Liège in Belgium gathers SNPs, or one-letter changes in DNA, that create or eliminate miRNA attachment sites. The site houses data on mice and humans. >> www.patrocles.org

SOFTWARE

Annotate While You Read

The tool CBioC can help biomedical researchers who are trawling abstracts for data on protein interactions and their connection to disease. Just launched by computer scientist Chitta Baral of Arizona State University, Tempe, and colleagues, CBioC (for Collaborative Bio Curation) combines computer-extracted information with human curation. The program runs while you search PubMed. When you open an abstract, the software displays the protein interactions and other data that it gleaned from the article or that other CBioC users posted previously. You can then vote on the listings' accuracy or contribute overlooked ones. The idea is that over time, CBioC's user-curators will build a consensus summary of the molecular relations in the paper. >> cbioc.eas.asu.edu

EDUCATION

Electronic Chem Lab

Aimed at beginning chemistry classes, this virtual lab from Thomas Greenbowe of Iowa State University in Ames features some 70 exercises and animations. Simulations illustrate concepts such as Boyle's law, which describes the relation between a gas's volume and pressure, and let students run experiments in electrochemistry (right) and other areas. Animations depict molecular interactions such as the formation of hydrogen bonds between water molecules or the reaction between silver ions and a lead electrode in a solution of silver nitrate. >> www.chem.iastate.edu/group/Greenbowe/sections/projectfolder/simDownload/index4.html

DATABASE

Mammoth Tusks and Cave Bear Toes

At Neogene of the Old World, paleontologists and other researchers can find out where fossils of extinct mammals such as the woolly rhinoceros (*Coelodonta antiquitatis*; below) have turned up. The database from the University of Helsinki in Finland stores information on mammal remains dating from 25 million years ago to about 10,000 years ago. Search by locality to unearth data on more than 1000 excavation sites sprinkled across Europe, Asia, and Africa. You can map the locales and call up a list of animals discovered at each one. >> www.helsinki.fi/science/now

Send site suggestions to >>
netwatch@aaas.org
Archive: www.sciencemag.org/netwatch

CREDITS (TOP TO BOTTOM): DAVID FLEAY; THOMAS GREENBOWE/IOWA STATE UNIVERSITY; CORBIS/ROUFFIGNAC CAVE, FRANCE

CALL FOR NOMINATIONS

AAAS Mentor Awards

The American Association for the Advancement of Science (AAAS) is seeking nominations for its 2006 Mentor Awards. These awards are given in two categories: **Lifetime Mentor Award** for the individual who has served as a mentor for 25 or more years and **Mentor Award** for the individual who has served less than 25 years.

Both awards recognize an individual who during their career has mentored and guided significant numbers of students from underrepresented groups to the completion of doctoral studies in science and engineering fields and careers, or who has impacted the climate of a department, college, or institution to significantly increase the diversity of students pursuing and completing doctoral studies.

Award recipients in both categories receive a $5,000 monetary prize, a commemorative plaque, complimentary registration, and reimbursement for reasonable travel and hotel expenses to attend the AAAS Annual Meeting.

**Underrepresented groups include: women of all racial or ethnic groups; African American, Native American, and Hispanic men; and people with disabilities*

Additional info & award requirements:
www.aaas.org/aboutaaas/awards/mentor/

DEADLINE: 31 JULY 2006

Big News

AAAS Science Journalism Awards
Call for Entries

The AAAS Science Journalism Awards honor distinguished reporting on science by professional journalists. The awards are an internationally recognized measure of excellence in science reporting for a general audience. They go to individuals (rather than institutions, publishers or employers) for coverage of the sciences, engineering and mathematics.

U.S. CATEGORIES

Awards will be presented for U.S. submissions in the following categories:

- **Large Newspaper**
- **Small Newspaper**
- **Magazine**
- **Online**
- **Television**
- **Radio**

INTERNATIONAL CATEGORY

Open to journalists worldwide, across all news media.

- **Children's Science News**

Deadline: August 1, 2006
www.aaas.org/SJAwards

SPONSORED BY
Johnson & Johnson PHARMACEUTICAL RESEARCH & DEVELOPMENT, L.L.C.

AAAS
ADVANCING SCIENCE, SERVING SOCIETY

NO DIAL FOR DOLLARS

Oxford University has turned down an unspecified share of a $1.6 million bequest because it doesn't want to move a sundial.

John Simmons, a Slavonic scholar at Oxford's All Souls College, died at 90 last year. A sundial aficionado, he had a thing about the one at the college designed by famed architect and scientist Christopher Wren, also an All Souls fellow. The sundial was installed in front of the college's chapel in 1658, but in the 1870s, it was moved to a different position in the quadrangle: the wall of the college's Codrington Library. Simmons for decades argued that this was a terrible mistake that upset the symmetry of the quadrangle. So he specified in his will that part of his estate would go to All Souls only if the sundial were restored to its original position.

The warden of All Souls, John Davis, said last week that the college was declining the bequest because the stipulations were too "onerous." No one was available to explain what that meant. But the university will not be losing out altogether: Ronald Milne of Oxford's famous Bodleian Library said in a statement that that library appears to stand next in line if All Souls rejects the bequest.

Pacific Preserve

President George W. Bush last week designated the Northwestern Hawaiian Islands as a national monument. That makes it the world's largest marine reserve, surpassing Australia's Great Barrier Reef. Fishing is to be phased out there, and even tourists will need permits for diving and photography.

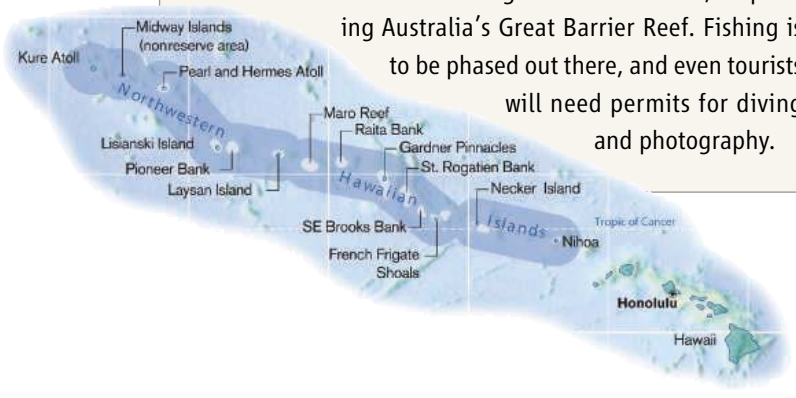

BACK TO THE FUTURE

Every language has metaphors that express time in terms of space; in English, for instance, one looks *forward* to next week or *back* to last year.

But in Aymara, spoken by about 2 million indigenous people in the Andean highlands of Bolivia, Peru, and Chile, it's the other way around. The word *nayra* can refer both to objects that are physically in front of the speaker and to events in the past. *Nayra mara*, for example, means "last year," explains Rafael Núñez, a cognitive scientist at the University of California (UC), San Diego. *Qhipa* means back or behind, so *qhipa mara* indicates "next year."

An Aymara man gestures back over his shoulder as he uses an expression referring to "next year."

This time concept extends to gestures as well as words. Speakers point backward or wave over their shoulders when talking about a future event and extend their hands forward to indicate the past—reaching farther out for events that happened long ago. Núñez and UC Berkeley linguist Eve Sweetser present their analysis of 20 hours of videotaped talk with 30 Aymara volunteers in the current issue of *Cognitive Science*.

"The Aymara seem to equate time with sources of knowledge," says David McNeill, a linguist at the University of Chicago in Illinois. To the Aymara, the forward direction is the source of the known: what's seen by the eyes, and what's happened in the past. Behind, where they can't see, lies the future.

A SMALL POLAR FOOTPRINT

Belgium plans to join the Antarctic scientific elite with a new polar research station, designed to be the most environment-friendly one ever built. The $8 million facility, dubbed Princess Elisabeth, will be constructed mostly of traditional materials such as wood, iron, and granite, and nontoxic, recyclable, high-tech materials.

To be built on a granite ridge near the Sør Rondane mountain range, the new base will house up to 20 people and use wind and solar energy to meet 98% of its energy needs. Half the wastewater will be recycled. Project manager Johan Berte says that figure could go up to 90% if guests can tolerate the idea.

Belgium's last Antarctic base was a short-lived one built in 1958 on the occasion of the International Geophysical Year, which led to the signing of the Antarctic Treaty. Construction of the new base will mark the 2007–08 International Polar Year.

"We would like to think that we are going to create a new culture" of nonintrusive research, says Berte. John Shears of the British Antarctic Survey says, "From what I have seen of the proposals, this station is at the forefront of environmental protection in Antarctica." He adds that it's important "not to exacerbate the problems, such as climate change, that we are investigating."

CREDITS (TOP TO BOTTOM): BRIAN MCMORROW; THE OCEAN CONSERVANCY; RAFAEL NÚÑEZ/UC SAN DIEGO; INTERNATIONAL POLAR FOUNDATION

Not so selfless
1727

A doomsday seedbank
1730

VOLCANOLOGY

Scientists Steal a Daring Look at Merapi's Explosive Potential

YOGYAKARTA, INDONESIA—It's an overcast and humid morning on 14 June as Supriyati Andreastuti and two colleagues embark on a routine mission to sample ash on the slopes of Mount Merapi. The researchers with the Merapi Volcano Observatory (MVO) are really scraping: Tarps set out to accumulate ash are barely flecked with gray. That isn't surprising. For several days, Indonesia's most active volcano has been relatively still. Working west across Merapi's southern flank, the trio, a *Science* journalist in tow, pulls into the Kaliurang Observation Station for a chat with Panut, chief observer. They park their jeep facing downhill, in case a quick getaway is in order.

Flat or fizzy? Scientists are assessing whether magma spilling from Merapi retains enough gas to possibly trigger an explosive eruption.

Panut isn't fooled by Merapi's tranquility. The current eruption may have cooled, he says, but he doesn't think it's over. As if on cue, the seismograph warbles. Huddling around it, Andreastuti and the others infer that a searing avalanche of volcanic rock, dust, and gas—a pyroclastic flow—is tumbling down the 3000-meter-tall mountain a few kilometers to the southeast, toward the Kaliadem tourist area.

Ten minutes pass, then 20. Andreastuti looks worried. "This one's dangerous," she says. It's impossible to discern from the seismograph how far the lethal clouds are traveling, but she knows that villages in the Kaliadem area are within striking range.

Merapi, the nemesis of Indonesian volcanologists, has roared back to life after a hiatus of 4 years. It began to stir in July 2005 with a swarm of tremors, then started dribbling lava in April. The eruption seemed to be subsiding at the end of last month when a magnitude-6.3 earthquake struck south of Yogyakarta, Java's ancient capital, on 27 May, killing 5780 people. Subsequently, growth of Merapi's lava dome surged. "The earthquake may have increased the ability of magma to move up into the conduit," says Birger Lühr, an applied geophysicist at the GeoForschungsZentrum in Potsdam, Germany.

Volcanologists are now racing to determine whether the latest uptick in Merapi's activity presages an explosive eruption—"no Krakatoa but … big enough to send pyroclastic flows in all directions," says Christopher Newhall, a volcanologist dispatched by the U.S. Geological Survey and the U.S. Agency for International Development to assist MVO. Although Newhall emphasizes that the odds of an explosive eruption are low, "we know Merapi is capable of quite nasty things."

Every few decades, on average, the volcano has a large eruption, and every several centuries it blows its top in a vertical plinian eruption—far more frequently than previously envisaged, Andreastuti and other researchers have found after analyzing ancient ash deposits and historical records. The most recent plinian eruption occurred roughly 500 years ago. Two lesser explosive eruptions in the 19th century killed thousands of villagers on the mountain's slopes; lava dome growth, says Newhall, appears to have preceded both events. By comparison, Merapi's outbursts in the 20th century were relatively tame. A 19th-century-sized eruption could put 80,000 villagers at risk.

Uncertainties abound. Merapi's behavior, as with other open-vent volcanoes, is notoriously unpredictable: Magma rises to the surface, loses some dissolved gases, and bleeds out or builds up in a lava dome. This can lead to pyroclastic flows and dome collapses or—under certain conditions—a gas-driven blast. Like others of its ilk, Merapi "doesn't give you many clues which way it will go," Newhall says.

Some Merapi eruptions have lasted months; there's no telling when this one will end. For MVO chief Antonius Ratdomopurdo and his staff, this translates as round-the-clock vigilance, and, says Newhall, "a hell of a lot of pressure."

Calculated risks

Andreastuti and her team drive east from Kaliurang for 15 minutes to the Merapi Golf Course near Kaliadem, 8 kilometers from the summit. They are hoping to observe the flow's aftermath from a closer vantage point. Andreastuti knows the billowing pyroclastic flow is a kilometer or so away but cannot see it. "That makes me much more nervous," she says. She has good reason to be wary. On 22 November 1994, she was with an MVO team on the north rim of Merapi's summit when, without warning, a pyroclastic flow tore down the south flank, killing 60 members of a wedding party and a few other villagers. The volcanologists were unharmed but shaken.

Around 3 p.m., after Andreastuti's crew reaches the Ngepos observation post, the seismograph is registering another pyroclastic flow barreling toward Kaliadem, bigger than the previous one. Scientists are on their cell phones, anxious to find out how bad the situation is in the east. Outside, coarse sand pellets ping and ricochet like sleet. Andreastuti and her team head northwest, to Babadan station, a mere 4.5 kilometers from the summit. The ash fall here is even heavier; eerie murkiness is punctuated by the distant plaintive voice of a muezzin calling villagers to a late afternoon prayer.

Back at headquarters that evening, the day's events are coming into focus. The first pyroclastic flow traveled more than 5 kilometers, scorching the uppermost village of Kaliadem. Just as a second MVO team had reached the scene and collected a few rock samples, they saw the second flow heading straight for them. "They had to high-tail it out of the danger zone," says Newhall. "They got out just in time"—as ▶

CREDIT: DITA ALANGKARA/AP PHOTO

Calm before the storm. Supriyati Andreastuti collects ash shortly before the first of two pyroclastic flows on 14 June.

did most of a search-and-rescue team. But two volunteers on the search team sought refuge in a bunker, one of several on the mountain built for such a contingency. The blast door was slightly ajar when rescuers dug down to the bunker the next day. The men had burned to death.

The mood at MVO is somber on 15 June. After 24 hours without another big pyroclastic flow, Newhall and two MVO scientists take a calculated risk. They duck back up to Kaliadem to retrieve additional samples, spending the minimum time necessary (20 minutes). "We wanted to see what's coming out right now to judge how fresh the magma might be," Newhall says. Older magma that has wallowed near the surface loses much of its gas, the way an opened can of soda loses its fizz. If fresh magma rises too fast, its higher concentration of gases could fuel an explosive eruption.

The rocks prove well worth the gamble. An initial look shows that the hardened magma is glassier than samples of earlier flows. Newhall anticipates that analyses will reveal that the magma is indeed fresher. At first blush, the samples resemble those from the 19th century eruptions; in contrast, magma from the tamer eruptions last century was largely degassed.

Even if further evidence points to a major explosion, however, officials may have trouble persuading villagers to clear out. Most are relying on guidance from their spiritual guardian Mbah Maridjan, who is advising villagers to stay put. "The level of risk people are willing to tolerate here is remarkable," says Newhall.

If Merapi were to regain its pre–20th century vigor, that obstinacy could be disastrous. "If you tell them, 'Tomorrow you'll be blown to smithereens,' that might have an effect," Newhall says. "But we don't know that. It might be the next day. It might be never." Merapi hasn't divulged that secret to the scientists. **–RICHARD STONE**

INFLUENZA

What Came Before 1918? Archaeovirologist Offers a First Glimpse

LISBON—After having resurrected the virus that caused the 1918 pandemic last year, a team of virologists is now trying to figure out which flu strains dominated the world before that global disaster.

At a meeting here last week,* Jeffery Taubenberger of the Armed Forces Institute of Pathology (AFIP) in Washington, D.C., said that RNA found in tissue samples from pneumonia patients who died in 1915 shows that the virus's hemagglutinin—an all-important coat protein—is a subtype called H3. If confirmed, "that's tremendously exciting," says molecular biologist Ian Wilson of the Scripps Research Institute in San Diego, California. Knowing the virus's entire genetic makeup—which Taubenberger believes is possible—would shed fresh light on where the 1918 killer flu may have originated, Wilson says.

Taubenberger spent almost 10 years piecing together the genome of the virus that caused the pandemic itself, using tissue samples stored at AFIP's massive repository as well as RNA scraps isolated from the frozen body of a woman who died during the pandemic in Alaska in 1918. He and others then rebuilt the virus from scratch and studied it in mice, chicken eggs, and human cells (*Science*, 7 October 2005, p. 77). The 1918 virus is a subtype called H1N1, based on its hemagglutinin (H) and neuraminidase (N) proteins.

What came before 1918 is a long-running question in virology, and the answer could help to explain what some believe is a natural cycle of flu subtypes succeeding each other (see graphic). In the 1950s and 1960s, a handful of researchers tested for hemagglutinin antibodies in people born before the 1918 pandemic. They proposed that an H2 strain swept the world during a pandemic in 1889, and H3 was introduced in another pandemic in 1900. A 1999 review of those same data concluded that H3 was more likely to have struck in the 1889 pandemic but warned that "seroarchaeology is not an exact science."

Only patient samples can yield solid answers, Taubenberger says. To find them, he teamed up with John Oxford of Queen Mary's School of Medicine at the University of London to explore a massive set of samples collected as early as 1905 and stored, along with patient records, in dusty cellars at the Royal London Hospital. Joanna Whitson, a medical student, found more than 200 suspected flu victims. So far, Taubenberger's team at AFIP has analyzed the lung tissue of only 12 of them, five of whom were confirmed to have had flu. And in four of those, sequencing of RNA snippets from the *hemagglutinin* gene—80 base pairs is the maximum length in these ancient samples—shows "it's absolutely an H3," Taubenberger says.

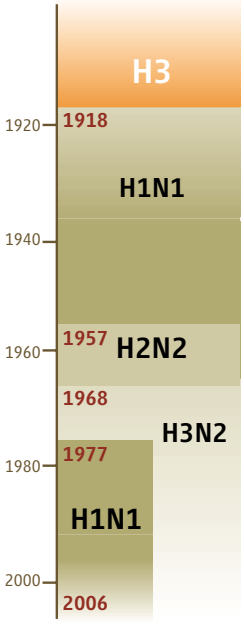

Coming and going. Preliminary results suggest that an H3 influenza strain circulated before H1N1 took over in the 1918 pandemic. Since then, several other subtypes have made their debuts.

The team plans to spend the next several years sequencing the entire viral genome. If viruses from before 1918 are completely different than the pandemic virus, that would support Taubenberger's contested theory that the pandemic virus jumped directly from an avian host into the human population, says virologist Albert Osterhaus of Erasmus University in Rotterdam, the Netherlands. "This could be the clincher," says Oxford.

–MARTIN ENSERINK

* 12th International Conference on Infectious Diseases, 15–18 June.

CREDIT: (TOP) R. STONE/*SCIENCE*

get*real*speed

Real-time PCR system Mastercycler® ep *realplex*

Innovative technology meets ultimate speed with the new, space-saving Mastercycler® ep *realplex* real-time PCR system.

Mastercycler ep *realplex* features high ramping speeds and short detection times, so you can complete more experiments each day—on even the tightest lab bench.

Eppendorf Mastercycler® ep *realplex*:

- High speed real-time PCR in <30 minutes
- Use reagent kits and consumables of your choice
- Intuitive software
- Modular concept provides ultimate flexibility
- Highly sensitive optical system

For more information visit
www.eppendorf.com/realplex

eppendorf

In touch with life

www.eppendorf.com · Email: info@eppendorf.com · Application support: 516-515-2258
In the U.S.: Eppendorf North America, Inc. 800-645-3050 · In Canada: Eppendorf Canada Ltd. 800-263-8715
Your local distributor: www.eppendorf.com/worldwide · Application support: Phone +49 180 366 67 89

PSYCHOLOGY

The Value of the Stick: Punishment Was a Driver of Altruism

A hallmark of humanity is that people help other people—not just relatives and friends but even complete strangers. Such altruism, which goes beyond the mere exchange of favors and forms the scaffolding of large-scale cooperation in human societies, has long been an evolutionary mystery. On page 1767, anthropologist Joseph Henrich of Emory University in Atlanta, Georgia, and his colleagues take a crack at solving the puzzle, concluding that such helpful behavior may have arisen as a result of punishment.

Playing by the rules. Joseph Henrich (*center*) and his colleagues found that the willingness to punish unfair acts is common to many societies, including members of Fiji's Yasawa population (*left*).

CREDIT: J. HENRICH *ET AL.*, *SCIENCE*

Reporting on experiments they conducted in 15 different societies on five continents, the researchers argue that altruism evolved hand in hand with a willingness to punish selfish behavior. Their results lend support to models of gene-culture coevolution that propose that cultural norms such as the punishment of unfair actions drive the selection of genes favoring altruism. "It's a pathbreaking study," says Ernst Fehr, an experimental economist at the University of Zurich in Switzerland and a proponent of gene-culture coevolution. But some evolutionary biologists, who believe that altruism toward nonrelatives evolved through repeated, mutually beneficial interactions, are unconvinced by the conclusions.

Researchers have studied the link between altruistic behavior and punishment in the past, but mainly among university students. To address whether all cultures reveal such a link, Henrich and his colleagues conducted game-playing experiments among populations such as a seminomadic community in the Kenyan savanna, inhabitants of Yasawa Island in Fiji, and farmers and wageworkers in Missouri. In one game, two players who remained anonymous to each other were given the local equivalent of 1 day's wages to divide between themselves. According to the rules, if the first player offered an amount that the second player rejected, both would walk away with nothing. The second player's decision thus provided one measure of willingness to punish.

In another game, a twist on the first one, a third person was added to the mix. If that third player felt that the first offered too little to the second, he could reduce the first player's winnings by 30%, but it would cost him a known portion of money he had been allotted. The choice of whether to ignore pure self-interest provided another measure of willingness to punish selfish acts. A final game was designed to measure altruism: Two anonymous players were given an amount to share, and one had to accept the other's offer.

The researchers found that individuals in all societies were willing to pay a price to punish unequal offers, both as the aggrieved party in the first game and as observers in the second game. Some societies were less punitive than others. And societies with a greater willingness to punish were more altruistic in the third game.

"You evolve into a more cooperative being if you grow up in a world where there are punishers," says Henrich. His evolutionary interpretation is that "punishment may have first emerged culturally. Those who violated social norms were punished while others flourished, leading to the genetic evolution of altruistic psychologies."

John Tooby, an evolutionary psychologist at the University of California, Santa Barbara, challenges Henrich's conclusion as a fanciful leap from games in which people remain anonymous. He notes that "in ancestral societies, people lived in small groups where everybody knew each other. In that environment, anonymous punitive interactions would have been rare to nonexistent, so there would have been no selection to adapt to such situations." Still, Tooby agrees that the study is a significant contribution to the ongoing debate on altruism "because it tests and reports on behavioral phenomena in a carefully parallel, cross-cultural fashion." **–YUDHIJIT BHATTACHARJEE**

Bank Shot

Gene hounds are keen on the idea of creating a massive DNA research database on the U.S. population, but planners need to do more homework first, according to a Department of Health and Human Services (HHS) advisory committee.

Several countries are launching population databases that researchers could mine for links between genes, the environment, and disease, such as the 500,000-person so-called biobank in the United Kingdom (*Science*, 17 March, p. 1535). Last month, the HHS Secretary's Advisory Committee on Genetics, Health, and Society weighed in on a similar proposal. The panel's draft report is "enthusiastic" about the idea, which could cost upward of $3 billion to recruit up to 1 million participants, analyze their DNA, and follow their health over a decade or more. But mindful of controversy over privacy and other matters that have dogged some biobanks, the panel says the government first needs to know whether the public wants to participate and study policy issues such as ethnic diversity and the effort's scientific value. HHS now plans to assess public opinion and is soliciting comment on the report until 31 July (see www4.od.nih.gov/oba/SACGHS/ public_ comments.htm).

– JOCELYN KAISER

Spanish Scientists: Home Alone

Young Spanish researchers are up in arms following recent comments by a government minister who referred to them as "postdoctoral and temporary." The roughly 2500 scientists, most Spanish-born, were lured back to their home country—many from tenure-track jobs abroad—for a fellowship program that promised "their integration in the Spanish science system." Now, with the first 5-year contracts in the Ramón y Cajal program nearing their end, many institutions have yet to offer secure employment, despite recent funding incentives from the government, although precise figures are not available.

Newly appointed Secretary of State for Universities and Research Miguel Ángel Quintanilla's words, published in the Spanish newspaper *El Mundo*, have only added to the scientists' discontent. The National Association of Ramón y Cajal Researchers deplored Quintanilla's "disrespectful and burlesque attitude." But the Ministry of Education and Science says it gave "generous" incentives to universities and research centers and "can't oblige [institutions] to contract anyone."

–ELISABETH PAIN

RESEARCH ETHICS

China's Science Ministry Fires a Barrage of Measures at Misconduct

BEIJING—Responding to a wave of scandals, China's Ministry of Science and Technology last week announced a slew of reforms aimed at discouraging and rooting out scientific misconduct. Although some researchers praised the initiatives, including a scheme to rate work performance and a public database of grant applications, many were skeptical they would lead to substantive change.

The Ministry of Science and Technology (MOST) outlined its proposals in a 26-point "Recommendations on Reforming Management of Science and Technology Programs," first released in January. The scientific community paid scant attention initially, researchers say, reading it as a recycling of similarly titled older materials. Previous reform plans "were not well implemented," admitted Vice Minister Shang Yong, who unveiled the array of more-specific measures at a press conference last week.

A promise of reform. Vice Minister Shang Yong outlined changes designed to increase government "transparency, equity, and fairness."

To limit the influence of grant managers, MOST plans to expand a database of experts it uses to review proposals and evaluate projects. Selection of reviewers will be random in the future, which MOST hopes will help reduce conflicts of interest. Another step involves setting up a "credit management system" to keep performance scores of experts who do evaluations and of institutions and individuals who undertake projects, explains Qin Yong, deputy director of the Department of Development Planning at MOST. Scores will be taken into account in making future grant decisions, he says.

The main goal, Shang says, is to increase "transparency, equity, and fairness" in program management. All nonconfidential projects administered by MOST will be handled online using a database searchable by the public. Everyone will be able to read applications, approvals, implementations, and appraisals, explains Qin. MOST says that expert reviewers' opinions will be kept confidential, however. Applications already must be submitted online, and an online evaluation system will be adopted later.

In a separate action, MOST enlisted 100 accounting firms to audit more than 2000 projects in 2004 and 2005, involving a total of $2 billion in funding. Some wrongdoers had been disciplined, MOST said but declined to elaborate on details.

In the past, MOST has been criticized for its dual role as both "umpire" and "player" in the research management game—selecting and implementing projects. This may be changing, says Liang Zheng, a researcher at the China Institute for Science and Technology Policy. He applauds what he views as an effort to limit managers' power in the new measures: It is "a step in the right direction, although slow in coming."

Zhu Bangfen, chair of the Physics Department at Qinghua University, praised the new measures as more workable than previous rules. But some observers such as Yu Lu, a theoretical physicist at the Chinese Academy of Sciences (CAS), consider them too vague. "Take the credit database for example; who gives scores to these experts? By what standards? Will it be credible?" he asks.

Others voiced doubts about the government's ability to carry out the reforms. Cao Zexian, a physicist at the CAS Institute of ▶

NATIONAL SCIENCE FOUNDATION

House Panel Tells NSF to Keep Eye on the Prize

A powerful member of Congress is leading the National Science Foundation (NSF) to water. But it's not clear whether he can get the agency to drink.

Representative Frank Wolf (R–VA) thinks NSF's bread-and-butter research grants aren't sufficient to attack some of the knottiest problems facing society—in particular, finding energy sources that don't contribute to global warming. So he has proposed that NSF launch a series of very large prizes to stimulate innovative research (*Science*, 10 March, p. 1363). And as chair of the House spending panel that oversees NSF and several other science agencies, he carries a powerful whip.

Last week his panel, in a report accompanying its endorsement of President George W. Bush's request to boost NSF's 2007 budget by 7.9%, told the foundation to use some of its $6.02 billion "for innovation-inducement prizes … of an appropriate scale." Wolf also gave NSF the green light to find potential backers for the prizes among high-tech companies and private foundations that share his concern about the health of the U.S. research enterprise. "I think it's a great way to generate interest in tackling these tough problems," he adds.

Last year, Wolf told NSF to consult with the National Academies on how to create a prize program, and its report is due in September. But the legislator says NSF "is not moving as fast as I had hoped," so this year's House report "strongly encourages NSF to leverage private sector involvement." Wolf says some of the $16 million he added to the president's request for NSF's education directorate, for example, could be used to leverage outside contributions.

NSF Deputy Director Kathie Olsen says that NSF already uses "a number of approaches to encourage innovation" and is waiting for advice from the academies before designing any competition. She adds that NSF must avoid even the appearance of a conflict of interest from donors: For example, a company might try to offer a prize for solving a problem that would enhance its products or industry. Still, Olsen predicts that prizes "will catch the attention" of many scientists, and she guesses that NSF "should at least be able to get an announcement out in 2007."

–JEFFREY MERVIS

CREDIT: GONG YIDONG

Physics, criticizes the proposed openness as a "matter of formality" and asks, if the public doesn't know how a program is approved, is there real transparency? Officials "often formulate measures that appear airtight, but I don't know how they will implement the rules concretely in practice," says Cao Nanyan, a professor at Qinghua University who researches scientific misconduct.

No matter how good the measures are, Liang says, they will only apply to a fraction of science and technology: "MOST alone can hardly stop scientific misconduct." The central government's R&D budget for 2006 is $9 billion, of which MOST will be distributing about $1.7 billion.

–GONG YIDONG AND HAO XIN

Gong Yidong writes for *China Features* in Beijing.

2007 NASA BUDGET

Space Scientists Score a Modest Victory in House Spending Bill

After months of fretting, arguing, and lobbying, earth and space scientists got some good news last week. The House panel that funds NASA proposed adding $75 million—mostly for research grants—to the agency's science programs next year. That is less than half of what the National Research Council (NRC) urged in a May report, but it demonstrates that researchers have the political muscle to battle the Administration's campaign to replace the space shuttle and return humans to the moon at the expense of several scientific projects.

Overall, the House appropriations subcommittee chopped $83 million from NASA's request for $16.8 billion, giving it only $86 million more than current levels. But lawmakers proved sympathetic to the science community. The spending bill includes $10 million to revive the Terrestrial Planet Finder and $15 million to restart planning for a mission to Jupiter's moon Europa, both of which NASA wants to postpone indefinitely to save money. Legislators added $50 million to a grants program that NASA proposed holding flat after this year, heeding the pleas of scientists for more money to analyze data from instruments yet to be launched. But the panel declined to restore funding for a host of small missions, in effect delaying them indefinitely.

Another look? Congress wants NASA to start work on a dedicated mission to Jupiter's moon Europa.

CREDIT: NASA/JPL/UNIVERSITY OF ARIZONA/UNIVERSITY OF COLORADO

"We're pleased they fixed at least one of our problems," says Lennard Fisk. An atmospheric chemist at the University of Michigan, Ann Arbor, Fisk chaired the NRC panel, which called for an additional $50 million for the research grants and $110 million across several small programs. Fisk also praised the low number of earmarks, which in recent years have eaten up an increasing share of science funding.

To offset the additions to science and a $100 million boost to the request for aeronautics research, the panel cut $151 million from President George W. Bush's $4 billion exploration effort, mostly in advanced technology work. But one NASA official said the agency isn't complaining, because it received nearly full funding for the space shuttle, the space station, and the shuttle-replacement program.

The Senate is likely to add both earmarks and research funds to its version of the bill later this year. Toward that end, senators Barbara Mikulski (D–MD), ranking minority member of the Senate panel, and Kay Bailey Hutchison (R–TX), who chairs the NASA authorizing panel, hope to meet soon with Vice President Dick Cheney to discuss an emergency funding bill to cover a long-term shortfall in shuttle, exploration, and science spending.

NASA, meanwhile, seems on the verge of reversing its plan to cancel the Stratospheric Observatory for Infrared Astronomy (SOFIA) (*Science*, 17 March, p. 1540). The same day that the House panel proposed its funding plan, NASA said SOFIA faces no further technical hurdles. But the search for the money to complete and launch SOFIA will spark yet another battle over the allocation of NASA's scarce research funds.

–ANDREW LAWLER

Lugar Backs Indian Nuke Deal

The chair of the Senate Foreign Relations Committee has gone to bat for the proposed U.S.-India nuclear technology agreement (*Science*, 10 March, p. 1356), raising the chances it will pass. Senator Richard Lugar (R–IN) told an audience last week at the Naval War College in Newport, Rhode Island, that the deal represents "the most important strategic diplomatic initiative undertaken by President Bush." Lugar's comments counter those made recently in *The Wall Street Journal* by nonproliferation activist and former senator Sam Nunn, who says the Senate should, among other things, demand that India halt its production of fissile material for weapons as a condition of passage.

The move suggests that "Congress is not going to turn the deal down," says Lawrence Korb of the Center for American Progress in Washington, D.C. Lugar's committee is expected to take up the issue sometime this month.

–ELI KINTISCH

Irish PIs Are Smiling

Ireland is rapidly becoming one of Europe's big R&D spenders. On 18 June, Irish Prime Minister Bertie Ahern announced new R&D spending of $4.8 billion between now and 2013. This will raise R&D investment to 2.5% of gross domestic product by 2013, above the European Union average of 2% and near the United States's 2.6%. The Irish government will spend billions beginning this year to accelerate research in areas such as agriculture and energy. Goals include doubling the number of Ph.D.s with grants nationwide and creating 350 new principal investigator–led research teams.

–SEAN DUKE

Vote Weakens Whaling Ban

Japan scored a symbolic victory in its quest to resume commercial whaling last week, winning support from the International Whaling Commission for its campaign to overturn a 20-year-long moratorium on the practice. The 33-to-32 vote, at the group's annual meeting on the Caribbean island of St. Kitts, approved a statement that declared that the moratorium "is no longer necessary," adding that "sustainable whaling is possible." Japan has encouraged several countries to join the commission in recent years, offering them foreign assistance.

Although the votes of three-quarters of the members are needed to end the moratorium, supporters of the ban are concerned by the latest step.

–DENNIS NORMILE

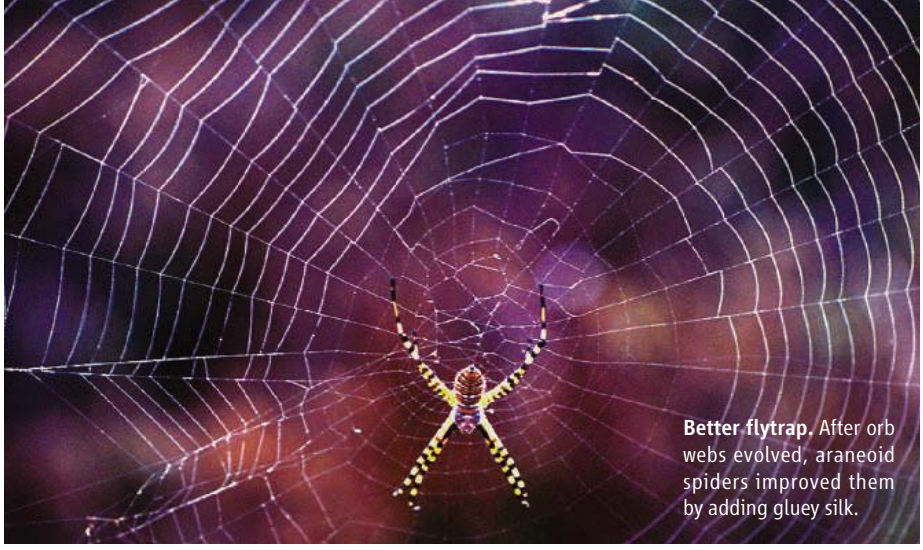

Better flytrap. After orb webs evolved, araneoid spiders improved them by adding gluey silk.

EVOLUTION

Spider Genes and Fossils Spin Tales Of the Original Worldwide Web

Building an orb web is no simple affair. Spiders suspend the silky equivalent of guy wires, attach radial spokes, and then weave in a sticky spiral to snare prey. Two groups of spiders—deinopoids and araneoids—make such webs. Their use of different kinds of adhesives for the "capture spiral" once made biologists think that the two spider lineages had evolved orb weaving independently. But the discovery of similar construction techniques made a single origin of orb webs seem more likely, and a new study of silk genetics on page 1762 strengthens the case.

"It's really cool to see this matched by the genetic evidence," says Gustavo Hormiga, an arachnologist at George Washington University in Washington, D.C., about a study led by Jessica Garb, a postdoc at the University of California, Riverside (UCR). Two other new papers describe fossils of spiders and their webs that further emphasize the antiquity of orb webs.

Deinopoids follow the more ancient silk recipe. They swathe their capture spirals in dry silk. First, a spider oozes fibrils just tens of nanometers in diameter from thousands of spigots on its abdomen. Then the spider combs the threads like cotton candy onto a support line that makes up the spiral. When a fly or other prey brushes up against the fibrils, electrostatic forces pin it to the web.

Araneoids simplified the process. Using a pair of glands that deinopoids lack, they simply dab a viscous glue onto the support line. That approach takes about one-tenth the effort of making dry silk, and the adhesive is 13 times stickier per unit volume. The web is also less visible to insects, because the silk doesn't reflect ultraviolet light. All these advantages may help explain why araneoids are 10 times more diverse than the deinopoids.

Scientists have extensively studied the genes and proteins that make spider silk stretchy and strong (*Science*, 25 February 2000, p. 1378), but most of the work has focused on araneoids. Garb decided to take the web less traveled by. Working with Cheryl Hayashi of UCR and others, she studied complementary DNA from silk glands of two kinds of deinopoids, *Deinopis spinosa* and *Uloborus diversus*.

The team found that the deinopoids had genes (known as *Flag*, *MaSp1*, and *MaSp2*) quite similar to those that araneoids use to make silk for the capture spiral and radial spokes—additional evidence for a single origin of orb webs. That's not a surprise to spider biologists, but it's pleasant confirmation that their previous observations "are as valid as we thought they were," says Brent Opell of Virginia Polytechnic Institute and State University in Blacksburg.

Two new fossils described this week underscore the long-lived success of orb webs. On page 1761, a team led by David Grimaldi of the American Museum of Natural History in New York City reports the oldest example of spider silk entrapping prey. In a chunk of 110-million-year-old amber from Spain, they found a fly and a mite ensnared in strands of gluey spider silk, possibly from an orb web. Meanwhile, in the 14 June online issue of *Biology Letters*, David Penney of the University of Manchester, U.K., and Vicente Ortuño of the Universidad de Alcalá, Madrid, describe the oldest true orb-weaving spider: an araneoid found in 115-million-year-old Spanish amber from a different site. The 2-millimeter-long spider, which they name *Mesozygiella dunlopi*, is remarkably similar to a living spider—showing that the basic, and successful, body plan appeared long ago. **–ERIK STOKSTAD**

SPECIES CONSERVATION

A 'Forever' Seed Bank Takes Root in the Arctic

LONGYEARBYEN, NORWAY—The prime ministers of five Nordic countries gathered here on the arctic archipelago of Svalbard last week to mark the beginning of a unique bunker: an underground vault that will hold up to 3 million seeds. Launched with $3 million from Norway, the project seeks to preserve the DNA of agricultural crops—the most complete such collection in the world by far. "It will contribute to ensuring our food security [and] protect our cultural heritage," says Norwegian Prime Minister Jens Stoltenberg.

The seed bank is intended as a backup for existing collections, which have proven to be vulnerable. Collections of seeds in Afghanistan and Iraq, for example, were destroyed by war, and some of the oldest seed banks in the world, including one in Russia and a collection of apple varieties in Kazakhstan, are deteriorating.

The Svalbard vault, carved into the side of a rocky, snow-streaked mountain near the town of Longyearbyen, will be built to withstand everything from nuclear war and bomb threats to global climate change. Its chief advantage is its location. Longyearbyen (population 1900) sits just ▶

Deep freeze. Norway's Prime Minister Jens Stoltenberg marks the launch of a mountainside seed vault.

CREDITS (TOP TO BOTTOM): MARK CHAPPELL; DAN CHARLES

1120 km from the North Pole. During the winter, residents endure complete darkness for almost 4 months. Thanks to the Gulf Stream, temperatures in summer usually rise a few degrees above freezing, but under the surface, the earth remains permanently frozen, easing the task of keeping seeds refrigerated at –18°C. Even if equipment fails, it would be many weeks or even months before the vault reached –3°C, the temperature of the surrounding sandstone.

The vault eventually will hold seeds representing almost the entire gene pool of the world's agricultural crops. Cary Fowler, executive director of the Global Crop Diversity Trust, calls the genetic diversity in existing seed collections "the most valuable natural resource in the world." Most of those varieties vanished from fields over the past century as farmers adopted the products of modern breeding programs. So when plant breeders are looking for genetic resistance to emerging plant diseases, or for genes that may improve yields further, they often are forced to turn to the gene banks.

But there will be a few gaping holes in the collection: China and a few African countries refused to include soybeans and peanuts in a recent international treaty that protects the free exchange of seeds among plant breeders. Those nations aren't likely to contribute copies of their important collections of those crops.

The first seeds to arrive at Longyearbyen will come from international centers such as the International Rice Research Institute in the Philippines or the International Center for Agricultural Research in the Dry Areas, located in Syria. After that, gene banks run by national governments will contribute additional samples. "We will limit this to unique seeds and try to avoid duplication," says Grethe Evjen of Norway's ministry of agriculture and food. But that may be difficult because many collections aren't well cataloged. Fowler's group plans to raise $100,000 a year to operate the seed bank.

Some scientists believe that preserving and deepening knowledge of these collections is as important as preserving the seeds themselves. "If the people who know about the collections are gone, I would say that 75% of the utility will be gone," said Major Goodman, a specialist on maize at North Carolina State University in Raleigh. Of the half-dozen top maize specialists worldwide, he said, almost all are nearing retirement: "For maize, we need at least eight young people trained in this area."

The prospects for so many positions appear bleak. But the Svalbard vault may help. "It's extremely good publicity," says Geoffrey Hawtin, former director of the International Plant Genetic Resources Institute in Rome. "It captures the public's imagination."

–DANIEL CHARLES

Daniel Charles is a freelance writer in Washington, D.C.

ARCHAEOLOGY

First Jewelry? Old Shell Beads Suggest Early Use of Symbols

A high school ring, a string of pearls on Oscar night—how we decorate our bodies says a lot about who we are. Archaeologists think such symbolic communication marks the mental leap that made art and language possible. But when did it begin? On page 1785, researchers claim that three grape-sized shells from the Levant and North Africa were worn as beads 100,000 or more years ago. If true, this would push back the earliest evidence for symbolism by at least 25,000 years.

"This is an important and exciting contribution," says archaeologist Christopher Henshilwood of the University of Bergen in Norway. Two years ago, Henshilwood reported finding 75,000-year-old marine shell beads at Blombos Cave in South Africa, then the earliest claimed ornaments (*Science*, 16 April 2004, p. 369). Yet archaeologists who were skeptical about Blombos also question the new claim. "The evidence seems weak to me," says Richard Klein of Stanford University in Palo Alto, California, who has long argued that the symbolic explosion took place in Europe and Africa about 40,000 years ago.

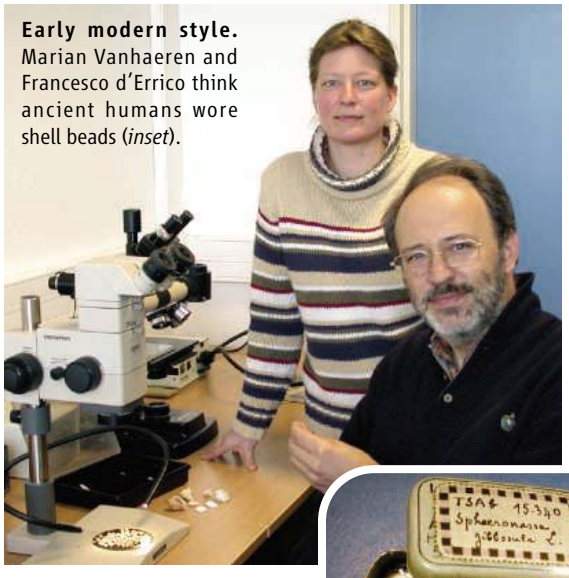

Early modern style. Marian Vanhaeren and Francesco d'Errico think ancient humans wore shell beads (*inset*).

The team, led by archaeologists Marian Vanhaeren of University College London and Francesco d'Errico of the research agency CNRS in Talence, France, found the beads in museum drawers. Two came from 1930s excavations at the Skhul rock shelter in Israel, where 10 burials of early *Homo sapiens* had been found. The other one came from the open-air site of Oued Djebbana in Algeria, excavated during the 1940s. Vanhaeren and d'Errico retrieved the shells and examined them for signs of use as ornaments.

All three suspected beads are shells of the marine snail *Nassarius gibbosulus*. Each has a distinctive type of indented perforation that turns up only rarely in reference collections. The team concluded that humans either made the holes or picked out perforated shells to string together as ornaments.

Recent dating of the Skhul burials has shown that they are 100,000 to 135,000 years old. (Oued Djebbana is poorly dated but is at least 35,000 years old and possibly much more.) To be sure that the Skhul shells came from the burial layer, Vanhaeren and d'Errico's team used scanning electron microscopy, x-ray diffraction, and chemical analysis to examine sediments stuck to one of the shells. The sediments matched those from the burial layer, suggesting that early modern humans did indeed create shell beads 100,000 or more years ago.

The team's findings are "particularly compelling evidence for symbolic use of the shells as beads," says anthropologist Alison Brooks of George Washington University in Washington, D.C. Such personal ornaments, Henshilwood adds, are "expressions of modern cognitive abilities" and also indirect evidence "for the acquisition of articulate oral language." And because neither Skhul nor Oued Djebbana was very close to the sea, says Steven Kuhn, an archaeologist at the University of Arizona in Tucson, humans must have carried the small shells—which have almost no food value—to the sites for symbolic purposes.

Nevertheless, Kuhn cautions that the Skhul shells could have come from a younger stratigraphic layer and picked up older sediment after they "filtered down" into lower layers. And Klein argues that even if they are beads, such artifacts are so rare at sites older than 40,000 years that their interpretation as full-blown symbolic behavior remains "debatable." Yet some researchers think more evidence will turn up—and not just in museum drawers. Says Henshilwood: "I believe this is the tip of the iceberg."

–MICHAEL BALTER

CREDITS: PHOTO COURTESY OF MARIAN VANHAEREN AND FRANCESCO D'ERRICO; (INSET) MARIAN VANHAEREN

SEISMOLOGY

The Strain Builds in Southern California

A fatalist would just observe that earthquakes happen, especially in California, and let it go at that. But seismologists and emergency-response planners would like to know where and when the next great quake—the Big One—is going to strike in California. This week in *Nature*, geophysicist Yuri Fialko of the Scripps Institution of Oceanography in San Diego, California, reports that the southernmost San Andreas fault is indeed building strain at a dangerous rate. If, as seems likely, strain has been accumulating there at the same clip since the last big strain-releasing quake, the next one will probably come within a few decades, according to one forecast.

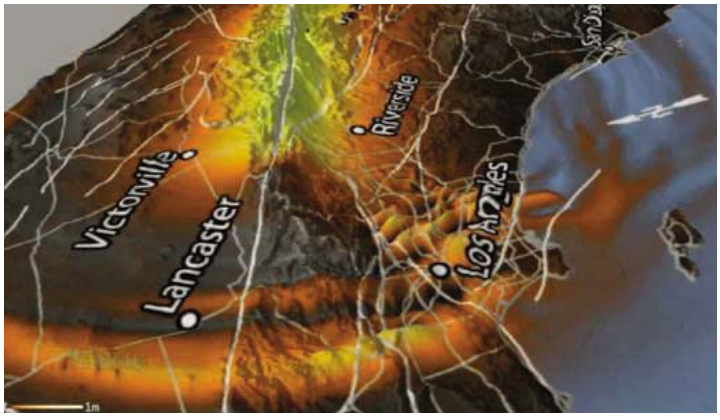

Big one. A simulated quake on the southernmost San Andreas shakes the near-fault region (color and exaggerated topography) and ripples into Los Angeles.

The 4 million people of Riverside and San Bernardino—and even distant Angelenos—should take note. "There's a lot of concern about this southernmost segment of the San Andreas," says paleoseismologist Ray J. Weldon of the University of Oregon, Eugene. It's now looking like "the most dangerous" fault in California.

The southernmost San Andreas has long been suspect. In the last 2 decades, paleoseismologists found signs of the last quake to rupture the 200 kilometers of fault running from San Bernardino and Riverside to beyond the Salton Sea. That quake struck more than 300 years ago. And the strain building on the fault was increasingly deforming the surface, geodesists found using precise distance-measuring instruments on the ground as well as the Global Positioning System. So the southernmost San Andreas appeared to be working up to its next big quake, probably something like a magnitude 7.5.

But southern California is a tectonic mess. The North American and Pacific plates don't simply jerk past each other along the San Andreas. Instead, fault slip—and earthquakes—occur on three or more adjacent faults, including the San Andreas and the San Jacinto fault, a side fault that joins the San Andreas at San Bernardino. Some plate motion might even occur without generating earthquakes.

To sort out how much strain is actually building on each fault, Fialko analyzed radar data that Europe's Earth Remote Sensing satellites ERS-1 and ERS-2 had gathered between 1992 and 2000. By combining sequential satellite passes using the interferometric synthetic aperture radar (InSAR) technique, Fialko found strain accumulating on both the San Andreas and San Jacinto but not on other subsidiary faults. "He's able to put a very solid number on the slip rate of the San Andreas," says geodesist Roland Burgmann of the University of California, Berkeley. "There's just no way around the result."

About 55% of the motion between the two plates occurs on the San Andreas, according to Fialko's results. That's enough to confirm researchers' concerns about the next big one. Weldon and colleagues have estimated a 70% probability that the southernmost San Andreas will rupture within the next 30 years. With the new InSAR data, says Weldon, "I think people are starting to believe it."

People in San Bernardino and Riverside would be within the zone of strongest shaking along the fault, and geologic crustal structure would focus seismic waves from a northward-propagating rupture into downtown Los Angeles. About 45% of plate motion is on the San Jacinto fault. That's more bad news for the San Bernardino–Riverside area. If true, the San Jacinto will have larger quakes than previously thought, says Weldon. Magnitude-7 quakes on the San Jacinto "could be as bad as a 7.5 on the San Andreas," he says.

On the bright side, having all the plate motion on just the two faults would mean that no significant motion would be left for faults such as the Elsinore, which reach into Los Angeles itself. **–RICHARD A. KERR**

EUROPEAN SCIENCE

E.U. Parliament Approves Funding for Human ES Cells

Scientists working with human embryonic stem (hES) cells in Europe breathed a sigh of relief last week as a final threat to Europe-wide funding of the work was lifted. On 15 June, the European Parliament voted down two amendments that would have restricted funding for hES cell research under the €50 billion ($63 billion) Framework 7 program, which will fund research in the E.U. from 2007 through 2013.

Among hundreds of suggested amendments to the Framework 7 proposal, the Parliament gave a broad endorsement to plans for the European Research Council, a new funding agency that would support top individual scientists across Europe, and made tweaks to the amount of money allocated to renewable energy and research by small businesses.

But the embryo issue was the most contentious. Many scientists hope hES cells will help them understand human development and treat disease in new ways, but the work is controversial because the cells are derived from week-old human embryos. The 25 E.U. member countries have different laws governing embryo research, ranging from very permissive to outright bans; some opposed spending E.U. money on it.

Under a compromise worked out in 2002, the current Framework 6 program can fund hES cell research if the work receives an ethical endorsement from the host country, an E.U.–level ethics committee, and a panel with representatives from all member countries. Scientists had lobbied to retain this policy in the face of two amendments that would have either blocked or restricted hES cell research. Both those amendments failed, however, and in a 284–249 vote, the Parliament approved a measure that continues the current policy.

Embryo research is a tiny but key slice of the Framework program, says Elena Cattaneo of the University of Milan in Italy. Cattaneo's lab received €10,000 to work on hES cells through EuroStemCell, a €12 million project funded by Framework 6. Although such work is not prohibited in Italy, she says, funding is unavailable from national sources.

Parliamentary and commission representatives will iron out their differences in meetings in the coming month. The revised Framework 7 program then needs the final endorsement of the Parliament and the research ministers of member countries.

–GRETCHEN VOGEL

CREDIT: SDSC AND SCEC

U.S. BIOETHICS

House Panel Finds Fault With How NIH Handles Tissue Samples

A congressional finding that a drug company paid a National Institutes of Health (NIH) scientist for spinal fluid samples has raised a larger question: What happens to NIH's archived patient samples? NIH's efforts to improve practices within its intramural program come as U.S. medical centers are trying to tighten controls over such materials.

At a 2-day hearing last week, Joe Barton (R–TX), chair of the House Energy and Commerce Committee, complained about the "lack of a centralized database [for patient samples] and a lack of oversight at NIH that could, and probably does, leave NIH laboratory[ies] vulnerable to the risks of theft and abuse." NIH officials testified they have already begun to improve their procedures.

But outside scientists agree with NIH that the agency needs time to organize its millions of stored specimens. "People have their samples everywhere," with details recorded on everything from paper notepads to computers, says Mark Sobel, a former NIH researcher who is now executive officer of the American Society for Investigative Pathology. Creating a central registry of NIH's holdings, he predicts, "is going to be a massive undertaking."

Barton's ethics investigation is an extension of an earlier one questioning large payments from drug companies to senior NIH scientists. That led NIH to ban industry consulting by its intramural scientists last August (*Science*, 2 September 2005, p. 1469). Last week's hearing focused on Alzheimer's disease researcher Trey Sunderland of the National Institute of Mental Health (NIMH) and his dealings with drug giant Pfizer.

The committee pursued a complaint from Susan Molchan, a former clinical researcher in Sunderland's lab, that Sunderland wouldn't provide her with some of her old spinal fluid samples. Staffers eventually learned that Sunderland had sent Pfizer about 3200 spinal fluid samples and 388 plasma samples he and others had collected since the early 1980s, including some from Molchan, along with clinical data, from Alzheimer's patients and controls. The company used them to study so-called biomarkers, proteins that might serve as indicators for the neurodegenerative disease.

Pfizer had signed a Material Transfer Agreement with NIMH for the samples in April 1998. Around the same time, Sunderland signed a consulting agreement with Pfizer that eventually paid him $285,000. A 26-page bipartisan report released last week by the Commerce Committee's oversight and investigations subcommittee found "reasonable grounds to believe" that Pfizer made the payments in exchange for the samples.

Exhibit A. Concerns that NIH researcher Trey Sunderland (with former co-worker Karen Putnam at a congressional hearing) was paid for patient tissue samples have triggered a call for a central NIH database.

CREDIT: CHRISTINE MCCARTY

Neither this agreement nor others with Pfizer, for which Sunderland was paid more than $300,000 over several years, were reported to NIH.

At the hearing, NIH officials said the transfer and consulting agreements would not have been approved because they improperly mixed official duties with consulting. "You could have both collaboration and consulting [but not] with the same agent," said NIMH Director Thomas Insel. Insel said Sunderland instead should have organized a cooperative agreement with the company for which he would not have been paid.

Sunderland and a co-worker, Karen Putnam, invoked their constitutional right to decline to answer questions before the committee. Sunderland has said that his staff simply failed to complete the proper paperwork, and his attorney Robert Muse says that "there is no truth to the allegation that Dr. Sunderland received a penny from Pfizer for the samples." NIH investigators earlier found that Sunderland had committed serious misconduct, and Insel suggested to the U.S. Public Health Service Commissioned Corps that he be terminated. The corps has put his retirement on hold, however, and the Department of Health and Human Services Inspector General's office and the Department of Justice are still investigating.

The committee's report also questions whether Sunderland had obtained proper informed consent from some patients for the Pfizer study. NIH officials told the subcommittee that they have tightened rules on the sharing of human tissues, including adding a requirement that investigators describe future plans for samples to an Institutional Review Board (IRB). In the mid-1990s, the policy was "very general," Insel said.

Indeed, a decade ago, researchers themselves often decided the fate of leftover samples, says bioethicist Mark Rothstein of the University of Louisville in Kentucky. Since bioethics council and other U.S. and international advisory bodies have called for better controls on the use of stored human tissue (*Science*, 18 December 1998, p. 2165). Reviews of old collections have revealed that informed consent forms are often missing, leaving IRBs to decide whether samples can be used, Rothstein says: "It's been a revelation."

But NIH officials say they need more time to figure out whether a central database of tissue specimens would make sense for the intramural program. The agency is looking at combining a new campuswide database of clinical trials with sample barcoding systems, says NIH Deputy Director for Intramural Research Michael Gottesman. And although extramural researchers have also traditionally tracked their samples individually, NIH's largest institute, the National Cancer Institute, is encouraging cancer centers to tally their tumor specimens in databases so sharing will be easier.

Insel warned that moving toward a central system too quickly could add "speed bumps" to the scientific process. Legislators haven't said if they plan to require a central database.

–JOCELYN KAISER

Groupthink. Social living may have fostered the evolution of intelligence.

A new generation of experiments reveals that group-living animals have a surprising degree of intelligence

Social Animals Prove Their Smarts

A Fox observed a Crow in a tree with a piece of cheese in her mouth. Hungry for the cheese, he thought up a ruse to get it. He said, "What a noble bird I see above me! Her beauty is without equal. If only her voice is as sweet as her looks are fair …"

The Crow was greatly flattered, and to show the Fox that she could sing, she opened her mouth and gave a loud caw. Down came the cheese. The Fox, snatching it up, said, "You have a voice, madam, I see: What you want is wits."

—Retelling of a fable by Aesop

In Aesop's time, it was common to endow animals with qualities of the human mind. In addition to the flattering fox, Aesop told of a deceitful eagle that lured a turtle to its death and a compassionate lion that exchanged favors with a shepherd. But although folktales often feature scheming or generous animals, scientists have spent most of the past few centuries thinking of other species as "dumb," or at least driven by innate behaviors. Even when biologists, anthropologists, and psychologists finally began to appreciate the complexity of animal cognition in the 1950s, they tended to focus on the mental advantages that still separated humans from the rest of the animal kingdom.

Even 10 years ago, most researchers considered the intellectual chasm between humans and animals too broad for even primates to begin to bridge. A few claimed that animals have advanced cognitive skills, but early studies were chiefly anecdotal and convinced few hard-core experimental biologists, says Michael Tomasello, a developmental psychologist at the Max Planck Institute for Evolutionary Anthropology in Leipzig, Germany. "From a scientific point of view, most of the evidence [for higher cognition] was not very good," he says.

In the past decade, however, the field of animal cognition has taken off, galvanized in part by a once-obscure idea that the development of social skills drove the evolution of general intelligence (see sidebar, p. 1737). The thinking is that the need to remember and track peers sharpened social animals' ability to do other useful cognitive tasks, such as remembering where and when particular fruit trees were ripe for the picking, or learning tool use from a particularly creative peer. From this perspective, abilities such as remembering the identity of dominant individuals are crucial steppingstones to the most advanced cognitive abilities, such as learning how to interact with those dominants for personal gain—something scientists assumed only humans could do.

Of course, humans are masters of social intelligence. We judge friend from foe and head honcho from underling by the raising of an eyebrow. We scheme, deceive, and sometimes help others with no gain to ourselves. But it turns out that other animals can do these things too, at least to some degree. Researchers using rigorous tests of such abilities in animals are finding numerous examples. Crows deceive each other, as do apes; hyenas keep track of social hierarchies. There are enough parallels that now "everyone is interested in

CREDIT: K & K AMMAN/GETTY IMAGES

discovering the similarities between animals and humans," says Bennett Galef, an emeritus animal behaviorist at McMaster University in Hamilton, Canada.

Together, the new studies, particularly those of apes and birds, are providing provocative evidence that perhaps humans aren't as special as we might like to think, says Brian Hare, a biological anthropologist also at the Max Planck Institute for Evolutionary Anthropology. What was once considered a sharp line separating humans from all other animals is becoming a blurry gray area, with various animals possessing certain parts of the set of skills that we consider advanced cognition.

In large part, that's because we're not the only species that has evolved to cope with the demands of living in groups, says Nicola Clayton, who studies animal cognition at the University of Cambridge, U.K. People in villages, chimps in troops, ravens in flocks, and hyenas in packs all need to be able to size each other up and modify their behaviors as needed.

Not all researchers are impressed with animals' newly demonstrated social ingenuity, and there is disagreement about its implications. All the same, says Marc Hauser of Harvard University, for cognitive scientists the research questions have changed, from what sets humans apart, to what animals reveal about the building blocks of higher cognition.

Tool savvy. An eager student learns how to retrieve a treat from outside its cage (*left*), while another ape takes a "grape-retrieval" tool to save for later use (*right*).

Understanding understanding

Throughout history, researchers have swayed back and forth on the question of animal intelligence. In the 1600s, nonhuman animals were considered little more than breathing machines. But after Darwin implied that differences between humans and other species were a matter of degree, dozens of examples of "smart" animals came to light, only to be subsequently debunked. During the 19th and early 20th centuries, the prevailing idea became that most animals, primates included, didn't reason but instead had sets of rules that dictated their behavior. And animal-cognition researchers avoided inferring states of mind from an animal's behavior. They took their cues from 19th century psychologist C. Lloyd Morgan, who argued that complex behaviors don't necessarily require complex thought, and that researchers should look for simple, mechanistic explanations for even the most complex animal behaviors.

But starting in the late 1970s, some researchers went against the grain. In 1976, psychologist Nicholas Humphrey of the London School of Economics stirred the pot by suggesting that getting along with others required more brainpower than other aspects of daily life, and that social animals might have humanlike smarts. "It was very much at odds with what everyone was thinking at the time," Humphrey recalls.

Two years later, psychologists David Premack and Guy Woodruff of the University of Pennsylvania proposed that chimpanzees might be able to think about what they are doing and to understand what others are thinking, an ability they called a "theory of mind." Even as children, humans can read each other's minds at least to some degree. Maybe chimps could as well, if we could only find a way to communicate with the apes, Premack and Woodruff proposed. And in the late 1980s, Andrew Whiten, an evolutionary psychologist at the University of St. Andrews in Fife, U.K., and his colleagues suggested that the relatively big brains of humans and other primates evolved not to see, smell, or fight better but to recognize and deal with social dilemmas.

Telling tales. Aesop's talking animals may not be true to life, but he might have been right about their intelligence.

But "it took a while for people to start thinking about these ideas," says Clayton. Today, psychologists recognize "theory of mind" as a critical cognitive skill, underlying teaching, deception, and perhaps even language (*Science*, 16 May 2003, p. 1079). It's also seen as a steppingstone to consciousness, or thinking about one's own thoughts—often considered the ultimate in higher cognition (*Science*, 25 June 1999, p. 2073).

Yet scientists disagree on exactly what theory of mind is, and the literature is filled with conflicting reports about its existence in animals. As recently as 6 years ago, Hauser argued that chimps didn't have even the basics of a theory of mind. Today, "the field has been completely turned upside down," says Hauser. "The provocative question is not do they have a theory of mind; it is thinking about the components that are going into theory of mind."

Reading the primate brain

Corporate meetings, playground games, and bargain shopping all require complex negotiation skills and a keen sense of who one's allies are. It makes sense that apes, our closest kin, should be political as well, but it has taken decades for scientists to come to grips with the idea that apes have street smarts akin to ours. Beginning in the 1960s, field researchers such as Jane Goodall were reporting sophisticated politics among

CREDITS: (TOP, LEFT TO RIGHT) ANDREW WHITEN; JOSEP CALL/MAX PLANCK; (BOTTOM) TIME LIFE PICTURES/GETTY IMAGES

Hide, no seek. Ravens (*inset*) turn away from each other to keep secret the location of their buried food.

chimps, for example, but controlled experimental evidence was rare.

Apes rarely did well on self-awareness, memory, gaze-following, gesture, spatial learning, and other tests at which even young children excel. For example, children will follow another person's gaze, showing that they are aware that the tester is in fact looking at something. But chimps confronted with humans with or without blindfolds on their heads didn't discriminate among who could see—and therefore deliver a reward—and who couldn't.

Then 6 years ago, Hare and his colleagues showed that under the right circumstances, chimps could pass some of these tests with flying colors. The secret was that chimps are exquisitely tuned in to their competition, particularly when food is involved, and will do everything they can to get a treat.

In one experiment published in 2001, Hare, Tomasello, and their colleagues paired a dominant chimp with a subordinate and manipulated the two apes' view and access to food. If both could see the food, the subordinate deferred. But if the dominant chimp couldn't see the treat, the subordinate quickly snapped it up.

The experiment, coupled with a related but simpler one published a year earlier, was revolutionary. "There was a big change in perspective," says Clayton, and a flurry of more ecologically appropriate experiments—geared to what motivates chimps in the wild—followed. For example, in a new study in *Cognition*, Hare and his colleagues designed another competition over food. They had chimps go head-to-head against a human who pulled food out of reach as a chimp went to grab it. If the chimps were given the option, they sneaked up behind a barrier to get to the food instead of approaching it directly. Thus, the chimps demonstrated not only that they knew what the human could see but also that they knew how to manipulate the situation to stay out of sight. Other studies have shown that chimps can recognize when a human is imitating them.

They can also sense the motives of others. A study a few months ago showed that chimps kept track of partners who best collaborated in retrieving inaccessible food and chose that same partner again in the next trial (*Science*, 3 March 2006, p. 1297). New experimental designs are helping to demonstrate chimp smarts outside the social realm, too: Studies show that they can reason about the movement of things they cannot directly see and plan for the future by taking account of past experiences.

Meal planning. Western scrub-jays remember where and when they buried wax worms in ice cube trays.

In parallel, other researchers are demonstrating that social primates are smart enough to help their cause through teaching and learning. Chimps apparently learn tool use from one another, and communities in different regions of Africa develop what some researchers consider cultural differences in tool use. The idea is still controversial, but field and, more recently, lab work are strengthening the case.

Last year, Whiten and his colleagues demonstrated "social learning" of traditions in two groups of captive chimpanzees. The researchers trained one female from each group either to pull or to lift a stick tool to retrieve a reward. After watching the female for just 20 minutes a day, each group learned its respective technique within a week. Not only were the chimps able to copy the lifting or the pulling, but lifters also almost never tried to pull or vice versa, suggesting a strong tendency to conform to the local norms, Whiten suggests.

Taken together, this work shows striking parallels with human abilities, says Hare. But do chimps have a theory of mind? They lack the most advanced skill identified by Woodruff and Premack: the ability to realize that another individual is thinking something wrong, or that it has a false belief, points out cognitive scientist Daniel Povinelli of the University of Louisiana in Lafayette. In his view, to have a theory of mind, a species must pass the false-belief test. And so far, chimps fail it. "People who [keep] insisting that 'It's got to be there, at least a little bit,' in dogs, cats, chimpanzees, my cousin Ned's horse are really missing the point," Povinelli says.

But Hare argues that theory of mind is "a whole suite of abilities." The new results indicating that chimps can judge what others are thinking, manipulate others through deception, and so on "are shooting down the all-or-none hypothesis about theory of mind," he says.

He adds that the false-belief test is so challenging that it foils children up to about age 4. In one test, for example, a child and a companion watch a tester put candy in a box. When the companion leaves, the candy is moved into a bucket. Because the child doesn't yet have a sense of false belief, she thinks the companion will know to look in the bucket, whereas an adult realizes that the companion still thinks the candy is in the box.

Hare argues that experimenters simply haven't found a good way to figure out where a chimp expects the companion to look for the

CREDITS (TOP TO BOTTOM): THOMAS BUGNYAR; PHOTO COURTESY OF NICOLA CLAYTON

Man's Best Friend(s) Reveal the Possible Roots of Social Intelligence

When a chimp sneaks a banana behind another chimp's back, it's showing social intelligence. So is the crow that buries worms behind a bush to prevent bystanders from spotting the location of its stash. Recent controlled experiments show that some social animals have evolved the flexibility and intelligence to deceive and benefit from others and even predict what their peers may do (see main text).

But why did these and related abilities evolve? In the 1970s, Nicholas Humphrey, now of the London School of Economics, proposed that natural selection favored the ability to distinguish anger from acceptance and to respond to changes in the moods of one's companions. Individuals with these kinds of social skills had advantages in gleaning food and mates—and avoiding violence, he suggested. But such evolutionary scenarios are hard to test. Now Brian Hare and Michael Tomasello of the Max Planck Institute for Evolutionary Anthropology in Leipzig, Germany, and their colleagues are gleaning some clues from studies of domestic dogs and their wild cousins, wolves and foxes.

Even as puppies, canines are adept at taking cues from their owners—more adept than chimps, who are rarely able to follow a human's eyes or hands to hidden food. That indicates a genetic component to this skill. For decades, anthropologists have hypothesized that this behavior began when dogs and humans were able to tolerate each others' company without aggression. Togetherness fostered dogs' social skills, helping ensure their access to food and other resources without having to resort to violence. Dogs better at reading human minds were favored by selection, leading to a cycle of interaction and cooperation.

That hypothesis is backed up by Hare's studies of foxes bred for the past 45 years to be comfortable with humans. These foxes understand human gestures—for example, when a human points to food—but untamed foxes don't, even after extensive efforts to train them, Hare and his colleagues reported in 2005. Studies done in 2002 and 2003 reveal "the exact same difference between dogs and wolves," says Hare. Selecting foxes for "togetherness" with humans also facilitated the evolution of the ability to understand their two-legged caretakers.

A similar cycle of tolerance leading to increased communication may have spurred the evolution of social intelligence within a species, says Hare. As social tolerance increased, group members could get close enough to an innovative, tool-using peer to imitate the behavior. Selection could also favor even more congenial relationships, say for cooperative food gathering or childcare, to the benefit of all involved.

Fellowship. Foxes bred to be tame are keenly tuned in to human behavior.

And the limits of social tolerance may partly explain differences in intelligence among species, says Tomasello. For example, chimps have competitive strategies down cold and can be quite sneaky. But they don't cooperate very effectively, at least not intentionally; they would have come to a bad end in Aesop's fable about the lion and the shepherd who traded favors. In contrast, although humans too are competitive, we also possess the capacity for more empathetic social skills. "We lie, but we can also cooperate and coordinate planning," says Tomasello. "It's not that humans have greater individual brainpower, it's that they have the ability to pool their cognitive resources and benefit from what others have learned."

This evolutionary scenario sounds reasonable, but it will be difficult to prove. Hare plans to compare higher cognition between bonobos and chimps, which exhibit different levels of social tolerance, to see whether the connection between sociability and cognition holds up. Bonobos are quite tolerant; when they meet strangers, they have sex, whereas chimps often wage war, he points out.

Even before these studies are done, other researchers are taking notice—although they have yet to be convinced. "Evolutionary modification of fearfulness and aggressive tendencies might be a critical precursor to the evolution of social intelligence," says ethologist Kay Holekamp of Michigan State University in East Lansing. "But I would certainly be surprised if that were all there were to [it]." **–E.P.**

treat, and that therefore we don't know yet whether chimps pass or fail this test. "We have not been able to come up with a convincing experiment with nonhumans," he says.

Picking bird brains

So far there's no evidence—and no good tests—of understanding false belief in birds. But contra the opinion of the fox in Aesop's tale, Clayton and her colleagues have found that crows and their relatives, including ravens and scrub-jays, have social intelligence on par with primates, apparently deceiving others in order to win more food. In Clayton's studies, she takes advantage of the natural tendency of many birds to stash surplus food in anticipation of lean times, and for other birds to steal those caches.

She and her husband Nathan Emery have recreated this behavior in her lab at the University of Cambridge, providing captive birds with sand-filled trays in which to bury wax worms. Sometimes the duo switches the food after it's been hidden; in other cases, they allow another bird to witness the burial. "They are putting birds in different situations and showing that the birds do all sorts of flexible things," says Hare.

Using this approach, Clayton and her Cambridge colleague Anthony Dickinson have shown that western scrub-jays remember what they have buried, and when and where they buried it, a phenomenon called mental time travel. They retrieve perishable food before it rots, for example, while waiting longer to retrieve nonperishable items. Many animals can remember where food has been placed, but rarely have researchers demonstrated that an animal can keep track of when an event occurred and use past events to figure out what to do in the future. This ability was demonstrated in bonobos and orangutans only recently, in an experiment published online in *Science* last month (16 June, p. 1662). The study showed that these primates could select the proper tool for a task even though they wouldn't need it until the next day. And in this week's issue of *Current Biology*, other researchers demonstrated that mangabeys, a primate found in Uganda, will take note of unripe fruit and come back to pick it after a few sunny days.

CREDIT: IRENE PLYUSNIA, PHOTO COURTESY OF BRIAN HARE

For birds, anticipating the future enables them to realize when they must take evasive action to protect stashed food. Working with Joanna Dally, then a graduate student, and Emery, Clayton showed in another experiment that western scrub-jays that see a potential thief will hide food far away from the other bird and sometimes move their supplies several times. In other cases, they wait to stash food until the onlooker is distracted. The jays take none of these precautions if no other birds are in sight. "There's flexibility at multiple levels," says Clayton.

Furthermore, birds who have been thieves themselves are more likely to take these evasive actions than birds who have not been so nefarious. The jays' behavior implies that they are aware of the onlooker's intentions and are using their past experience to predict the future actions of the potential thief, says Clayton.

In addition, like apes, the jays track the social status of their competitors and change their behavior accordingly. In the lab, scrub-jays try hard to hide food from dominants but not from breeding partners, whose pilfering is tolerated, Clayton's group reported. All this hints that jays do have elements of a theory of mind, says Clayton.

Lab work on ravens supports this idea. In most cases, a raven poised to grab another raven's stashed food doesn't hesitate to act when bystanders might beat them to it, Thomas Bugnyar and Bernd Heinrich of the University of Vermont in Burlington reported in 2005. But if the stash belongs to a dominant member of the flock, the thief will briefly search elsewhere, as if to allay suspicion. Such actions seem intentional and suggest that the thieves understand what other birds are seeing, says Bugnyar. "There's no question that birds are more intelligent than anyone thought they would be," Tomasello says.

But researchers still don't agree on how to interpret these results. Cognitive ethologist Marc Beckoff of the University of Colorado, Boulder, sees little difference in social prowess between humans and other species, and he suggests that animals should be treated more like humans.

Other researchers still draw a line separating the minds of humans and animals, even other social species. The new experiments highlight how "various species have remarkable cognitive skills for the problems they must solve," but they stop short of showing a theory of mind or other advanced cognitive skills, says Povinelli. Humans, by virtue of having language, have a fundamentally novel cognitive system, he points out. Tomasello agrees, noting that humans excel at many skills: They are better teachers, for example.

Furthermore, what looks like humanlike cognition may not be. Dogs, for example, seem to know what their owners are thinking. But "they are not reading people's minds but our behavior," cautions Clive Wynne, a psychologist at the University of Florida, Gainesville. For example, those ravens avoiding the wrath of dominant birds could be picking up on subtle behavioral cues that humans can't read, he says.

To resolve whether external cues or internal decision-making underlie seemingly intelligent behavior, researchers need to expand their studies to include more species, Wynne says. "We're only studying a tiny, tiny fraction of animals," he says. "We really don't know what's out there."

Those studies are beginning, and by looking across the animal kingdom, researchers are gleaning the conditions that predispose a species toward social intelligence. For example, Kay Holekamp, an ethologist at Michigan State University in East Lansing, has observed hyenas for 18 years and concludes that these scavengers can recognize not just their own status relative to the pack leader but also the status relationships of other pack members. Other researchers are trying to measure social intelligence, albeit often in indirect ways, in ungulates, elephants, and dolphins. And in this week's issue of *Current Biology*, researchers demonstrated that fringe-lipped bats learn to listen for unfamiliar prey from fellow bats.

All these studies suffer from the same limitation, however. Researchers still can't read the minds of their subjects, warns behavioral ecologist Anne Engh of the University of Pennsylvania: "Until we can come up with creative methods of testing, we won't know whether complex behaviors are the result of animals actually knowing what they are doing or whether they are able to do complex things using cognitive short cuts."

Galef is particularly skeptical of researchers who have concluded that chimps respond to peer pressure, that wolves and capuchin monkeys have a sense of fairness, or that jackdaws are the avian equivalent of the Good Samaritan. "It's gotten a little out of hand," he complains. And not one species has yet passed the false-belief test, he points out.

But does that matter? "It's not clear to me that you need [a complete] theory of mind to be very skilled socially," says Hare. And for much of the animal kingdom, those skills are good enough. Just ask Aesop.

–ELIZABETH PENNISI

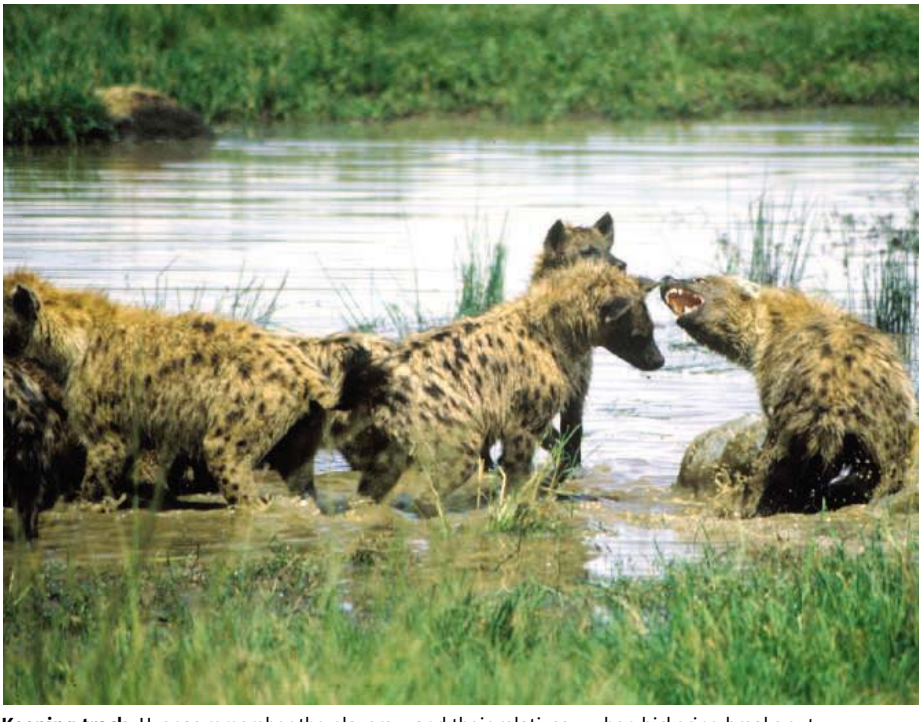

Keeping track. Hyenas remember the players—and their relatives—when bickering breaks out.

CREDIT: LAURA SMALE

Additional Reading

- J. Dally *et al*., "Food-caching western scrub-jays keep track of who was watching when." *Science* **312**, 1662 (2006).
- B. Hare *et al*., "Chimpanzees deceive a human competitor by hiding." *Cognition* online, 17 January 2006. (doi:10.1016/j.cognition. 2005.01.011)
- B. Hare and M. Tomasello, "Human-like social skills in dogs?" *TRENDS in Cognitive Sciences* **9**, 439 (2005).
- N. Emery and N. Clayton, "The Mentality of Crows: Convergent Evolution of Intelligence in Corvids and Apes." *Science* **306**, 1903 (2004).

Line of descent. Lucy's discoverer Donald Johanson and Maurice Taieb (*left and center*) meet the cast of Toumaï, discovered by Michel Brunet (*right*).

CREDIT: FRÉDÉRIC PAUVAREL

PALEOANTHROPOLOGY

A Rare Meeting of the Minds

At a historic meeting in France, rival paleoanthropologists gathered to review their field's progress and sketch its future

AIX-EN-PROVENCE, FRANCE—For an elite group of fossil hunters of a certain generation, life can be split into two time periods: B.L. and A.L., or Before Lucy and After Lucy. The "Lucy" in question, of course, is the petite, 3.2-million-year-old skeleton discovered in Ethiopia in 1974, which revolutionized our view of human origins. Famous fossil hunters, who rarely meet together, gathered here for 3 days last week to celebrate the 32nd anniversary of Lucy's discovery; they also came to pay tribute to French geologist Maurice Taieb, the man who found where Lucy and other famed hominids lived and died (see sidebar, p. 1740).

The 30-plus scientists at the invitation-only conference* are members of one of the world's most exclusive clubs by dint of having discovered crucial hominid fossils. But they aren't exactly chummy: Several have not spoken to each other or been in the same room in more than a decade. So it's no surprise that they fought bitterly over questions of fossil interpretation and access. But their battles also provide a road map to where the field is headed: Was Lucy really our direct ancestor? Who came before her? When and where was our lineage born, and what sets it apart from other apes?

When a young American named Donald Johanson found the famed partial skeleton, researchers thought that Lucy's species, *Australopithecus afarensis*, was the earliest member of the human family, and that upright walking had evolved in the open savanna 3 million to 4 million years ago. But researchers have now glimpsed hominids nearly twice as old. And animal fossils, pollen, and geological clues at Hadar, Ethiopia, have revealed that Lucy's species walked in a grassy woodland with deciduous trees, reported Taieb, now of the Centre Européen de Recherche et d' Enseignement des Géosciences de l'Environnment (CEREGE).

Johanson, now a paleoanthropologist at Arizona State University in Tempe and a prominent popularizer of science, reported that the portals into past environments had shown that Lucy's species, found across Africa, was also remarkably adaptable. At last count, researchers had found 370 fossils of *A. afarensis* at Hadar alone, including males and females, infants, and adults who were alive 3 million to 3.4 million years ago. As the habitat became drier and more open, the species adapted. Their bodies and jaws grew, probably as they ate less fruit and more tuberous roots. The once-radical idea that these fossils were all members of one species that gave rise to our genus, *Homo*—and eventually led to modern humans—is now accepted by many researchers, said Johanson.

But despite the wealth of data on Lucy's species, old differences of opinion linger. Courtly paleoanthropologist Yves Coppens of the Collège de France in Paris—who co-discovered Lucy's species—politely demurred with Johanson's view at the meeting. Coppens maintains that two species of hominids lived at Hadar—and that neither led to modern humans.

That old feud has now burned down to embers, in part because emphasis has shifted to newly discovered fossils that spark heated debate. On the meeting's second day, talk turned to these more ancient and fragmentary specimens, most discovered in the past decade, that are vying for status as our earliest ancestor. First up was paleontologist Michel Brunet of the University of Poitiers, who brandished a jawbone of the oldest putative hominid, *Sahelanthropus tchadensis*, discovered in the Djurab Desert of Chad and dated to as early as 7 million years ago.

Brunet, who radiates both charm and an edgy humor, reviewed the traits that tie this stunning skull, nicknamed Toumaï, to human ancestors. The fossil is 95% complete, and Brunet says that the angle at which it sat atop the spine suggests it walked upright—a defining trait of humans and their ancestors but not apes. "Toumaï is not a chimpanzee. It is not a gorilla," Brunet pronounced. That was a dig at two colleagues in the room, geologist Martin Pickford of the Collège de France and paleontologist Brigitte Senut of France's National Museum of Natural History, who have proposed Toumaï as an ancestor of apes rather than people. They repeat this view this week in the online journal *PaleoAnthropology*.

Soon it was time for Senut, one of the few women who co-leads a team. (The other leading woman, Meave Leakey, was invited but did not attend.) Senut showed new fossils of teeth and a thumb of a 6-million-year-old hominid called *Orrorin tugenensis* that she and Pickford discovered in the Tugen Hills in Kenya. *Orrorin*'s teeth are primitive, but the shape of the thumb suggests that it was opposable and more modern than the thumb of Lucy's species, Senut said. That trait adds to their claim, based on a partial thighbone, that *Orrorin* walked in a more human way than Lucy did.

If *Orrorin* was more modern than Lucy, it must have given rise to the *Homo* lineage that led to modern humans, Senut and Pickford say. That would bump most of the fossils found by the other teams in the room, including Lucy, off the line leading to *Homo*.

Robert Eckhardt of Pennsylvania State University in State College then attempted to support *Orrorin*'s claim to fully human walking by resurrecting controversial computed tomography (CT) scans of the interior of its thighbone (*Science*, 24 September 2004, p. 1885). Such scans, x-rays, and photographs can show the internal pattern of bone distribution, which can reveal whether an animal walked upright. But Tim White of the University of California, Berkeley, and his

* "Lucy, 30 years later," 12–14 June, Aix-en-Provence, France.

Paleoanthropology's Unsung Hero

In 1871, Charles Darwin speculated in the *Descent of Man* that humans had evolved in Africa. And he predicted that it would likely be geologists who found the missing fossil trail that led to where our lineage arose.

Almost 100 years later, the man who has best fulfilled Darwin's prophecy is indeed a geologist: Maurice Taieb, 71, of the French research lab CEREGE in Aix-en-Provence. Taieb has the rare distinction of discovering two of the most important sites in human evolution, both in Ethiopia. Although geological groundwork is critical for hominid paleontology, it is less glamorous than finding fossil bones, and so Taieb is far less famous than some of his fossil-hunting colleagues.

But for him, fieldwork has been its own reward. Born and reared in Tunisia, he calls the desert "magic." As a graduate student back in the 1960s, he set out to explore the scorched earth of the Afar Depression, seeking signs of ancient lakes. He traveled only with an Afar guide, often on foot or with a donkey, and slept under little more than a mosquito net.

One day in 1969, Taieb had driven well beyond the end of the road, as was his habit, across a gravel-strewn plateau in the Awash valley, and come to an abrupt stop at the edge. When he stood on the rim overlooking the valley of Hadar, he was stunned by the layers of ancient sediments laid down over millions of years. After hiking down into the valley—alone, because his guide feared trouble from local tribes—he was overwhelmed by the fossils he found. Elephant bones and tusks were sticking out of the sandstone, and rhino and hippo bones were strewn on the surface. Taieb took photos, collected a few bones, and returned to Paris. There, he invited paleoanthropologist Yves Coppens to work with him; the pair was later joined by a young American named Donald Johanson and others.

In 1974, Johanson discovered the famous hominid skeleton called Lucy, transforming our view of human origins and establishing a new standard for international research in human origins. "Lucy was a turning point," says paleoanthropologist Tim White of the University of California, Berkeley, who helped analyze her bones. "Lucy had a fundamental role in changing the structure of paleoanthropology in east Africa."

Taieb also was the first to discover the site of Aramis, in the Middle Awash, which turned out to be the resting place of the 4.4-million-year-old hominid *Ardipithecus ramidus.* White thinks *Ardipithecus* may be a distant ancestor of Lucy—and our own lineage. Taieb never worked at Aramis, but he generously told White about it, paving the way for more than a decade of fruitful fieldwork in what White has dubbed the Grand Canyon of human origins.

Last week, at a rare face-to-face meeting of hominid discoverers organized by Taieb (see main text), two generations of researchers praised him. "Paleoanthropology is a field fraught with intense fighting and intense competition," says Johanson. "Maurice is a man who, rather than usurping areas for his own aggrandizement, offered others opportunities." **–A.G.**

colleagues, who discovered a younger hominid, *Ardipithecus*, that they say is bipedal and may have led to Lucy, contend that the scans are of low quality and unreliable. For several years, White has repeatedly asked Pickford and Senut to provide a simple photograph of the interior of the thighbone at a point where it was broken and glued.

After seeing the 4-year-old scans yet again on-screen, White, who is known for his acerbic wit and has co-authored a state-of-the-art paper on how to use the CT method, blasted Eckhardt and called details of his talk a "diversionary tactic." Eckhardt said he would like new CT scans but lacked permission and funding. (Ironically, their exchange took place against the backdrop of one of Eckhardt's slides that proposed: "Beginning of real cooperation on the structure of thought about hominid origins.")

Pickford then made the startling revelation that he did not control access to fossils his team has found. He offered to provide access if he could. "Anyone is free to see the specimens. You need to contact Eustace Gitonga," he said. Gitonga is director of the Community Museums of Kenya, which has custody of the *Orrorin* specimens, and issues permits to Pickford and Senut to search for fossils.

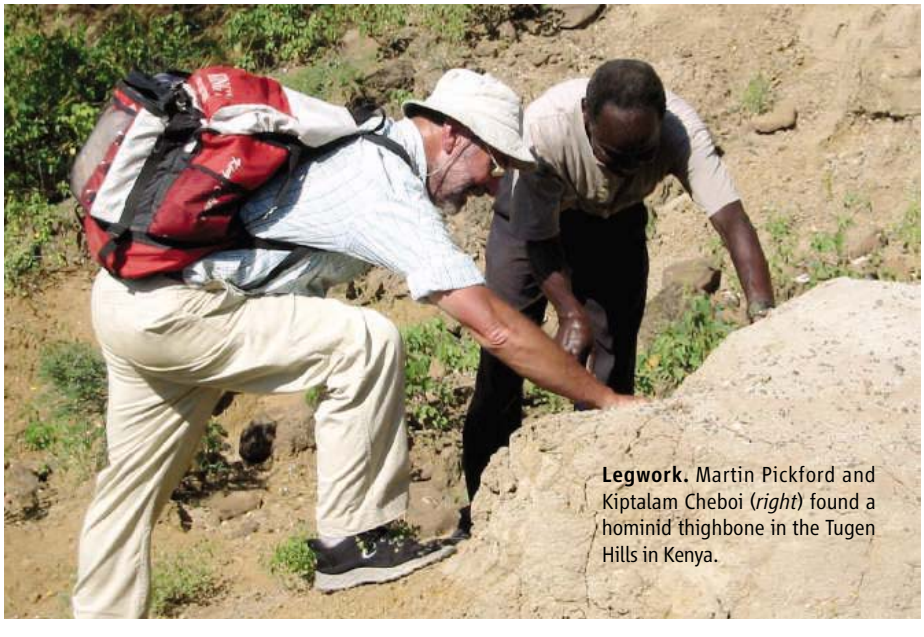

Legwork. Martin Pickford and Kiptalam Cheboi (*right*) found a hominid thighbone in the Tugen Hills in Kenya.

CREDIT: A. GIBBONS

Brunet piped up that "it's not so difficult … to take a picture. I'm just asking why [no picture]?" Johanson, who was moderator, then ended the session, muttering that "everyone makes mistakes."

The next day, Johanson applied a little spin control. "Every person here has a slightly different idea how to draw the [human family] tree," he told a group of French science teachers invited to the last session. "But you should not let this distract you that there is probably more consensus about human origins today than ever before." For example, although researchers argue over which early fossil was even a hominid, much less the first, each of the competing teams has independently concluded that their primate lived in the forest, not the savanna. White's colleague Doris Barboni of CEREGE reported, for example, that the 4.4-million-year-old *Ardipithecus ramidus* lived in a tropical woodland with palm trees.

Another positive trend was the easy camaraderie of the younger researchers, both during sessions and at breaks. At least a half-dozen were scientists from Ethiopia and Chad reporting on their impressive array of newly discovered hominid fossils. There were no Africans with Ph.D.s in human evolution research 30 years ago, noted the Tunisian-born Taieb. Now, he said, "there is a new generation."

–ANN GIBBONS

EDITED BY YUDHIJIT BHATTACHARJEE

Movers

CONSERVING FORESTS. The Center for International Forestry Research (CIFOR) in Indonesia has chosen policy research manager Frances Seymour to advance its efforts to conserve forests and help local communities use forest resources wisely. Seymour, now at the World Resources Institute in Washington, D.C., will move this fall to the center's headquarters in Bogor Barat to succeed director general David Kaimowitz, who is joining the Ford Foundation.

"It's at that sweet spot between academic research and pure advocacy," Seymour, 47, says about her new job at the center, whose $17-million-a-year budget comes mainly from national governments and the World Bank. "We make the case for the contribution of forests to the development agenda and poverty reduction."

At CIFOR, Seymour hopes to manage forests in a way that "meets the needs of the poor" by working with communities and agencies on a local and national level. That may include developing technologies for forest management and improving governments' capacity for research. "I think the real challenge is to get the message out to those who don't think of themselves as caring about forests," she says.

MOVERS

BACK IN BUSINESS. British biochemist Michael Morgan, who once managed the genomics portfolio of the United Kingdom's biggest private sponsor of biomedical research, has been hired to set Canada's primary genome research program on a new course. Genome Canada is abandoning open competitions in favor of directed grantsmaking in thematic areas proposed by scientists, and Morgan hopes to inspire researchers to "think outside the box" and come up with bold proposals.

Morgan, 63, retired in 2002 as chief executive officer of the Wellcome Trust Genome Campus in Hinxton, U.K., to become an international consultant but is eager "to get back into the scientific harness" as chief scientific officer for an organization that has spent $560 million since it was created in 2000.

He "is a fantastic catch," says Thomas Hudson, a genomicist at McGill University in Montreal, Canada. "With Genome Canada shifting to a problem-based approach, you need a consensus builder [like him]."

ON CAMPUS

STORM'S OVER. The embattled dean of Oregon State University's College of Forestry, Hal Salwasser, has won a campus vote of confidence in his attempts to heal the bitterly divided college.

Long-simmering tensions within the college blew up in January when a group of faculty members tried to delay the publication of a high-profile paper about ecological damage from postfire logging (*Science*, 10 February, p. 761). Salwasser was criticized for not supporting the graduate students who were among the authors and for appearing to side with the logging industry.

In last week's nonbinding online vote—by faculty, students, and staff—66% said they have confidence in Salwasser's ability to lead. And 63% favored his ideas for change. Salwasser plans to appoint two additional faculty members to the college's leadership committee and keep asking for input. "I'm taking advantage of lessons learned," he says.

AWARDS

BENCH TO BEDSIDE. Although translational medicine is a buzzword in biomedical research these days, it's still rare for scientists to shepherd their discoveries from the lab to the clinic. Cancer biologist Napoleone Ferrara of Genentech in San Francisco, California, did just that with vascular endothelial growth factor (VEGF) and reaped a rich reward for it last week: the $250,000 General Motors Cancer Research Prize.

Ferrara began the research at Genentech in 1988, taking advantage of a company policy that allows scientists to pursue their own projects on company time. After discovering that VEGF guides new blood-vessel growth, Ferrara developed an antibody that targeted VEGF and injected it into mice with cancer. Their tumors melted away. The work led to the development of the drug Avastin, which was approved by the U.S. in 2004 to treat advanced colorectal cancer. Last year, Genentech reaped revenues of more than $1 billion for Avastin.

"Even at the very beginning, [VEGF looked] very unique," says Ferrara. He's still puzzling over why some patients are resistant to the drug. Meanwhile, the find has spawned another anti-VEGF drug for macular degeneration.

Got a tip for this page? E-mail people@aaas.org

They Said It . . .

"I didn't fancy the thought of being handed over to the Inquisition like Galileo."

—Cosmologist Stephen Hawking, joking about a comment made by the late Pope John Paul II at a cosmology conference some years ago that scientists should not study the beginning of the universe because it was God's work. Hawking recounted the pope's remarks during a lecture at the Hong Kong University of Science and Technology last week.

CREDITS (TOP TO BOTTOM): WORLD RESOURCES INSTITUTE; OREGON STATE UNIVERSITY; GENENTECH; EMPICS

Check out what's hot in your field

Scopus helps you find who's publishing leading research. Spot research trends across the articles you choose with the Scopus Citation Tracker. Get an easy overview of an author's papers, citations and co-authors with the Scopus Author Identifier. Stay up-to-date with highly cited articles using Scopus alerts. It's a fast and easy way to accelerate your research.

Scopus is the largest abstract and citation database of research literature and quality web sources.

Try it! You will like what you find.

Visit www.scopus.com

SCOPUS™
Find out.

Earthquakes in modernizing Japan 1749

Gene expression and repair 1752

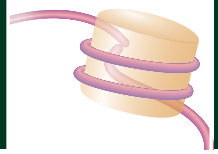

Tracking phosphorus 1758

LETTERS | BOOKS | POLICY FORUM | EDUCATION FORUM | PERSPECTIVES

LETTERS

edited by Etta Kavanagh

Looking at Biofuels and Bioenergy

THE EDITORIAL "GETTING SERIOUS ABOUT BIOFUELS" (S. E. KOONIN, 27 JAN., P. 435) EMPHASIZES three important societal concerns that are addressed by a conversion to bioenergy: security of supply, lower greenhouse gas emissions, and support for agriculture.

We believe that bioenergy production and policies need to be based on a broad cost-and-benefit analysis at multiple scales and for the entire production chain. This is particularly true for bioenergy's impact on agriculture. One of the major problems in modern, intensive agriculture is the lost link between livestock and land (*1*). This separation between different agricultural production systems, environmental problems, and the consumers is largely unaccounted for in the development of economies and agricultural practices. Mitigation actions are needed to ensure global sustainability. It is possible that growth in bioenergy production (*2*) will add to these problems, reducing the overall benefits of conversion. A recent study on organic farming and bioenergy production (*3*) looked for solutions to such problems. Organic food production integrated with short rotation coppice and biogas utilization suggested a number of win-win solutions, for example, lower energy use per unit produced, water quality protection, recycling of nutrients, reduced nitrous oxide emissions, and increased soil carbon storage. Ecologically sound bioenergy production should aim for closed cycles of mass and optimization of net energy yields and efficiencies.

TOMMY DALGAARD,[1] UFFE JØRGENSEN,[1] JØRGEN E. OLESEN,[1] ERIK STEEN JENSEN,[2] ERIK STEEN KRISTENSEN[3]

[1]Department of Agroecology, Danish Institute of Agricultural Sciences, DK-8830 Tjele, Denmark. [2]Risø National Laboratory, DK-4000 Roskilde, Denmark. [3]Danish Research Centre for Organic Farming, DK-8830 Tjele, Denmark.

References

1. R. Naylor *et al.*, *Science* **310**, 1621 (2006).
2. A. J. Ragauskas *et al.*, *Science* **311**, 484 (2006).
3. U. Jørgensen *et al.*, *Biomass Bioenergy* **28**, 237 (2005).

YOUR RECENT ARTICLES ON BIOFUEL ("GETTING serious about biofuels," S. E. Koonin, Editorial, 27 Jan., p. 435; "The path forward for biofuels and biomaterials," A. J. Ragauskas *et al.*, Reviews, 27 Jan., p. 484; "Ethanol can contribute to energy and environmental goals," A. E. Farrell *et al.*, Reports, 27 Jan., p. 506) are arousing unreasonable expectations for its potential contribution to energy and environmental goals. Although biofuel's contribution can be positive, it will remain small, being restricted by the ability of the natural environment to provide both fuel and food for a large and energy-demanding world population.

It requires production equivalent to 0.5 ton of grain to feed one person for one year, a value sufficiently large to allow some production to be used as seed for the next crop, some to be fed to animals, and some land to be diverted to fruit and vegetable crops. Compare this value with that for a car running 20,000 km/year at an efficient consumption of 7 liters/100 km. The required 1400 liters of ethanol would be produced from 3.5 ton grain (2.48 kg grain/liter), requiring an agricultural production seven times the dietary requirement for one person.

Agriculture now provides, with some shortfalls, food for 6 billion people and will need to feed 9 billion by 2050, while conserving natural resources. From an agronomic perspective, increasing food production to this level during the next 50 years is an enormous challenge.

The above calculations demonstrate that major reliance on biofuel, even for private motoring alone, would place an additional demand on agricultural production greater than would providing an adequate diet for 9 billion people by 2050. Positive energy gain and reduced greenhouse gas emissions are not sufficient to establish biofuel as an economic and ecologically friendly solution to current problems of energy supply and ecological sustainability. Anything but a marginal contribution from biofuel would pose a serious threat to both food security and the natural resource base of land, soils, and water.

DAVID CONNOR[1] AND INÉS MÍNGUEZ[2]

[1]Department of Agriculture and Food Systems, University of Melbourne, Victoria 3010, Australia. E-mail: djconnor@unimelb.edu.au. [2]ETSI Agrónomos, Universidad Politécnica de Madrid, Madrid 28040, Spain. E-mail: ines.minguez@upm.es

Poplar

I READ WITH INTEREST S. E. KOONIN'S EDITORIAL "Getting serious about biofuels" (27 Jan., p. 435) and applaud his support of alternative fuels. Unfortunately, his optimistic analysis provides the same shortsighted view of biomass production and resource sustainability that is driving the misdirected efforts of the ethanol industry today. Koonin's analysis does not address the environmental costs (specifically land degradation) of producing biofuels. He optimistically suggests that "with plausible technology developments, biofuels could supply some 30% of global demand in an environmentally responsible manner without affecting food production." Although encouraging, this type of logic includes flawed assumptions: (i) that biofuels will be produced "responsibly"; (ii) that food crop production and consumption will be sustained at current levels on existing footprints; and (iii) that the use of soil

CREDIT: MANFRED MIELKE/FORESTRY IMAGES

resources for production of transportation biofuels is ethical. As an illustration, the corn grain ethanol (the primary biofuel produced in the United States) that is produced on 3.5 million hectares of prime cropland (~12% of U.S. corn acreage on soils that are uniquely productive) yields less than 2% of our current fuel consumption. Year-round corn crops, encouraged by biofuel production, cause long-term soil degradation. This type of degradation cannot be repaired by fertilization, nor can fertilizer be used as "soil energy currency" in accounting for biofuel production costs. The real cost of this form of land use will not be realized by this or even the next generation, but will be borne by future generations who have no say in the energy policy of today. Biomass certainly has a place in our country's fuel mix, but in a nation that averages a paltry fuel economy of 20.8 miles/gallon, the production of relatively inefficient transportation fuels at the expense of soil resources and in the face of increasing global populations is irresponsible.

THOMAS H. DELUCA

Department of Ecosystem and Conservation Science, University of Montana, 32 Campus Drive, Missoula, MT 59812, USA.

Response

DALGAARD *ET AL.*, CONNOR AND MÍNGUEZ, AND DeLuca all raise important systems-level issues about biofuels. Their comments are well aligned with the principal point of the Editorial: Biofuels produced incidentally to food-crop agriculture are suboptimal in several dimensions, but the cellulose from engineered energy crops, processed in new ways, offers the prospect of significant improvement and material benefit for transport fuels. I agree that sustainability is an essential consideration as the system design space is being explored.

STEVEN E. KOONIN

Chief Scientist, BP, 1 St. James's Square, London SW1Y 4PD, UK.

Measuring the Efficiency of Biomass Energy

IN A SOPHISTICATED JOURNAL SUCH AS *SCIENCE*, we expect the topic of energy policy to be illuminated by use of arithmetic and other analytical tools. The Review "The path forward for biofuels and biomaterials" (A. J. Ragauskas *et al.*, 27 Jan., p. 484) presents its most important datum, 10^{20} joules per year of sustainable biomass energy, without any attempt to relate it to energy consumption. The United States uses more than 400 million kilowatts of electrical power, or a little more than one kilowatt per capita. If we multiply this quantity by the number of seconds in a year ($3600 \times 24 \times 365$), the result is 1.26×10^{19} joules per year. Production of one unit of electrical energy requires three units of fuel energy; thus, the corresponding demand on biomass energy would be 0.38×10^{20} joules per year. For itself, the United States would use approximately 40% of the world's biomass energy just for electricity. The remainder of the energy, and more besides, would be consumed by transportation, space heating, and manufacturing. Nothing would be left over for the rest of the world. Because wind and solar energy have less potential than biomass energy, it is obvious that the global community must rely mainly on petroleum and coal.

KAY R. BROWER

Department of Chemistry, Emeritus, New Mexico Institute of Technology, 1306 Vista Drive, Socorro, NM 87801, USA.

Response

WE AGREE WITH THE CORE POINT OF BROWER, that it would be foolish in the extreme to base energy needs solely on biomass or indeed any other source. The best security for energy provision will derive from the use of a range of technologies. For this very reason, our Review does not make claims for the "supremacy" of bioenergy. It is clear, however, that the use of biomass to supplement and replace oil for liquid transportation fuel will inevitably happen as oil supplies decline and become more costly. Our Review argues for the development of biorefinery technologies that optimally extract the greatest benefit from biomass resources. In addition, the form and flexibility of biofuels are advantages for transportation fuels.

Nevertheless, there are certain missed assumptions in Brower's figures. First, based on Parikka (*1*) and further on Kaltschmitt (*2*), who have used the International Energy Agency energy balance methods with physical energy content methodology, the current state of energy conversion efficiency is already included in the 100 EJ/year estimate, so the value does not need to be multiplied by three again. Second, Parikka reports the current sustainable biomass potential. This is the amount of biomass that is being produced but is underutilized throughout the world at present. Further gains could come from more efficiency, more productive land use, increased use of biomass wastes, etc. In addition, Perlack *et al.* (*3*) report current U.S. bioenergy where 190 million dry tons biomass become 2.9 Quads of bioenergy (a Quad is about 1 EJ); thus, the ultimate potential with improved production of 1.3 billion dry tons biomass might become 19 EJ/year electricity (even though transportation fuel appears a better use). Thus, the United States alone could meet an appreciable fraction of its domestic energy. Likewise, on a global scale, the World Energy Council and World Energy Assessment project that bioenergy could supply a maximum of 250 to 450 EJ/year (perhaps a quarter of global energy demand) by 2050.

BRIAN H. DAVISON,[1] ARTHUR J. RAGAUSKAS,[3] RICHARD TEMPLER,[4] TIMOTHY J. TSCHAPLINSKI,[2] JONATHAN R. MIELENZ[1]

[1]Life Sciences Division, [2]Environmental Sciences Division, Oak Ridge National Laboratory, Oak Ridge, TN 37831, USA. [3]School of Chemistry and Biochemistry, Georgia Institute of Technology, Atlanta, GA 30332, USA. [4]Division of Biology, Imperial College London, London SW7 2AZ, UK.

References

1. M. Parikka, *Biomass Bioenergy* **27**, 613 (2004).
2. M. Kaltschmitt, L. Dinkelbach, in *Biomass Gasification and Pyrolysis—State of the Art and Future Prospects*, M. Kaltschmitt, A. V. Bridgwater, Eds. (CPL Scientific, Newbury, UK, 1997).
3. R. D. Perlack *et al., Biomass as Feedstock for a Bioenergy and Bioproducts Industry: The Technical Feasibility of a Billion-Ton Annual Supply* (U.S. Department of Energy and U.S. Department of Agriculture, April 2005; available at feedstockreview.ornl.gov/pdf/billion_ton_vision.pdf).

Harvesting Our Meadows for Biofuel?

TWO PAPERS ("THE PATH FORWARD FOR BIOfuels and biomaterials," A. J. Ragauskas *et al.*, Reviews, p. 484; "Ethanol can contribute to energy and environmental goals," A. E. Farrell *et al.*, Reports, p. 506) and an Editorial ("Getting serious about biofuels," S. E. Koonin, p. 435) in the 27 January issue outline some of the promises of plant-derived ethanol for satisfying energy demands. Switchgrass (*Panicum virgatum*), which grows naturally throughout most of the continent, is a promising source material. The prospect of a native grass dominating an agricultural landscape is intriguing and potentially ecologically sound.

In nature, however, switchgrass almost invariably grows intermixed with other C_4 grasses such as bluestems. It is unclear whether vast monocultures of switchgrass can be sustainable, especially given that pathogen sources are likely to be present in natural populations of this species. It is also not clear whether these other C_4 grasses may be promising candidates for biofuels.

Biofuel engineers should consider the use of mixed-species, C_4-dominated grasslands as biofuel sources. This would not only avoid the potential instability of monocultures, but could help promote native biodiversity. In the southern Great Plains, vast areas of native tallgrass prairie are being lost due to the lack of fire (causing encroachment of woody plants) and due to development. Highly diverse native hay meadows, mowed annually, were once an important part of the landscape in Oklahoma but are now in serious decline.

CREDIT: JAMES H. MILLER/FORESTRY IMAGES

If we "bring back the meadows" and convert the harvest to fuel, we might simultaneously fill our gas tanks and conserve our natural heritage.

MICHAEL W. PALMER

Department of Botany, Oklahoma State University, Stillwater, OK 74078–3013, USA.

Response

THE ANSWER TO THE QUESTION OF WHETHER monocultures will be used to produce bioenergy feedstocks depends on what it is you are trying to accomplish. Conventional wisdom suggests the following points:

i) There is every reason to believe that, at least from small-scale plots and some larger ones, we are receiving really good stand regeneration and yield per unit area from mixed stands of grasses (*1*).

ii) We have received some pretty strong indication from managers of Conservation Reserve Program (CRP) lands that mixed stands are appropriate for managing conservation acreage for purposes of soil stabilization, providing wildlife amenities, and improved seasonal stand proliferation and extended cover (*1*).

iii) We understand fairly well, at least at some relevant scale, the wildlife advantages of mixed grasses. Species populate the stands at different times of varying cover and find suitable nesting resources (*1*).

iv) We currently farm largely monocultures, especially in annual cropping scenarios, but we think that long-term perennial stands might be more productive, withstand disease or variation in climate and soils better, and use less water than a stand of a single or two species of switchgrass (*1*).

Finally, the biorefinery industry needs to think about the ramifications of farming perennial species as monocultures as opposed to mixed grass stands. Even planted acreage of trees for pulp and paper clearly demonstrates a kind of monoculture—loblolly pine and other pines in the southeast and hybrid poplar and hybrid willow in other areas. Some of the beetle infestation and forest fire risk ramifications are pretty demonstrative of the effects of closely spaced monocultures. There may be trade-offs in productivity, but ignoring the real substantive sustainability issues would be more costly.

MARK DOWNING

Environmental Science Division, Oak Ridge National Laboratory, Oak Ridge, TN 37831, USA.

Reference
1. Much of this evidence comes from results of U.S. Department of Agriculture (USDA) Crop Development Center, Land Grant Institution, and U.S. Department of Energy– and USDA-funded research.

Energy Returns on Ethanol Production

IN THEIR REPORT "ETHANOL CAN CONTRIBUTE to energy and environmental goals" (27 Jan., p. 506), A. E. Farrell *et al.* focus in part on whether biomass-derived ethanol fuel delivers positive net energy [i.e., whether energy return on energy invested (EROI) exceeds 1:1; see (*1*)]. Their analysis neither resolves nor clarifies the fundamental issues that make net energy important and contentious. First, in their comparison of ethanol and gasoline, they confuse EROI—a productivity index—with the energy efficiency of an oil refinery. Second, their use of energy break-even as a litmus test is a red herring; it is more crucial that EROI is high compared with competing energy sources. Exploration for domestic petroleum in the 1930s returned 100 Joules for each Joule invested; the EROI for oil production today is ~15:1 (*2*). Because the present EROI of fossil fuels is high, the ~90 net Quads (1 Quad = ~1 exajoule) delivered annually to the U.S. economy results from an investment of only about 10 Quads (*2*). To provide that same 90 net Quads from corn-derived ethanol would require an investment of 145 to 500 Quads (based on an EROI = ~1.6:1 to 1.2:1, implied by Farrell *et al.*'s fig. 1). The current transportation system cannot be maintained on a fuel system delivering only a 1.6:1 return. Third, the focus on petroleum inputs is too limited. Natural gas is often the principal input to biomass fuel production, but its future is no more certain than oil's; we already import more than 15% of what we use (*3*). Fourth, the authors ignore the energy cost of repairing soil erosion.

Finally, the one (speculative) result for an energy technology based on cellulose in fig. 1 implies an EROI of ~50:1. This (very uncertain) EROI indicates that this source of biomass could be potentially useful, but ethanol from corn remains too marginal to survive without heavy economic subsidy.

CUTLER J. CLEVELAND,[1]
CHARLES A. S. HALL,[2]
ROBERT A. HERENDEEN[3]
[1]Center for Energy and Environmental Studies, Boston University, 675 Commonwealth Avenue, Boston, MA 02215, USA. [2]College of Environmental Science and Forestry, Syracuse, NY 13210, USA. [3]Illinois Natural History Survey, Champaign, IL 61821, USA.

References
1. C. J. Cleveland, R. Costanza, C. A. S. Hall, R. Kaufmann, *Science* **225**, 890 (1984).
2. C. J. Cleveland, *Energy* **30**, 769 (2005).
3. Official U.S. Energy Information Web page, eia.doe.gov.

IN THEIR REPORT "ETHANOL CAN CONTRIBUTE to energy and environmental goals" (27 Jan., p. 506), A. E. Farrell and colleagues offer hopeful opinions about corn-based ethanol. Their analysis suggests that, since the ratio of ethanol produced to fossil fuel used is positive, ethanol should be further developed. If replacing oil is our goal, we must look at two parameters of this approach: (i) energy return on investment (EROI) including environmental impacts on soil, water, climate change, ecosystem services, etc.; and (ii) scalability and timing. Farrell and colleagues' most optimistic EROI of 1.2:1 (which does not include tractors, labor, or environmental impacts) implies that we need to produce 6 MJ of ethanol to net 1 MJ of energy for other endeavors. Thus, the yield of ethanol would not be 360 gallons per acre gross yield, but rather a mere 60 gallons per acre net yield, not even two fill-ups for an SUV. The entire state of Iowa, if planted in corn, would yield approximately five days of gasoline alternative.

To devote half the nation's corn crop to ethanol would require an input of 3.42 billion barrels of oil (almost half our current national use) to net 684 million barrels of "new" ethanol energy. We would also lose food and soil nutrients, suffer ecosystem damage, and use massive amounts of water for irrigation.

We need alternative energy. But ethanol from corn is neither scalable nor sustainable. Let's pursue better options.

NATHAN HAGENS, ROBERT COSTANZA, KENNETH MULDER
Gund Institute for Ecological Economics, University of Vermont, Burlington, VT 05405, USA.

IN THEIR REPORT "ETHANOL CAN CONTRIBUTE to energy and environmental goals" (27 Jan., p. 506), A. E. Farrell *et al.* address the energy balance and greenhouse gas (GHG) emissions of ethanol from corn and show the pessimistic analysis of these issues by Pimentel and Patzek (*1*) to be wrong. Pimentel and Patzek are also wrong in their analysis of cellulose-derived ethanol.

Hammershlag's (*2*) estimates for the energy return per nonrenewable energy invested for near-term cellulosic ethanol technology range from 4.4:1 to 6.6:1, and Farrell *et al.* calculate a value of 8.3:1. The energy return for mature cellulosic ethanol technology is expected to be over 10:1 (*3*). Pimentel and Patzek estimate the energy return for cellulosic ethanol at 0.69:1. Why such a striking discrepancy? The primary reason is that Pimentel and Patzek estimate the externally supplied processing energy to be over 25 MJ/liter ethanol, whereas in all other studies this value is zero, since it is met by lignin from cellulosic biomass.

Whether energy return and greenhouse gas emissions of ethanol production are favorable depends on how the process is configured and designed. The fact that Pimentel and Patzek's

process does not have positive energy returns should not be used to measure the potential of this promising energy path.

The science is clear; it's time to move on from the energy balance debate and focus on policies that encourage the greatest oil savings and reductions in greenhouse gas emissions from both corn and cellulosic ethanol.

LEE LYND,[1] NATHANAEL GREENE,[2] BRUCE DALE,[3] MARK LASER,[1] DAN LASHOF,[4] MICHAEL WANG,[5] CHARLES WYMAN[6]

[1]Thayer School of Engineering, Dartmouth College, 8000 Cummings Hall, Hanover, NH 03755, USA. [2]Senior Policy Analyst, Natural Resources Defense Council, 40 West 20th Street, New York, NY 10011, USA. [3]Chemical Engineering Department, Michigan State University, 2527 Engineering, East Lansing, MI 48824–1226, USA. [4]Senior Director, Climate Center, Natural Resources Defense Council, 1200 New York Avenue, NW, Suite 300, Washington, DC 20005, USA. [5]Center for Transportation Research, Argonne National Laboratory, 9700 South Cass Avenue, Building 362/B215, Argonne, IL 60439, USA. [6]Bourns College of Engineering, Center for Environmental Research and Technology (CE-CERT), University of California, Riverside, 1084 Columbia Avenue, Riverside, CA 92507, USA.

References

1. D. Pimentel, T. D. Patzek, *Nat. Resources Res.* **14**, 65 (2005).
2. R. Hammershlag, *Environ. Sci. Technol*., in press.
3. N. Greene *et al.*, Growing Energy, www.nrdc.org/air/energy/biofuels/contents.asp (2004).

THE METHODOLOGICAL FLAWS IN A. E. FARRELL *et al.*'s Report "Ethanol can contribute to energy and environmental goals" (27 Jan., p. 506) are revealed in the authors' fig. 1b, which shows that motor gasoline has a negative net energy and the highest input/output ratio, while ethanol technologies have positive net energies and lower input/output ratios. These numbers imply that motor gasoline is the marginal fuel seeking to displace biomass fuels.

This contradiction is caused by inconsistencies in the boundaries that are used to analyze their energy balance. For motor gasoline, the authors add the energy content of the gasoline to the effort used to produce it. The energy used to produce motor gasoline is much less than its energy content —estimates for the total energy input/energy output ratio are about 0.06 (*1*).

For biomass fuels, the authors report only the petroleum input/output ratio. Other fuels used in the process should also be included; these cannot be assumed to be sustainable (as exemplified by natural gas shortages) The biomass fuels are not used as liquids—(much of the co-products are used to generate electricity), which also needs to be taken into account. Including these additional fuels raises the input/output ratio to 0.79 (ethanol today) or 0.82 (CO_2 intensive). If the U.S. economy used oil with an energy input/output ratio of about 0.8, the energy equivalent of about 80 million barrels per day of oil would be used to generate the 20 million barrels per day of refined petroleum products that the United States uses outside of the oil sector.

Once the boundaries are made equivalent, motor gasoline has a much higher energy surplus and a lower energy input/energy out ratio than biomass fuels. This result matches the economic reality described by the authors' first paragraph—biomass fuels, not motor gasoline, need subsidies and tax breaks.

ROBERT K. KAUFMANN

Center for Energy and Environmental Studies, Boston University, 675 Commonwealth Avenue, Boston, MA 02215, USA.

Reference

1. C. J. Cleveland, *Energy* **30** (no. 5), 769 (2005).

IN THE NET-ENERGY ANALYSIS IN THEIR REPORT "Ethanol can contribute to energy and environmental goals" (27 Jan., p. 506), A. E. Farrell *et al.* do not (i) define the system boundaries, (ii) conserve mass, and, consequently, (iii) conserve energy. Most of the current First Law net-energy models of the industrial corn-ethanol cycle are based on nonphysical assumptions and should be discarded.

When properly formulated, mass and First Law energy balances of corn fields and ethanol refineries account for the photosynthetic energy, some of the environment restoration work, and the co-product energy (*1*). These show that production of ethanol from corn is two to four times less favorable than production of gasoline from petroleum. From thermodynamics, it also follows that the ecological devastation wrought by industrial biofuel production must be severe. With the DDGS coproduct energy credit, 3.9 gallons of ethanol displace on average the energy in 1 gallon of gasoline. Without the DDGS energy credit, this average number is 6.2 gallons of ethanol. Equivalent CO_2 emissions from the corn ethanol cycle are 50% higher than those from gasoline and become 100% higher if methane emissions from cows fed with DDGS are accounted for.

The U.S. ethanol industry has consistently inflated its ethanol yields by counting 5 volume percent of #14 gasoline denaturant (8% of energy) as ethanol. Also, imports from Brazil and longer chain alcohols seem to have been counted as U.S. ethanol (*1*). A detailed statistical analysis of 401 corn hybrids from Illinois reveals that the highest possible yield of ethanol is 2.64 ± 0.05 (SD) gallons EtOH/bu (*1*). The commonly accepted U.S. Department of Agriculture estimate of mean ethanol yield in the United States, 2.682 gallons EtOH/bu (*2*), is one standard deviation above this estimate.

TAD W. PATZEK

Department of Civil and Environmental Engineering, University of California at Berkeley, Berkeley, CA 94720, USA.

References and Notes

1. The detailed calculations and arguments can be found at http://petroleum.berkeley.edu/patzek/BiofuelQA/Materials/RealFuelCycles-Web.pdf.
2. H. Shapouri, P. Gallagher, M. S. Graboski, USDA's 1998 Ethanol Cost-of-Production Survey, Agricultural Economic Report No. 808 (U.S. Department of Agriculture, Economic Research Service, Office of Energy and New Uses, Washington, DC, 2002).

Response

WE THANK THE LETTER AUTHORS FOR THEIR comments. As Lynd *et al*. and Cleveland *et al.* point out, the potential benefits of cellulosic ethanol technologies would include a shift away from intensely farmed monocultures such as corn and positive effects on soil erosion, fertilizer runoff, and biodiversity. In addition, because cellulosic technologies can use a wide variety of feedstocks, their flexibility may allow for more applications worldwide. Similarly, we agree with Hagens *et al*. and Patzek that we need more sustainable processes than current corn ethanol production.

However, Hagens *et al*. are mistaken that our analysis excludes tractors or labor; these were included. And Cleveland *et al.* and Kaufmann incorrectly state that we ignored natural gas or coal inputs. These are explicitly included in the ERG Biofuels Analysis Meta-Model (EBAMM, cells N6, N28, N30, N37 and N38 in worksheet "Net Energy") (*1*).

We agree with Hagens *et al*., Cleveland *et al.*, and Patzek that meaningful measurement of environmental impacts is critical to an appropriate evaluation of biofuels. However, including incommensurable quantities such as soil erosion and climate change into a single metric requires an arbitrary determination of their relative value. We stressed the advantages of individual metrics for petroleum consumption and greenhouse gas emissions and encouraged the development of specific metrics for environmental effects such as soil erosion. In addition to exposing trade-offs among competing objectives, multiple metrics permit more focused analysis and help reduce uncertainty (see related correction on page 1748).

Hagens *et al*., Cleveland *et al.*, and Kaufmann incorrectly assert that our paper focused on energy return on investment (EROI). The Supporting Online Material explains why ratios such as EROI are methodologically inferior to the additive metric we use (*1*). Even a quality-adjusted EROI is a single metric that has the problems noted above. Furthermore, such aggregation can lead to mischaracterizations. For example, Hagens *et al.* inappropriately label total energy input into ethanol production as gasoline or petroleum, even though it is predominantly coal and natural gas.

Patzek's Letter is based on a non–peer-reviewed online document that has changed several times since its receipt. Nonetheless, much of his analysis appears to be rigorous in detail but erroneous overall. For instance, extractable starch only applies to wet milling, which presently produces approximately 30% of U.S. ethanol. Almost all new ethanol plants

are dry mills, for which total fermentable starch is a better measure of ethanol yield, and that yield at least 5% more ethanol per unit mass of corn than wet milling (*2*, *3*). Further, Patzek arbitrarily assumes that spreading coproduct animal feed on agricultural land is the best way to maintain soil quality, ignoring among other things the potential of alternative cropping systems (*4*).

These Letters focus on different questions than did our paper. EROI measures the efficiency of primary energy production, but is not useful for comparing different ways of using fossil energy resources to create liquid transportation fuels, which was the point of our paper (*1*). Life-cycle assessments such as ours are not designed to balance mass and energy; they are designed to evaluate environmental implications of the production, use, and disposal of products and fuels.

In retrospect, we should have labeled our metric not as net energy value (NEV) but as Fossil Energy Value (FEV), which, following, is calculated as FEV = $E_{out} - (F_F + P_F)$, where E_{out} is the energy content in the delivered fuel, F_F is primary fossil energy in feedstocks, and P_F is the primary fossil input energy in nonfeedstocks (*5*). For biomass, F_F is zero, which explains the seeming inconsistency in system boundaries that Kaufmann reports (*2*). The system boundaries of EBAMM are clearly defined in Equations S-1 through S-7, even if not explicitly labeled as such.

Like the Letter authors, we believe that ethanol can contribute to energy and environmental goals only as part of an overall strategy that also includes more efficient vehicles, other sustainable energy sources, and careful monitoring of ethanol production. The magnitude and timing of this contribution will depend on the development of better methods of producing ethanol than today's corn-based approach. To encourage these changes, we should measure what we care about—greenhouse gas emissions and soil erosion, for example—and provide strong incentives to ethanol producers to improve their performance in these areas. A close reading of our paper and supporting material reveals far more agreement among us all than these Letters suggest.

ALEXANDER E. FARRELL,[1] RICHARD J. PLEVIN,[1] BRIAN T. TURNER,[1,2] ANDREW D. JONES,[1] MICHAEL O'HARE,[2] DANIEL M. KAMMEN[1,2,3]

[1]Energy and Resources Group, [2]Goldman School of Public Policy, [3]Renewable and Appropriate Energy Laboratory, University of California, Berkeley, Berkeley, CA 94720–3050, USA.

References

1. Available online at http://rael.berkeley.edu/EBAMM.
2. S. Butzen, D. Haefele, P. Hilliard, *Crop Insights* **13**, 1 (2003).
3. H. Shapouri, P. W. Gallagher, "2002 Ethanol Cost-of-Production Survey" (U.S. Department of Agriculture, Washington, DC, 2003).
4. S. Kim, B. E. Dale, *Biomass Bioenergy* **29**, 426 (2005).
5. D. V. Spitzley, G. A. Keoleian, "Life Cycle Environmental and Economic Assessment of Willow Biomass Electricity" (University of Michigan, Ann Arbor, MI, 2005).

CORRECTIONS AND CLARIFICATIONS

News of the Week: "Court revives Georgia sticker case" by C. Holden (2 June, p. 1292). The article incorrectly characterizes the Discovery Institute in Seattle, Washington, as a think tank for the creationist movement. The institute is a public policy organization that operates many different programs, including the Center for Science & Culture, which supports the work of scholars who explore challenges to evolution and promote the concept of intelligent design.

News of the Week: "RU-486–linked deaths open debate about risky bacteria" by J. Couzin (19 May, p. 986). The story mistakenly implied that a woman's risk of death from a *Clostridium sordellii* infection after a nonsurgical abortion is about 1 in 100,000. In fact, this is the estimated risk of contracting a *C. sordellii* infection following a nonsurgical abortion; to date, the infections are invariably fatal.

Reports: "Ethanol can contribute to energy and environmental goals" by A. E. Farrell *et al.* (27 Jan. 2006, p. 506). Michael Wang of Argonne National Laboratory has raised interesting and important issues associated with greenhouse gas (GHG) emissions from corn (maize) ethanol production in this Report. The U.S. Department of Agriculture (USDA) confirmed that the data reported for lime application had been calculated incorrectly and kindly updated these values. The custom report and an updated version of the Supporting Online Material that discusses the issues raised in this erratum in more detail are downloadable from http://rael.berkeley.edu/EBAMM. The corrected data are expected to be available on the USDA Web site in the coming months. In conducting a reanalysis, even larger uncertainties were discovered in the emissions factor of lime and the emission factor for nitrous oxide (N_2O) resulting from nitrogen fertilizer application. With these refinements, the *Ethanol Today* case now yields a point estimate of net greenhouse gases for corn ethanol at 18% below conventional gasoline, very close to the initially reported value of 15% below gasoline, but with an expanded uncertainty band of –36% to +29%.

TECHNICAL COMMENT ABSTRACTS

COMMENT ON "Nature of Phosphorus Limitation in the Ultraoligotrophic Eastern Mediterranean"

Michelle S. Hale and Richard B. Rivkin

Thingstad *et al*. (Reports, 12 August 2005, p. 1068) reported that in situ mesoscale phosphorus enrichment of the eastern Mediterranean Sea altered selected biological parameters and concluded that the added phosphorus was rapidly transferred from bacteria to mesozooplankton. However, because of a lack of replication and a misinterpretation of their statistical analyses, that conclusion is not supported by the data.

Full text at www.sciencemag.org/cgi/content/full/312/5781/1748c

RESPONSE TO COMMENT ON "Nature of Phosphorus Limitation in the Ultraoligotrophic Eastern Mediterranean"

T. F. Thingstad, C. S. Law, M. D. Krom, R. F. C. Mantoura, P. Pitta, S. Psarra, F. Rassoulzadegan, T. Tanaka, P. Wassmann, C. Wexels Riser, T. Zohary

With no requirement for synoptic treated (IN) and control (OUT) stations, analysis of covariance is an interesting statistical technique for testing IN-OUT differences in Lagrangian experiments, but it has inherent limitations due to its assumption of linear responses. With this limitation properly considered, we find that analysis of covariance strengthens, not weakens, experimental support for the food-web transfer mechanisms we proposed.

Full text at www.sciencemag.org/cgi/content/full/312/5781/1748d

Caution on Nominee to Head USGS

IN THE NEWSMAKERS ITEM "NEW USGS HEAD" (19 May, p. 995) on the nomination of Mark Myers to head the U.S. Geological Survey (USGS), I was quoted by the writer Erik Stokstad as saying that Myers "has a significant amount of integrity." I have no direct knowledge of Myers and therefore have no basis for evaluating his fitness for the job. However, his background is in such contrast to previous USGS directors that I said to Stokstad that Congress must ask some very tough questions of Myers before confirming him.

As I said to Stokstad, because of the Bush Administration's history of interfering with the integrity of science conducted at agencies and of being overly friendly to the oil and gas industry, Congress should demand full answers from Myers regarding his view on the independence of the government's main science agency and whether he would stand up to an administration that has shown no qualms about dismissing good science when it conflicts with political goals.

KAREN WAYLAND

Legislative Director, Natural Resources Defense Council, 1200 New York Avenue, NW, Washington, DC 20005, USA.

Letters to the Editor

Letters (~300 words) discuss material published in *Science* in the previous 6 months or issues of general interest. They can be submitted through the Web (www.submit2science.org) or by regular mail (1200 New York Ave., NW, Washington, DC 20005, USA). Letters are not acknowledged upon receipt, nor are authors generally consulted before publication. Whether published in full or in part, letters are subject to editing for clarity and space.

GEOPHYSICS

Building on Shaken Ground

Iain Stewart

In the famous Japanese woodblock prints that depict a whale-like catfish carrying the archipelago on its back, the animal whose movements trigger earthquakes is not always a ferocious creature bent on destruction. Instead, it often has a benign character—a representation in folklore that earthquakes have the potential to set right social, political, and economic injustice. In the wake of the great earthquake that devastated Edo (modern Tokyo) in 1855, the catfish was popularly seen as a god who would equally distribute all wealth and create an ideal fortune—a reminder that out of disaster comes opportunity. The opportunism that emerged gradually from the ruins of Edo was that of Western engineering know-how, which effectively pitted the apparently fragile wooden townscapes of Japan—prone as much to fire as quakes—against the solidity and strength of brick-built American and European cities.

Earthquake Nation: The Cultural Politics of Japanese Seismicity, 1868–1930 details the changing fortunes of wood and masonry in the retrofitting of a modernizing Japan under Western supervision. In doing so, it eloquently charts the rise of two nascent disciplines—architecture and seismology—through the final quarter of the 19th century, when the technological changes following the Meiji Restoration were underpinned by foreign (mostly British) scientists, architects, and engineers. From the tectonic solidity of western Europe and the eastern United States, the Japanese landscape of timber temples, houses, and arched bridges quickly became the object of elaborate denigration. Wooden pagodas that had withstood centuries of shakes were not structures designed to withstand earthquakes, they were just lucky. The intricate work of the Japanese carpenter might be ingenious, but it was artistically indulgent and effectively useless in the face of the earthquake threat. Clearly, what was needed was strength. In a multiple-choice examination for the new breed of Japanese architects, one question that asked about the future of their domestic architecture offered the following options for materials: "either brick and stone, brick and terracotta, entirely brick, or entirely stone." Wooden Japan, foreign architects and engineers had decided, would be rebuilt in masonry.

Earthquake Nation
The Cultural Politics of Japanese Seismicity, 1868–1930

by Gregory Clancey

University of California Press, Berkeley, CA, 2006. 345 pp. $49.95, £32.50. ISBN 0-520-24607-1.

Gregory Clancey, a historian of technology at the National University of Singapore, explores how this West-inspired vision of Japan's future ultimately crumbled in the Great Nōbi Earthquake of 1891, a calamitous event that shook down brick mills and factories as readily as it did traditional wooden structures. From the wreckage of the new Western constructions, and spurred on by growing nationalism, came an explosion of changed practice. Japanese architecture reconnected with its traditional past and sought out fresh homegrown ways of protecting against and resisting earthquakes. Architects and builders were helped by a new breed of scientist interested in how earthquakes worked. A dominating presence among these was John Milne, now regarded as the father of modern seismology—he developed the seismograph and wrote an early text on the discipline (*1*). Milne arrived in Japan from England in 1876 to teach geology and mining. His remarkable tenacity in establishing an earthquake-monitoring network, first of observers and then of seismographs, was coupled to his detailed observations of the actual effects of earthquake motion, both from the field (*2*) and from elementary shaking tables. Through this interdisciplinary approach, Milne became convinced of the superiority of indigenous constructional design over imported techniques (*3*). His conclusions found favor among the younger generation of Japanese seismologists and architects.

Clancey follows a fascinating series of twists and turns through the evolving struggle for supremacy between Japanese architecture and seismology that ultimately resulted in a fusion into earthquake engineering. Along the way, each new earthquake reset the various scientific arguments and personal feuds that fueled a debate that formed the Japanese centerpiece of a cultural schism between West and East. After Nōbi, Japan's earthquake science declared war on earthquakes, and, indeed, Clancy regards the national response to the 1891 earthquake as a dress rehearsal for the landmark nationalizing event of the 1894–1895 Sino-Japanese war. Japanese expansionism in the political and military arenas was mirrored by an increasing international preeminence in the seismological domain, as Japanese seismologists such as Fusakichi Ōmori traveled beyond their homeland's shores to document the urban fragility in Western seismic catastrophes like the 1906 San Francisco and the 1908 Messina (Italy) earthquakes.

Bricks fall, wood stands. One of the three panels of Baidō Kokunimasu's woodblock print of Nagoya during the Great Nōbi Earthquake of 1891.

CREDIT: NAGOYA CITY MUSEUM/COURTESY UNIVERSITY OF CALIFORNIA PRESS

It is always fascinating to see a discipline depicted from the outside—in this case from the architectural wings—but in fact what Clancey reveals to us in *Earthquake Nation* is the inside story of the birth of modern seismology. In fine detail, he charts the economic, social, and political factors that allowed a new, controversial science to take root in a remarkable and unique cultural melting pot. Driving a subplot of the book are the contrasting earthquake ethnographies that continue to subtly underpin "Eastern" and "Western" perspectives on seismology and seismic engineering. Center stage, one finds the careful dissection of a remarkable period of history during which much of what we know of as modern earthquake science came to be.

The reviewer is at the School of Earth, Ocean, and Environmental Sciences, University of Plymouth, Plymouth, PL4 8AA, UK. E-mail: istewart@plymouth.ac.uk

References

1. J. Milne, *Seismology* (Kegan, Paul, Trench, Truber, London, 1898).
2. J. Milne, W. K. Burton, *The Great Earthquake in Japan, 1891* (Stanford, London, 1892).
3. J. Milne, Ed., "Construction in Earthquake Countries." Special issue of *Trans. Seismol. Soc. Jap.* **14** (1889).

10.1126/science.1130280

ECOLOGY

Coral Reefs and the Global Network of Marine Protected Areas

Existing marine reserves are largely ineffective and as a whole remain insufficient for the protection of coral reef diversity.

Camilo Mora,[1,2]* Serge Andréfouët,[3] Mark J. Costello,[1] Christine Kranenburg,[4] Audrey Rollo,[1] John Veron,[5] Kevin J. Gaston,[6] Ransom A. Myers[2]

Coral reefs worldwide are suffering massive declines in their diversity in response to human activities (*1*, *2*). The accelerating decay of this and other marine and terrestrial ecosystems has motivated multinational efforts to reduce biodiversity loss such as the 2002 World Summit on Sustainable Development (*3*) and the 2003 World Parks Congress (*4*). The latter recommends that 20 to 30% of all major ecosystems should lie within strictly protected reserves by 2012 (*4*).

Enhanced online at www.sciencemag.org/cgi/content/full/312/5781/1750

Protected reserves should reduce pressure from harvesting and other human activities, which should in turn facilitate the ability of species to cope with natural disturbances (*5*–*7*). Although much discussion has surrounded the success of protected areas at small spatial scales (*7*), little evaluation has been done at the global scale (*5*, *8*). Here we provide a global assessment on the extent, effectiveness, and gaps in the coverage of coral reefs by Marine Protected Areas (MPAs).

A major challenge to quantifying the extent of coverage of any ecosystem by a network of MPAs is the dynamic nature of the network itself and of information about it. To address this problem, we built a database of coral reef MPAs for every country (*9*), contacted local managers and researchers, and used recent published reports (*2*, *10*, *11*) to ensure that verification was available for each country. This process resulted in the deletion of 521 MPAs from a previous standard list, and the addition of 157 further MPAs. The final verified database contains 980 MPAs and covers 98,650 km^2 (18.7%) of the world's coral reef habitats. We will provide general conclusions in the text; detailed methodology and data can be found in the supporting online material.

Protected areas are managed for different purposes, and, therefore, this protection can have varied effects on particular taxa. Growing evidence for coral reefs suggests that their resilience is strongly dependent on the presence of a range of functional groups, including large herbivorous and predatory fishes (*1*). Consequently, those areas used for harvesting may be of limited benefit (*1*, *7*). Of the world's roughly 527,072 km^2 of coral reefs, 5.3% lie inside extractive MPAs, 12% inside multipurpose MPAs, and 1.4% inside no-take MPAs (see figure, this page). Regional coverage of coral reefs by multipurpose and no-take MPAs ranges from 69% in Australia, to 7% in the central Pacific and western Indian Ocean, to ~2% in the central Indian Ocean (fig. S1A, table S1).

Each year over the past 10 years, about 40 new MPAs have been created worldwide that include coral reefs (fig. S2A). Unfortunately, the establishment of MPAs is rarely followed by good management and enforcement (*10*, *11*), which means that the numbers of MPAs and their coverage can be misleading indicators of effective conservation. Using levels of poaching as an indirect measurement of management performance (*9*), we found that only 88 coral reef MPAs (fig. S1B), covering 1.6% of the world's coral reefs (table S1), are managed in such a way as to prevent such activities. Less than 0.1% of the world's coral reefs are within MPAs classified as no take with no poaching (see figure, this page). Management performance varies worldwide but, troublingly, it is particularly low in areas of high coral diversity such as the Indo-Pacific and the Caribbean (fig. S1B, table S1) (*10*, *11*).

MPAs are specifically intended to limit human activities at particular locations. However, many coral reefs still remain vulnerable to risks that arise from beyond their boundaries, such as sedimentation, pollution, coastal development, and overfishing (*7*, *12*). Using a risk index of these threats (*9*), we found that 147 coral reef MPAs (fig. S1C), covering almost 10.8% of the world's corals (table S1) are at low risk from such threats. Less than 0.01% of the world's corals are within MPAs defined as no take with no poaching and at low risk (see figure, below).

One of the main impacts of effective MPAs on marine organisms is the prevention of harvesting, which reduces mortality and which, in turn, should generate larger body sizes, increases in abundance, and greater fecundity (*6*, *7*). However, populations can also be influenced by the movement of their individuals (*6*). Extensive movement can expose juvenile and adult individuals to harvesting outside the boundaries of the MPAs (*6*, *7*, *13*), whereas the arrival of new recruits can be favored if source populations are protected (*6*, *14*). Therefore, the scales of adult movement and propagule dispersal can be critical to the effectiveness of an MPA network (*6*, *7*).

Data on species' home ranges is improving, particularly for coral reef fishes (*13*). Although, for most species, home ranges are small (<1 km^2), for large herbivorous and predatory fishes,

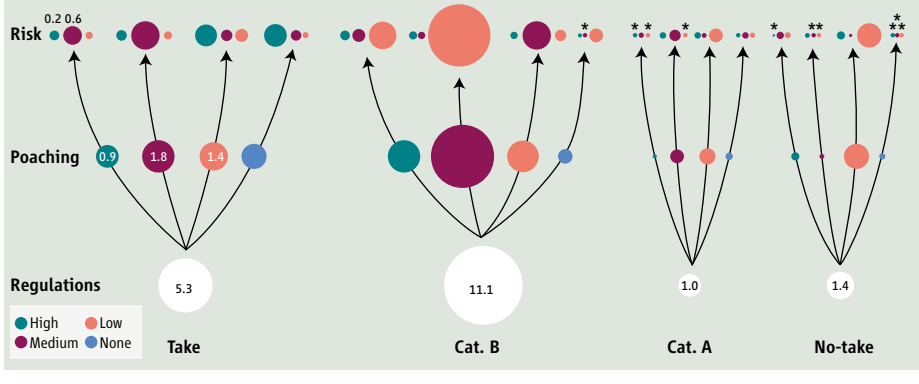

Effectiveness of the global network of coral reef MPAs. The area of coral reefs covered by the network of MPAs (18.7% of the world total) was classified by their regulations on extraction as either no take, take, or multipurpose. Multipurpose MPAs were divided into those that prohibit commercial harvesting (category A) and those that do not (category B). The subdivision of reefs on each of those MPA categories was then analyzed according to attributes of poaching and risk (according to the combined threat risk index described above). Sizes of circles indicate percentage of world coral reef area; in a few cases, numbers are shown within the circles to indicate sizes and method of subdivision. Asterisks indicate percentages smaller than 0.01.

[1]Leigh Marine Laboratory, University of Auckland, Post Office Box 349, Warkworth, New Zealand. [2]Department of Biological Sciences, Dalhousie University, Halifax, NS, Canada, B3H 4J1. [3]Institut de Recherche pour le Développement, Boite postale A5-98848, Noumea cedex, New Caledonia. [4]Institute for Marine Remote Sensing, University of South Florida, St. Petersburg, FL 33701, USA. [5]Australian Institute of Marine Sciences, Townsville 4810, Australia. [6]Biodiversity and Macroecology Group, Department of Animal and Plant Sciences, University of Sheffield, Sheffield, S10 2TN, UK.

*Author for correspondence. E-mail: moracamilo@hotmail.com

Conservation of MPAs. (**Top**) Status of the global network. Location and shape of all 980 MPAs are shown. Categorization of MPAs was based on the average of the attributes analyzed (*9*). The percent of coral reefs per region covered by MPAs in those categories is shown on the bar charts. (**Bottom**) MPAs needed for an optimum coverage of the world's coral reefs. Dots represent MPAs of 10 km^2 and spaced at 15 km from each other.

which are often the targets of fishermen, these can cover several square kilometers (*6*, *7*, *13*). About 40% of the areas in the current global network of coral reef MPAs are smaller than 1 to 2 km^2 (fig. S2B). This suggests that in a large portion of the network, vagile, and usually also key, species can be lost directly to harvesting because they can move beyond the boundaries of small MPAs. Such losses can also trigger negative indirect effects on resilience of coral reefs through trophic cascades (*1*).

Propagule dispersal in coral reef organisms may be on scales on the order of a few tens of kilometers (*6*, *14*, *15*). Thus, it has been recommended that MPAs should be 10 to 20 km in diameter and/or in spacing from each other to ensure exchange of propagules among protected benthic populations (*14*). At the global scale, there are only a handful of MPAs sufficiently large to accommodate such dispersal within their boundaries (fig. S2B), while their average spacing (63 km) is too broad for this network to be functional in this regard (fig. S2C). Given the scattered distribution of coral reefs, an optimum global network of MPAs, each 10 km^2 in area [to protect the "neighborhood" of a broad group of vagile species (*6*)] and spaced 15 km apart from one another [to ensure "safe" levels of larval connectivity (*14*)], would require 2559 MPAs in addition to those that already exist (see figure, this page, top). These results suggest a major need for expanding and establishing new MPAs. This expansion of MPAs only requires the protection of 25,590 km^2, or ~5% of the world's coral reefs distributed over a sparser network.

The different attributes of MPAs discussed so far are likely to interact to different extents in determining the overall effect of a given MPA. Finally, we combined all the attributes analyzed in this study (i.e., regulations on extraction, poaching, external risks, MPA size, and MPA isolation) into a single index of overall conservation status (*9*). From this, we found that only 2% of the world's coral reefs are within MPAs that combine adequate conditions of the analyzed attributes. No one regional network covers more than 10% of its regional coral reefs within MPAs with such quality (see figure, page 1750, and table S1). Our analysis of the performance of the global network of MPAs in protecting coral reefs reveals that this network is very inefficient.

We have identified major discrepancies between the quantity and the quality of efforts invested toward minimizing biodiversity loss in coral reefs. Even if all existing coral reef MPAs are considered effective, as a whole, it is troubling that they are still insufficient for the global protection of coral reef diversity. Recent studies have also indicated important gaps in the global coverage of terrestrial vertebrates by protected areas (*8*); our analysis suggests that these shortcomings are worse than previously anticipated if the effectiveness of protected areas is taken into account. Given the current worldwide decline of coral reefs (*1*, *2*), our report highlights the serious vulnerability of this ecosystem and the need for immediate reassessment of global-scale conservation strategies.

References and Notes

1. D. Bellwood *et al.*, *Nature* **429**, 827 (2004).
2. C. Wilkinson, *Status of Coral Reef of the World* (Australian Institute of Marine Science, Townsville, Australia, 2004).
3. A. Balmford *et al.*, *Science* **307**, 212 (2005).
4. (www.iucn.org/themes/wcpa/wpc2003/pdfs/outputs/ wpc/recommendations.pdf).
5. S. Chape *et al.*, *Philos. Trans. R. Soc. London Ser. B* **360**, 443 (2005).
6. S. R. Palumbi, *Annu. Rev. Environ. Resources* **29**, 31 (2004).
7. P. F. Sale *et al.*, *Trends Ecol. Evol.* **20**, 74 (2005).
8. A. S. Rodrigues *et al.*, *Nature* **428**, 640 (2004).
9. Methods and results are available as supporting material on *Science* Online.
10. L. Burke, L. Selig, M. Spalding, *Reefs at Risk in Southeast Asia* (World Resources Institute, Washington, DC, 2002).
11. L. Burke, J. Maidens, *Reefs at Risk in the Caribbean* (World Resources Institute, Washington, DC, 2004).
12. D. M. Stoms *et al.*, *Front. Ecol. Environ*. **3**, 429 (2005).
13. D. L. Kramer, M. R. Chapman, *Environ. Biol. Fish*. **55**, 65 (1999).
14. A. L. Shanks *et al.*, *Ecol. Appl*. **13**, S159 (2003).
15. C. Mora, P. F. Sale, *Trends Ecol. Evol.* **17**, 422 (2002).
16. We thank all the managers, researchers, and institutions who provided data. R. Metzger helped in data gathering and P. Wong and D. Egli provided Geographic Information Systems advice. We are grateful for the comments of P. Sale, J. Montgomery, D. Pelletier, P. Usseglio, D. Egli, M. Spalding, R. Taylor, T. Langlois, A. Cozens, and J. McPherson. Funding was provided by the Owen Glenn bequest for marine sciences at University of Auckland and the Sloan Foundation Census of Marine Life through the Future of Marine Animal Populations and the Ocean Biogeographic Information System. The Millennium Coral Reef Mapping project was funded by the National Aeronautics and Space Administration to S.A and F. Muller-Karger at University of South Florida.

Supporting Online Material
www.sciencemag.org/cgi/content/full/312/5781/1750/DC1

10.1126/science.1125295

TRANSCRIPTION

Gene Expression Needs a Break to Unwind Before Carrying On

The molecular events that change a quiescent gene within compacted chromatin into one actively transcribing RNA are not yet clear. Unexpectedly, enzymes that create and repair DNA breaks seem to be necessary.

Jean-François Haince, Michèle Rouleau, Guy G. Poirier

The lengthy genomic DNA of a eukaryotic cell manages to fit within the relatively small confines of its nucleus by spooling. Twisting ribbons of DNA are tightly wrapped around core histone proteins, forming compact nucleosomes that constitute chromatin, the substance of chromosomes. Although this compacted structure is a means to handle space constraint, it presents a barrier to regulated genomic activity, including gene expression and maintenance of genomic integrity. However, cells are not adversely affected by such tight packaging because this highly structured assembly is compliant and dynamic, displaying varying degrees of compaction that allows regulated access to protein complexes in response to various stimuli. To operate within this overcrowded area, protein complexes locally remodel chromatin. But precisely how defined areas of chromatin adopt different conformations, allowing regulated access to specific DNA regions, is a captivating question. On page 1798 of this issue, Ju *et al*. (*1*) provide molecular evidence that the enzyme DNA topoisomerase IIβ (TopoIIβ) activates transcription by generating a break in double-stranded DNA within a nucleosome. This enzyme, which is associated with a DNA-repair machinery, allows chromatin to relax, which is needed to drive gene expression (see the figure).

Until recently, the role of topoisomerase II in transcriptional regulation was restricted to resolving topological problems regarding the passage of RNA polymerase II, as it transcribes genes into messenger RNA. Remarkably, Ju *et al*. report that regulated gene transcription involves the unexpected recruitment and unique enzymatic function of TopoIIβ. This enzyme produces a transient nucleosome-specific DNA double-strand break that is required for transcriptional activation. They first observed this process with the hormone estradiol 17β, a ligand for a specific nuclear receptor (which happens to be a transcription factor), that activates the target gene pS2. Cleverly, the authors developed an exclusive procedure—nucleosome-chromatin immunoprecipitation—to determine the precise position of the double-strand break in the hormone-responsive promoter region of the target gene. In this method, the transient TopoIIβ-DNA complex was stabilized by an inhibitor that blocks the enzyme's DNA ligation activity. They further demonstrate that the presence of the transient double-strand break is mechanistically due to the action of the TopoIIβ component of a complex, which also includes two enzymes that sense DNA damage—poly(ADP-ribose) polymerase–1 (PARP-1) and DNA-dependent protein kinase (DNA-PK). The authors report that this DNA-strand break–dependent activation of gene expression occurs at other genes activated by nuclear receptors, suggesting that the mechanism is a prevailing strategy for gene activation.

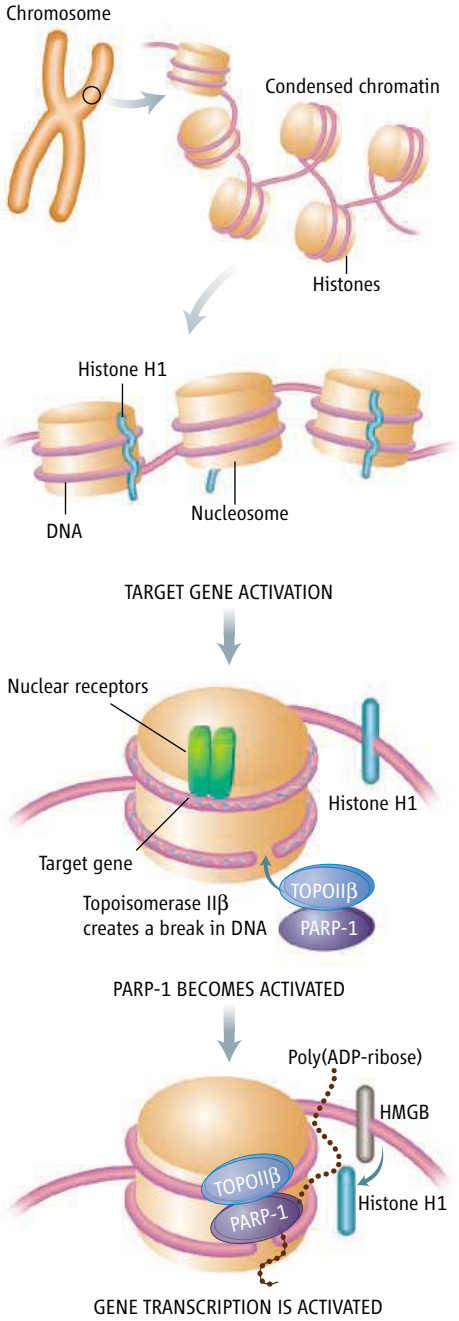

TopoIIβ and PARP-1 assemble in regulated gene transcription. Proposed regulatory mechanism required for gene expression mediated by a transient TopoIIβ-dependent DNA double-strand break. Upon binding of nuclear receptors to the target gene, TopoIIβ creates a nucleosome-specific DNA double-strand break. This likely triggers PARP-1's intrinsic catalytic activity, resulting in poly(ADP-ribosyl)ation of chromatin-associated proteins. Exchange of histone H1 for high mobility group B (HMGB) proteins appears to depend on the activation of PARP-1 during this gene-specific transcriptional activation.

PARP-1 has long been studied as a DNA damage–responsive enzyme because it is rapidly activated by DNA strand breaks, for which it has high affinity (*2*). Activated PARP-1 synthesizes large amounts of a highly negatively charged polymer, poly(ADP-ribose). It mostly attaches this molecule onto itself (automodification), but also onto histones H1, H2A, and H2B. This rapid but reversible poly(ADP-ribosyl)ation induces local relaxation of the chromatin structure, which in turn facilitates access of repair proteins to damaged DNA (*3*). The transient nature of poly(ADP-ribosyl)ation is regulated by poly(ADP-ribose) glycohydrolase (PARG), which restores the original state of modified proteins by hydrolyzing poly(ADP-ribose). Although PARP-1 interacts with several transcriptional complexes (*4*), it is unclear whether the intrinsic enzymatic activity of PARP-1 triggered by DNA-strand breaks is involved in the initiation of gene expression. Tulin and Spradling (*5*) first demonstrated that puffs (relaxed chromatin in actively transcribed regions) in polytene chromosomes of *Drosophila melanogaster* present increased amounts of poly(ADP-ribose) and require PARP-1 enzymatic function at sites of transcriptional activity induced by heat shock. Although the finding of massive poly(ADP-ribose) accumulation at puffs suggested that PARP-1 activation is important for local loosening of chromatin and transcriptional activation, the trigger of PARP-1 activation in this context remained obscure.

But various studies indicate that the regulation and function of PARP-1 are multifaceted. Ju *et al*. previously reported (*6*) that PARP-1 is a crucial component of the Groucho-transducin-

The authors are in the Health and Environment Unit, Faculty of Medicine, Laval University Medical Research Center, 2705 Boulevard Laurier, Quebec City, QC, G1V 4G2, Canada. E-mail: guy.poirier@crchul.ulaval.ca

like Enhancer-of-split corepressor complex that blocks transcription. In this context, PARP-1 activity is dispensable. However, upon stimulation of neuronal differentiation, PARP-1 activity is key to the dissociation of the corepressor complex and the assembly of a transcription activator complex, leading to expression of the transcription factor MASH1 (mammalian achaete-scute homolog 1). Surprisingly, the authors showed that PARP-1 phosphorylation by calcium-calmodulin–dependent protein kinase IIδ triggers PARP-1 activation. Recently, the nucleosome-binding properties of PARP-1 were shown to promote the formation of nuclease-resistant chromatin structures that are transcriptionally repressed, similar to what is observed upon the binding of the linker histone H1 to DNA (*7*). In the presence of nicotinamide adenine dinucleotide, PARP-1 is automodified and released from chromatin, promoting the formation of an open chromatin conformation that is permissive to transcription. These findings thus suggested that PARP-1 activation occurs in the absence of strand breaks and is important for transcriptional activation.

In contrast, others have presented convincing data supporting PARP-1 as a transcriptional coactivator, independent of its enzymatic activity. PARP-1 can act as a gene-specific coactivator of the transcription factor nuclear factor κB (NF-κB) in vitro (*8*). In response to inflammatory stimuli, acetylation of PARP-1 by p300/CREB-binding protein is required for NF-κB activation (*9*). Similarly, PARP-1 is required for retinoic acid–dependent transcription independently of its catalytic domain (*10*). By chromatin immunoprecipitation, the study found that direct interaction of PARP-1 with two proteins—the retinoic acid receptor and Mediator, a transcriptional coactivator—at the retinoic acid receptor (RARβ2) gene promoter was indeed sufficient to initiate transcription. It is therefore conceivable that PARP-1 might be required for at least two dependent functions: as a fundamental structural component of chromatin and, conversely, as a modulator of chromatin structure through its intrinsic enzymatic activity.

The new work by Ju *et al*. finally identifies a connection between initiation of transcription and sensing and repair of DNA double-strand breaks. Their findings reveal a new chromatin-specific function for TopoIIβ and suggest an active role for PARP-1 in transcription, in agreement with its function as a sensor of DNA breaks. However, beyond the mechanistic model proposed by Ju *et al*. and others, intriguing questions remain about the involvement of TopoIIβ–PARP-1–DNA-PK and poly(ADP-ribosyl)ation in transcription initiation. Elucidating the precise biochemical interactions that underlie the nucleosome-specific recruitment of TopoIIβ–PARP-1–DNA-PK repair complex awaits further study. Furthermore, the requirement for the DNA-damage repair proteins DNA-PK and PARP-1 remains unexplored. It will be interesting to define the precise role of PARP-1 activity in the exchange of histone H1 for high mobility group B proteins (chromatin-associated nucleoproteins that bend DNA and facilitate the binding of various transcription factors to their DNA targets) during gene-specific transcription initiation. Finally, current models overlook the role of PARG, the enzyme responsible for poly(ADP-ribose) hydrolysis, in transcriptional regulation. Yet, this enzyme appears to be as critical for the regulation of transcriptional events, as is PARP-1 (*11*). Nevertheless, the present work will undoubtedly stimulate new conceptual views about transcriptional control mechanisms and the interplay between regulated gene transcription and the DNA damage response.

References

1. B.-G. Ju *et al.*, *Science* **312**, 1798 (2006).
2. D. D'Amours, S. Desnoyers, I. D'Silva, G. G. Poirier, *Biochem. J.* **342**, 249 (1999).
3. M. Rouleau, R. A. Aubin, G. G. Poirier, *J. Cell Sci.* **117**, 815 (2004).
4. M. Y. Kim, T. Zhang, W. L. Kraus, *Genes Dev.* **19**, 1951 (2005).
5. A. Tulin, A. Spradling, *Science* **299**, 560 (2003).
6. B. G. Ju *et al.*, *Cell* **119**, 815 (2004).
7. M. Y. Kim, S. Mauro, N. Gevry, J. T. Lis, W. L. Kraus, *Cell* **119**, 803 (2004).
8. P. O. Hassa, M. Covic, S. Hasan, R. Imhof, M. O. Hottiger, *J. Biol. Chem.* **276**, 45588 (2001).
9. P. O. Hassa *et al.*, *J. Biol. Chem.* **280**, 40450 (2005).
10. R. Pavri *et al.*, *Mol Cell* **18**, 83 (2005).
11. A. Tulin, N. M. Naumova, A. K. Menon, A. C. Spradling, *Genetics* **172**, 363 (2006).

10.1126/science.1129808

PLANETARY SCIENCE

Our Local Astrophysical Laboratory

The behavior of the orbiting bodies within Saturn's rings, now being closely observed by the Cassini spacecraft, can inform our understanding of the birth of extrasolar planets.

Joseph A. Burns and Jeffrey N. Cuzzi

Saturn's elegant rings (see the figure, top and inset) embody all that is wondrous and exotic about the universe (*1*). Planetary rings are surely beautiful, but they also provide astronomers with nearby—albeit imperfect—analogs (*2*) for the very remote, massive protoplanetary disks (see the figure, bottom left) that surround many young stars and form the nurseries of extrasolar planets (*3*). Although the events deep within protoplanetary disks are obscured by dust and can only be inferred, ongoing observations of the Saturn system by the capable Cassini spacecraft (*1*) let us view—in real time—the complex dynamics that operate in our neighborhood's astrophysical disk. As described below, some of the processes that Cassini has observed address questions relevant to the solar system's origin: how hordes of orbiting bodies crowd together, how material accumulates in such systems to form moons or planets, and how nearby masses disturb—and are perturbed by—adjacent disks.

Saturn's rings and protoplanetary disks are both composed of innumerable small objects orbiting a dominant central mass. In the former case, centimeter- to meter-sized chunks of water ice orbit within a few planetary radii; in the latter, planetesimals (kilometer- to Mars-sized) circle at tens to hundreds of stellar radii. When such swarms of orbiting bodies collide with one another, they lose energy while conserving angular momentum. As a result, the systems flatten rapidly to thin disks that then inexorably spread radially unless some process halts their drift. In Saturn's rings, this evolution is interrupted at resonances, those specific orbital radii where the local orbital period is a simple ratio of a nearby perturbing satellite's orbital period. Resonances presumably play a comparable role in protoplanetary disks; indeed, the truncation of our asteroid belt's outer edge at a resonance with Jupiter gives evidence of a similar process having occurred in the early solar system. Adjacent to such resonant locations, a moon's gravity systematically perturbs a ring's mass distribution, thereby initiating spiral density or bending waves, which transfer angular momentum between the moons and the rings and ultimately drive them apart. An analogous process supposedly pushed many extrasolar planets unexpectedly close to their stars. This paradigm can be tested if, by mission's end, Cassini's precise observations identify changes in any moon's motion.

J. A. Burns is in the Departments of Astronomy and Theoretical and Applied Mechanics, Cornell University, Ithaca, NY 14853, USA. E-mail: jab16@cornell.edu J. N. Cuzzi is in the Space Science Division, NASA-Ames Research Center, Moffett Field, CA 94035, USA.

By causing satellites and rings to repel one another, this process can truncate rings and pry open gaps. Two of the most prominent clearings in Saturn's rings contain embedded moons: Pan amidst the broad Encke Gap (see the figure, inset) and the less massive Daphnis lurking in the narrower Keeler Gap. The comparison between Saturn's two examples of moon/gap configurations indicates that our angular momentum scaling law is basically correct. By surveying the distorted edges (shown in green in the figure inset) of the gaps where these embedded moons reside, one can watch the shepherding mechanism at work. A similar mechanism is likely responsible for the inferred openings in protoplanetary disks. Observations of the interactions between the dominant moonlets and other debris in these gaps may elucidate how planets continued to grow even after they cleared openings in protoplanetary disks.

The elementary model in which ring edges are maintained by satellite resonances predicts that a ring's periphery should contain an integer number of graceful sinusoidal scallops. For example, Saturn's A ring, which halts at Janus' 7:6 resonance, should exhibit seven oscillations. To examine this, Cassini is scanning the various ring edges around the ring's full circumference with unprecedented radial and longitudinal resolution (*4*). The shapes of the main rings' perimeters grossly fit our picture, but they are not nearly as simple as had been forecast. Elsewhere too, such as along the rims of the Encke and Keeler gaps, wavy edges change amplitude and form, bobbing along in unanticipated ways, only to later regain their previous shapes. Near most crisp ring boundaries and in other strongly perturbed regions, where angular momentum is most effectively exchanged, images intriguingly show that the ring's texture becomes ropy in places and strawlike elsewhere (*1*). What, if anything, might this anomalous behavior imply for angular momentum transfer in rings and protoplanetary disks?

Cassini's remote-sensing instruments have monitored the visibility of several bright stars as they drifted behind the nonuniform curtain that the rings present. The opacity of various ring regions can thereby be observed with exceptionally fine resolution. At many resonant locations, textbook-quality spiral density waves are sighted during these occultations and in other observations (*1*). Owing to the rings' small mass and proximity to Saturn, the waves are very tightly coiled—unlike the arms of spiral galaxies, which share their physics. In addition, occultation signals are abruptly cut off (in less than 10 m) at the sharpest ring boundaries (*5*), indicating very thin structures but also challenging our understanding of how satellite resonances can restrain material so effectively across such brief spans.

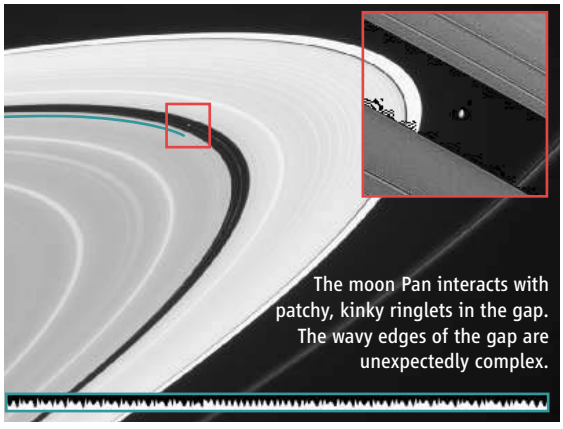

Occultations also probe the ring's microstructure on scales far too fine to observe any other way. Rather than being randomly distributed, the ensemble of ring particles aggregates into sausage-shaped clumps 5 to 10 m high, typically separated by ~100 m (*6*, *7*), especially in the outer regions of Saturn's rings. These tubes are canted relative to the orbital direction and have mostly cleared lanes between them. In numerical simulations (see the figure, bottom right), such structures are spontaneously and continuously generated as gravity attempts to assemble the numerous particles (*8*), but Saturn's tides shear them apart before they can fully agglomerate into small moons. Essentially, these particle concentrations are the manifestations of marginal gravitational instabilities in Saturn's disk. Many astronomers assume that such instabilities in the protoplanetary nebula's midplane particle layer led directly through collapse to planetesimals, but obviously that is not true here. The analogy may be imperfect, however, because nebular gas strongly alters the dynamics of 1-km and smaller bodies within a protoplanetary disk.

In protoplanetary disks, these processes lead eventually to the accretion of planets (*2*). However, in the case of planetary rings, growth is frustrated by tides and by strong radial velocity shears owing to the nearby planet. Thus, the presence of Pan and Daphnis within Saturn's disk is prima facie evidence that at least some saturnian ring particles arise from fragmentation of a larger body, most likely a primordial moon (*9*), rather than being the progeny of condensation/accumulation processes. The breakup scenario is further supported by Cassini's recent discovery of strong circumstantial evidence for the presence of 100-m ring particles that lie along the same power-law size distribution as the little moons (*10*). The interaction of these larger ring denizens with background material provides the opportunity to directly observe processes similar to those experienced by a planetesimal growing in a protoplanetary disk.

The Cassini mission, currently scheduled to end in summer 2008, may be extended for another 2 years. If so, it will observe dynamical events that should further test our theories. At equinox in fall 2009, the Sun will cross the ring plane to start warming the rings' northern side that had been shadowed for 15 years; any dusty rings that are susceptible to radiation forces will be driven southward. Late that year, the moon Prometheus will brush against its contiguous F ring, mimicking the overlapping orbits that once encouraged planets to grow in the solar nebula. As 2010 begins, the co-orbital moons Janus and Epimetheus will exchange positions, thus shifting their ring resonances slightly and initiating new density waves at these positions. Cassini's final observing sequences will give opportuni-

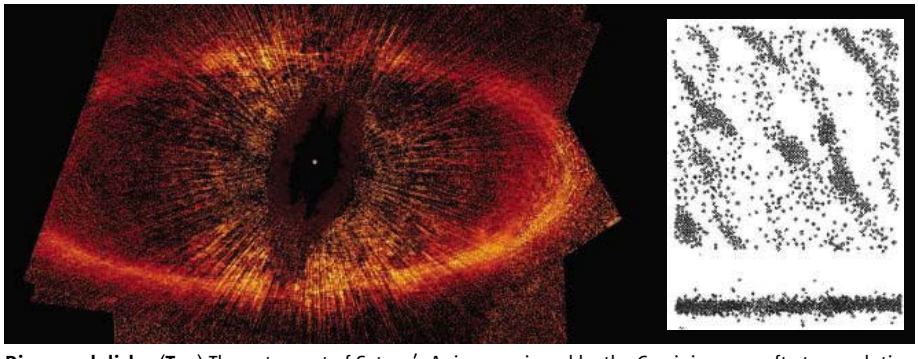

Rings and disks. (**Top**) The outer part of Saturn's A ring, as viewed by the Cassini spacecraft at a resolution of 10.4 km per pixel and a phase angle of 92.5°, shows several structures that are believed to have analogs in protoplanetary disks: The outer edges of the A ring and of the B ring (not shown) are caused by resonances with satellites that lie just beyond the ring system; small moons pry open the Encke and Keeler gaps, narrow dark arcs in the outer part of the A ring, as well as sculpting associated ringlets and gap edges. The sawtooth pattern at the bottom shows the radial structure of the green section of the inner edge of the Encke Gap. (**Inset**) The Encke Gap, taken at a resolution of 3.8 km per pixel at a phase angle of 18.5°, contains the embedded moon Pan. (**Bottom left**) False-color optical coronagraphic image taken by the Advanced Camera for Surveys on the Hubble Space Telescope shows a debris ring at Kuiper Belt distances surrounding Fomalhaut (HD 216956) with resolution of 0.5 astronomical units (*11*). (**Bottom right**) Particle positions after 15 orbital periods in a numerical simulation for a 112 m by 112 m patch containing 1600 gravitating and dissipative bodies that reside at 110,000 km in Saturn's rings (*8*).

CREDIT: SATURN IMAGES, NASA/JPL/SPACE SCIENCE INSTITUTE, ASSEMBLED BY M. TISCURENO/CORNELL UNIVERSITY; HUBBLE IMAGE, NASA/SPACE TELESCOPE SCIENCE INSTITUTE

ties to emphasize those measurements of our local astrophysical laboratory that will best illuminate how these fundamental cosmic entities operate. Moreover, observations to date already indicate that the Saturn system is literally changing before our eyes. We anticipate that even more dramatic transformations in our neighborhood's astrophysical laboratory will be monitored by Cassini's instruments over the next several years.

References and Notes

1. Special Issue on Cassini at Saturn, *Science* **307** (25 February 2005).
2. J. J. Lissauer, J. N. Cuzzi, in *Protostars and Planets II*, D. C. Black, M. S. Matthews, Eds. (Univ. of Arizona Press, Tucson, AZ, 1985), pp. 920–958.
3. Special Issue on Disks in Space, *Science* **307** (7 January 2005).
4. M. S. Tiscareno *et al.*, paper presented at the American Geophysical Union fall meeting, 5 to 9 December 2005, San Francisco (abstract FM-P33B0245T2005).
5. J. E. Colwell, personal communication.
6. J. E. Colwell, L. W. Esposito, M. Sremcevic, *Geophys. Res. Lett.* **33**, L07201 (2006).
7. M. M. Hedman, P. D. Nicholson, B. D. Wallis, paper presented at the American Geophysical Union fall meeting, 5 to 9 December 2005, San Francisco (abstract FM-P31D02H2005).
8. H. Salo, *Icarus* **117**, 287 (1995).
9. A. W. Harris, in *Planetary Rings*, R. J. Greenberg, A. Brahic, Eds. (Univ. of Arizona Press, Tucson, AZ, 1984), pp. 641–658.
10. M. S. Tiscareno *et al.*, *Nature* **440**, 648 (2006).
11. P. Kalas, J. R. Graham, M. Clampin, *Nature* **435**, 1067 (2005).

12. Support from the Cassini project is gratefully acknowledged. We thank M. Tiscareno, M. Hedman, and P. Nicholson for comments.

10.1126/science.1114856

CLIMATE CHANGE

Threats to Water Supplies in the Tropical Andes

Climate models predict that greenhouse warming will cause temperatures to rise faster at higher than at lower altitudes. In the tropical Andes, glaciers may soon disappear, with potentially grave consequences for water supplies.

Raymond S. Bradley, Mathias Vuille, Henry F. Diaz, Walter Vergara

According to general circulation models of future climate in a world with double the preindustrial carbon dioxide (CO_2) concentrations, the rate of warming in the lower troposphere will increase with altitude. Thus, temperatures will rise more in the high mountains than at lower elevations (see the figure) (*1*). Maximum temperature increases are predicted to occur in the high mountains of Ecuador, Peru, Bolivia, and northern Chile. If the models are correct, the changes will have important consequences for mountain glaciers and for communities that rely on glacier-fed water supplies.

Is there evidence that temperatures are changing more at higher than at lower elevations? Although surface temperatures may not be the same as in the free air, in high mountain regions the differences are small (*2*), and changes in temperature should thus be similar at the surface and in the adjacent free air. Unfortunately, few instrumental observations are available above ~4000 m. The magnitude of recent temperature change in the highest mountains is therefore poorly documented. An analysis of 268 mountain station records between 1°N and 23°S along the tropical Andes indicates a temperature increase of 0.11°C/decade (compared with the global average of 0.06°C/decade) between 1939 and 1998; 8 of the 12 warmest years were recorded in the last 16 years of this period (*3*). Further insight can be obtained from glaciers and ice caps in the very highest mountain regions, which are strongly affected by rising temperatures. In these high-altitude areas, ice masses are declining rapidly (*4*–*6*). Indeed, glacier retreat is under way in all Andean countries, from Columbia and Venezuela to Chile (*7*).

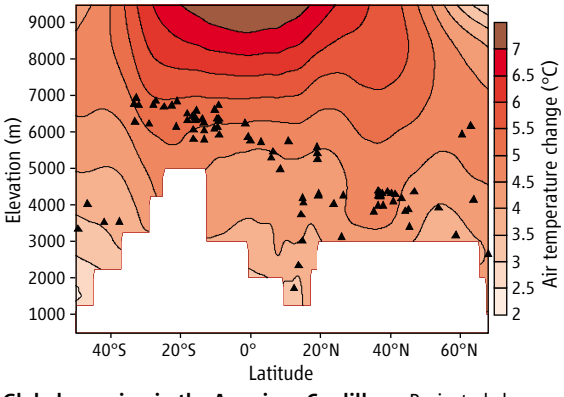

Global warming in the American Cordillera. Projected changes in mean annual free-air temperatures between (1990 to 1999) and (2090 to 2099) along a transect from Alaska (68°N) to southern Chile (50°S), following the axis of the American Cordillera mountain chain. Results are the mean of eight different general circulation models used in the 4th assessment of the Intergovernmental Panel on Climate Change (IPCC) (*15*), using CO_2 levels from scenario A2 in (*16*). Black triangles denote the highest mountains at each latitude; areas blocked in white have no data (surface or below in the models). Data from (*15*).

A convergence of factors contribute to these changes. Rising freezing levels (the level where temperatures fall to 0°C in the atmosphere) (*8*, *9*) lead to increased melting and to increased exposure of the glacier margins to rain rather than snow (*10*). Higher near-surface humidity leads to more of the available energy going into melting snow and ice, rather than sublimation, which requires more energy to remove the same mass of ice. Therefore, during humid, cloudy conditions, there is often more ablation than during drier, cloud-free periods (*6*). In some areas, changes in the amount of cloud cover and the timing of precipitation may have contributed to glacier mass loss through their impact on albedo (surface reflectivity) and the net radiation balance (*11*). As these processes continue and snow is removed, more of the less reflective ice is exposed and absorption of the intense high-elevation radiation increases, thus accelerating the changes under way through positive feedbacks.

The processes involved in mass-balance changes at any one location are complex, but temperature is a good proxy (*12*) for all these processes, and most of the observed changes are linked to the rise in temperature over recent decades (*5*). Further warming of the magnitude shown in the figure will thus have a strong negative impact on glaciers throughout the Cordillera of North and South America. Many glaciers may completely disappear in the next few decades, with important consequences for people living in the region (*7*).

Although an increase in glacier melting initially increases runoff, the disappearance of glaciers will cause very abrupt changes in streamflow, because of the lack of a glacial buffer during the dry season. This will affect the availability of drinking water, and of water for agriculture and hydropower production.

In the High Andes, the potential impact of such changes on water supplies for human con-

R. S. Bradley and M. Vuille are at the Climate System Research Center, Department of Geosciences, University of Massachusetts, Amherst, MA 01003, USA. H. F. Diaz is at the Earth System Research Laboratory, National Oceanic and Atmospheric Administration, Boulder, CO 80303, USA. W. Vergara is in the Latin America Environment Department, World Bank, 1850 I Street, NW, Washington, DC 20433, USA. E-mail: rbradley@geo.umass.edu (R.S.B.)

sumption, agriculture, and ecosystem integrity is of grave concern. Many large cities in the Andes are located above 2500 m and thus depend almost entirely on high-altitude water stocks to complement rainfall during the dry season. For example, Ecuador's capital Quito currently receives part of its drinking water from a rapidly retreating glacier on Volcano Antizana. Other cities, like La Paz in Bolivia and many smaller population centers, likewise partially depend on glacier sources for drinking water. In many dry inter-Andean valleys, agriculture relies on glacier runoff; for instance, ~40% of the dry-season discharge of the Rio Santa, which drains the Cordillera Blanca in Peru, comes from melting ice that is not replenished by annual precipitation (*13*). As these water-resource buffers shrink further (and, in some watersheds, disappear completely), alternative water supplies may become very expensive and/or impractical in the face of increased demand as population and per-capita consumption rise.

Furthermore, in most Andean countries, hydropower is the major source of energy for electricity generation. As these water resources are affected by reductions in seasonal runoff, these nations may have to shift to other energy sources, resulting in large capital outlays, higher operational and maintenance costs, and—most probably—an increased reliance on fossil fuels.

We have focused here on changes taking place in the mountains of the tropical Andes, but the same situation prevails in high mountain regions elsewhere in the Tropics. Glaciers are disappearing rapidly in East Africa and New Guinea, though there is far less reliance on glacier-fed water supplies in those regions. It is in the tropical Andes that climate change, glaciers, water resources, and a dense (largely poor) population meet in a critical nexus. Some glaciers have already reached the threshold at which they are destined to disappear completely; for many more, this threshold may be reached within the next 10 to 20 years. Therefore, governments must plan without delay to avoid large-scale disruption to the people and economy of those regions (*14*).

Practical measures to prepare for, and adapt to, these changes could include conservation of (or price controls on) water supplies in urban areas, a shift to less water-intensive agriculture, the creation of highland reservoirs to stabilize the cycle of seasonal runoff, and a shift to power generation from resources other than hydropower. At the same time, more detailed scenarios of future climate change in these topographically complex regions are urgently needed. High-resolution regional climate models allow for a better simulation of climate in mountain regions than do general circulation models. Coupled with tropical glacier–mass balance models, these regional models will help us to better understand and predict future climate changes and their impacts on tropical Andean glaciers and associated runoff.

Recent high-resolution (grid size ~10 km) regional climate simulations for the Colombian Andes indicate that even at relatively low altitudes, projected temperature increases and changes in rainfall patterns have the potential to disrupt water and power supplies to large segments of the population (*14*). Such simulations must be used to inform decision-makers of the steps they need to take to avoid a very problematical future in the region.

References and Notes

1. R. S. Bradley, F. T. Keimig, H. F. Diaz, *Geophys. Res. Lett.* **31**, L16210 (2004).
2. D. J. Seidel, M. Free, *Clim. Change* **59**, 53 (2003).
3. M. Vuille, R. S. Bradley, M. Werner, F. T. Keimig , *Clim. Change* **59**, 75 (2003).
4. E. Ramirez *et al*., *J. Glaciol*. **47**, 187 (2001).
5. B. Francou, M. Vuille, P. Wagnon, J. Mendoza, J.-E. Sicart, *J. Geophys. Res*. **108**, 4154 (2003).
6. G. Kaser, C. Georges, I. Juen, T. Molg, in *Global Change and Mountain Regions: A State of Knowledge Overview*, U. Huber, H. K. M. Bugmann, M. A. Reasoner, Eds. (Kluwer, New York, 2005), pp. 185–195.
7. A. Coudrain, B. Francou, Z. W. Kundzewicz, *Hydrol. Sci. J.* **50**, 925 (2005).
8. J. F. Carrasco, G. Casassa, J. Quintana, *Hydrol. Sci. J.* **50**, 933 (2005).
9. H. F. Diaz, N. E. Graham, *Nature* **383**, 152 (1996).
10. B. Francou, M. Vuille, V. Favier, B. Cáceres, *J. Geophys. Res.* **109**, D18106 (2004).
11. P. Wagnon, P. Ribstein, B. Francou, J.-E. Sicart, *J. Glaciol*. **47**, 21 (2001).
12. From 1999 to 2002, some glaciers had neutral or slightly positive mass balance as a result of a prolonged La Niña episode. Since 2002, glaciers are again retreating everywhere, and temperatures have rebounded upwards.
13. B. G. Mark, J. M. McKenzie, I. J. Gómez, *Hydrol. Sci. J.* **50**, 975 (2005).
14. W. Vergara, *Adapting to Climate Change. Latin America and Caribbean Region Sustainable Development Working Paper 25* (World Bank, Washington, DC, 2005).
15. www-pcmdi.llnl.gov/ipcc/about_ipcc.php
16. Nebojsa Nakicenovic, Rob Swart, Eds., *Special Report on Emissions Scenarios* (Cambridge Univ. Press, Cambridge, U.K., 2000).

17. We acknowledge the international modeling groups for providing their data for analysis; the Program for Climate Model Diagnosis and Intercomparison (PCMDI) for collecting and archiving the model data; the Johnson Space Center/Climate Variability and Predictability (JSC/CLIVAR) Working Group on Coupled Modelling (WGCM) and their Coupled Model Intercomparison Project (CMIP) and Climate Simulation Panel for organizing the model data analysis activity; and the IPCC WG1 Technical Support Unit for technical support. The IPCC Data Archive at Lawrence Livermore National Laboratory is supported by the Office of Science, U.S. Department of Energy (DOE). This research was supported by the Office of Science (Office of Biological and Environmental Research), U.S. DOE, grant DE-FG02-98ER62604 and NSF grant EAR-0519415.

10.1126/science.1128087

CELL SIGNALING

A New Way to Burn Fat

Jaap G. Neels and Jerrold M. Olefsky

Acetyl-CoA carboxylase controls fat storage and utilization in adipose cells. An important regulator of this enzyme modulates its degradation and is a potential therapeutic target for treatment of insulin resistance and obesity.

Storage of body fat creates an energy reserve for times of starvation, but excess body fat, or obesity, substantially increases the risk for diabetes, cardiovascular disease, and other disorders. So the appropriate balance between fat storage and utilization is clearly important. Adipose tissue acetyl–coenzyme A (CoA) carboxylase (ACC) plays a crucial role in maintaining this balance, and regulation of this enzyme is tied to the overall control of energy metabolism. On page 1763 of this issue, Qi *et al*. (*1*) show that the mammalian protein TRB3 mediates degradation of adipose tissue ACC, providing a new level of metabolic regulation for this key enzyme.

ACC regulates lipid storage and overall energy metabolism by catalyzing the formation of malonyl-CoA from acetyl-CoA (*2*). In turn, malony-CoA has two important functions with respect to overall triglyceride storage (see the figure). It serves as the essential substrate for fatty acid synthesis, but it also blocks the uptake of fatty acids from the cytosol into the mitochondria, where they undergo oxidative metabolism to generate adenosine 5′-triphosphate (*2*). Through these effects, malonyl-CoA is a key control point for fat metabolism in peripheral tissues, including adipose tissue, suggesting that it may also have central effects within the hypothalamus to regulate energy balance (*3*).

There are two major isoforms of ACC in rodents and humans, each the product of a separate gene. ACC1 is highly expressed in lipogenic tissues such as liver, adipose, and lactating mammary gland, whereas ACC2 is predominantly expressed in heart and skeletal muscle and, to a lesser extent, in the liver (*2*). ACC1 is a cytosolic enzyme and ACC2 is associated with the mitochondria. The tissue distribution and intracellular localization of each isoform suggest that mitochondrial-associated ACC2 generates the malonyl-CoA that is

The authors are in the Department of Medicine, University of California, San Diego, 9500 Gilman Drive, La Jolla, CA 92093–0673, USA. E-mail: jolefsky@ucsd.edu

tightly coupled to inhibition of mitochondrial fatty acid oxidation. Cytosolic ACC1 produces malonyl-CoA destined for lipogenesis. Consistent with this notion, ACC2-deficient mice are leaner than wild-type mice due to increased fat oxidation in heart and skeletal muscle (*4*), whereas mice specifically lacking hepatic ACC1 show significantly less de novo fatty acid synthesis and triglyceride accumulation in the liver (*5*). In rats, blocking expression of both isoforms markedly reduces the concentrations of long-chain acyl-CoAs, diacylglycerol, and triglycerides in the liver, improving hepatic insulin sensitivity (*6*).

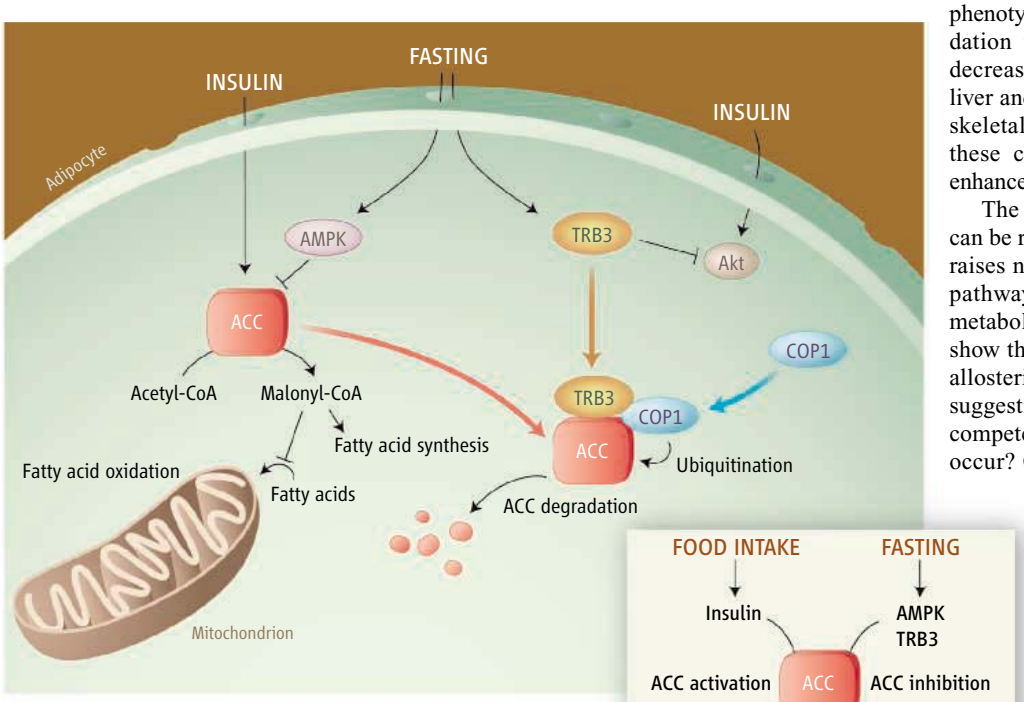

Balancing fat storage and utilization. Integration of signaling pathways regulating ACC enzymatic activity in response to fasting or food intake. The protein TRB3 controls ACC degradation. AMPK, adenosine monophosphate–dependent protein kinase.

ACC activity is acutely regulated by allosteric effectors and phosphorylation reactions (*2*). For example, citrate and other carboxylic acids can activate the enzyme by allosteric mechanisms. Insulin signaling leads to phosphorylation and dephosphorylation of ACC (on different sites), but the net effect is to activate the enzyme. Activation of adenosine monophosphate–dependent protein kinase (AMPK) by fasting, exercise, or hormonal stimulation inhibits ACC activity through yet a different set of phosphorylation sites (*2*).

TRB3, the other molecule studied by Qi *et al.*, strongly resembles tribbles, a protein in *Drosophila melanogaster* that promotes ubiquitination and proteasomal degradation of other proteins (*7*). Like tribbles, TRB3 lacks detectable kinase activity and is thought to function as an adaptor protein. TRB3 expression is induced by fasting and by "stress" in the endoplasmic reticulum (such as the accumulation of misfolded proteins). It is also overexpressed in mouse models of insulin resistance (*8, 9*). TRB3 specifically blocks the actions of insulin in the liver by binding to the enzyme Akt. Thus, Akt cannot be phosphorylated and activated in response to insulin (*8*). Because stimulation of Akt inhibits glucose production by the liver, excess TRB3 should cause hepatic insulin resistance. In agreement with this, overexpression of TRB3 in isolated rat liver cells blocks the action of insulin, and in transgenic mice, overexpression of TRB3 in the liver promotes hyperglycemia by increasing hepatic glucose production (*8*). In contrast, inhibition of TRB3 expression in mouse liver improves insulin sensitivity and lowers hepatic glucose production (*10*).

Qi *et al.* report a new Akt-independent effect of TRB3. In addition to blocking insulin's action in the liver through inhibition of Akt, TRB3 regulates the cellular protein level of ACC (*1*). The authors show that TRB3 acts as an adaptor protein between ACC, a protein called constitutive photomorphogenic protein 1 (COP1), and other components of an E3 ubiquitin ligase. The ubiquitin-proteasome system is the major pathway of selective protein degradation in eukaryotic cells (*11*). Therefore, by mediating an interaction between COP1 and ACC, TRB3 triggers the ubiquitination and subsequent degradation of ACC. Indeed, adipocytes deficient in TRB3 accumulate larger amounts of ACC protein than do wild-type cells, and this should shift the balance of energy metabolism toward fatty acid oxidation. Not surprisingly, transgenic mice that overexpress TRB3 in adipose tissue eat more food but gain less weight than wild-type mice. Although these TRB3-overexpressing mice have a higher caloric intake, they also exhibit increased fatty acid oxidation, converting more fat into energy. Their increase in core body temperature suggests that this excess energy is released in the form of heat. This lean phenotype is driven by increased fatty acid oxidation in adipose tissue and also leads to decreased triglyceride accumulation in the liver and, although not measured, probably in skeletal muscle. As would be expected from these changes, these animals also display enhanced insulin sensitivity.

The surprising finding that energy balance can be regulated through degradation of ACC raises new questions about how the different pathways that control this key step in lipid metabolism converge on one another. Qi *et al.* show that ubiquitination of ACC inhibits the allosteric activation of the enzyme by citrate, suggesting that these two regulatory pathways compete with each other. But how might this occur? One possibility is that ACC ubiquitination disrupts the binding motif of the allosteric activator, resulting in competition between these two regulatory pathways. This also raises the question of how formation of the ACC-TRB3-COP1 complex and/or ubiquitination affects regulation of ACC by phophorylation, or whether phosphorylation or insulin treatment affects ubiquitination of ACC. Do these regulatory pathways also compete with each other, or do they act in concert?

In a broader sense, the Qi *et al.* findings strengthen the notion that under certain circumstances it may be beneficial to disrupt insulin signaling, and TRB3 can play a dual role in this. For example, in the adaptations to fasting, anabolic pathways, such as those stimulated by insulin, are suppressed and catabolic mechanisms are activated. This action is mediated by the fasting-induced fall in circulating insulin concentrations and the induction of hepatic TRB3 expression. Both effects favor glycogenolysis and gluconeogenesis, allowing maintenance of glucose production by the liver to provide a continuous supply of glucose for the central nervous system. In fat and muscle, insulin promotes lipogenesis, and because TRB3 causes ACC degradation, this shifts the balance of fatty acid metabolism away from lipogenesis to oxidation, allowing these tissues to derive their energies from fatty acids rather than glucose during fasting. These studies again show the parsimony of metabolic design. TRB3, a relatively new player on the metabolic

stage, accomplishes its tissue-specific tasks of counterbalancing insulin action through two unique mechanisms. In the liver, TRB3 blocks insulin action by interfering with Akt activation. In fat tissue, whereas insulin promotes lipogenesis, TRB3 causes ACC degradation, shifting the balance of fatty acid metabolism away from lipogenesis to oxidation. Together, the regulatory pathways acting on ACC, and in particular the novel role of TRB3, provide interesting therapeutic targets for the treatment of insulin resistance and obesity.

References

1. L. Qi *et al.*, *Science* **312**, 1763 (2006).
2. R. W. Brownsey, A. N. Boone, J. E. Elliott, J. E. Kulpa, W. M. Lee, *Biochem. Soc. Trans.* **34**, 223 (2006).
3. Z. Y. Hu, S. H. Cha, S. Chohnan, M. D. Lane, *Proc. Natl. Acad. Sci. U.S.A.* **100**, 12624 (2003).
4. L. Abu-Elheiga, M. M. Matzuk, K. A. H. Abo-Hashema, S. J. Wakil, *Science* **291**, 2613 (2001).
5. J. Mao *et al.*, *Proc. Natl. Acad. Sci. U.S.A.* **103**, 8552 (2006).
6. D. B. Savage *et al.*, *J. Clin. Invest.* **116**, 817 (2006).
7. A. R. Saltiel, *N. Engl. J. Med.* **349**, 2560 (2003).
8. K. Du, S. Herzig, R. N. Kulkarni, M. Montminy, *Science* **300**, 1574 (2003).
9. C. A. Corcoran *et al.*, *Cancer Biol. Ther.* **4**, 1063 (2005).
10. S. H. Koo *et al.*, *Nat. Med.* **10**, 530 (2004).
11. D. Nandi, P. Tahiliani, A. Kumar, D. Chandu, *J. Biosci.* **31**, 137 (2006).

10.1126/science.1130476

OCEANOGRAPHY

A Direct Proxy for Oceanic Phosphorus?

New results suggest that deep-sea corals record the concentration of phosphorus in the deep sea. If proven reliable, this method may provide insights into past ocean circulation patterns.

Edward A. Boyle

There are many reasons why we would like to know the distribution of oceanic nutrients in the oceans of the past. The biogeochemical cycling of dissolved inorganic phosphorus (P) and other nutrients serves as a tracer of deep-ocean water masses and of ocean circulation patterns that influence climate. Phosphorus is also a key requirement for marine life. It depends on the rock-weathering cycle for its steady supply to the ocean (in contrast to equally important nitrogen, which is fixed biologically from atmospheric N_2). Because of biotic uptake of carbon dioxide, changes in oceanic phosphorus affect past atmospheric CO_2 concentrations. Paleophosphorus data could thus help to elucidate the effect of changing phosphorus distributions on marine biota and on global climate. On page 1788 of this issue, Montagna *et al.* (*1*) propose that the phosphorus concentration of solitary deep-sea corals is a reliable indicator of past ocean phosphorus concentrations.

Past ocean circulation patterns can be studied through indirect tracers such as carbon isotopes or cadmium in calcareous foraminifera. These tracers are linked to the phosphorus cycle by biological uptake in the upper ocean and subsequent decay of sinking organic matter with approximately fixed C:P:Cd ratios and $\delta^{13}C$ values. Phosphorus concentrations can be inferred from these tracers only by making assumptions that may not hold at all times. For example, the absolute deep-sea phosphorus concentration can be estimated from measurements of carbon isotopes in coexisting planktonic (surface-dwelling) and benthic (bottom-dwelling) foraminifera by assuming that the C:P ratio in biogenic organic matter is precisely fixed. But this assumption has been challenged; for example, it has been suggested that the organic C:N ratio is fixed but the marine C:P ratio adapts to the availability of phosphorus (*2*, *3*).

A direct phosphorus tracer (or proxy) is thus highly desirable, but previous efforts to establish such a proxy have not been fruitful. Studies of the phosphorus concentrations of foraminifera shells (see the figure, top panel) (*4*, *5*) have shown that foraminiferal phosphorus resides mainly in inorganic coatings (such as ferromanganese phases) on the surface. These coatings can be removed by chemical cleaning in the laboratory, but it is then seen that there is very little phosphorus substitution into the crystalline calcite lattice. These reactive surface coatings probably form during sediment diagenesis and are not likely to be reliable indicators of deep-sea phosphorus concentrations. Fe:P ratios in particles from hydrothermal vent plumes are clearly related to the phosphorus levels of the deep sea, and it has been proposed that perhaps hydrothermal sediments might preserve this chemical relationship (*6*). However, studies of phosphorus in hydrothermal sediments have not established a consistent relation (*7*), probably as a result of early sedimentary diagenesis and the incorporation of other phosphorus-bearing phases such as fish teeth. Hence, there are no previous reports of a reliable direct tracer for deep-sea phosphorus levels.

Tracing phosphorus. A benthic foraminifera shell (*Cibicidoides wuellerstorfi*, **top**, diameter ~1 mm) is not a good tracer of deep-ocean phosphorus concentrations, whereas the deep-sea coral (*Desmophyllum dianthus*, **bottom**, diameter ~10 cm) appears to be, most likely because of different calcification mechanisms.

Montagna *et al*. now propose that the phosphorus concentration of certain portions of the solitary deep-sea coral *Desmophyllum dianthus* (see the figure, bottom panel) is a reliable indicator of oceanic phosphorus concentrations. Their suggestion is based on laser ablation inductively coupled plasma mass spectrometry (LA-ICPMS) measurements of phosphorus in six deep-sea corals that grew in waters with dissolved inorganic phosphorus concentrations ranging from 0.2 to 2 μmol/kg. The measurements were restricted to the aragonite fibers on the outer faces of each septum (leaf-like structural elements), avoiding early-mineralizing centers of calcification that make up the central midplane of each septum.

The phosphorus concentrations in these corals ranged linearly from 0.1 to 1.3 mmol P per mole of Ca, with a $[P/Ca]_{coral}$:$[P/Ca]_{water}$ ratio of ~7. Note that LA-ICPMS does not determine the chemical form of the phosphorus, so we are not

The author is in the Department of Earth, Atmospheric and Planetary Sciences, Massachusetts Institute of Technology, Cambridge, MA 02139, USA. E-mail: eaboyle@mit.edu

CREDITS: (TOP TO BOTTOM) ED BOYLE; TOM KLEINDINST/WOODS HOLE OCEANOGRAPHIC INSTITUTION

certain whether the phosphorus is bound in the inorganic lattice or in organic phases or ferromanganese coatings. The authors argue against the importance of the latter phases, but others will demand direct proof eventually.

Why do corals appear to slightly concentrate phosphorus relative to calcium and to consistently record its concentration values, whereas foraminifera discriminate against phosphorus, leaving no trace of its concentration in their shells? One obvious difference is that these corals are aragonitic, whereas the benthic foraminifera are calcitic (aragonite and calcite are two different crystal forms of $CaCO_3$). But I suspect that the crystal form is not the cause of these differences.

Rather, I would point to differences between the modes of calcification between foraminifera and corals. Foraminifera engulf vacuoles of seawater into their interiors and then chemically modify these vacuoles as they are transported to the site of calcification (*8*). In contrast, coral anemone polyps transport Ca^{2+} and H^+ ions and gaseous CO_2 across their cell membrane into an extracellular reservoir at the base of the polyp, where the fluid is drawn from external seawater (*9*). As a result of this difference in the mode of calcification, the chemical compositions of corals are quite different from those of foraminifera, with coral elemental concentration ratios values close to seawater values for many elements such as Sr/Ca and U/Ca, whereas foraminifera—including an aragonitic species—strongly discriminate against these elements.

Montagna *et al.* also provide data from an older coral that indicate much higher deep-sea phosphorus in the Mediterranean Sea at 11,200 years ago, some time after the end of the Younger Dryas cold event [~12,900 to 11,600 years ago (*10*)]. The authors attribute this increase in nutrients to extra inputs of phosphorus into the Mediterranean caused by an intensification of the African monsoon. This example indicates that deep-sea nutrient changes occur and can be studied by this new tracer archive.

The report by Montagna *et al.* will probably set off a gold rush by other laboratories attempting to test and verify the calibration data set with different samples and analytical methods, and to establish whether this proxy is free from artifacts. If the calibration proves robust, dated coral samples from the deep Atlantic and deep Pacific oceans must be tested to see whether the global average ocean phosphorus concentration increases during glaciations—as was originally suggested by Broecker (*11*) but subsequently discounted because of inconsistencies with other proxy tracers—and whether this direct phosphorus proxy verifies conclusions drawn from the indirect carbon isotope and cadmium proxies.

Many other problems can also be tackled by the collection of solitary corals from different times and places. For example, deep-sea corals can provide direct pictures of deep-sea phosphorus distributions to complement the radiocarbon age information that the corals also provide. Alternatively, solitary corals from Antarctic continental shelves might finally determine whether Antarctic waters were nutrient-depleted during glacial maxima, as supposed by some theories of glacial atmospheric CO_2.

Now, if only we could find a direct proxy for oceanic nitrate!

References

1. P. Montagna *et al.*, *Science* **312**, 1788 (2006).
2. M. B. McElroy, *Nature* **302**, 328 (1983).
3. W. S. Broecker, G. M. Henderson, *Paleoceanography* **13**, 352 (1998).
4. M. R. Palmer, *Earth Planet. Sci. Lett.* **73**, 285 (1985).
5. B. A. Sherwood, S. L. Sager, H. D. Holland, *Geochim. Cosmochim. Acta* **51**, 1861 (1987).
6. R. A. Feely, J. H. Trefry, G. T. Lebon, C. R. German, *Geophys. Res. Lett.* **25**, 2253 (1998).
7. T. Schaller, J. Morford, S. R. Emerson, R. A. Feely, *Geochim Cosmochim. Acta* **64**, 2243 (2000).
8. J. Erez, *Rev. Mineral. Geochem.* **54**, 115 (2003).
9. J. F. Adkins, E. A. Boyle, W. B. Curry, A. Lutringer, *Geochim. Cosmochim. Acta* **67**, 1129 (2003).
10. R. B. Alley *et al.*, *J. Geophys. Res.* **102**, 26367 (1997).
11. W. S. Broecker, *Geochim. Cosmochim. Acta* **46**, 1689 (1982).

10.1126/science.1129723

ASTRONOMY

Very Energetic γ-Rays from Microquasars and Binary Pulsars

Compact astrophysical objects produce some of the highest energy light in the universe. The challenge is to determine what mechanism produces these photons.

I. F. Mirabel

A new window on the universe is presently being opened by ground-based telescopes that survey the sky by detecting very-high-energy (VHE) photons, which have energies greater than 100 gigaelectron volts (GeV). Because of their high sensitivity, and high angular and energy resolution, these telescopes are identifying a plethora of new extragalactic and galactic sources of VHE radiation. The galactic center, supernovae remnants, pulsar-wind nebulae, and a new class of binary stars called γ-ray binaries have all been identified as VHE sources in the Milky Way. On page 1771 of this issue, Albert *et al.* (*1*) confirm the identification of the object designated LSI +61 303 as the third γ-ray stellar binary known so far, and report a time variability in the signal that may point to a mechanism for the VHE emission.

A microquasar-jet (*2*) model (see the figure, left panel) has been proposed to account for the VHE emission from another γ-ray binary, LS 5039 (*3*). For LSI +61 303, Albert *et al.* favor a mechanism, called inverse Compton scattering, by which relativistic electrons collide with stellar and/or synchrotron photons and boost their energies to the VHE range (*4*, *5*). VHE photons have also been detected from blazars, namely, active galactic nuclei (AGN) whose jets are closely aligned with our line of sight. Because the particle energy in microquasar jets is comparable to that of particles in AGN jets (*2*), it is expected that microquasars with jets pointing to the Earth may appear as scaled-down versions of blazars, which have been named microblazars (*6*). This idea has been strengthened by recent observations showing that the kinetic power of microquasar jets may be more than 10^{39} ergs s^{-1}, which is larger than the radiated power (*7*). Furthermore, microquasar jets trigger shocks where electrons are accelerated up to teraelectron-volt energies (*8*), providing the necessary conditions for VHE emission.

Alternatively, relativistic particles can be injected into the surrounding medium by the wind from a young pulsar (*9*). In this scenario the slowing rotation of a young pulsar provides stable energy to the nonthermal relativistic particles in the shocked pulsar-wind material flowing outward from the binary companion (see the figure, right panel). As in the microquasar-jet model proposed for LSI +61 303 by Albert *et al.*, the γ-ray emission is produced by inverse Compton scattering of the electrons from the pulsar wind on stellar photons. In this context, LSI +61 303 would resemble the γ-ray binary PSR B1259-63, a radio pulsar in an eccentric orbit around a star of spectral type Be (*10*).

The compact objects in these three γ-ray

The author is at the European Southern Observatory in Chile, Alonso de Cordova 3107, Santiago, Chile, on leave from Commissariat à l'Energie Atomique, Saclay, Gif-sur-Yvette, France 91191. E-mail: fmirabel@eso.org

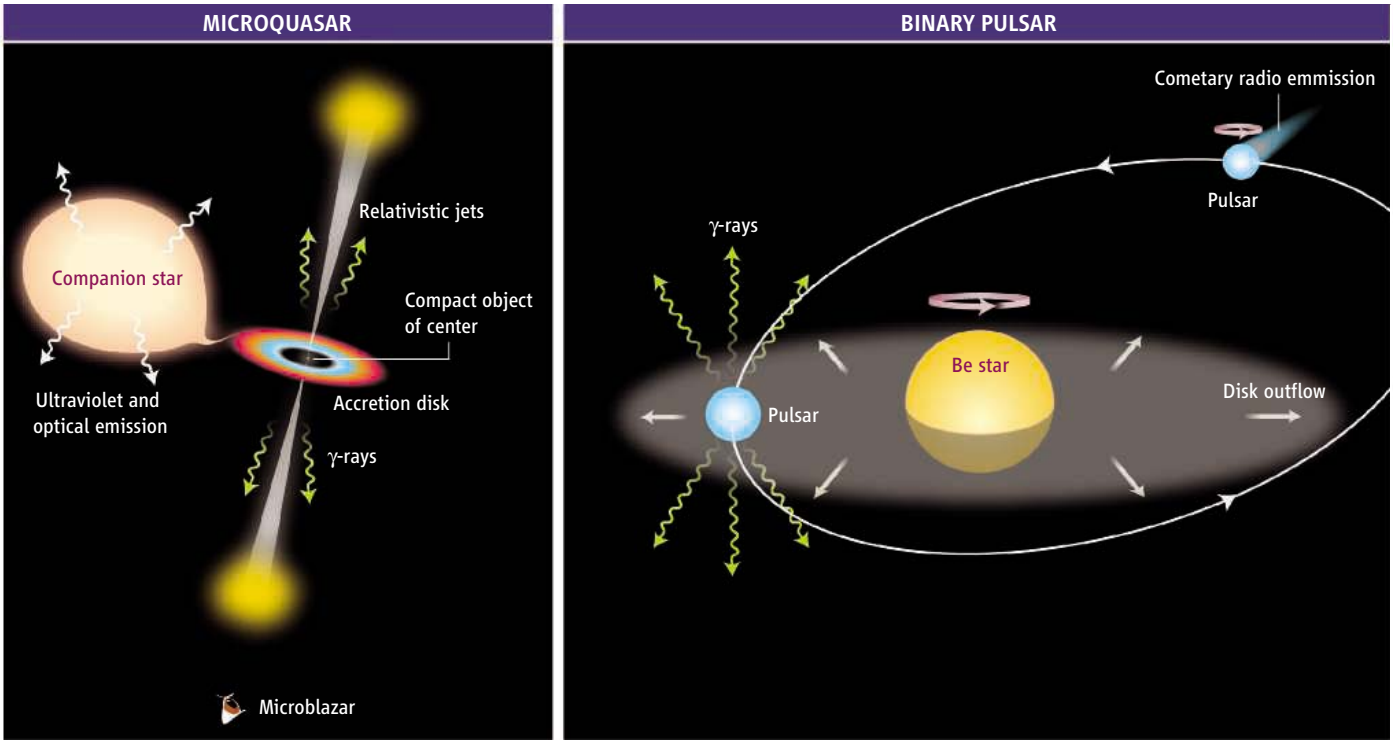

Alternative models for very energetic γ-ray binaries. (**Left**) Microquasars are powered by compact objects (neutron stars or stellar-mass black holes) via mass accretion from a companion star. This produces collimated jets that, if aligned with our line of sight, appear as microblazars. The jets boost the energy of stellar photons to the range of very energetic γ-rays. (**Right**) Pulsar winds are powered by the rotation of neutron stars; the wind flows away to large distances in a comet-shaped tail. Interaction of this wind with the companion-star outflow may produce very energetic γ-rays.

binaries (LS 5039, LSI +61 303, and PSR B1259-63) have eccentric orbits around stars with masses in the range of 10 to 23 solar masses, and these stars provide the seed photons to be scattered by the inverse Compton effect to VHEs. PSR B1259-63 contains a pulsating neutron star, but in LS 5039 and LSI +61 303, the precise nature of the compact stars is not known. Certainly, they are no more than 4 solar masses, which is consistent with neutron stars and/or black holes of low mass. Both the microquasar-jet model and the pulsar-wind model yield similar mechanisms to produce the VHE emission (that is, the inverse Compton effect). Thus, the fundamental question that remains open is whether the relativistic electrons in LS 5039 and LSI +61 303 come from accretion-powered jets or from the rotational energy of pulsars that are spinning down as in PSR B1259-63.

The pulsar-wind model requires γ-ray binaries with neutron stars young enough to provide large spin-down energies. In fact, as in PSR B1259-63, LS 5039 and LSI +61 303 contain young compact objects. Kinematic studies show that LS 5039 has been shot out from the plane of the galaxy (*11*) and LSI +61 303 from a cluster of massive stars (*12*) sometime during the past 1 million years by supernova explosions produced when the compact objects were formed. Furthermore, it has been proposed that LSI +61 303 is a pulsar-wind source because the time variability and the radio and x-ray spectra resemble those of young pulsars (*13*). Besides, LSI +61 303 contains a Be-class star like PSR B1259-63, and the high-energy emission in both objects seems to be produced at specific phases of orbital motions of the compact objects around the Be stars. All Be/x-ray binaries known so far contain neutron stars, and none is known to host a black hole.

However, the pulsar-wind model (*13*) does not satisfactorily explain the GeV γ-ray and radio wavelength fluxes observed in LSI +61 303 and LS 5039. In addition, contrary to what would be expected in the radio emission from a young pulsar, the jets in LS 5039 are steady and two-sided, and seem to have bulk motions of 0.2 to 0.3 times the speed of light, as do the compact jets in black hole microquasars. Furthermore, in LS 5039, no major radio outbursts are observed similar to those in PSR B1259-63.

The detection of pulsations would be a definitive proof for the pulsar-wind mechanism in γ-ray binaries. On the other hand, detection of VHE emission from a black hole binary (for example, Cygnus X-1, V 4641, or GX 339-4) would provide definitive observational ground to the microquasar-jet model. Another direct way to distinguish between accretion and rotational powered γ-ray binaries may be to use radio images with higher sensitivity and angular resolution that would establish clearly whether the high-energy particles that trigger the VHE emission emanate as pulsar winds or as highly collimated microquasar jets.

γ-ray binaries are becoming subjects of topical interest in high-energy astrophysics, and their study has important implications. As microblazars, they would serve as valuable nearby laboratories to gain insight into the physics of distant blazars. As pulsar-wind γ-ray binaries, they are important because they are the likely precursors of a much larger population of high-mass x-ray binaries in the Milky Way, and may provide clues to understand the early evolution of the enshrouded hard x-ray binaries being discovered from space with satellite telescopes such as the European Space Agency's International Gamma Ray Astrophysics Laboratory (INTEGRAL).

References

1. J. Albert *et al.*, *Science* **312**, 1771 (2006); published online 18 May 2006 (10.1126/science.1128177).
2. I. F. Mirabel, L. F. Rodríguez, *Nature* **392**, 673 (1998).
3. F. Aharonian *et al.*, *Science* **309**, 746 (2005).
4. A. M. Atoyan, F. Aharonian, *Mon. Not. R. Astron. Soc.* **302**, 253 (1999).
5. V. Bosch-Ramon. G. E. Romero, J. M. Paredes, *Astron. Astrophys.* **447**, 263 (2006).
6. I. F. Mirabel, L. F. Rodríguez, *Annu. Rev. Astron. Astrophys.* **37**, 409 (1999).
7. E. Gallo *et al.*, *Nature* **436**, 819 (2005).
8. S. Corbel *et al.*, *Science* **298**, 196 (2002).
9. L. Maraschi, A. Treves, *Mon. Not. R. Astron. Soc.* **194**, 1P (1981).
10. F. Aharonian, *Astron. Astrophys.* **442**, 1 (2005).
11. M. Ribó *et al.*, *Astron. Astrophys.* **384**, 954 (2002).
12. I. F. Mirabel, I. Rodrigues, Q. Z. Liu, *Astron. Astrophys.* **422**, L29 (2004).
13. G. Dubus, http://arxiv.org/abs/astro-ph/0605287 (2006).

10.1126/science.1129815

Early Cretaceous Spider Web with Its Prey

Enrique Peñalver,[1] David. A. Grimaldi,[1]* Xavier Delclòs[2]

Spider silk is uncommonly fossilized, primarily in amber and usually as isolated strands. The oldest record is from the Early Cretaceous, which is a single silk strand with droplets in Lebanese amber (*1*). Here we describe an association of insects trapped within a spider web made by Araneoidea preserved in an aerial, cylindrical stalactitic mass of amber from the San Just site in Spain, which is Early Cretaceous in age (~110 million years ago).

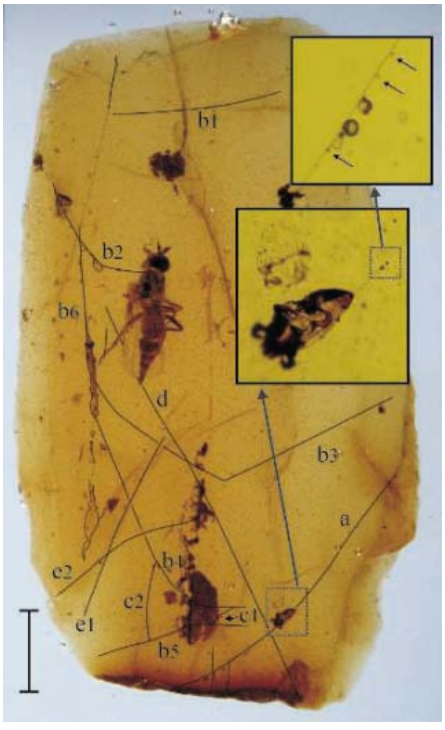

Fig. 1. Spider web with adhered arthropods from the Early Cretaceous of Spain (strands are not visible in the photomicrograph, so they have been drawn in here). A map of silk strands in the amber portion, with a *Microphorites* fly and a mite (CPT-963 and CPT-964), also shows details of the rectilinear strand with droplets to which a mite adheres (upper box shows the measured droplets, two big and three small, arrows). Five strands are in the same plane and have a similar orientation and thickness (b1 to b5), and three of them are connected perpendicularly to an incomplete strand (b6), but the other two strands are possibly also connected. Two consecutive main strands are connected by two very thin strands (c1 and c2); one of them was broken inside the resin and appears bent (c1). Another long strand is crossed by a longer rectilinear strand with the same thickness (d). These two strands cross at an acute angle, like the intersection of two silks in this amber portion but which lie in a different plane and are unconnected to the main group (e1 and e2). Other views of the amber piece reveal a more extensive web. Scale bar, 1 mm.

The amber stalactite, originally 18 mm × 7.5 mm, was prepared in three small sections of amber embedded in epoxy resin to stabilize it. There are at least 26 silk strands in the three amber sections that are rectilinear or slightly curved, but two strands have the shape of hanks (fig. S1). Glue droplets are visible on two strands (diameter 3.4 μm; two droplets have a large diameter, 11.3 to 13.0 μm, surely a result of water absorption); the droplets are unusually small compared with the size range of other fossil droplets, but they are within the range of extant species, as in the case of Linyphiidae with 2 to 10 μm (*2*). The two viscid strands are one rectilinear, long strand with an adhering mite (Fig. 1) and another with an adhering beetle (Cucujidae). The longest strand is 5.7 mm in length. The thickness of the silk strands ranges from 0.6 to 1.9 μm.

The most interesting web fragment is in the amber section with a *Microphorites* fly and a mite trapped by the strands. This section contains 16 silk strands, 5 of which are in the same plane and have a similar orientation and thickness. Three of these five strands are connected perpendicularly to an incomplete strand, but the other two strands are possibly also connected. Two consecutive main strands are connected by two thin strands that can be interpreted as two contiguous strands of a sticky spiral between two consecutive radii (Fig. 1). The above-described web portion suggests an orb web, but the overall geometry preserved indicates that other kind of webs are possible, e.g., a comb-footed spider cobweb. In another amber section (fig. S1), there is a thicker bifurcate thread, which is made up of numerous thinner strands without droplets and which snagged one leg of a *Cretevania* wasp.

Two strands in the amber pieces without droplets but forming hanks indicate that the silk had great elasticity. The web apparently made partial contact with the resin and then some of the strands contracted violently because of the release of tension from breaking. Elasticity allows the web to absorb the kinetic energy of flying prey. The web had a vertical orientation, because the longest main strands of the three amber portions were originally oriented in a similar direction as the longitudinal axis of the runnel. The high diversity of Araneoidea compared with Deinopoidea is associated with the replacement of primitive cribellar capture thread by viscous adhesive thread and with a change from a horizontal to a vertical orb-web orientation. As a consequence, the changes increased the orb web's capacity to intercept and retain winged insects (*3*).

The diversification of spiders is thought to be related to the radiation of insects (*4*), and this is likely the case for aerial webs and winged (pterygote) insects. Many paraneopterans are of appropriate size for capture in webs, but the most diverse flying insects are the four large orders in the Holometabola: Coleoptera, Diptera, Hymenoptera, and Lepidoptera. Major radiations within each of these and several other orders occurred with the angiosperm radiations in the Cretaceous (*5*). Small (1- to 2-mm-long) Diptera, then Hymenoptera, then Coleoptera are the most abundant prey of modern araneid spiders (*6*), and these are represented as the prey items in the fossil web. Spider webs may have imposed substantial selection pressures for Cretaceous insects, and this amber record confirms that araneoid web capture is indeed old enough to have affected the early evolution of diverse groups of flying insects.

References and Notes

1. S. Zschokke, *Nature* **424**, 636 (2003).
2. S. Zschokke, *European Arachnology* **2003**, 367 (2004).
3. J. E. Bond, B. D. Opell, *Evolution* **52**, 403 (1998).
4. D. Penney, *Trans. R. Soc. Edinb. Earth Sci.* **94**, 275 (2004).
5. D. A. Grimaldi, M. S. Engel, *Evolution of the Insects* (Cambridge Univ. Press, New York, 2005).
6. W. Nentwig, *Oecologia* **66**, 580 (1985).
7. We thank C. Soriano, M. Engel, A. Melic, J. I. Ruiz Omeñaca, and M. Marco for providing information. We also thank Diputación General de Aragón and L. Alcalá of the Fundación Conjunto Paleontológico de Teruel-Dinopólis. Research was sponsored with Spanish-French Scientific Research Program no. HF2004-0053 and grant no. CGL2005-00046, both from Research Projects of the Spanish Ministry of Education and Science.

Supporting Online Material

www.sciencemag.org/cgi/content/full/312/5781/1761/DC1
Figs. S1 and S2

23 February 2006; accepted 12 May 2006
10.1126/science.1126628

[1]Department of Entomology, American Museum of Natural History, New York, NY 10024, USA. [2]Departament d'Estratigrafia, Paleontologia i Geociències Marines, Facultat de Geologia, Universitat de Barcelona, 08028 Barcelona, Spain.

*To whom correspondence should be addressed. E-mail: grimaldi@amnh.org

Silk Genes Support the Single Origin of Orb Webs

Jessica E. Garb,* Teresa DiMauro, Victoria Vo, Cheryl Y. Hayashi

The spider orb web is an impressive example of animal architecture. This silken net consists of a frame and supporting radii overlaid with a sticky capture spiral. Because an orb web must absorb the enormous kinetic impact of flying prey, silks composing the web have exceptional mechanical properties (*1*). Orb weaving is characteristic of species in two lineages: Araneoidea and Deinopoidea (Fig. 1A). Araneoid and deinopoid orb weavers use nearly identical behavioral sequences and spinning apparatuses to produce architecturally similar webs. However, there are notable differences between the adhesive mechanisms of capture spirals spun by araneoids (aqueous glue) and deinopoids (dry fibrils) (*2*). Thus, the two types of orb webs were widely considered a dramatic example of convergent evolution (*3*).

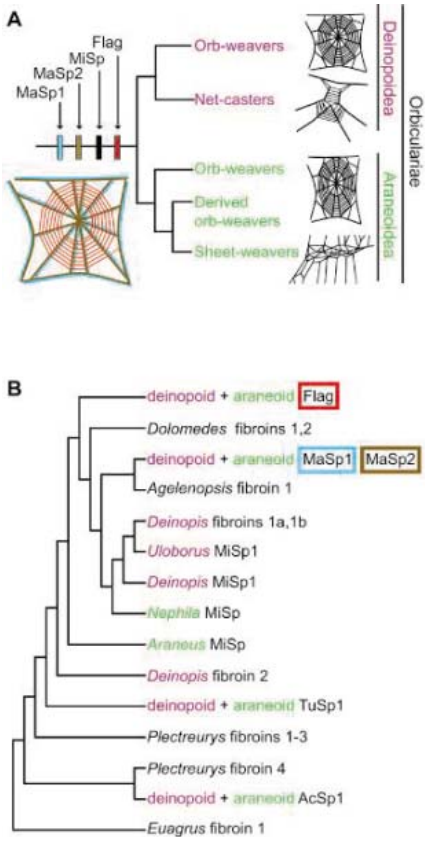

Fig. 1. Relationships of orb-weaving spiders and spidroins. (**A**) Deinopoid (purple) and araneoid (green) lineages (*2*), depicting inferred ancestral web and spidroins. Orb-web frame and radii composed of MaSp1 (blue) and MaSp2 (brown) are shown along with temporary spiral with MiSp (black) and capture spiral with Flag (red). (**B**) Summarized phylogeny of spidroin family members. The full tree is shown in fig. S2.

Spider silks are composed of proteins (spidroins) synthesized in specialized abdominal glands. Three types of glands produce the fibers used in orb-web construction: (i) major ampullates for frame and radial fibers, (ii) minor ampullates for temporary spiral scaffolding, and (iii) flagelliforms for capture spiral axial fibers (*4*). Whereas silk cDNAs were described from these glands in araneoids, none are known from deinopoids. If Araneoidea and Deinopoidea are sister taxa (Orbiculariae), then the simplest explanation for similarities between their orb webs is that they were acquired from a common orb-weaving ancestor (*2*). Thus, deinopoids are expected to have counterparts to araneoid silk proteins used in orb-web construction. To test this hypothesis, we characterized silk gland cDNAs from representatives of both deinopoid families: a net-casting spider, *Deinopis spinosa* (Deinopidae), and a feather-legged orb weaver, *Uloborus diversus* (Uloboridae) (*5*).

Among the deinopoid cDNAs, we identified the following orthologs of araneoid silks used in orb webs: (i) MaSp1 and MaSp2, major ampullate proteins of the frame and radii, (ii) MiSp, minor ampullate scaffolding protein, and (iii) Flag, flagelliform protein of capture spirals (*4*) (fig. S1). Given the diversification of silk glands and fiber types that accompanied spider evolution (*6*), the distribution of certain spidroins should uniquely define particular clades. Spidroins have been reported from six nonorbicularian species (*4*), but MiSp and Flag are exclusively known from araneoids, and major ampullate cDNAs that encode MaSp1-like spidroins but not MaSp2 are known from nonorbicularians. Because minor and major ampullate gland spigots are broadly distributed in nonorbicularians (*6*), the use of MiSp and MaSp1 by araneoids and deinopoids is interpreted as plesiomorphic. However, araneoids and deinopoids are united by their shared use of MaSp2. Moreover, araneoids and deinopoids are the only spiders that have flagelliform-like spigots and make capture spirals with silk from these spigots (*2*). The discovery of Flag and MaSp2 in deinopoids consequently identifies these spidroins as molecular synapomorphies (shared derived traits) supporting orbicularian monophyly.

Phylogenetic analyses of spidroin C-termini substantiate close relationships between deinopoid and araneoid spidroins used in orb webs (Fig. 1B). The analyses do not consistently recover a grouping of MiSp-like sequences, but the resulting trees do contain clades of the following: (i) deinopoid and araneoid Flag, (ii) deinopoid and araneoid MaSp1 and MaSp2, (iii) deinopoid and araneoid AcSp1 (prey-wrapping silk protein), and (iv) deinopoid and araneoid TuSp1 (egg-case silk protein). The collective combination of Flag, MiSp, MaSp1, and MaSp2 in araneoid and deinopoid spiders implies that the orbicularian ancestor was equipped with the molecular elements necessary for orb-web construction. Based on fossil evidence, this ancestor minimally dates from the Lower Cretaceous, 136 million years ago (*7*). Accordingly, the birth of Flag, MiSp, MaSp1, and MaSp2 must have occurred by this time. Since their ancient origins, these silks have diversified during the subsequent radiation of Orbiculariae (>10,000 species) (*2*), thus greatly expanding the designs available for the production of high-performance biomimetic materials.

References and Notes

1. F. Vollrath, D. P. Knight, *Nature* **410**, 541 (2001).
2. C. E. Griswold, J. A. Coddington, G. Hormiga, N. Scharff, *Zool. J. Linn. Soc.* **123**, 1 (1998).
3. W. A. Shear, Ed., *Spiders: Webs, Behavior, and Evolution.* (Stanford Univ. Press, Stanford, CA, 1986).
4. J. Gatesy, C. Hayashi, D. Motriuk, J. Woods, R. Lewis, *Science* **291**, 2603 (2001).
5. Materials and methods are available as supporting material on *Science* Online.
6. N. Platnick, J. Coddington, R. Forster, C. Griswold, *Am. Mus. Novit.* **3016**, 1 (1991).
7. P. A. Selden, *Nature* **340**, 711 (1989).
8. N. Nguyen, P. Paquin, and M. Stowe provided assistance. N. Ayoub, T. Blackledge, J. Gatesy, M. McGowen, D. Reznick, and A. Suarez commented on drafts. Work was supported by NSF grant no. DEB-0236020 and by the Army Research Office grant no. DAAD19-02-1-0358. Sequences were deposited in GenBank with accession codes DQ399323 to DQ399335.

Supporting Online Material

www.sciencemag.org/cgi/content/full/312/5781/1762/DC1
Materials and Methods
Figs. S1 and S2
References

27 March 2006; accepted 28 April 2006
10.1126/science.1127946

Department of Biology, University of California, Riverside, CA 92521, USA.

*To whom correspondence should be addressed. E-mail: jessica.garb@ucr.edu

TRB3 Links the E3 Ubiquitin Ligase COP1 to Lipid Metabolism

Ling Qi,[1*] Jose E. Heredia,[1*] Judith Y. Altarejos,[1] Robert Screaton,[1] Naomi Goebel,[1] Sherry Niessen,[2] Ian X. MacLeod,[2] Chong Wee Liew,[3] Rohit N. Kulkarni,[3] James Bain,[4] Christopher Newgard,[4] Michael Nelson,[1] Ronald M. Evans,[1] John Yates,[2] Marc Montminy[1]†

During fasting, increased concentrations of circulating catecholamines promote the mobilization of lipid stores from adipose tissue in part by phosphorylating and inactivating acetyl–coenzyme A carboxylase (ACC), the rate-limiting enzyme in fatty acid synthesis. Here, we describe a parallel pathway, in which the pseudokinase Tribbles 3 (TRB3), whose abundance is increased during fasting, stimulates lipolysis by triggering the degradation of ACC in adipose tissue. TRB3 promoted ACC ubiquitination through an association with the E3 ubiquitin ligase constitutive photomorphogenic protein 1 (COP1). Indeed, adipocytes deficient in TRB3 accumulated larger amounts of ACC protein than did wild-type cells. Because transgenic mice expressing TRB3 in adipose tissue are protected from diet-induced obesity due to enhanced fatty acid oxidation, these results demonstrate how phosphorylation and ubiquitination pathways converge on a key regulator of lipid metabolism to maintain energy homeostasis.

Obesity is a major risk factor in the development of type 2 diabetes, which is characterized by a loss of insulin signaling in muscle, liver, pancreatic islets, and adipose tissue (*1*). Mice with a knockout of the insulin receptor (IR) in specific tissues show varying degrees of deterioration in metabolic function (*2*, *3*), but mice with an IR knockout in fat (FIRKO) are phenotypically lean, display enhanced insulin sensitivity in peripheral tissues, and live longer than control littermates (*4*). The mechanism by which loss of insulin signaling in adipose tissue improves metabolic function in FIRKO mice is unclear, but it is thought to be a consequence of enhanced lipolysis and fatty acid oxidation (FAO).

Profiling studies on adipocytes with a knockout of insulin receptor substrate (IRS) genes point to a number of candidate genes that may contribute to the salutary effects of IR or IRS knockouts on metabolic function (*5*). Loss of insulin signaling increases expression of the gene encoding Tribbles 3 (TRB3), a pseudokinase that accumulates in response to fasting and binds to and inhibits the activation of the serine-threonine kinase Akt in the liver (*6*, *7*). Indeed, humans with a gain-of-function mutation in TRB3 have a higher incidence of insulin resistance and diabetes-associated complications (*8*).

TRB3 and its paralogs—TRB1 and TRB2—are catalytically inactive because they lack adenosine 5′-triphosphate (ATP)–binding and catalytic core motifs within their Ser-Thr kinase domains, and they are thought to have evolved instead as adaptor proteins (*9*–*12*). Consistent with this idea, studies in lower organisms have pointed to a potential link between TRBs and the ubiquitin ligase machinery (*9*–*12*). The *Drosophila* protein tribbles, the founding member of this family, coordinates mitosis and morphogenesis during gastrulation by promoting the proteasome-mediated degradation of the G_2-M phase cell cycle regulator String (also called CDC25) (*9*). Tribbles also regulates oogenesis by stimulating the ubiquitination and proteasomal degradation of Slbo, the *Drosophila* homolog of mammalian CCAAT enhancer-binding protein alpha (*11*).

In the process of characterizing TRB3, we found an unexpected role for this pseudokinase in promoting lipid metabolism during fasting through an association with the E3 ligase COP1 (*13*). Confirming its proposed function as an adaptor protein, TRB3 enhanced the COP1-dependent ubiquitination and inactivation of a key regulatory enzyme

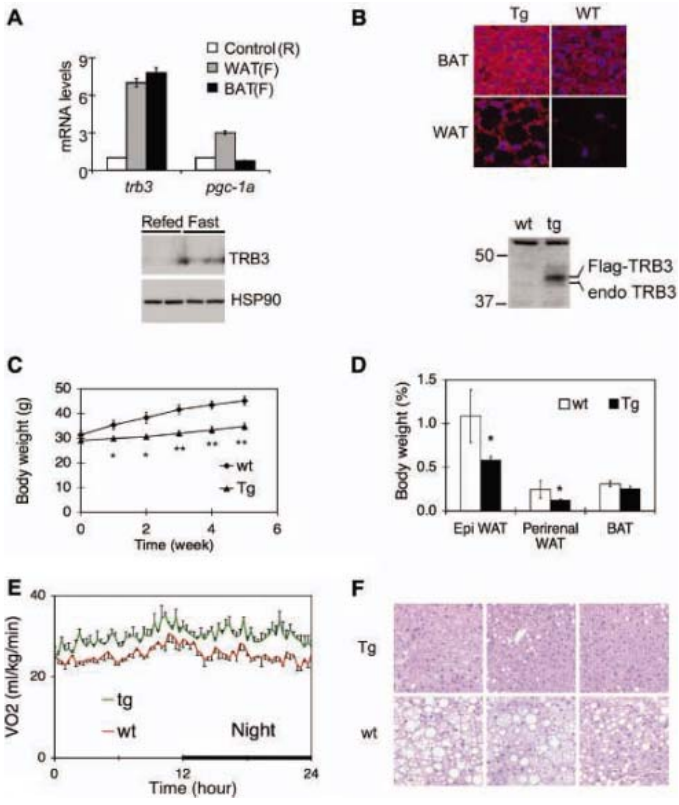

Fig. 1. Protection of transgenic mice expressing TRB3 in adipose tissue from diet-induced obesity. (**A**) (Top) Effect of fasting (F) on amounts of TRB3 and PGC-1α mRNA [fold increase relative to refed (R) levels (set at 1)] in WAT and BAT from wild-type mice. (Bottom) Western blot showing amounts of endogenous TRB3 protein in WAT from wild-type mice under fasting or refed conditions. Amounts of heat shock protein 90 (HSP90) are also shown. (**B**) Immunofluorescence staining (top) and Western blot (bottom) analysis of WAT from overnight-fasted wild-type (wt) littermates and transgenic (Tg) mice expressing TRB3 (F-TRB3) under control of the white and brown adipose-specific aP2 promoter. TRB3 protein was detected with polyclonal antiserum to TRB3. Endogenous (endo) and Flag-tagged TRB3 proteins are indicated. (**C**) Effect of high-fat diet on weight gain in F-TRB3 and control littermates over a 5-week period ($n = 8$) (n, sample size for each cohort). $^*P < 0.05$, $^{**}P < 0.01$. (**D**) Relative mass of WAT [epididymal (Epi) or perirenal] and BAT in control and F-TRB3 (Tg) mice, expressed as percentage of total body weight ($n = 3$). (**E**) Relative oxygen consumption (VO_2) of wild-type and F-TRB3 mice over a 24-hour period ($n = 4$). Mice were maintained on a high-fat diet. (**F**) Protection of F-TRB3 mice from hepatic steatosis under high-fat diet conditions. Representative sections from livers of three F-TRB3 transgenic and three wild-type mice on a high-fat diet for 22 weeks. Data in (A) and (C) to (E) are shown as means ± SEM.

[1]Peptide Biology Laboratories and Gene Expression Laboratories, Salk Institute for Biological Studies, La Jolla, CA 92037, USA. [2]The Scripps Research Institute, 10550 North Torrey Pines Road, La Jolla, CA 92037, USA. [3]Joslin Diabetes Center, One Joslin Place, Boston, MA 02215, USA. [4]Sarah W. Stedman Nutrition and Metabolism Center, Duke University Medical Center, 4321 Medical Park Drive, Suite 200, Durham, NC 27704, USA.

*These authors contributed equally to this work.
†To whom correspondence should be addressed. E-mail: montminy@salk.edu

in the fatty acid synthesis pathway during fasting. Our results may help explain the beneficial effects of disrupting insulin signaling in adipose tissue and may also shed light on TRB function in *Drosophila* during development.

Lean phenotype of TRB3 transgenic mice. We generated two independent lines of transgenic mice expressing Flag-tagged TRB3 from the adipose-specific aP2 promoter (F-TRB3 mice) (*14*). In wild-type mice, amounts of TRB3 mRNA and protein in brown and white adipose tissue (BAT and WAT, respectively) were greater in fasting animals than in animals that had been fed after fasting (Fig. 1A). In F-TRB3 mice, TRB3 mRNA and protein levels in WAT and BAT were 2 to 4 times as high as those of wild-type animals under either fasting or feeding conditions and were similar to TRB3 levels in IRS1 (−/−) adipocytes (*5*) (Fig. 1B and fig. S1).

F-TRB3 mice were indistinguishable from control littermates at birth, but gained weight more slowly and had about 10% lower body mass at 8 weeks of age on a normal chow diet (fig. S2). Under high-fat diet conditions, however, F-TRB3 mice showed lower weight gains than did wild-type littermates (Fig. 1C). Epididymal and perirenal fat pads were each reduced in weight by about 50% in F-TRB3 mice, whereas BAT mass did not significantly decrease (Fig. 1D). Histologically, BAT and WAT tissues from F-TRB3 animals had comparable cellularity to those of wild-type littermates, but average adipocyte size was lower in F-TRB3 adipose tissues, suggesting that the metabolism of fat is enhanced in these mice (figs. S3 and S4).

We conducted metabolic studies to determine why adiposity is reduced in F-TRB3 mice. Although physical activity was comparable between both groups, F-TRB3 mice actually consumed 20% more calories than did their wild-type littermates (fig. S5). Under high-fat diet conditions, F-TRB3 mice showed increased O_2 consumption [31.04 ± 0.30 ml O_2/kg/min for F-TRB3 mice versus 26.22 ± 0.32 ml O_2/kg/min for wild-type mice, where the error is SD (Fig. 1E)] as well as a persistent increase in core body temperatures (fig. S5) indicating that F-TRB3 mice are lean in part because of increased energy expenditure.

A high-fat diet is thought to trigger insulin resistance in part by promoting lipid accumulation in the liver (hepatic steatosis). Hepatic steatosis was readily observed in control littermates on a high-fat diet; but lipid accumulation was less pronounced in livers of F-TRB3 mice (Fig. 1F). Correspondingly, F-TRB3 animals exhibited lower circulating concentrations of glucose and insulin (fig. S5), and they appeared to be more sensitive to insulin than were wild-type littermates in an insulin tolerance test (fig. S6).

In view of their increased energy expenditure, F-TRB3 mice could be protected from hepatic steatosis through increased metabolism of fat. Supporting this idea, basal rates of FAO in BAT and WAT were 1.5 to 2 times as high in animals fed normal chow and 3 times as high in animals on a high-fat diet when F-TRB3 mice were compared with control littermates (Fig. 2A and fig. S7). Correspondingly, increased expression of genes encoding enzymes that function in FAO was observed in WAT and BAT from F-TRB3 mice. mRNAs for key transcriptional regulators [peroxisome proliferator-activated receptor α (PPARα), PPARδ, and PPAR gamma coactivator (PGC)–1α] and FAO enzymes carnitine palmitoyltransferase 1 were more abundant in F-TRB3 animals (Fig. 2B). Consistent with the increased core body temperatures, amounts of uncoupling protein 1 (UCP1) mRNA were nearly 14 times as high in WAT from F-TRB3 relative to those in wild-type mice, indicating that TRB3 may protect against diet-induced obesity by enhancing rates of fatty acid oxidation and dissipating this energy in part through thermogenesis.

TRB inhibits ACC activity. We attempted to identify cellular proteins that associate with TRB3 by performing mass spectrometry analysis on endogenous proteins coimmunoprecipitated with Flag-tagged TRB3 in transfected human embryonic kidney (HEK293T) cells. The protein complex was digested with trypsin and directly analyzed with the use of multidimensional liquid chromatography–tandem mass spectrometry together with the SEQUEST database searching software [multidimensional protein identification technology (MudPIT)] (*15*). We identified acetyl-coenzyme carboxylase 1 (ACC1), the rate-limiting enzyme in fatty acid synthesis (*16*) (fig. S8). The TRB3-ACC interaction was also observed in transfected HEK293T cells with the use of epitope-tagged TRB3 and ACC1 polypeptides (fig. S9), and association of the native proteins was detected in WAT of wild-type mice under fasting conditions but not after postfast feeding (Fig. 2C). Other enzymes in the fatty acid synthesis pathway, such as fatty acid synthase (FASN), did not interact with TRB3.

Similar to F-TRB3 mice, mice with a knockout of the *ACC2* gene exhibit a lean phenotype and are resistant to diet-induced obesity, in part because of an increase in fatty acid oxidation in adipose tissue (*17*, *18*). We therefore tested whether the metabolic ef-

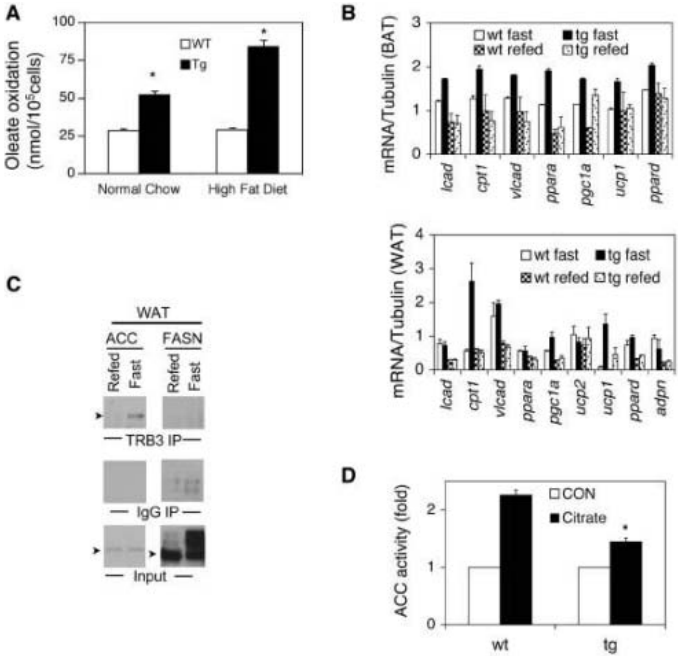

Fig. 2. Effects of TRB3 to promote fatty acid oxidation and disrupt ACC activity. (**A**) Fatty acid oxidation was measured in primary brown adipocytes from refed wild-type and F-TRB3 mice fed a normal chow or high-fat diet. BAT was isolated, and fatty acid oxidation was measured in adipocytes cultured for 12 hours in Roswell Park Memorial Institute (RPMI)–1640 medium containing 0.6 mM oleate (2.5 μCi/ml, [9,10-^{3}H]). (**B**) Quantitative real-time fluorescence polymerase chain reaction analysis of mRNAs for fatty acid oxidation and thermogenic genes in BAT (top) and WAT (bottom) from F-TRB3 and wild-type littermates maintained on a high-fat diet for 22 weeks, under fasting or refed conditions. (**C**) Western blot assay showing recovery of endogenous ACC or FASN from immunoprecipitates (IPs) with antiserum to TRB3 or control rabbit immunoglobulin G (IgG) prepared from WAT of fasted or refed wild-type mice. Input levels (10% of total) of ACC and FASN are shown. (**D**) Fold change in ACC activity [measured as counts per minute (cpm) (^{14}C)/g tissue/min] in WAT from F-TRB3 transgenic mice relative to control littermates. The effect of citrate, an allosteric activator of ACC, is shown. CON, control. Data in (A), (B), and (D) are shown as the means + SEM of three experiments. *$P < 0.05$.

fects of TRB3 in adipose tissue are linked to its association with ACC. In enzymatic assays, ACC activity in WAT from F-TRB3 mice was about one-half that in WAT from normal littermates (Fig. 2D). Infection of 3T3-L1 cells with an adenovirus vector encoding TRB3 also inhibited ACC activity acutely (fig. S10), suggesting that the effects of TRB3 on ACC are likely cell-autonomous.

TRB3 associates with the E3 ubiquitin ligase COP1. Because the *Drosophila* gene *tribbles* (*TRB*) inhibits certain regulatory targets by promoting their proteasomal degradation, we hypothesized that TRB3 might inhibit ACC by a similar mechanism. We performed mass spectroscopy experiments to identify endogenous proteins associated with adenovirus-expressed Flag-tagged TRB3 in 3T3 L1 adipocytes. TRB3 immunoprecipitates contained the E3 ubiquitin ligase constitutive photomorphogenic protein 1 (mCOP1), as well as de-etiolated-1 (DET1) and DNA damage binding protein 1 (DDB1), components of a cullin 4A (Cul4A) ubiquitin ligase (*19*, *20*) (fig. S11). We confirmed the interaction of TRB3 with COP1 in transfected HEK293T cells with the use of epitope-tagged constructs (Fig. 3A). Endogenous TRB3-COP1 complexes were also detected in WAT from fasted mice and at lower levels after postfast feeding (Fig. 3A).

To determine whether TRB3 binds to COP1 and ACC through a direct mechanism, we performed immunoblotting assays with recombinant glutathione *S*-transferase (GST)–TRB3 proteins. Full-length TRB3 bound directly to both ACC1 and COP1 proteins (Fig. 3B), and a truncated TRB3 polypeptide lacking the C-terminal 40 residues (amino acids 315 to 354) associated with ACC1 but not COP1. The C-terminal region of TRB3 contains a sequence similar to the consensus COP1 binding motif ([Asp or Glu] [Asp or Glu]…Val-Pro [Asp or Glu]) (*20*–*22*) that is present in all TRB family members (fig. S13). Mammalian TRB1 also associated with COP1 in transfected HEK293T cells (fig. S14), and a mutant TRB3 polypeptide called Val Pro mutant (VPmt), which contains alanine substitutions at three residues in the COP1 binding motif (Asp^{333}, Val^{336}, and Pro^{337}) was unable to associate with COP1 in transfected HEK293T cells (Fig. 3C).

TRB3 recruits COP1 to ACC. On the basis of its ability to associate with both COP1 and ACC, apparently through distinct surfaces, TRB3 might be expected to mediate an interaction between these proteins and to trigger ubiquitination of ACC1. TRB3 enhanced the interaction of COP1 with ACC1 and ACC2 as detected by coimmunoprecipitation from extracts of transfected HEK293T cells (Fig. 3D and fig. S15). TRB3 also stimulated the ubiquitination of ACC1 and ACC2 by COP1 (Fig. 4A and fig. S15). Confirming the importance of the TRB3:COP1 interaction in this setting, ACC was not ubiquitinated by COP1 in cells expressing COP1 interaction–defective VPmt TRB3 protein (Fig. 4A).

Given our evidence that TRB3 promotes the COP1-dependent ubiquitination of ACC, we tested whether this modification was sufficient to inhibit ACC enzymatic activity. Wild-type TRB3 alone caused a small decrease in ACC1 activity in HEK293T cells, which express small amounts of endogenous COP1 relative to those in 3T3 L1 adipocytes (Fig. 4A). However, ACC activity was reduced to about one-third of that in control cells in cells coexpressing COP1 and TRB3 (Fig. 4A). VPmt TRB3 had no effect on ACC1 activity (Fig. 4A). Taken together, these results suggest that TRB3 may promote loss of fat by mediating the COP1-dependent ubiquitination and inactivation of ACC.

In keeping with the increased abundance of endogenous TRB3 during fasting, amounts of ubiquitinated ACC in WAT were also higher in fasted compared with refed wild-type mice (Fig. 4B). Amounts of ubiquitinated ACC were increased in BAT from F-TRB3 mice compared with those of wild-type littermates (Fig. 4B). Supporting the proposed role of TRB3 as an adaptor protein, amounts of endogenous COP1 associated with endogenous ACC in BAT were higher in F-TRB3 mice than in controls. Amounts of COP1 and ACC associated with TRB3 were also increased in adipose tissue from F-TRB3 mice (fig. S16).

The increased ubiquitination of ACC induced by TRB3 would be predicted to enhance ACC degradation. Under high-fat diet conditions, total amounts of ACC protein in WAT and BAT of F-TRB3 mice were smaller than those in control littermates (Fig. 4C). Conversely, reduction of TRB3 by infection of 3T3-L1 cells with an adenovirus encoding a small interfering RNA against mouse TRB3 induced accumulation of ACC protein and an increase in its enzymatic activity (Fig. 4C and fig. S17), and coexpression of an RNA interference (RNAi)–resistant form of TRB3 protein blocked the induction of ACC by TRB3 RNAi (fig. S18). Reduction of TRB3 in primary cultures of brown adipocytes also increased amounts of ACC protein (Fig. 4C). Amounts of COP1 protein in BAT are much greater than in other tissues such as liver, which may explain in part the distinct metabolic effects of TRB3 in these tissues (Fig. 4C). Taking these results together, we propose that TRB3 may protect against diet-induced

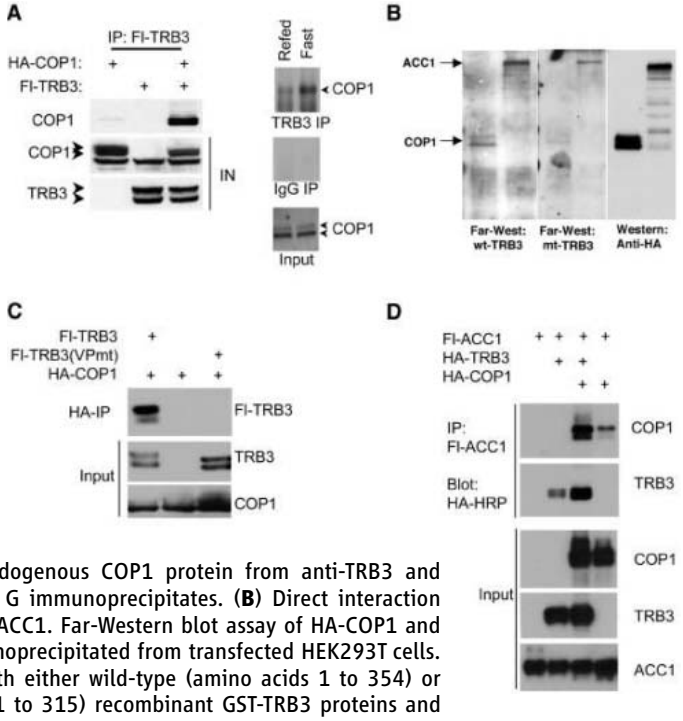

Fig. 3. TRB3-mediated binding of ACC to the E3 ubiquitin ligase COP1. (**A**) (Left) Western blot assay showing recovery of hemagglutinin (HA)–tagged COP1 from immunoprecipitates (IPs) of Flag-TRB3 prepared from transfected HEK293T cells. Input (IN) levels (10%) of each protein indicated. The TRB3 doublet in these studies corresponds to Ser^{51} and Ser^{323} phosphorylated and dephosphorylated forms of the protein (fig. S12). (Right) Western blot assay of WAT extracts from fasted or refed wild-type mice showing recovery of endogenous COP1 protein from anti-TRB3 and control immunoglobulin G immunoprecipitates. (**B**) Direct interaction of TRB3 with COP1 and ACC1. Far-Western blot assay of HA-COP1 and HA-ACC1 proteins immunoprecipitated from transfected HEK293T cells. Blots were incubated with either wild-type (amino acids 1 to 354) or truncated (amino acids 1 to 315) recombinant GST-TRB3 proteins and then developed with antiserum to GST to detect binding of TRB3. The Western blot assay on the right shows immunoprecipitated COP1 and ACC1 proteins. (**C**) Western blot assay comparing the recoveries of wild-type and COP1 interaction–defective VPmt mutant Flag-TRB3 from immunoprecipitates of HA-tagged COP1 prepared from transfected HEK293T cells. (**D**) Effect of TRB3 on association of COP1 with ACC1. Western blot assay shows recovery of HA-tagged TRB3 and HA-tagged COP1 from immunoprecipitates of Flag-tagged ACC1 prepared from transfected HEK293T cells. Input levels (10%) of each protein are shown.

obesity by stimulating fatty acid oxidation in adipose during fasting through the COP1-mediated ubiquitination and degradation of ACC (Fig. 4D).

Parallel fasting pathways. In the fasted state, mammals maintain energy balance by mobilizing triglyceride stores in response to hormonal signals. Triggering of cyclic adenosine 3′, 5′ monophosphate and energy-sensing adenosine monophosphate-dependent protein kinase (AMPK) pathways promote lipolysis and fatty acid oxidation in part by inhibiting ACC, the rate-limiting enzyme in fatty acid synthesis (*16*). ACC activity is modulated acutely by phosphorylation and allosteric regulation and chronically at the levels of biosynthesis and degradation.

Our results indicate that fasting signals also trigger fat metabolism in adipose by increasing amounts of TRB3 protein. Indeed, transgenic mice expressing TRB3 were protected from diet-induced obesity through the disruption of ACC activity and subsequent increase in fatty acid oxidation, metabolic effects similar to those in ACC2-knockout mice (*18*, *23*).

TRB3 appears to inhibit ACC activity by functioning as an adaptor for COP1. The role of TRB3 in this context appears limited, given that we observed no effect of TRB3 on ubiquitination or degradation of other COP1 substrates such as c-Jun and p53 (*19*, *20*). First described in *Arabidopsis* as negative regulators of light-activated genes (*24*–*26*), COP1 and DET1 also modulate genes involved in fatty acid metabolism in plants (*27*). It is possible that the oscillation of COP1 activity with light and dark cycles in plants has its mammalian counterpart in the regulation of metabolic programs during the feeding-to-fasting transition.

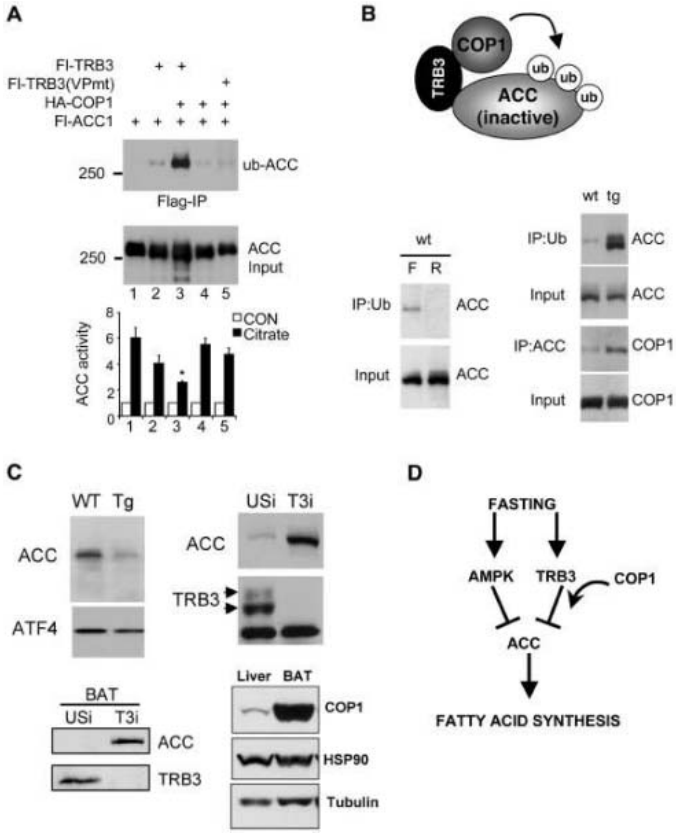

Fig. 4. Effects of TRB3 on ubiquitination (ub) and degradation of ACC by COP1. (**A**) (Top) Effect of overexpression of wild-type and COP1 interaction–defective (VPmt) TRB3 on ubiquitination of ACC1 in HEK293T cells expressing exogenous COP1 as indicated. Amounts of ACC ubiquitination were determined by coexpressing Myc-tagged ubiquitin; top panel shows Western blot of Myc-ubiquitin recovered from immunoprecipitates of Flag-ACC1. Input levels of Flag-tagged ACC (10%) are shown. (Bottom) Effect of wild-type or COP1 interaction–defective (VPmt) TRB3 on >ACC enzymatic activity in HEK293T expressing COP1 in the presence or absence of 2 mM citrate. Numbered sets of bars correspond to numbered lanes in blot above. CON, control. Data are shown as means + SEM. $*P < 0.05$. (**B**) TRB3 promotion of ACC ubiquitination in adipose tissue during fasting. (Left) Western blot assay showing recovery of endogenous ACC from immunoprecipitates with anti-ubiquitin prepared from WAT of wild-type mice under fasting (F) or refed (R) conditions. Input amounts of ACC (10%) are shown. (Right) Relative amounts of ubiquitinated ACC in BAT from wild-type and F-TRB3 transgenic mice. Blot shows amounts of ACC recovered from immunoprecipitates of BAT extracts with anti-ubiquitin. Input levels (10%) of ACC are shown. Below, a Western blot shows the amounts of endogenous COP1 recovered from immunoprecipitates of endogenous ACC prepared from BAT of wild-type and transgenic mice as indicated. (**C**) Promotion of ACC degradation by TRB3. (Top left) Western blot showing amounts of ACC in WAT from control and transgenic littermates under high-fat diet conditions. ATF4, activating transcription factor 4. (Top right) Western blot assay showing TRB3 and ACC protein amounts in control (USi) and Ad-TRB3 RNAi (T3i) expressing 3T3-L1 adipocytes. (Bottom left) Effect of control (USi) and lenti-TRB3 RNAi (T3i) on amounts of TRB3 and ACC protein in primary cultures of brown adipocytes. (Bottom right) Western blot showing relative amounts of COP1 in BAT and liver extracts of wild-type mice. (**D**) Model showing that fasting signals inhibit fatty acid synthesis by means of parallel pathways (AMPK and TRB3) that inactivate ACC by means of phosphorylation- and ubiquitin-dependent mechanisms, respectively. TRB3 promotes ACC ubiquitination by functioning as an adaptor for COP1 during fasting.

References and Notes

1. A. R. Saltiel, *Cell* **104**, 517 (2001).
2. A. Nandi, Y. Kitamura, C. R. Kahn, D. Accili, *Physiol. Rev.* **84**, 623 (2004).
3. C. R. Kahn, *Trans. Am. Clin. Climatol. Assoc.* **114**, 125 (2003).
4. M. Bluher, B. B. Kahn, C. R. Kahn, *Science* **299**, 572 (2003).
5. Y. H. Tseng *et al.*, *Nat. Cell Biol.* **7**, 601 (2005).
6. K. Du, S. Herzig, R. N. Kulkarni, M. Montminy, *Science* **300**, 1574 (2003).
7. S. H. Koo *et al.*, *Nat. Med.* **10**, 530 (2004).
8. S. Prudente *et al.*, *Diabetes* **54**, 2807 (2005).
9. J. Grosshans, E. Wieschaus, *Cell* **101**, 523 (2000).
10. J. Mata, S. Curado, A. Ephrussi, P. Rorth, *Cell* **101**, 511 (2000).
11. P. Rorth, K. Szabo, G. Texido, *Mol. Cell* **6**, 23 (2000).
12. T. C. Seher, M. Leptin, *Curr. Biol.* **10**, 623 (2000).
13. C. Yi, X. W. Deng, *Trends Cell Biol.* **15**, 618 (2005).
14. Methods and Materials are available as supporting material on *Science* Online.
15. SEQUEST; J. Eng, J. Yates, The Scripps Research Institute (http://fields.scripps.edu/sequest).
16. N. B. Ruderman, A. K. Saha, E. W. Kraegen, *Endocrinology* **144**, 5166 (2003).
17. L. Abu-Elheiga, W. Oh, P. Kordari, S. J. Wakil, *Proc. Natl. Acad. Sci. U.S.A.* **100**, 10207 (2003).
18. W. Oh *et al.*, *Proc. Natl. Acad. Sci. U.S.A.* **102**, 1384 (2005).
19. D. Dornan *et al.*, *Nature* **429**, 86 (2004).
20. I. E. Wertz *et al.*, *Science* **303**, 1371 (2004).
21. E. Bianchi *et al.*, *J. Biol. Chem.* **278**, 19682 (2003).
22. M. Holm, C. S. Hardtke, R. Gaudet, X. W. Deng, *EMBO J.* **20**, 118 (2001).
23. L. Orci *et al.*, *Proc. Natl. Acad. Sci. U.S.A.* **101**, 2058 (2004).
24. X. W. Deng *et al.*, *Cell* **71**, 791 (1992).
25. A. Pepper, T. Delaney, T. Washburn, D. Poole, J. Chory, *Cell* **78**, 109 (1994).
26. A. G. von Arnim, X. W. Deng, *Cell* **79**, 1035 (1994).
27. J. Hu *et al.*, *Science* **297**, 405 (2002).

28. This work was supported by the Juvenile Diabetes Research Foundation (L.Q.) and Hillblom Foundation, the Keikhefer Foundation, the American Diabetes Assocation, the Foundation for Medical Research, and by NIH grant DK064142 (M.M.). We thank Weimin He for aP2 construct and members of the Montminy laboratory for helpful discussions.

Supporting Online Material

www.sciencemag.org/cgi/content/full/312/5781/1763/DC1
Materials and Methods
Figs. S1 to S18
References

2 December 2005; accepted 16 May 2006
10.1126/science.1123374

Costly Punishment Across Human Societies

Joseph Henrich,[1]* Richard McElreath,[2] Abigail Barr,[3] Jean Ensminger,[4] Clark Barrett,[5] Alexander Bolyanatz,[6] Juan Camilo Cardenas,[7] Michael Gurven,[8] Edwins Gwako,[9] Natalie Henrich,[1] Carolyn Lesorogol,[10] Frank Marlowe,[11] David Tracer,[12] John Ziker[13]

Recent behavioral experiments aimed at understanding the evolutionary foundations of human cooperation have suggested that a willingness to engage in costly punishment, even in one-shot situations, may be part of human psychology and a key element in understanding our sociality. However, because most experiments have been confined to students in industrialized societies, generalizations of these insights to the species have necessarily been tentative. Here, experimental results from 15 diverse populations show that (i) all populations demonstrate some willingness to administer costly punishment as unequal behavior increases, (ii) the magnitude of this punishment varies substantially across populations, and (iii) costly punishment positively covaries with altruistic behavior across populations. These findings are consistent with models of the gene-culture coevolution of human altruism and further sharpen what any theory of human cooperation needs to explain.

For tens of thousands of years before formal contracts, courts, and constables, human societies maintained important forms of cooperation in domains such as hunting, warfare, trade, and food sharing. The scale of cooperation in both contemporary and past human societies remains a puzzle for the evolutionary and social sciences, because, first, neither kin selection nor reciprocity appears to readily explain altruism in very large groups of unrelated individuals and, second, canonical assumptions of self-regarding preferences in economics and related fields appear equally ill-fitted to the facts (*1*). Reputation can support altruism in large groups; however, some other mechanism is needed to explain why reciprocity should be linked to prosociality rather than selfish or neutral behavior (*2*). Recent theoretical work suggests that substantial cooperation can evolve, even among non-kin, in situations devoid of reputation or repeat interaction if cooperators also engage in the costly punishment of non-cooperative norm violators (*3*–*10*). Consistent with these models, behavioral experiments have now confirmed the (i) existence of costly punishment, (ii) effectiveness of punishment in sustaining cooperation (*11*, *12*), and (iii) willingness by uninvolved third parties to punish in anonymous situations (*13*). Such experiments have even begun to probe the neural underpinnings of punishment (*14*, *15*).

These results are important, because the existence of costly punishment can explain important pieces of the puzzle of large-scale human cooperation. However, like previous experimental games used to study altruism, these experiments have been conducted almost exclusively among university students. We do not know whether such findings represent the peculiarities of students and/or people from industrialized societies or whether they are indeed capturing species characteristics. Our earlier research used experimental games in 15 diverse societies to measure other-regarding behavior (*1*, *16*). We found that canonical self-interest could not explain the results in any of the 15 societies studied. We also found much more variation in game behavior than previous studies with university students had found. Similarly, until costly punishment is studied in more societies and outside of university students, it is difficult to judge its importance for explaining human cooperation.

In addition to estimating how widespread it is, knowing whether costly punishment covaries with altruistic behavior is valuable. Models of the evolution of costly punishment suggest that societies in which costly punishment is common will exhibit stronger norms of fairness and prosociality, because the

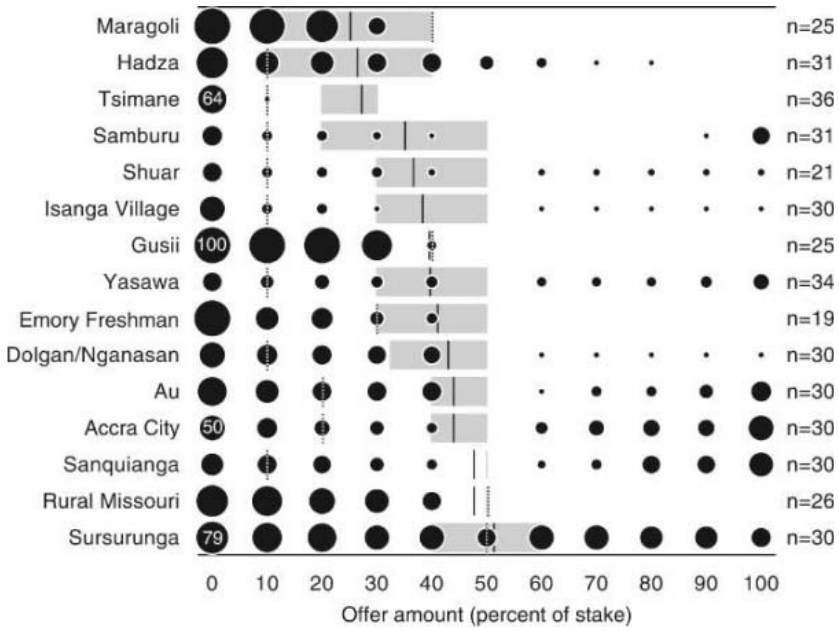

Fig. 1. UG results displayed as the distributions of rejections across possible offers in the UG, which overlay the mean offers and interquartiles. For each population labeled along the vertical axis, the areas of the black bubbles, reading horizontally, show the fraction of the sample of player 2s who were willing to reject that offer. For reference, inside some of the bubbles we noted the percentage illustrated by that bubble. The dashed vertical bars mark the IMO for each population. The solid vertical bars mark the mean offer for each population, with the gray shaded rectangle highlighting the interquartile of offers. Populations were ordered by their mean offers (from low to high). Counts on the right (*n*) refer to numbers of pairs of players.

[1]Department of Anthropology, Emory University, 1557 Dickey Drive, Atlanta, GA 30322, USA. [2]Department of Anthropology, Graduate Group in Ecology, Animal Behavior Graduate Group, Population Biology Graduate Group, University of California Davis, One Shields Avenue, Davis, CA 95616, USA. [3]GPRG, Department of Economics, University of Oxford, Manor Road, Oxford, OX1 3UQ, UK. [4]Division of the Humanities and Social Sciences, California Institute of Technology, Pasadena, CA 91125, USA. [5]Department of Anthropology, UCLA, 341 Haines Hall, Box 951553, Los Angeles, CA 90095, USA. [6]Department of Anthropology, College of DuPage, Glen Ellyn, IL 60137, USA. [7]Facultad de Economia, CEDE, Universidad de Los Andes, K1 No. 18A-70, Bogotá, Colombia. [8]Department of Anthropology, University of California, Santa Barbara, CA 93106, USA. [9]Department of Sociology and Anthropology, Guilford College, 5800 West Friendly Avenue, Greensboro, NC 27410, USA. [10]George Warren Brown School of Social Work, Washington University, 1 Brookings Drive, St. Louis, MO 63130, USA. [11]Department of Anthropology, Harvard University, 11 Divinity Avenue, Cambridge, MA 02138, USA. [12]Department of Anthropology, University of Colorado at Denver and Health Sciences Center, Post Office Box 173364, Campus Box 103, Denver, CO 80217, USA. [13]Department of Anthropology, Boise State University, 1910 University Drive, Boise, ID 83725, USA.

*To whom correspondence should be addressed. E-mail: jhenric@emory.edu

existence of costly punishment is what allows such norms to remain stable against invading defectors. Thus, the status of costly punishment as a viable explanation of human prosociality depends on it being found outside of students as well as its association with cooperative norms and institutions across cultures.

In this article, we present a round of field experiments that address the nature of costly punishment. Field experiments are valuable tools because they allow for better comparability and control of causal factors, and these particular experiments were designed by economists to specifically test the predictions of a canonical model of narrow self-interest (*16*). We used two behavioral experiments, the ultimatum and third party punishment games, among 1762 adults sampled from 15 diverse populations from five continents, representing the breadth of human production systems. In addition to explicitly measuring costly punishment via a strategy method that provides more information about behavior than the method used in the previous study, this study represents greater methodological standardization than the previous round of experiments [Supporting Online Material (SOM) Text]. Although our findings revealed some consistent patterns of punishment in all populations, we also found substantial variation across populations in their willingness to punish, including several populations with a willingness to punish "excessive generosity" (a phenomenon not observed in typical student subject pools). By using a third experiment, the dictator game, we also show that punishment correlates positively with altruism across populations in a manner consistent with coevolutionary theories (*4*).

Experiments. In our first experiment, the ultimatum game (UG), two anonymous players are allotted a sum of real money (the stake) in a one-shot interaction (*17*). The first player (player 1) can offer a portion of this sum to a second player, player 2 (offers were restricted to 10% increments of the stake). Player 2, before hearing the actual amount offered by player 1, must decide whether to accept or reject each of the possible offers, and these decisions are binding. If player 2 specified acceptance of the actual offer amount, then he or she receives the amount of the offer and player 1 receives the rest. If player 2 specified a rejection of the amount actually offered, both players receive zero. If people are motivated purely by self-interest, player 2s will always accept any positive offer; knowing this, player 1 should offer the smallest nonzero amount. Because this is a one-shot anonymous interaction, player 2's willingness to reject provides one measure of costly punishment, termed second-party punishment.

In our second experiment, the third party punishment game (3PPG), two players are allotted a sum of real money (the stake), and a third player gets one-half of this amount (*13*). Player 1 must decide how much of the stake to give to player 2 (who makes no decisions). Then, before hearing the actual amount player 1 allocated to player 2, player 3 has to decide whether to pay 10% of the stake (20% of his or her allocation) to punish player 1, causing player 1 to suffer a deduction of 30% of the stake from the amount kept. Player 3's punishment strategy is elicited for all possible offers by player 1. For example, suppose the stake is $100: if player 1 gives $10 to player 2 (and keeps $90) and player 3 wants to punish this offer amount, then player 1 takes home $60; player 2, $10; and player 3, $40. If player 3 had instead decided not to punish offers of 10%, then the take-home amounts would have been $90, $10, and $50, respectively. In this anonymous one-shot game, a purely self-interested player 3 would never pay to punish player 1. Knowing this, a self-interested player 1 should always offer zero to player 2. Thus, an individual's willingness to pay to punish provides a direct measure of the person's taste for a second type of costly punishment, third-party punishment.

To get behavioral measures of altruism, we also conducted dictator games (DG) in each population. The DG is the same as the UG except that player 2 cannot reject (*18*). Player 1 merely dictates the portions of the stake received by himself or herself and player 2. In this one-shot anonymous game, a purely self-interested individual would offer zero; thus, offers in the DG provide a measure of a kind of behavioral altruism that is not directly linked to kinship, reciprocity, reputation, or the immediate threat of punishment (*19*).

Here, we highlight several key aspects of our standardized procedures, protocols, and scripts (for further details, see SOM Text). First, to guarantee motivation and attention to the experiments, we standardized the stake of each game to 1 day's wage in the local economy. Players were also paid a show-up fee equal to 20% of a day's wage. Second, by using the method of back translation, all of our game scripts were administered in a local language by fluent speakers. Third, our protocol prevented those waiting to play from talking about the game and from interacting with experienced players during a game session. Fourth, individualized instruction using a fixed script, set of examples, and preplay test questions guaranteed that all players understood the game well enough to correctly answer at least two consecutive test questions (*19*).

We drew adults from a diverse set of populations scattered across the globe. Table 1

Table 1. Summary of populations studied. The column labeled "Economic base" classifies the production systems. Horticulturalists, for example, rely primarily on slash-and-burn agriculture, whereas pastoralists rely primarily on herding. "Residence" classifies societies according to the nature and frequency of their social groups' movements.

Group	Continent	Nation, region	Environs	Economic base	Residence
Accra City	Africa	Ghana	Urban	Wage work	Sedentary
Gusii	Africa	Kenya, Nyamira	Fertile high plains	Mixed farming, wage work	Sedentary
Hadza	Africa	Tanzania	Savannah-woodlands	Foraging	Nomadic
Isanga village	Africa	Tanzania, Mbeya	Mountainous forest	Agriculture, wage work	Sedentary
Maragoli	Africa	Kenya	Fertile plains	Mixed farming, wage work	Sedentary
Samburu	Africa	Kenya	Semi-arid savanna	Pastoralism	Semi-nomadic
Emory freshman	N. America	U.S., southeast	Temperate forest, urban	Students	Temporary residence
Missouri	N. America	U.S., rural and urban midwest	Prairie	Wage work and farming	Sedentary
Sanquianga	S. America	Colombia, Pacific coast	Mangrove forest	Fisheries (fish, clams, shrimp)	Sedentary
Shuar	S. America	Ecuador, Amazonia	Tropical forest	Horticulture	Sedentary
Tsimane	S. America	Bolivia, Amazonia	Tropical forest	Horticulture-foraging	Semi-nomadic
Dolgan/Nganasan	Asia	Russian Federation, Siberia	Tundra-taiga	Hunting/fishing and wage work	Semi-sedentary
Au	Oceania	Papua New Guinea, West Sepik	Mountainous tropical forest	Horticulture-foraging	Sedentary
Sursurunga	Oceania	Papua New Guinea, New Ireland	Coastal tropical island	Horticulture	Sedentary
Yasawa	Oceania	Fiji, Yasawa Island	Coastal tropical pacific	Horticulture and marine foraging	Sedentary

provides the nation, region, environment, economic base, and predominant residence pattern for each population. As points of reference, we also ran these games with students at Emory University and nonstudent adults in both rural and urban Missouri. The Missouri samples provide the appropriate U.S. points of comparison with our diverse sample of societies, whereas the student sample links us to the subject populations used in most work. In considering the student data (vis-à-vis the nonstudent data), it is important to realize that behavior in these experiments continues to change through the university years and does not reach the adult plateau until the participants reach their mid-twenties (*20*–*23*). Thus, because we want to explore the variation among adult populations and avoid confounding maturational effects, we used only the nonstudent samples in comparative analyses (*24*).

Punishment results. Our two measures of costly punishment revealed both a universal pattern, with an increasing proportion of individuals from every society choosing to punish as offers approach zero, and substantial differences across populations in their overall willingness to punish unequal offers. Figure 1 summarizes our UG data. For every population studied, the probability of rejection decreased as offers increase from 0% to 50%. At the lowest offer for which punishment is costly (10% offers), 56.5% of players rejected overall. However, the magnitude of this effect varied substantially across groups. In five societies, the Tsimane, the Shuar, Isanga village, Yasawa, and the Samburu, less than 15% of the population were willing to reject 10% offers. In contrast, over 60% of the samples in four populations rejected such offers. Another, although indirect, measure of a population's willingness to punish is its income-maximizing offer (IMO), which is the offer that maximizes player 1's expected income, given the observed rejection probabilities in that society. Marked with a dashed line, the IMO varied from 10% (little punishment) in eight of the populations to 50% (strong punishment) in two.

To assess whether the observed variation in punishment between populations can be explained by demographic and economic differences among them, we conducted a set of three linear regression analyses using player 2s' minimum acceptable offer (MAO), the lowest offer between zero and 50% that a player would accept, as the dependent variable. For example, if an individual rejected an offer of zero but then accepted 10 through 50, the MAO is 10. First, regressing MAO on population dummy variables showed that 34.4% of the variation occurs between population means. Second, adding measures of players' sex, age, education, household size, income, and wealth increased the variance explained to 41.5%, implying that these capture about 7% of the variance within populations. Third, removing the dummies from the regression decreased the variance explained to 15.8%, indicating that a substantial portion of the between-population variance cannot be explained by these individual predictors (SOM Text).

Shown in Fig. 1 is that 6 of our 14 nonstudent populations also display a willingness to reject increasingly unequal UG offers as they rise from 50% to 100%, with upwards of half of the sample rejecting offers of 100% in two populations. Originally noted by Tracer in Papua New Guinea (*25*), this willingness to reject hyperfair offers (offers greater than 50%) now appears to be widespread, having also been documented in Russia (*26*) and China (*27*). Milder versions of this phenomenon have been detected among students in the U.S. and Europe by using more sensitive bargaining instruments (*28*, *29*), and we argue that these hyperfair rejections are unlikely to result from players' confusion (SOM Text).

To study the hyperfair rejections, we also calculated the maximum acceptable offer (MXAO), which is the highest offer above 50% that a player will accept. If a player accepted all offers above 50%, his MXAO was set at 100. First, regressing MXAO on our population dummies showed that 17% of the variation in MXAO occurs between populations. Then, adding age, sex, educa-

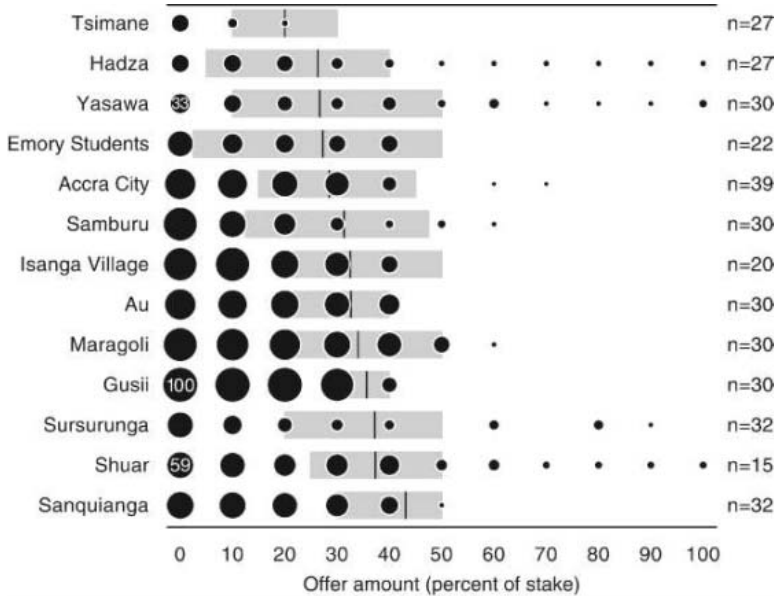

Fig. 2. 3PP results displayed as the distributions of decisions to punish across the possible offers in the 3PPG. For each population, the areas of the bubble display the fraction that was willing to punish at that offer amount. Counts on right (*n*) refer to numbers of triads of players. Inside some of the bubbles, we noted the precise percentage the bubble represents, for reference. For player 1 offers, the solid vertical bar marks the mean offer for each group, with the gray shaded rectangles highlighting the interquartiles. Populations ordered by mean offers (low to high). Emory students here are a general undergraduate sample, not the same freshman in Fig. 1.

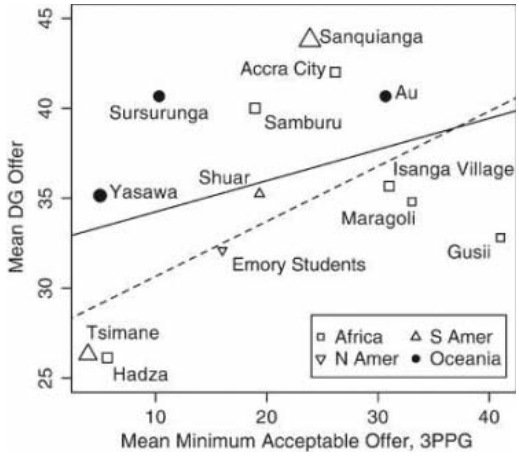

Fig. 3. Relationship between 3PP and altruism shown as the relationship between mean MAOs in the 3PPG and mean offers in the DG. The different symbols indicate geographic proximity or continent. The size of each symbol is proportional to the number of DG pairs at each site. The dotted line gives the weighted regression line, with continental controls, of mean DG offers on mean MAO-3PP. The solid line gives the simple linear regression. Emory students were not included in the regression analysis, although we have plotted them for comparison.

tion, household size, income, and wealth increased the variance explained to 24%. Third, removing the dummies dropped the variance explained to 5%, suggesting that very little of the variation among populations can be explained by measured differences in these economic and demographic variables.

Our findings for the Au, the Hadza, and the Tsimane largely replicated previous experimental work among these populations that used another version of the UG (*30*–*32*). Because these populations have provided some of the more unusual results, this robustness suggests that (i) at a population level, these findings are stable and (ii) basic patterns in the data are not substantially shifted by minor adjustments in the UG protocol.

The 3PPG revealed patterns similar to those seen in the UG, with all societies showing a decreasing frequency of punishment as offers increase to 50% (*19*), as well as substantial differences between populations (Fig. 2). Overall, two-thirds of player 3s were willing to pay 20% of their endowment (half of 1 day's wage) to punish player 1 for allocating zero to player 2. However, this fraction varied from around 28% among the Tsimane and the Hadza to over 90% among the Gusii and the Maragoli.

By using the same technique described above for MAO, we calculated the MAO-3PP for each player 3. Regressing MAO-3PP first on the group dummies showed that 38.2% of the variation occurs between groups. Adding our standard set of predictors increased the variation explained to 41%. Then, removing the dummies dropped the variance explained to 11%, indicating that a substantial portion of the between-population variation cannot be captured by our economic and demographic measures.

If costly punishment culturally coevolves with an intrinsic motivation for certain forms of altruism, societies with high degrees of punishment will also exhibit more altruistic behavior. Figure 3 plots the relationship between punishment, based on the mean MAO-3PP, and altruism, based on mean offers in the DG. To examine this relationship, we first regressed the mean DG offer from each population on the respective mean MAO-3PP. This yielded a coefficient of 0.17, with a 95% confidence interval (CI) from 0.031 to 0.51 (*33*). Second, because the population means are derived from somewhat different sample sizes, we re-ran the same regression weighted by our sample sizes. The coefficient increased to 0.23 (CI from 0.075 to 0.38). Lastly, because our samples may be correlated due to shared history (shared cultural phylogenies), we added continental dummy variables to our weighted linear regression. The coefficient for MAO-3PP then increased to 0.31 (CI from 0.13 to 0.51). In addition, measures of punishment other than the group means also correlate with mean DG offers (SOM Text).

Conclusions. We have shown three things about costly punishment as measured in one-shot anonymous experiments. First, costly punishment is present across a highly diverse range of human populations and emerges in a patterned fashion in each population. In every population, less-equal offers were punished more frequently. Second, we also find substantial variation among populations, with some societies showing very little overall willingness to punish, others demonstrating substantial willingness to punish, and still others revealing a willingness to punish offers that are either too generous or too stingy. Given the critical importance of costly punishment in maintaining cooperation in experimental studies (*12*, *34*), the observed variation here suggests that the same institutional forms may function quite differently in different populations (*33*). Third, at the population level, this willingness to punish covaries with a behavioral measure of altruism.

These three results are consistent with recent evolutionary models of altruistic punishment (*3*, *4*, *9*). In particular, culture-gene coevolutionary models that combine strategies of cooperation and punishment predict that local learning dynamics generate between-group variation as different groups arrive at different "cultural" equilibria (*36*, *37*). These local learning dynamics create social environments that favor the genetic evolution of psychologies that predispose people to administer, anticipate, and avoid punishment (by learning local norms). Alternative explanations of the costly punishment and altruistic behavior observed in our experiments have not yet been formulated in a manner that can account for stable between-group variation or the positive covariation between altruism and punishment (*38*, *39*). Whether the coevolution of cultural norms and genes or some other framework is ultimately correct, these results more sharply delineate the species-level patterns of social behavior that a successful theory of human cooperation must address.

References and Notes

1. J. Henrich *et al.*, *Behav. Brain Sci.* **28**, 795 (2005).
2. K. Panchanathan, R. Boyd, *Nature* **432**, 499 (2004).
3. R. Boyd, H. Gintis, S. Bowles, P. J. Richerson, *Proc. Natl. Acad. Sci. U.S.A.* **100**, 3531 (2003).
4. E. Fehr, U. Fischbacher, *Nature* **425**, 785 (2003).
5. A. Gardner, S. A. West, *Am. Nat.* **164**, 753 (2004).
6. H. Gintis, *J. Theor. Biol.* **206**, 169 (2000).
7. H. Gintis, *J. Theor. Biol.* **220**, 407 (2003).
8. K. Sigmund, C. Hauert, M. A. Nowak, *Proc. Natl. Acad. Sci. U.S.A.* **98**, 10757 (2001).
9. J. Henrich, R. Boyd, *J. Theor. Biol.* **208**, 79 (2001).
10. R. Boyd, P. Richerson, *Ethol. Sociobiol.* **13**, 171 (1992).
11. E. Fehr, S. Gachter, *Am. Econ. Rev.* **90**, 980 (2000).
12. E. Fehr, S. Gächter, *Nature* **415**, 137 (2002).
13. E. Fehr, U. Fischbacher, *Evol. Hum. Behav.* **25**, 63 (2003).
14. A. G. Sanfey, J. K. Rilling, J. A. Aronson, L. E. Nystrom, J. D. Cohen, *Science* **300**, 1755 (2003).
15. D. J. de Quervain *et al.*, *Science* **305**, 1254 (2004).
16. C. F. Camerer, E. Fehr, in *Foundations of Human Sociality: Economic Experiments and Ethnographic Evidence from Fifteen Small-Scale Societies*, J. Henrich *et al.*, Eds. (Oxford Univ. Press, Oxford, 2004), pp. 55–95.
17. W. Guth, R. Schmittberger, B. Schwarze, *J. Econ. Behav. Organ.* **3**, 367 (1982).
18. R. Forsythe, J. L. Horowitz, N. E. Savin, M. Sefton, *Games Econ. Behav.* **6**, 347 (1994).
19. See methods discussion in the supplemental online materials.
20. M. Sutter, M. Kocher, "Trust and reciprocity across different age groups," 2005 (www.mpiew-jena.mpg.de/esi/alumni/sutter/pdfs/children_trust_36.pdf).
21. J. Carter, M. Irons, *J. Econ. Perspect.* **5**, 171 (1991).
22. W. T. Harbaugh, K. Krause, *Econ. Inq.* **38**, 95 (2000).
23. W. T. Harbaugh, K. Krause, S. G. Liday, working paper, 2002 (http://econpapers.repec.org/paper/oreuoecwp/2002-04.htm).
24. We only have DG data for urban Missouri and no 3PPG data for rural Missouri. Because the rural and urban Missouri samples cannot be distinguished, we have combined them in all analyses. Similarly, we have treated the Dolgan and Nganasan as one sample. The Dolgan/Nganasan did not play the 3PPG.
25. D. Tracer, in *Foundations of Human Sociality: Economic Experiments and Ethnographic Evidence from Fifteen Small-Scale Societies*, J. Henrich *et al.*, Eds. (Oxford Univ. Press, Oxford, 2004), pp. 232–259.
26. D. L. Bahry, R. K. Wilson, *J. Econ. Behav. Organ.* **60**, 37 (2006).
27. H. Hennig-Schmidt, Z.-Y. Li, C. Yang, working paper, 2004 (http://ideas.repec.org/p/bon/bonedp/bgse22_2004.html).
28. S. Huck, *J. Econ. Psychol.* **20**, 183 (1999).
29. J. Andreoni, M. Castillo, R. Petrie, *Am. Econ. Rev.* **93**, 672 (2003).
30. F. W. Marlowe, in *Foundations of Human Sociality: Economic Experiments and Ethnographic Evidence from Fifteen Small-Scale Societies*, J. Henrich *et al.*, Eds. (Oxford Univ. Press, Oxford, 2004), pp. 168–193.
31. M. Gurven, in *Foundations of Human Sociality: Economic Experiments and Ethnographic Evidence from Fifteen Small-Scale Societies*, J. Henrich *et al.*, Eds. (Oxford Univ. Press, Oxford, 2004), pp. 194–231.
32. D. Tracer, *Curr. Anthropol.* **44**, 432 (2003).
33. All confidence intervals here were calculated by resampling (10,000 times) the means from each population and then recalculating the regression coefficient.
34. O. Gurerk, B. Irlenbusch, B. Rockenbach, *Science* **312**, 108 (2006).
35. S. Gächter, B. Herrmann, C. Thoni, *Behav. Brain Sci.* **28**, 822 (2005).
36. R. Boyd, P. Richerson, *J. Theor. Biol.* **215**, 287 (2002).
37. J. Henrich, *J. Econ. Behav. Organ.* **53**, 3 (2004).
38. M. Price, J. Tooby, L. Cosmides, *Evol. Hum. Behav.* **23**, 203 (2002).
39. K. Haley, D. M. T. Fessler, *Evol. Hum. Behav.* **26**, 245 (2005).

40. We first thank our study participants, who welcomed us into their homes, lives, and communities. This research was funded primarily by the NSF in the United States (grant BCS-0136761), with additional support from the MacArthur Foundation's Norms and Preferences Network. Thanks also to our many research assistants.

Supporting Online Material

www.sciencemag.org/cgi/content/full/312/5781/1767/DC1
Materials and Methods
SOM Text
Figs. S1 and S2
Tables S1 to S8
References

13 March 2006; accepted 9 May 2006
10.1126/science.1127333

Variable Very-High-Energy Gamma-Ray Emission from the Microquasar LS I +61 303

J. Albert,[1] E. Aliu,[2] H. Anderhub,[3] P. Antoranz,[4] A. Armada,[2] M. Asensio,[4] C. Baixeras,[5] J. A. Barrio,[4] M. Bartelt,[6] H. Bartko,[7] D. Bastieri,[8] S. R. Bavikadi,[9] W. Bednarek,[10] K. Berger,[1] C. Bigongiari,[8] A. Biland,[3] E. Bisesi,[9] R. K. Bock,[7] P. Bordas,[11] V. Bosch-Ramon,[11] T. Bretz,[1] I. Britvitch,[3] M. Camara,[4] E. Carmona,[7] A. Chilingarian,[12] S. Ciprini,[13] J. A. Coarasa,[7] S. Commichau,[3] J. L. Contreras,[4] J. Cortina,[2] V. Curtef,[6] V. Danielyan,[12] F. Dazzi,[8] A. De Angelis,[9] R. de los Reyes,[4] B. De Lotto,[9] E. Domingo-Santamaría,[2] D. Dorner,[1] M. Doro,[8] M. Errando,[2] M. Fagiolini,[14] D. Ferenc,[15] E. Fernández,[2] R. Firpo,[2] J. Flix,[2] M. V. Fonseca,[4] L. Font,[5] M. Fuchs,[7] N. Galante,[14] M. Garczarczyk,[7] M. Gaug,[8] M. Giller,[10] F. Goebel,[7] D. Hakobyan,[12] M. Hayashida,[7] T. Hengstebeck,[16] D. Höhne,[1] J. Hose,[7] C. C. Hsu,[7] P. G. Isar,[7] P. Jacon,[10] O. Kalekin,[16] R. Kosyra,[7] D. Kranich,[3,15] M. Laatiaoui,[7] A. Laille,[15] T. Lenisa,[9] P. Liebing,[7] E. Lindfors,[13] S. Lombardi,[8] F. Longo,[17] J. López,[2] M. López,[4] E. Lorenz,[3,7] F. Lucarelli,[4] P. Majumdar,[7] G. Maneva,[18] K. Mannheim,[1] O. Mansutti,[9] M. Mariotti,[8] M. Martínez,[2] K. Mase,[7] D. Mazin,[7] C. Merck,[7] M. Meucci,[14] M. Meyer,[1] J. M. Miranda,[4] R. Mirzoyan,[7] S. Mizobuchi,[7] A. Moralejo,[2] K. Nilsson,[13] E. Oña-Wilhelmi,[2] R. Orduña,[5] N. Otte,[7] I. Oya,[4] D. Paneque,[7] R. Paoletti,[14] J. M. Paredes,[11] M. Pasanen,[13] D. Pascoli,[8] F. Pauss,[3] N. Pavel,[16*] R. Pegna,[14] M. Persic,[19] L. Peruzzo,[8] A. Piccioli,[14] M. Poller,[1] G. Pooley,[20] E. Prandini,[8] A. Raymers,[12] W. Rhode,[6] M. Ribó,[11] J. Rico,[2]† B. Riegel,[1] M. Rissi,[3] A. Robert,[5] G. E. Romero,[21,22] S. Rügamer,[1] A. Saggion,[8] A. Sánchez,[5] P. Sartori,[8] V. Scalzotto,[8] V. Scapin,[8] R. Schmitt,[1] T. Schweizer,[16] M. Shayduk,[16] K. Shinozaki,[7] S. N. Shore,[23] N. Sidro,[2]† A. Sillanpää,[13] D. Sobczynska,[10] A. Stamerra,[14] L. S. Stark,[3] L. Takalo,[13] P. Temnikov,[18] D. Tescaro,[2] M. Teshima,[7] N. Tonello,[7] A. Torres,[5] D. F. Torres,[2,24] N. Turini,[14] H. Vankov,[18] V. Vitale,[9] R. M. Wagner,[7] T. Wibig,[10] W. Wittek,[7] R. Zanin,[8] J. Zapatero[5]

Microquasars are binary star systems with relativistic radio-emitting jets. They are potential sources of cosmic rays and can be used to elucidate the physics of relativistic jets. We report the detection of variable gamma-ray emission above 100 gigaelectron volts from the microquasar LS I +61 303. Six orbital cycles were recorded. Several detections occur at a similar orbital phase, which suggests that the emission is periodic. The strongest gamma-ray emission is not observed when the two stars are closest to one another, implying a strong orbital modulation of the emission or absorption processes.

Microquasars are binary star systems consisting of a compact object of a few solar masses (either a neutron star or a black hole) and a companion star that loses mass into an accretion disk around the compact object. The most relevant feature of microquasars is that they display relativistic jets—outflows of matter from regions close to accreting black holes and neutron stars. These jets are among the most spectacular astrophysical phenomena, yet they remain poorly explained (*1*). In microquasars, the time scales of relevant processes, because they are correlated with the compact object's mass, are shorter than those in quasars by more than six orders of magnitude, allowing the study of a different range of variability. In addition, microquasars could measurably contribute to the density of galactic cosmic rays (*2*). It is noteworthy that photons up to very high energy (VHE) are an expected by-product of cosmic ray production.

Two GeV sources detected by the Energetic Gamma-Ray Experiment Telescope (EGRET) (*3*) are positionally compatible with microquasars. One of these, LS 5039 (*4*) in the Southern Hemisphere, was recently confirmed as a TeV emitter (*5*) by the High Energy Stereoscopic System (HESS). The other, LS I +61 303 (*6*), can be observed from the Northern Hemisphere and was thus a natural target for the Major Atmospheric Gamma-ray Imaging Cherenkov (MAGIC) telescope.

LS I +61 303 is a B0 main-sequence star with a circumstellar disc (i.e., a Be star) located at a distance of ~2 kpc (*7*). A compact object of unknown mass is orbiting around it every 26.496 days (*8*, *9*). The eccentricity of the orbit is 0.72 ± 0.15, and the periastron passage (the point where the two stars are closest to one another) is at phase 0.23 ± 0.02. The nature of the compact object is still debated (*10*). Radio outbursts are observed every orbital cycle from this system (*11*) at phases varying between 0.45 and 0.95 (*12*) with a modulation of 4.6 years. The monitoring of LS I +61 303 at x-ray energies (*13*–*15*) revealed x-ray outbursts starting around phase 0.4 and lasting up to phase 0.6. The detection of extended jetlike and likely rapidly precessing radio-emitting structures at angular extensions of 0.01 to 0.05 arc sec has been interpreted as unambiguous evidence of the microquasar nature of LS I +61 303 (*16*, *17*).

The gamma-ray source 3EG J0241+6103 (also known as 2CG 135+01) was discovered by Cosmic Ray Satellite B (COS-B) at energies above 100 MeV (*18*). Despite its large uncertainty (~1°) in position, the source was proposed to be the high-energy counterpart of the 26.5-day periodic radio outburst source GT 0236+610, which turned out to be the early-type star LS I +61 303 (*11*). The large uncertainty of the position of 3EG J0241+6103 did not allow unambiguous association with LS I +61 303. The GeV gamma-ray emission from this EGRET source is clearly variable (*19*). Even though the GeV data remain scarce in this regime, an increased emission has been suggested for the periastron passage (*20*) and was firmly reported around phase 0.5 (*6*), coincident with the x-ray outbursts.

MAGIC, located on La Palma, Canary Islands (Spain), is an imaging air Cherenkov telescope (IACT). This kind of instrument images the Cherenkov light produced in the particle cascade initiated by a gamma ray in the atmosphere. MAGIC (*21*, *22*) includes several innovative techniques and technologies in its design and is currently the largest single-dish telescope (diameter 17 m) in this energy band. It is equipped with a 576-pixel photomultiplier camera with a 3.5° field of view. The telescope's sensitivity above 100 GeV is ~2.5% of the Crab Nebula flux (the calibration standard candle for IACTs) in 50 hours of observations. The angular resolution is ~0.1°, and the energy

[1]Universität Würzburg, D-97074 Würzburg, Germany. [2]Institut de Física d'Altes Energies, E-08193 Bellaterra (Barcelona), Spain. [3]Eidgenössische Technische Hochschule Zürich, CH-8093 Zürich, Switzerland. [4]Universidad Complutense, E-28040 Madrid, Spain. [5]Universitat Autónoma de Barcelona, E-08193 Bellaterra, Spain. [6]Universität Dortmund, D-44227 Dortmund, Germany. [7]Max-Planck-Institut für Physik, D-80805 München, Germany. [8]Università di Padova and Istituto Nazionale di Fisica Nucleare (INFN), I-35131 Padova, Italy. [9]Università di Udine and INFN Trieste, I-33100 Udine, Italy. [10]University of Lodz, PL-90236 Lodz, Poland. [11]Universitat de Barcelona, E-08028 Barcelona, Spain. [12]Yerevan Physics Institute, 375036 Yerevan, Armenia. [13]Tuorla Observatory, FI-21500 Piikkiö, Finland. [14]Università di Siena and INFN Pisa, I-53100 Siena, Italy. [15]University of California, Davis, CA 95616, USA. [16]Humboldt-Universität zu Berlin, D-12489 Berlin, Germany. [17]Università di Trieste and INFN Trieste, I-34100 Trieste, Italy. [18]Institute for Nuclear Research and Nuclear Energy, BG-1784 Sofia, Bulgaria. [19]Osservatorio Astronomico and INFN Trieste, I-34100 Trieste, Italy. [20]Cavendish Laboratory, University of Cambridge, Cambridge CB3 0HE, UK. [21]Facultad de Ciencias Astronómicas y Geofísicas, UNLP, 1900 La Plata, Argentina. [22]Instituto Argentino de Radioastronomía CC5, 1894 Villa Elisa, Argentina. [23]Università di Pisa and INFN Pisa, I-56100 Pisa, Italy. [24]Institut de Ciències de l'Espai/Consejo Superior de Investigaciones Cientificas, E-08193 Bellaterra (Barcelona), Spain.

*Deceased.

†To whom correspondence should be addressed. E-mail: nsidro@ifae.es (N.S.); jrico@ifae.es (J.R.)

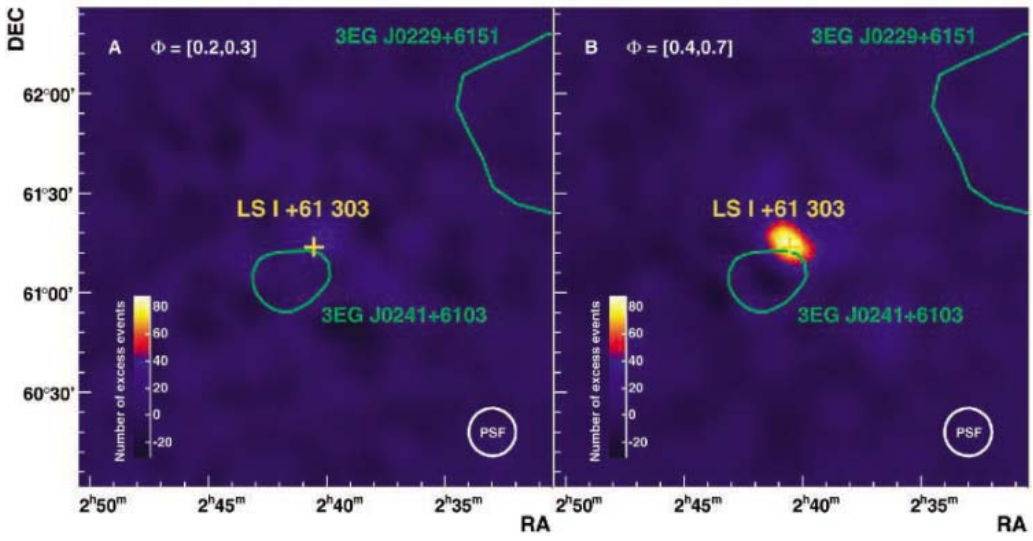

Fig. 1. Smoothed maps of gamma-ray excess events above 400 GeV around LS I +61 303. (**A**) Observations over 15.5 hours corresponding to data around periastron (i.e., between orbital phases 0.2 and 0.3). (**B**) Observations over 10.7 hours at orbital phase between 0.4 and 0.7. The number of events is normalized in both cases to 10.7 hours of observation. The position of the optical source LSI +61 303 (yellow cross) and the 95% confidence level contours for 3EG J0229+6151 and 3EG J0241+6103 (green contours) are also shown. The bottom right circle shows the size of the point spread function of MAGIC (1σ radius). No significant excess in the number of gamma-ray events is detected around periastron passage, whereas it shows up clearly (9.4σ statistical significance) at later orbital phases, in the location of LS I +61 303.

resolution above 200 GeV is better than 30%. MAGIC can provide gamma-ray source localization in the sky with a precision of ~2′.

LS I +61 303 was observed during 54 hours (after standard quality selection, discarding bad-weather data) between October 2005 and March 2006. MAGIC is unique among IACTs in its capability to operate in the presence of the Moon. This allows the duty cycle to be increased by up to 50%, thus considerably improving the sampling of variable sources. In particular, 22% of the data used in this analysis were recorded under moonlight. The data analysis was carried out using the standard MAGIC analysis and reconstruction software (*21*, *22*).

The reconstructed gamma-ray map (Fig. 1) during two different observation periods, around periastron passage and at higher (0.4 to 0.7) orbital phases, clearly shows an excess in the latter case. The excess is located at (J2000) $\alpha = 2^h40^m34^s$, $\delta = 61°15'25''$, with statistical and systematic uncertainties of ±0.4′ and ±2′, respectively, in agreement with the position of LS I +61 303. The distribution of gamma-ray excess is consistent with a pointlike source. In the natural case in which the VHE emission is produced by the same object detected at EGRET energies, this result identifies a gamma-ray source that resisted classification during the past three decades.

Our measurements show that the VHE gamma-ray emission from LS I +61 303 is variable. The gamma-ray flux above 400 GeV coming from the direction of LS I +61 303 (Fig. 2) has a maximum corresponding to ~16% of the Crab Nebula flux and is detected around phase 0.6. The combined statistical significance of the three highest flux measurements is 8.7σ, for an integrated observation time of 4.2 hours. The probability for the distribution of measured fluxes to be a statistical fluctuation of a constant flux (obtained from a χ^2 fit of a constant function to the entire data sample) is 3×10^{-5}. The fact that the detections occur at similar orbital phases suggests a periodic nature of the VHE gamma-ray emission. Contemporaneous radio observations of LS I +61 303 were carried out at 15 GHz with the Ryle Telescope covering several orbital periods of the source. The peak of the radio outbursts was at phase 0.7, just after the increase of the VHE gamma-ray flux (fig. S1).

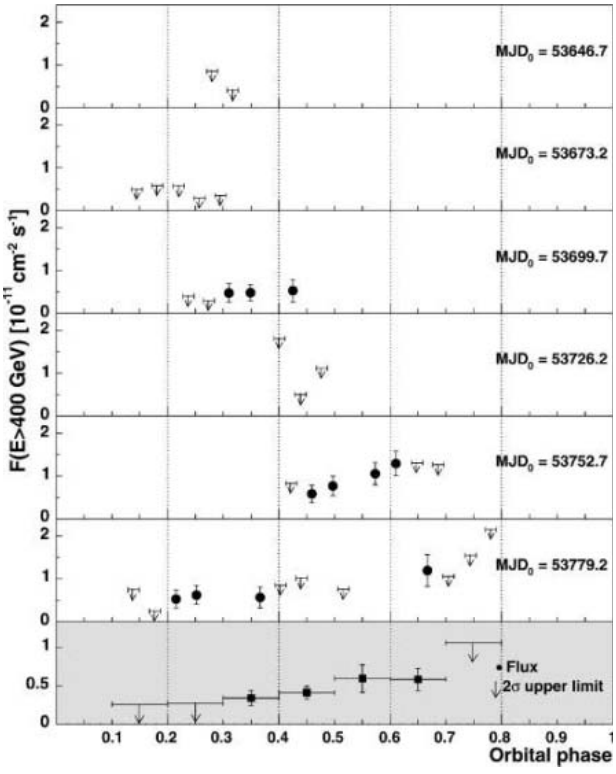

Fig. 2. VHE gamma-ray flux of LS I +61 303 as a function of orbital phase for the six observed orbital cycles (six upper panels, one point per observation night) and averaged for the entire observation time (bottom panel). Vertical error bars include 1σ statistical error and 10% systematic uncertainty on day-to-day relative fluxes. Only data points with more than 2σ significance are shown, and 2σ upper limits (*33*) are derived for the rest. The modified Julian date (MJD) corresponding to orbital phase 0 is indicated for every orbital cycle. The orbital phase is computed with orbital period of 26.4960 days and zero phase at JD 2443366.775 (*9*); periastron takes place at phase 0.23 (*10*). Marginal detections occur between orbital phases 0.2 and 0.4 in different cycles, whereas a significant increase of flux is detected from phase ~0.45 to phase ~0.65 in the fifth cycle, peaking at ~16% of the Crab Nebula flux on MJD 53769 (phase 0.61). During the following cycle, the highest flux is measured on MJD 53797 (phase 0.67). This behavior suggests that the VHE gamma-ray emission from LS I +61 303 has a periodic nature.

The VHE spectrum derived from data between ~200 GeV and ~4 TeV at orbital phases between 0.4 and 0.7 is fitted reasonably well (χ^2/ndf = 6.6/5) by a power-law function: $dN_\gamma/(dA/dt/dE) = (2.7 \pm 0.4 \pm 0.8) \times 10^{-12} E^{(-2.6 \pm 0.2 \pm 0.2)}$ cm^{-2} s^{-1} TeV^{-1}, where $N\gamma$ is the number of gamma rays reaching Earth per

unit area A, time t, and energy E, and E is expressed as TeV. Errors quoted are statistical and systematic, respectively (fig. S2). This spectrum is consistent with that of EGRET for a spectral break between 10 and 100 GeV. We estimate that the flux from LS I +61 303 above 200 GeV corresponds to an isotropic luminosity of $\sim 7 \times 10^{33}$ ergs s^{-1} at a distance of 2 kpc. The intrinsic luminosity of LS I +61 303 at its maximum is higher than that of LS 5039 by a factor of ~6 and is lower than the combined upper limit ($<8.8 \times 10^{-12}$ cm^{-2} s^{-1} above 500 GeV) obtained by Whipple (*23*) by a factor of ~2. LS I +61 303 displays more luminosity at GeV than at x-ray energies, a behavior shared also by LS 5039 (*4*).

Different models have been put forward to explain putative gamma-ray emission from LS I +61 303. Maraschi and Treves (*24*) proposed that the GeV emission measured by COS-B could be due to the wind from a pulsar interacting with that of the stellar companion. However, the detection of radio jets (*16*, *17*) favored an accretion scenario. The observation of jets has also triggered the study of different microquasar gamma-ray emission models. Some of these models are based on hadronic mechanisms: Relativistic protons in the jet interact with nonrelativistic stellar wind ions, producing gamma rays via neutral pion decay (*25*, *26*). Others are based on leptonic mechanisms such as inverse Compton (IC) scattering of relativistic electrons in the jet on stellar and/or synchrotron photons (*27*–*29*).

The TeV flux maximum is detected at phases 0.5 to 0.6 (Fig. 2), overlapping with the x-ray outburst and the onset of the radio outburst. The maximum flux is not detected at periastron, when the accretion rate is expected to be the largest (*30*). This result seems to favor the leptonic over the hadronic models, because the IC efficiency is likely to be higher than that of proton-proton collisions at the relatively large distances from the companion star at this orbital phase. With respect to energetics, a relativistic power on the order of 10^{36} ergs s^{-1} could explain the nonthermal luminosity of the source from radio to VHE gamma rays. This power can be extracted from accretion in a slow inhomogeneous wind along the orbit (*30*).

The variable nature of the TeV emission on time scales of ~1 day constrains the emitting region to be smaller than 10^{15} cm (or ~0.1 arc sec at 2 kpc). This is compatible with the emission being produced within the binary system, where there are large densities of seed photons for IC interaction. Under these strong photon fields, opacity effects certainly play a role in the modulation of the emitted radiation (*31*). Indeed, VHE gamma-ray emission that peaks after periastron passage has been recently predicted with models that consider electromagnetic cascading within the binary system (*32*). In addition, the detection of VHE gamma-ray emission associated with both LS I +61 303 and LS 5039 observationally confirms high-mass microquasars as a population of galactic TeV gamma-ray sources.

LS I +61 303 is an excellent laboratory to study the VHE gamma-ray emission and absorption processes taking place in massive x-ray binaries. The high eccentricity of the binary system provides very different physical conditions to be tested on time scales of less than 1 month.

References and Notes

1. I. F. Mirabel, L. F. Rodríguez, *Annu. Rev. Astron. Astrophys.* **37**, 409 (1999).
2. S. Heinz, R. A. Sunyaev, *Astron. Astrophys.* **390**, 751 (2002).
3. R. C. Hartman *et al.*, *Astrophys. J.* **123** (suppl.), 79 (1999).
4. J. M. Paredes, J. Martí, M. Ribó, M. Massi, *Science* **288**, 2340 (2000).
5. F. Aharonian *et al.*, *Science* **309**, 746 (2005); published online 7 July 2005 (10.1126/science.1113764).
6. D. A. Kniffen *et al.*, *Astrophys. J.* **486**, 126 (1997).
7. D. A. Frail, R. M. Hjellming, *Astron. J.* **101**, 2126 (1991).
8. J. B. Hutchings, D. Crampton, *Pub. Astron. Soc. Pac.* **93**, 486 (1981).
9. P. C. Gregory, *Astrophys. J.* **575**, 427 (2002).
10. J. Casares, I. Ribas, J. M. Paredes, J. Martí, C. Allende Prieto, *Mon. Not. R. Astron. Soc.* **360**, 1105 (2005).
11. P. C. Gregory, A. R. Taylor, *Nature* **272**, 704 (1978).
12. J. M. Paredes, R. Estalella, A. Rius, *Astron. Astrophys.* **232**, 377 (1990).
13. P. Goldoni, S. Mereghetti, *Astron. Astrophys.* **299**, 751 (1995).
14. A. R. Taylor, G. Young, M. Peracaula, H. T. Kenny, P. C. Gregory, *Astron. Astrophys.* **305**, 817 (1996).
15. F. A. Harrison, P. S. Ray, D. A. Leahy, E. B. Waltman, G. G. Pooley, *Astrophys. J.* **528**, 454 (2000).
16. M. Massi, M. Ribó, J. M. Paredes, M. Peracaula, R. Estalella, *Astron. Astrophys.* **376**, 217 (2001).
17. M. Massi *et al.*, *Astron. Astrophys.* **414**, L1 (2004).
18. W. Hermsen *et al.*, *Nature* **269**, 494 (1977).
19. M. Tavani, D. Kniffen, J. R. Mattox, J. M. Paredes, R. Foster, *Astrophys. J.* **497**, L89 (1998).
20. M. Massi, *Astron. Astrophys.* **422**, 267 (2004).
21. J. Albert *et al.*, *Astrophys. J.* **638**, L101 (2006).
22. J. Albert *et al.*, *Astrophys. J.* **637**, L41 (2006).
23. S. J. Fegan *et al.*, *Astrophys. J.* **624**, 638 (2005).
24. L. Maraschi, A. Treves, *Mon. Not. R. Astron. Soc.* **194**, 1P (1981).
25. G. E. Romero, D. F. Torres, M. M. Kaufman Bernadó, I. F. Mirabel, *Astron. Astrophys.* **410**, L1 (2003).
26. G. E. Romero, H. R. Christiansen, M. Orellana, *Astrophys. J.* **632**, 1093 (2005).
27. A. M. Atoyan, F. Aharonian, *Mon. Not. R. Astron. Soc.* **302**, 253 (1999).
28. V. Bosch-Ramon, J. M. Paredes, *Astron. Astrophys.* **425**, 1069 (2004).
29. V. Bosch-Ramon, G. E. Romero, J. M. Paredes, *Astron. Astrophys.* **447**, 263 (2006).
30. J. Martí, J. M. Paredes, *Astron. Astrophys.* **298**, 151 (1995).
31. G. Dubus, *Astron. Astrophys.* **451**, 9 (2006).
32. W. Bednarek, *Mon. Not. R. Astron. Soc.* **368**, 579 (2006).
33. W. A. Rolke, A. M. López, J. Conrad, *Nucl. Instrum. Methods A* **551**, 493 (2005).

34. We thank the Instituto de Astrofísica de Canarias for the excellent working conditions at the Observatory Roque de los Muchachos in La Palma. Supported by the Bundesministerium für Bildung und Forschung and Max-Planck-Gesellschaft (Germany), INFN (Italy), Comisión Interministerial de Ciencia y Tecnología and Ministerio de Educación y Ciencia grant AYA2004-07171-C02-01 (Spain), ETH (Switzerland) research grant TH-34/04-3, and Ministerstwo Nauki i Informatyzacji (Poland) grant 1P03D01028.

Supporting Online Material

www.sciencemag.org/cgi/content/full/1128177/DC1
Figs. S1 and S2

31 March 2006; accepted 8 May 2006
Published online 18 May 2006;
10.1126/science.1128177
Include this information when citing this paper.

The Spiral Structure of the Outer Milky Way in Hydrogen

E. S. Levine,* Leo Blitz, Carl Heiles

We produce a detailed map of the perturbed surface density of neutral hydrogen in the outer Milky Way disk, demonstrating that the Galaxy is a non-axisymmetric multiarmed spiral. Spiral structure in the southern half of the Galaxy can be traced out to at least 25 kiloparsecs, implying a minimum radius for the gas disk. Overdensities in the surface density are coincident with regions of reduced gas thickness. The ratio of the surface density to the local median surface density is relatively constant along an arm. Logarithmic spirals can be fit to the arms with pitch angles of 20° to 25°.

Mapping the Milky Way's spiral structure is traditionally difficult because the Sun is imbedded in the Galactic disk; absorption by dust renders optical methods ineffective at distances larger than a few kpc. Radio lines like the 21-cm hyperfine transition of atomic hydrogen (HI) are not affected by this absorption and are therefore well suited to looking through the disk. The density of HI is roughly proportional to the intensity of the emission, barring optical depth effects. Maps are constructed by using the Doppler shift of the emission line in combination with the rotation structure to determine where in the Galaxy the emission originates. The first maps of the HI density in the midplane of the Milky Way (*1*) made with the use of the 21-cm transition offered the promise that HI mapping of the Galactic plane would reveal its spiral structure by highlighting regions with HI overdensities. The task is easiest outside of the Sun's orbit

Astronomy Department, University of California, 601 Campbell Hall, Berkeley, CA 94720, USA.

*To whom correspondence should be addressed. E-mail: elevine@astron.berkeley.edu

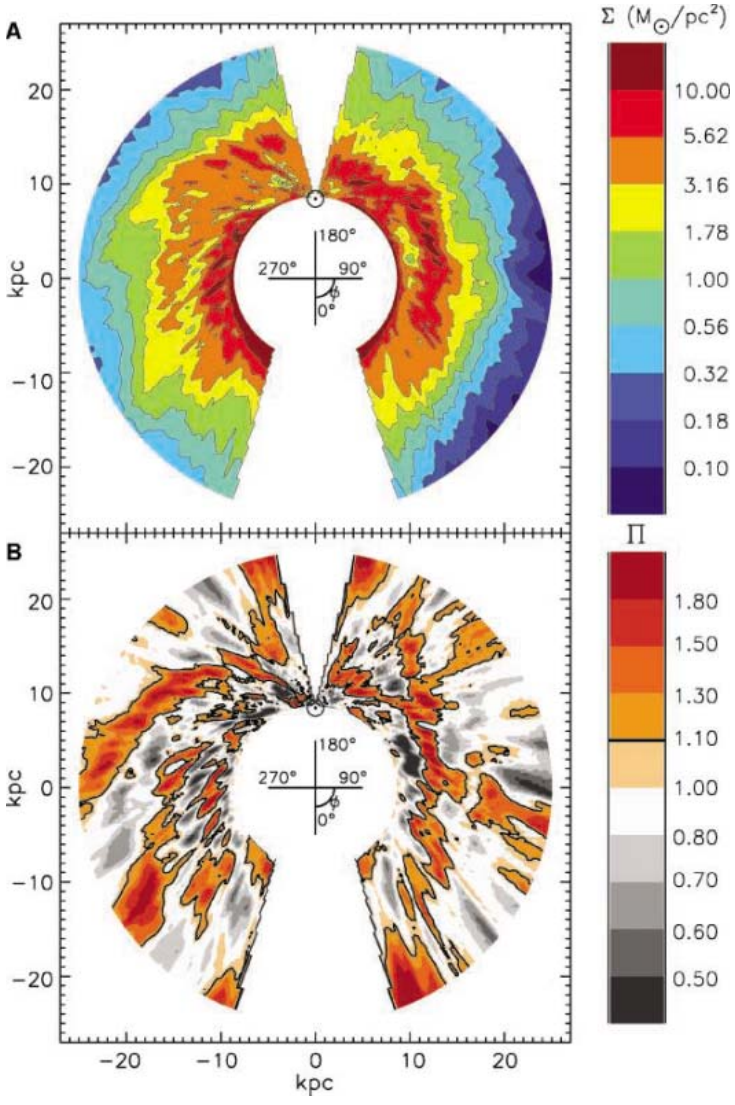

Fig. 1. (**A**) Contour plot of the surface density $\Sigma(R,\phi)$. The location of the Sun is marked at (0, 8.5 kpc) by the solar symbol ⊙. The regions excluded because of unreliable distances are the large blank wedges near the Sun-Galactic center line. (**B**) Contour plot of $\Pi(R,\phi)$ as defined in the text. Colored regions are overdense compared with the local median, whereas grayscale regions are underdense. The solid contour marks the line $\Pi = 1.1$. The values of Π for the different contour levels are given by the color bar.

Fig. 2. A contour plot of the perturbations in the gas thickness, $\Gamma(R,\phi)$. Colored regions have reduced thickness compared with the local median, whereas grayscale regions have larger thicknesses. The perturbation levels for the different contour levels are given by the color bar. The solid contour marks the line $\Pi = 1.1$, the same as in Fig. 1, to show the alignment of the overdense surface densities with the thinner gas regions.

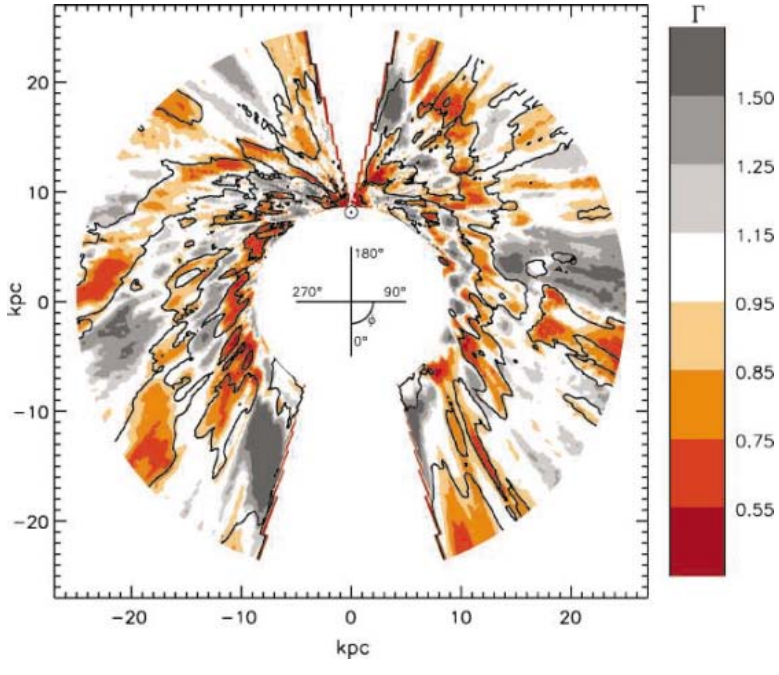

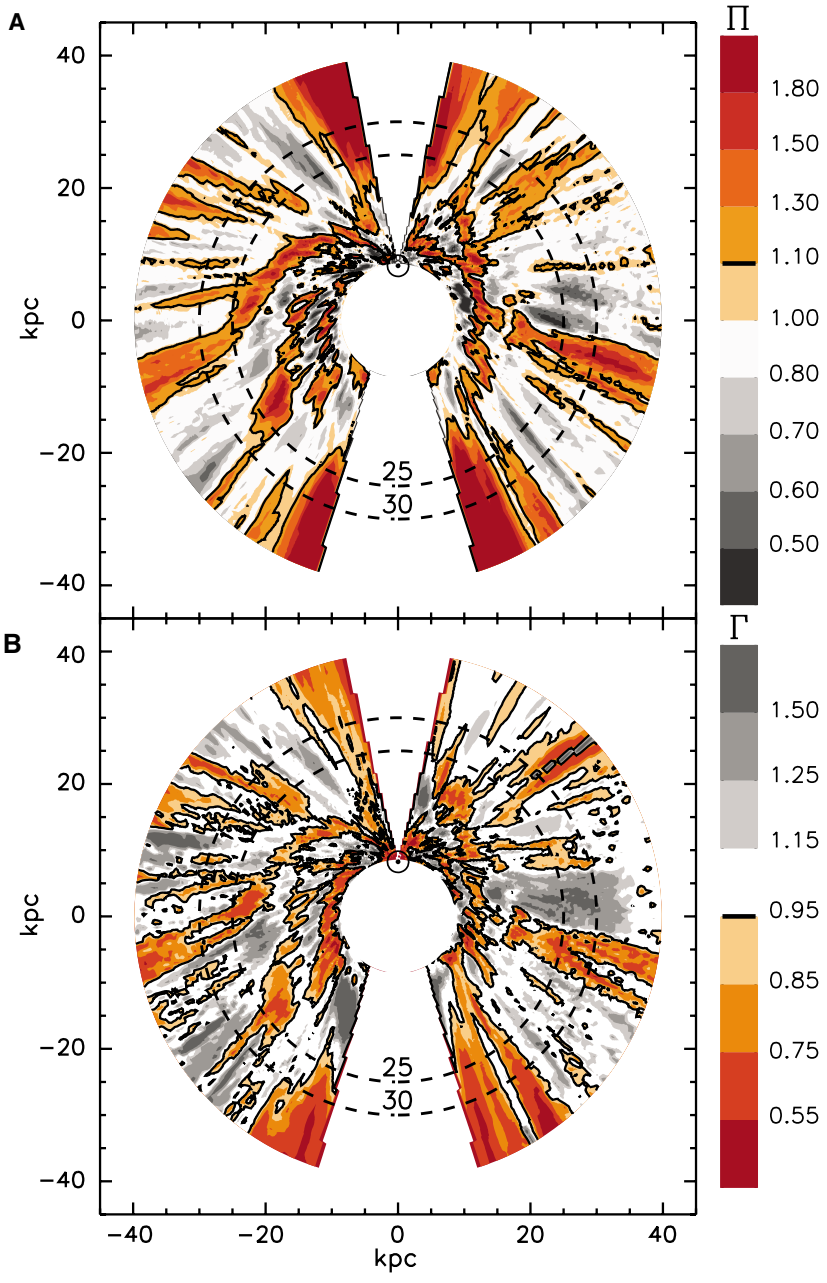

Fig. 3. (**A**) A contour map of the modified unsharp masked surface density, $\Pi(R,\phi)$, out to 40 kpc. (**B**) A contour map of the modified unsharp masked disk thickness, $\Gamma(R,\phi)$. The dashed circles are lines of constant Galactocentric radius, marked in kpc.

around the Galactic center, because velocities in this region map into distances uniquely; in the inner Galaxy, however, each velocity corresponds to two distinct distances from the Sun, so an unambiguous velocity-to-position mapping is impossible. When observations of the southern plane of the Galaxy made in Australia were combined with northern sky data from the Netherlands (*2*), a picture of spiral structure of the inner Milky Way was seen, but it did not clearly resemble that of a typical spiral galaxy; the spiral structure in the outer Galaxy (outside the Solar orbit) was less apparent. More recent maps of HI in the outer Galaxy have improved on the early work (*3*).

In this paper, we present a map of perturbations on the HI surface density in the outer Milky Way using a modified unsharp masking technique. By subtracting a blurred copy from the original image, this technique emphasizes low-contrast features in both bright and dim regions (*4*), such as spiral structure. In previous maps [e.g., (*3*) and Fig. 1], spiral arms were difficult to discern on top of the surface density's global falloff with radius.

We constructed a grid of the HI density for the outer Galactic disk, ρ, as a function of Galactocentric radius, R, angle, ϕ, and height off the plane, z, from the Leiden-Argentine-Bonn (LAB) Galactic HI survey (*5*–*8*). The

Table 1. Fits to pitch angles, ψ, and angles at which the arms cross the Solar circle, ϕ_0. The arm numbers correspond to Fig. 4A.

Arm	ψ (°)	ϕ_0 (°)
1	24	56
2	24	135
3	25	189
4	21	234

density was recovered from the measured intensity by assuming a constant spin temperature of 155 K and by using the Doppler shift velocity to determine distance along the line of sight. We applied a median filter to remove small features not associated with the disk (such as other galaxies) and a thickness filter to remove larger-scale features like clouds and spurs coming off the disk. We adopted the International Astronomical Union standard value of $R_0 = 8.5$ kpc for the Sun-Galactic center distance; recent measurements suggesting that this value may be too high would result in a proportional rescaling of the disk (*9*, *10*). We constructed the surface density map, $\Sigma(R,\phi)$, by summing the grid $\rho(R,\phi,z)$ over z (Fig. 1). For our rotation structure, we used circular orbits with a frequency $m = 1$ epicyclic streamline correction and a circular velocity of 220 km/s constant with radius (*11*). The epicyclic correction is necessary because previous studies of HI spiral arms that used purely circular orbits resulted in grossly discontinuous surface density contours near the Sun-Galactic center line [e.g., (*3*)]; the magnitude of the correction is fit to minimize this discontinuity. The maximum line-of-sight velocities of the corrections were fixed to lie along the Sun-Galactic center line. We excluded from the map regions within ±15° of the Sun-Galactic center line because of the difficulty of determining reliable distances in these directions. Our radial grid runs over the Galactocentric range from 8.6 kpc to 40 kpc.

For each point on our grid, we calculated $\eta(R,\phi)$, the median surface density of the points within 25° in ϕ and 2 kpc in R; this local median is analogous to the blurred image used in unsharp masking. It is well suited for looking for perturbations in surface density, because it takes into account the falloff in surface density with radius and adjusts if the Galaxy has a lopsided or lumpy distribution. For points within 2 kpc of the inner and outer radial borders of our grid, we narrowed the radial range so that the median is evenly balanced with surface densities inside and outside the point. We then compared the surface density at each point to the median value:

$$\Pi(R,\phi) = \Sigma(R,\phi)/\eta(R,\phi) \qquad (1)$$

This is a dimensionless quantity and therefore is a direct measure of the strength of the

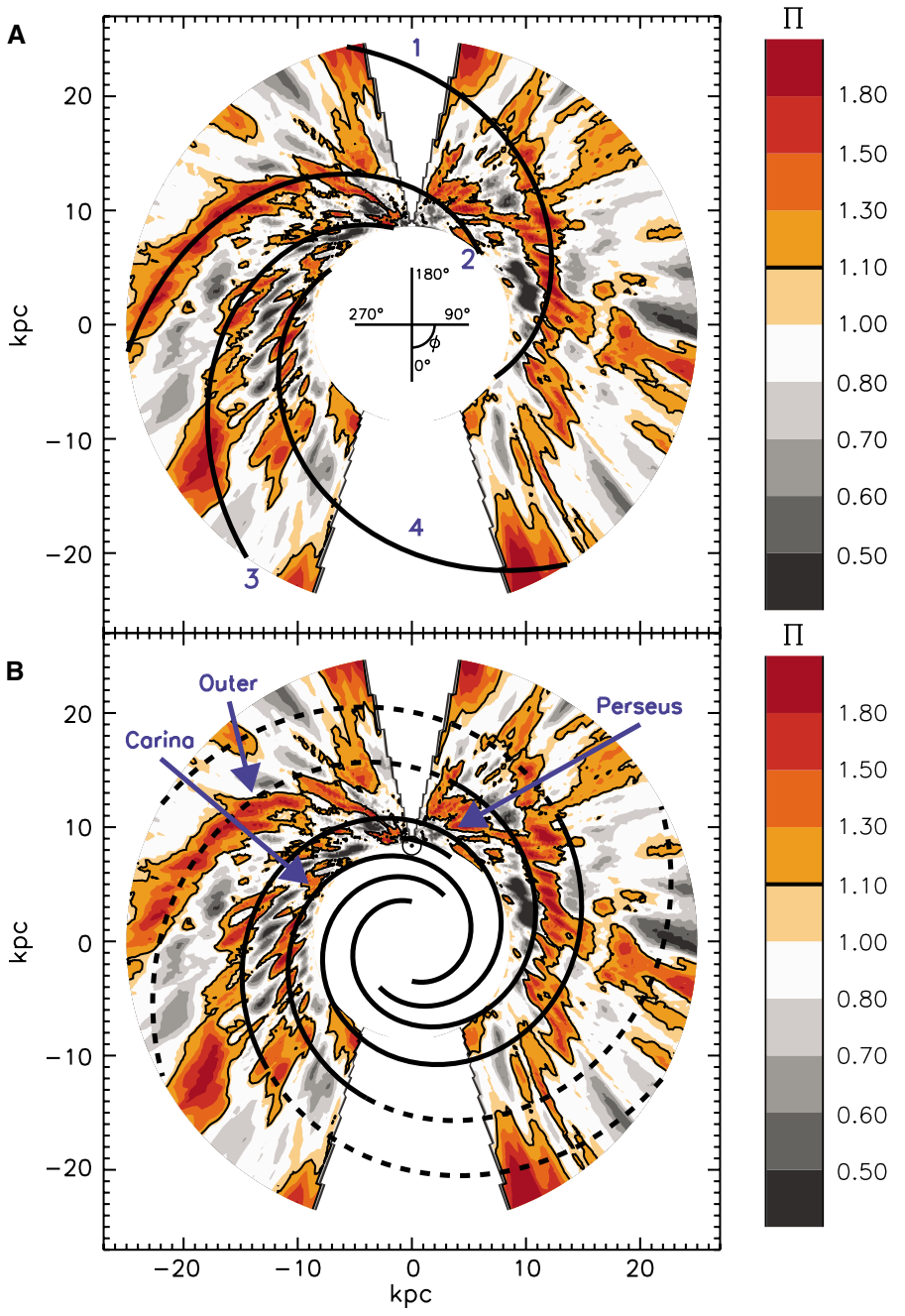

Fig. 4. (**A**) The same contour plot as in Fig. 1B, with a four-armed logarithmic spiral fit overplotted. The fitting method is described in the text. Other fits that connect different features are possible. (**B**) The same contour plot as in Fig. 1B, with the four-armed symmetric spiral model overplotted (*23*). The solid lines represent the model over its claimed range of validity; the dashed lines are an extension beyond that range. The unlabeled short line near the Sun is the local Orion arm. The width of the model arms is arbitrary.

surface density perturbations (Fig. 1). Dividing by the local median rather than subtracting, as is normally done in unsharp masking, compensates for the change in the surface density by more than an order of magnitude over the radial range of the map.

Values of surface density ratios in Fig. 1 range from a minimum of $\Pi = 0.13$ to a maximum of 10.36. The vast majority of points have values in the range from 0.6 to 1.8, implying that the arm-to-interarm surface density ratio is about 3. The typical value of Π does not vary strongly as a function of R along an arm or even from arm to arm. The $\Pi = 1$ line does not signify the border of a spiral arm, so Fig. 1 does not provide a meaningful description of the width of the arms. Furthermore, the intrinsic velocity dispersion serves to widen the apparent arms, especially at large radii.

Several long spiral arms appear clearly on the map, but the overall structure does not have the reflection through the origin symmetry of a "grand design" spiral. Easily identified spiral arms cover a larger area in the south than in the north; there are three arms in the southern half of the diagram. Calculating η over a smaller range of R and ϕ reveals more structure in the arms but does not change their positions. Each of these arms has already been detected in previous maps out to about 17 kpc for the two arms closer to the anticenter (*3*) and out to 24 kpc for the outer arm (*12*). The modified unsharp masking technique allows us to trace the arms further; these arms run coherently over a length of nearly 30 kpc in the outer Galaxy alone. Near the Sun, the overdense region in Fig. 1 at $R \approx 10$ kpc and $\phi \approx 160°$ is associated with the Perseus arm; however, there is a well-known discrepancy between photometrically and kinematically determined distances in this region (*13*, *14*). The well-defined underdense interarm regions in the south are also quite striking. There are clear underdense regions between all three of the arms in the south. In the north, a strongly underdense region is apparent inside the arm at $R \approx 13$ kpc.

When using the Doppler shift velocity of an emission line to find the distance to the emitting gas, small-scale velocity perturbations result in distortions of the distance measure because the assumed rotation structure is inaccurate. In fact, peaks in 21-cm emission intensity are more likely to result from a combination of density and velocity perturbations (*15*, *16*) than solely from HI overdensities. Physically, this occurs because a peak can be explained by a local density maximum or by nearby gas flowing into or out of that location. If velocity perturbations result from spiral structure as described in density wave theory (*17*), then Fig. 1 will not represent the true perturbed surface density but will still be a reasonable representation of the spiral pattern (*3*). A dynamical model that self-consistently incorporates density and velocity perturbations is required to compensate for this effect but is beyond the scope of this paper.

We also mapped the thickness of the HI gas as a function of position by calculating the second moment, T, of the density distribution ρ for each point in (R,ϕ). When we performed the modified unsharp masking on $T(R,\phi)$ to create $\Gamma(R,\phi)$, spiral structure is evident (Fig. 2). The quantity Γ is a direct equivalent to Π as defined in Eq. 1. The value of Γ ranges in magnitude from 0.32 to 3.29, although the dynamic range of the majority of the points lies within 0.55 to 1.5. We plot the $\Pi = 1.1$ overdensity contour from the surface density perturbation map (Fig. 1) on top of the thickness perturbation map (Fig. 2), showing that there is a good match between the arm positions as calculated from the surface density and the thickness; the thickness of the HI layer is smaller in the arms

than in the rest of the disk. The correlation remains notable even if we do not apply a thickness filter to the data or if we use another definition of the thickness (3, 11). The two maps are not independent, however; changing the density distribution in the arms will necessarily produce changes in the measured thickness unless the perturbations are distributed in the same way as the initial distribution. The alignment of overdensities with regions of reduced thickness was suggested previously (3). This alignment has not been observed in other galaxies because surface density maps are most easily made for face-on galaxies where there is no information about the thickness of the gas layer.

The radial profile of the HI disk has been a matter of controversy for many years. A sharp falloff in HI emission as a function of velocity has long been known (*18*), but this need not correspond to an abrupt radial cutoff in the disk density (*19*). Velocity dispersion will cause features to be smeared along the line of sight by confusing the velocity-distance transformation, resulting in the radially elongated features near the edges of maps (Fig. 3). The radial extent of the spiral arms provides a minimum cutoff radius for the Galactic gas disk; in other words, it is not possible for the gas to have spiral structure beyond where the HI disk ends. This radius is only a lower limit, because it is possible that there is gas beyond where the spiral structure ends that does not participate in the spiral structure or that past some radius the arms are too weak to be detected by the unsharp masking. Near 25-kpc Galactocentric radius, both the surface density and the thickness perturbation maps (Fig. 3) change from spiral patterns to features elongated along the line of sight. This is most clearly seen in the south; the transition radius is not immediately obvious in the north. Thus, the HI gas disk must extend to at least 25 kpc from the Galactic center in the south, about three times the Sun-Galactic center distance. A related conclusion is that gas within the cutoff radius is kinematically settled into a disk; otherwise it would be unlikely to respond to the spiral density waves.

It is useful to fit four-armed models to our density perturbation map. We used logarithmic spiral arms that start at the Solar circle:

$$\log(R/R_0) = [\phi(R) - \phi_0]\tan\psi \qquad (2)$$

where ψ is the pitch angle and ϕ_0 is the Galactocentric azimuth at the Solar circle. Our fitting method was designed to trace the regions of gas overdensity. For each of the four arms apparent in Fig. 1, we investigated an evenly spaced grid of these two free parameters for ranges of values that connect the overdense contours. For each combination of ψ and ϕ_0, we linearly interpolated the value of Π for the locus of points along each arm. Any points that fall in the excluded regions were ignored. We used the median of the list of interpolated values as a measure of the goodness of fit for each curve. In this scheme, arms with values of ψ and ϕ_0 that trace overdense regions will naturally have a large median and thus a large goodness of fit. The best fit values of ψ and ϕ_0 for each of the four arms are given (Table 1). Other fits that connect a different set of features in the map could be drawn, because assigning a unique arm pattern to a map is not possible. We find pitch angles for the outer arms in the range from 20° to 25°; this is larger than the value of $\psi \approx 13°$ averaged over a variety of tracers (*20*). This does not necessarily imply a disagreement, however, because the arms could be unwinding in their outer regions.

Various models of the locations of the arms have been proposed. We compared our map to a model derived from regions of ionized hydrogen (*21–23*); the model consists of two pairs of mirror symmetric arms following logarithmic spirals. We denoted this as the symmetric model (Fig. 4). The symmetric model fits Π reasonably well over much of the southern sky; the agreement is poor in the north where the spiral structure is less prominent, possibly because of the larger thickness of the northern gas (*11*). Gas that is dynamically warmer is less likely to respond to spiral density waves, and the azimuthally averaged thickness of the northern gas is nearly twice that of the southern gas at $R = 20$ kpc.

There are several places where the symmetric model deviates from the data. For example, the arm in the north ($R \approx 13$ kpc) falls in between two of the model's arms; forcing the arms to be mirror-imaged pairs is too strong a restriction. Features near the excluded regions could result from a large-scale ordered velocity structure that has not been included in our rotation model. Elliptical streamlines with $m = 2$ could cause such an effect (*11*). Images of other galaxies suggest that the spiral arms may bifurcate into spurs in the outer disk. The structure of the Perseus and Carina arms past $R \approx 20$ kpc is suggestive of this behavior.

References and Notes

1. H. C. van de Hulst, C. A. Muller, J. H. Oort, *Bull. Astron. Inst. Neth.* **12**, 117 (1954).
2. F. Kerr, G. Westerhout, in *Galactic Structure*, vol. 5 of *Stars and Stellar Systems*, A. Blaauw, M. Schmidt, Eds. (Univ. Chicago Press, Chicago, IL, 1965), pp. 167–202.
3. A. P. Henderson, P. D. Jackson, F. J. Kerr, *Astrophys. J.* **263**, 116 (1982).
4. D. Malin, *Am. Astron. Soc. Photo Bull.* **16**, 10 (1977).
5. P. M. W. Kalberla *et al.*, *Astron. Astrophys.* **440**, 775 (2005).
6. D. Hartmann, W. B. Burton, *Atlas of Galactic Neutral Hydrogen* (Cambridge Univ. Press, Cambridge, 1997).
7. E. Bajaja *et al.*, *Astron. Astrophys.* **440**, 767 (2005).
8. E. M. Arnal, E. Bajaja, J. J. Larrarte, R. Morras, W. G. L. Pöppel, *Astron. Astrophys. Suppl. Ser.* **142**, 35 (2000).
9. M. J. Reid, *Annu. Rev. Astron. Astrophys.* **31**, 345 (1993).
10. R. P. Olling, M. R. Merrifield, *Mon. Not. R. Astron. Soc.* **297**, 943 (1998).
11. E. S. Levine, L. Blitz, C. Heiles, *Astrophys. J.* **643**, 881 (2006).
12. N. M. McClure-Griffiths, J. M. Dickey, B. M. Gaensler, A. J. Green, *Astrophys. J.* **607**, L127 (2004).
13. J. S. Miller, *Astrophys. J.* **151**, 473 (1968).
14. Y. Xu, M. J. Reid, X. W. Zheng, K. M. Menten, *Science* **311**, 54 (2006); published online 7 December 2005 (10.1126/science.1120914).
15. W. B. Burton, *Astron. Astrophys.* **10**, 76 (1971).
16. M. A. Tuve, S. Lundsager, *Astron. J.* **77**, 652 (1972).
17. C. Yuan, *Astrophys. J.* **158**, 871 (1969).
18. N. H. Dieter, *Astron. Astrophys.* **12**, 59 (1971).
19. G. R. Knapp, S. D. Tremaine, J. E. Gunn, *Astron. J.* **83**, 1585 (1978).
20. J. P. Vallée, *Astron. J.* **130**, 569 (2005).
21. W. W. Morgan, A. E. Whitford, A. D. Code, *Astrophys. J.* **118**, 318 (1953).
22. Y. M. Georgelin, Y. P. Georgelin, *Astron. Astrophys.* **49**, 57 (1976).
23. R. J. Wainscoat, M. Cohen, K. Volk, H. J. Walker, D. E. Schwartz, *Astrophys. J. Suppl. Ser.* **83**, 111 (1992).

24. We thank P. Kalberla for providing a copy of the LAB HI survey and J. Peek, C. Laver, and T. Robishaw for helpful advice regarding plots. E.S.L. and L.B. were supported by NSF grant AST 02-28963. C.H. was supported by NSF grant AST 04-06987.

7 April 2006; accepted 22 May 2006
Published online 1 June 2006;
10.1126/science.1128455
Include this information when citing this paper.

Optical Conformal Mapping

Ulf Leonhardt

An invisibility device should guide light around an object as if nothing were there, regardless of where the light comes from. Ideal invisibility devices are impossible, owing to the wave nature of light. This study develops a general recipe for the design of media that create perfect invisibility within the accuracy of geometrical optics. The imperfections of invisibility can be made arbitrarily small to hide objects that are much larger than the wavelength. With the use of modern metamaterials, practical demonstrations of such devices may be possible. The method developed here can also be applied to escape detection by other electromagnetic waves or sound.

According to Fermat's principle (*1*), light rays take the shortest optical paths in dielectric media, where the refractive index n integrated along the ray trajectory defines the path length. When n is spatially varying, the shortest optical paths are not straight lines, but are curved. This light bending is the cause of many optical illusions. Imagine a situation where a medium guides light around a hole in it. Suppose that all parallel bundles of incident rays are bent around the hole and recombined in precisely the same direction as they entered the medium. An

observer would not see the difference between light passing through the medium or propagating across empty space (or, equivalently, in a uniform medium). Any object placed in the hole would be hidden from sight. The medium would create the ultimate optical illusion: invisibility (*2*).

However, it has been proved (*3*, *4*) that perfect invisibility is unachievable, except in a finite set of discrete directions where the object appears to be squashed to infinite thinness and for certain objects that are small as compared with the wavelength (*5*, *6*). In order to carry images, though, light should propagate with a continuous range of spatial Fourier components, i.e., in a range of directions. The mathematical reason for the impossibility of perfect invisibility is the uniqueness of the inverse-scattering problem for waves (*3*): the scattering data, i.e., the directions and amplitudes of the transmitted plane-wave components determine the spatial profile of the refractive index (*3*). Therefore, the scattering data of light in empty space are only consistent with the propagation through empty space. Perfect illusions are thus thought to be impossible due to the wave nature of light.

On the other hand, the theorem (*3*) does not limit the imperfections of invisibility—they may be very small—nor does it apply to light rays, i.e., to light propagation within the regime of geometrical optics (*1*). This study develops a general recipe for the design of media that create perfect invisibility for light rays over a continuous range of directions. Because this method is based on geometrical optics (*1*), the inevitable imperfections of invisibility can be made exponentially small for objects that are much larger than the wavelength of light.

To manufacture a dielectric invisibility device, media are needed that possess a wide range of the refractive index in the spectral domain where the device should operate. In particular, Fermat's Principle (*1*) seems to imply that $n < 1$ in some spatial regions, because only in this case the shortest optical paths may go around the object without causing phase distortions. In our example, n varies from 0 to about 36. In practice, one could probably accept a certain degree of visibility that substantially reduces the demands on the range of the refractive index.

Extreme values of n occur when the material is close to resonance with the electromagnetic field. Metamaterials (*7*) with man-made resonances can be manufactured with appropriately designed circuit boards, similar to the ones used for demonstrating negative refraction (*8*). The quest for the perfect lens (*9*) has led to recent improvements (*7*, *10*–*13*) mainly focused on tuning the magnetic susceptibilities. In such metamaterials, each individual circuit plays the role of an artificial atom with tunable resonances. With these artificial dielectrics, invisibility could be reached for frequencies in the microwave-to-terahertz range. In contrast, stealth technology is designed to make objects of military interest as black as possible to radar where, using impedance matching (*14*), electromagnetic waves are absorbed without reflection, i.e., without any echo detectable by radar. Recently, nanofabricated metamaterials with custom-made plasmon resonances have been demonstrated (*13*) that operate in the visible range of the spectrum and may be modified to reach invisibility.

The method used here is general and also applicable to other forms of wave propagation—for example, to sound waves, where the index n describes the ratio of the local phase velocity of the wave to the bulk value, or to quantum-mechanical matter waves, where external potentials act like refractive-index profiles (*1*). For instance, one could use the profiles of n described here to protect an enclosed space from any form of sonic tomography. This study examines the simplest nontrivial case of invisibility, an effectively two-dimensional situation, by applying conformal mapping (*15*) to solve the problem—an elegant technique used in research areas as diverse as electrostatics (*14*), fluid mechanics (*16*), classical mechanics (*17*–*20*), and quantum chaos (*21*, *22*).

Consider an idealized situation: a dielectric medium that is uniform in one direction and light of wave number k that propagates orthogonal to that direction. In practice, the medium will have a finite extension and the propagation direction of light may be slightly tilted without causing an appreciable difference to the ideal case. The medium is characterized by the refractive-index profile $n(x,y)$. To satisfy the validity condition of geometrical optics, $n(x,y)$ must not vary by much over the scale of an optical wavelength $2\pi/k$ (*1*). To describe the spatial coordinates in the propagation plane, complex numbers $z = x + iy$ are used with the partial derivatives $\partial_x = \partial_z + \partial_z^*$ and $\partial_y = i\partial_z - i\partial_z^*$, where the asterisk symbolizes complex conjugation. In the case of a gradually varying refractive-index profile, both amplitudes ψ of the two polarizations of light obey the Helmholtz equation (*1*)

$$(4\partial_z^*\partial_z + n^2k^2)\,\psi = 0 \qquad (1)$$

written here in complex notation with the Laplace operator $\partial_x^2 + \partial_y^2 = 4\partial_z^*\partial_z$. Suppose we introduce new coordinates w described by an analytic function $w(z)$ that does not depend on z^*. Such functions define conformal maps (*15*) that preserve the angles between the coordinate lines. Because $\partial_z^*\partial_z = |dw/dz|^2\partial_w^*\partial_w$, we obtain in w space a Helmholtz equation with the transformed refractive-index profile n' that is related to the original one as

$$n = n'\left|\frac{dw}{dz}\right| \qquad (2)$$

Suppose that the medium is designed such that $n(z)$ is the modulus of an analytic function $g(z)$. The integral of $g(z)$ defines a map $w(z)$ to new coordinates where, according to Eq. 2, the transformed index n' is unity. Consequently, in w coordinates, the wave propagation is indistinguishable from empty space where light rays propagate along straight lines. The medium performs an optical conformal mapping to empty space. If $w(z)$ approaches z for $w \to \infty$, all incident waves appear at infinity as if they have traveled through empty space, regardless

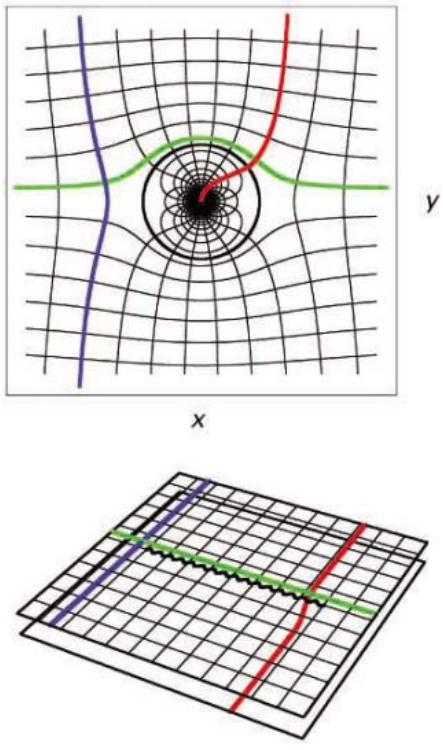

Fig. 1. Optical conformal map. A dielectric medium conformally maps physical space described by the points $z = x + iy$ of the complex plane onto Riemann sheets if the refractive-index profile is $|dw/dz|$ with some analytic function $w(z)$. The figure illustrates the simple map (3) where the exterior of a circle in the picture above is transformed into the upper sheet in the lower picture, and the interior of the circle is mapped onto the lower sheet. The curved coordinate grid of the upper picture is the inverse map $z(w)$ of the w coordinates, approaching a straight rectangular grid at infinity. As a feature of conformal maps, the right angles between the coordinate lines are preserved. The circle line in the figure above corresponds to the branch cut between the sheets below indicated by the curly black line. The figure also illustrates the typical fates of light rays in such media. On the w sheets, rays propagate along straight lines. The rays shown in blue and green avoid the branch cut and hence the interior of the device. The ray shown in red crosses the cut and passes onto the lower sheet where it approaches ∞. However, this ∞ corresponds to a singularity of the refractive index and not to the ∞ of physical space. Rays like this one would be absorbed, unless they are guided back to the exterior sheet.

School of Physics and Astronomy, University of St Andrews, North Haugh, St Andrews KY16 9SS, Scotland. E-mail: ulf@st-andrews.ac.uk

of what has happened in the medium. However, as a consequence of the Riemann Mapping Theorem (*15*), nontrivial w coordinates occupy Riemann sheets with several ∞, one on each sheet. Consider, for example, the simple map

$$w = z + \frac{a^2}{z}, \quad z = {}^1\!/_2\left(w \pm \sqrt{w^2 - 4a^2}\right) \quad (3)$$

illustrated in Fig. 1, that is realized by the refractive-index profile $n = |1 - a^2/z^2|$. The constant a characterizes the spatial extension of the medium. The function (3) maps the exterior of a circle of radius a on the z plane onto one Riemann sheet and the interior onto another. Light rays traveling on the exterior w sheet may have the misfortune of passing the branch cut between the two branch points $\pm 2a$. In continuing their propagation, the rays approach ∞ on the interior w sheet. Seen on the physical z plane, they cross the circle of radius a and approach the singularity of the refractive index at the origin. For general $w(z)$, only one ∞ on the Riemann structure in w space corresponds to the true ∞ of physical z space and the others to singularities of $w(z)$. Instead of traversing space, light rays may cross the branch cut to another Riemann sheet where they approach ∞. Seen in physical space, the rays are irresistibly attracted toward some singularities of the refractive index. Instead of becoming invisible, the medium casts a shadow that is as wide as the apparent size of the branch cut. Nevertheless, the optics on Riemann sheets turns out to serve as a powerful theoretical tool for developing the design of dielectric invisibility devices.

All we need to achieve is to guide light back from the interior to the exterior sheet, i.e., seen in physical space, from the exterior to the interior layer of the device. To find the required refractive-index profile, we interpret the Helmholtz equation in w space as the Schrödinger equation (*1*) of a quantum particle of effective mass k^2 moving in the potential U with energy E such that $U - E = -n'^2/2$ (*1*). We wish to send all rays that have passed through the branch cut onto the interior sheet back to the cut at precisely the same location and in the same direction in which they entered. This implies that we need a potential for which all trajectories are closed. Assuming radial symmetry for $U(w)$ around one branch point w_1, say $+2a$ in our example, only two potentials have this property: the harmonic oscillator and the Kepler potential (*17*). In both cases the trajectories are ellipses (*17*) that are related to each other by a transmutation of force according to the Arnol'd-Kasner theorem (*18–20*). The harmonic oscillator corresponds to a Luneburg lens (*23*) on the Riemann sheet with the transformed refractive-index profile

$$n'^2 = 1 - \frac{|w - w_1|^2}{r_0^2} \quad (4)$$

where r_0 is a constant radius. The Kepler potential with negative energy E corresponds to an Eaton lens (*23*) with the profile

$$n'^2 = \frac{r_0}{|w - w_1|} - 1 \quad (5)$$

Note that the singularity of the Kepler profile in w space is compensated by the zero of $|dw/dz|$ at a branch point in physical space such that the total refractive index (2) is never singular. In both cases (4) and (5), r_0 defines the radius of the circle on the interior w sheet beyond which n'^2 would be negative and hence inaccessible to light propagation. This circle should be large enough to cover the branch cut. The inverse map $z(w)$ turns the outside of the circle into the inside of a region bounded by the image $z(w)$ of the circle line in w space. No light can enter this region. Everything inside is invisible.

Yet there is one more complication: Light is refracted (*1*) at the boundary between the exterior and the interior layer. Seen in w space, light rays encounter here a transition from the refractive index 1 to n'. Fortunately, refraction is reversible. After the cycles on the interior sheets, light rays are refracted back to their original directions (Fig. 2). The invisibility is not affected, unless the rays are totally reflected. According to Snell's Law (*1*), rays with angles of incidence θ with respect to the branch cut enter the lower sheet with angles θ' such that $n'\sin\theta' = \sin\theta$. If $n' < 1$, this equation may not have real solutions for θ larger than a critical angle Θ. Instead of entering the interior layer of the device, the light is totally reflected (*1*). The angle Θ defines the acceptance angle of the dielectric invisibility device, because beyond Θ, the device appears silvery instead of invisible. The transformed refractive-index profiles (4) and (5) at the boundary between the layers are lowest at the other branch point w_2 that limits the branch cut, $w_2 = -2a$, in our example. In the case of the harmonic-oscillator profile (4), n' lies always below 1, and we obtain the acceptance angle

$$\Theta = \arccos\left(\frac{|w_2 - w_1|}{r_0}\right) \quad (6)$$

For all-round invisibility, the radius r_0 should approach infinity, which implies that the entire

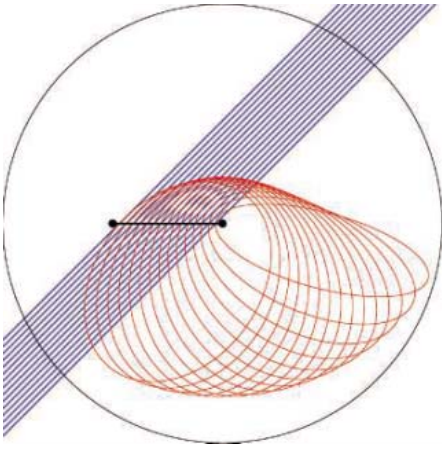

Fig. 2. Light guiding. The device guides light that has entered its interior layer back to the exterior, represented here using two Riemann sheets that correspond to the two layers, seen from above. Light on the exterior sheet is shown in blue and light in the interior, in red. At the branch cut, the thick line between the two points in the figure (the branch points), light passes from the exterior to the interior sheet. Here light is refracted according to Snell's law. On the lower sheet, the refractive-index profile (5) guides the rays to the exterior sheet in elliptic orbits with one branch point as focal point. Finally, the rays are refracted back to their original directions and leave on the exterior sheet as if nothing has happened. The circle in the figure indicates the maximal elongations of the ellipses. This circle limits the region in the interior of the device that light does not enter. The outside of the circle corresponds to the inside of the device. Anything beyond this circle is invisible.

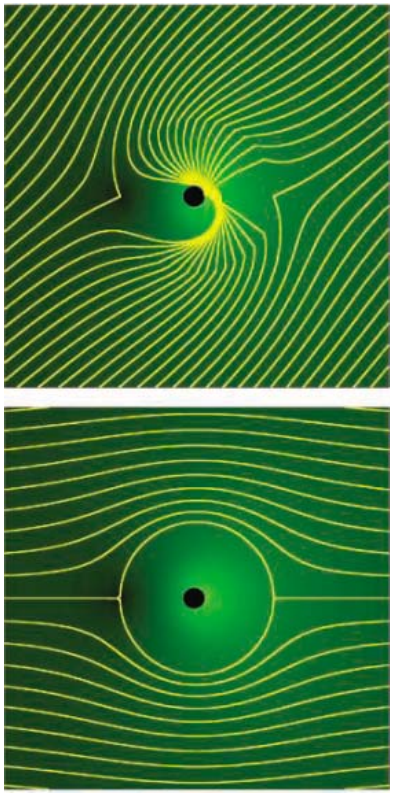

Fig. 3. Ray propagation in the dielectric invisibility device. The light rays are shown in yellow. The brightness of the green background indicates the refractive-index profile taken from the simple map (3) and the Kepler profile (5) with $r_0 = 8a$ in the interior layer of the device. The invisible region is shown in black. The upper panel illustrates how light is refracted at the boundary between the two layers and guided around the invisible region, where it leaves the device as if nothing were there. In the lower panel, light simply flows around the interior layer.

interior sheet is used for guiding the light back to the exterior layer. Fortunately, the Kepler profile (5) does not lead to total reflection if $r_0 \geq 2|w_2 - w_1|$. In this case, the invisible area is largest for

$$r_0 = 2|w_2 - w_1| \quad (7)$$

Figure 3 illustrates the light propagation in a dielectric invisibility device based on the simple map (3) and the Kepler profile (5) with $r_0 = 8a$. Here n ranges from 0 to about 36, but this example is probably not the optimal choice. One can choose from infinitely many conformal maps $w(z)$ that possess the required properties for achieving invisibility: $w(z) \sim z$ for $z \to \infty$ and two branch points w_1 and w_2. The invisible region may be deformed to any simply connected domain by a conformal map that is the numerical solution of a Riemann-Hilbert problem (*16*). We can also relax the tacit assumption that w_1 connects the exterior to only one interior sheet, but to m sheets where light rays return after m cycles. If we construct $w(z)$ as $af(z/a)$ with some analytic function $f(z)$ of the required properties and a constant length scale a, the refractive-index profile $|dw/dz|$ is identical for all scales a. Finding the most practical design is an engineering problem that depends on practical demands. This problem may also inspire further mathematical research on conformal maps in order to find the optimal design and to extend our approach to three dimensions.

Finally, we ask why our scheme does not violate the mathematical theorem (*3*) that perfect invisibility is unattainable. The answer is that waves are not only refracted at the boundary between the exterior and the interior layer, but also are reflected, and that the device causes a time delay. However, the reflection can be substantially reduced by making the transition between the layers gradual over a length scale much larger than the wavelength $2\pi/k$ or by using anti-reflection coatings. In this way, the imperfections of invisibility can be made as small as the accuracy limit of geometrical optics (*1*), i.e., exponentially small. One can never completely hide from waves, but can from rays.

References and Notes

1. M. Born, E. Wolf, *Principles of Optics* (Cambridge Univ. Press, Cambridge, 1999).
2. G. Gbur, *Prog. Opt.* **45**, 273 (2003).
3. A. I. Nachman, *Ann. Math.* **128**, 531 (1988).
4. E. Wolf, T. Habashy, *J. Mod. Opt.* **40**, 785 (1993).
5. M. Kerker, *J. Opt. Soc. Am.* **65**, 376 (1975).
6. A. Alu, N. Engheta, *Phys. Rev. E* **72**, 016623 (2005).
7. D. R. Smith, J. B. Pendry, M. C. K. Wiltshire, *Science* **305**, 788 (2004).
8. R. A. Shelby, D. R. Smith, S. Schultz, *Science* **292**, 77 (2001).
9. J. B. Pendry, *Phys. Rev. Lett.* **85**, 3966 (2000).
10. A. Grbic, G. V. Eleftheriades, *Phys. Rev. Lett.* **92**, 117403 (2004).
11. T. J. Yen *et al.*, *Science* **303**, 1494 (2004).
12. S. Linden *et al.*, *Science* **306**, 1351 (2004).
13. A. N. Grigorenko *et al.*, *Nature* **438**, 335 (2005).
14. J. D. Jackson, *Classical Electrodynamics* (Wiley, New York, 1998).
15. Z. Nehari, *Conformal Mapping* (McGraw-Hill, New York, 1952).
16. M. J. Ablowitz, A. S. Fokas, *Complex Variables* (Cambridge Univ. Press, Cambridge, 1997).
17. L. D. Landau, E. M. Lifshitz, *Mechanics* (Pergamon, Oxford, 1976).
18. V. I. Arnol'd, *Huygens & Barrow, Newton & Hooke* (Birkhäuser Verlag, Basel, 1990).
19. T. Needham, *Am. Math. Mon.* **100**, 119 (1993).
20. T. Needham, *Visual Complex Analysis* (Clarendon, Oxford, 2002).
21. M. Robnik, *J. Phys. A* **16**, 3971 (1983).
22. M. Robnik, M. V. Berry, *J. Phys. A* **19**, 669 (1986).
23. M. Kerker, *The Scattering of Light* (Academic Press, New York, 1969).

24. I am grateful to L. Boussiakou, L. Davila-Romero, M. Dennis, M. Dunn, G. Gbur, C. Gibson, J. Henn, and A. Hindi for the discussions that led to this paper. My work has been supported by the Leverhulme Trust and the Engineering and Physical Sciences Research Council.

21 February 2006; accepted 26 April 2006
Published online 25 May 2006;
10.1126/science.1126493
Include this information when citing this paper.

Controlling Electromagnetic Fields

J. B. Pendry,[1]* D. Schurig,[2] D. R. Smith[2]

Using the freedom of design that metamaterials provide, we show how electromagnetic fields can be redirected at will and propose a design strategy. The conserved fields—electric displacement field D, magnetic induction field B, and Poynting vector B—are all displaced in a consistent manner. A simple illustration is given of the cloaking of a proscribed volume of space to exclude completely all electromagnetic fields. Our work has relevance to exotic lens design and to the cloaking of objects from electromagnetic fields.

To exploit electromagnetism, we use materials to control and direct the fields: a glass lens in a camera to produce an image, a metal cage to screen sensitive equipment, "blackbodies" of various forms to prevent unwanted reflections. With homogeneous materials, optical design is largely a matter of choosing the interface between two materials. For example, the lens of a camera is optimized by altering its shape so as to minimize geometrical aberrations. Electromagnetically inhomogeneous materials offer a different approach to control light; the introduction of specific gradients in the refractive index of a material can be used to form lenses and other optical elements, although the types and ranges of such gradients tend to be limited.

A new class of electromagnetic materials (*1*, *2*) is currently under study: metamaterials, which owe their properties to subwavelength details of structure rather than to their chemical composition, can be designed to have properties difficult or impossible to find in nature. We show how the design flexibility of metamaterials can be used to achieve new electromagnetic devices and how metamaterials enable a new paradigm for the design of electromagnetic structures at all frequencies from optical down to DC.

Progress in the design of metamaterials has been impressive. A negative index of refraction (*3*) is an example of a material property that does not exist in nature but has been enabled by using metamaterial concepts. As a result, negative refraction has been much studied in recent years (*4*), and realizations have been reported at both GHz and optical frequencies (*5*–*8*). Novel magnetic properties have also been reported over a wide spectrum of frequencies. Further information on the design and construction of metamaterials may be found in (*9*–*13*). In fact, it is now conceivable that a material can be constructed whose permittivity and permeability values may be designed to vary independently and arbitrarily throughout a material, taking positive or negative values as desired.

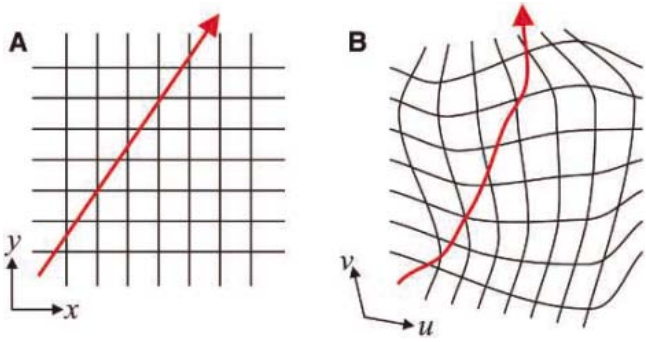

Fig. 1. (**A**) A field line in free space with the background Cartesian coordinate grid shown. (**B**) The distorted field line with the background coordinates distorted in the same fashion. The field in question may be the electric displacement or magnetic induction fields **D** or **B**, or the Poynting vector **S**, which is equivalent to a ray of light.

[1]Department of Physics, Blackett Laboratory, Imperial College London, London SW7 2AZ, UK. [2]Department of Electrical and Computer Engineering, Duke University, Box 90291, Durham, NC 27708, USA.

*To whom correspondence should be addressed. E-mail: j.pendry@imperial.ac.uk

If we take this unprecedented control over the material properties and form inhomogeneous composites, we enable a powerful form of electromagnetic design. As an example of this design methodology, we show how the conserved quantities of electromagnetism—the electric displacement field **D**, the magnetic field intensity **B**, and the Poynting vector **S**—can all be directed at will, given access to the appropriate metamaterials. In particular, these fields can be focused as required or made to avoid objects and flow around them like a fluid, returning undisturbed to their original trajectories. These conclusions follow from exact manipulations of Maxwell's equations and are not confined to a ray approximation. They encompass in principle all forms of electromagnetic phenomena on all length scales.

We start with an arbitrary configuration of sources embedded in an arbitrary dielectric and magnetic medium. This initial configuration would be chosen to have the same topology as the final result we seek. For example, we might start with a uniform electric field and require that the field lines be moved to avoid a given region. Next, imagine that the system is embedded in some elastic medium that can be pulled and stretched as we desire (Fig. 1). To keep track of distortions, we record the initial configuration of the fields on a Cartesian mesh, which is subsequently distorted by the same pulling and stretching process. The distortions can now be recorded as a coordinate transformation between the original Cartesian mesh and the distorted mesh

$$u(x,y,z), v(x,y,z), w(x,y,z) \qquad (1)$$

where (u, v, w) is the location of the new point with respect to the x, y, and z axes. What happens to Maxwell's equations when we substitute the new coordinate system? The equations have exactly the same form in any coordinate system, but the refractive index—or more exactly the permittivity ε and permeability μ—are scaled by a common factor. In the new coordinate system, we must use renormalized values of the permittivity and permeability:

$$\varepsilon'_u = \varepsilon_u \frac{Q_u Q_v Q_w}{Q_u^2},$$
$$\mu'_u = \mu_u \frac{Q_u Q_v Q_w}{Q_u^2}, \text{ etc.} \qquad (2)$$
$$E'_u = Q_u E_u,\ H'_u = Q_u H_u, \text{ etc.} \qquad (3)$$

where,

$$Q_u^2 = \left(\frac{\partial x}{\partial u}\right)^2 + \left(\frac{\partial y}{\partial u}\right)^2 + \left(\frac{\partial z}{\partial u}\right)^2$$
$$Q_v^2 = \left(\frac{\partial x}{\partial v}\right)^2 + \left(\frac{\partial y}{\partial v}\right)^2 + \left(\frac{\partial z}{\partial v}\right)^2$$
$$Q_w^2 = \left(\frac{\partial x}{\partial w}\right)^2 + \left(\frac{\partial y}{\partial w}\right)^2 + \left(\frac{\partial z}{\partial w}\right)^2 \qquad (4)$$

As usual,

$$\mathbf{B}' = \mu_0 \boldsymbol{\mu}' \mathbf{H}', \quad \mathbf{D}' = \varepsilon_0 \boldsymbol{\varepsilon}' \mathbf{E}' \qquad (5)$$

We have assumed orthogonal coordinate systems for which the formulae are particularly simple. The general case is given in (*14*) and in the accompanying online material (*15*). The equivalence of coordinate transformations and changes to ε and μ has also been referred to in (*16*).

Now let us put these transformations to use. Suppose we wish to conceal an arbitrary object contained in a given volume of space; furthermore, we require that external observers be unaware that something has been hidden from them. Our plan is to achieve concealment by cloaking the object with a metamaterial whose function is to deflect the rays that would have struck the object, guide them around the object, and return them to their original trajectory.

Our assumptions imply that no radiation can get into the concealed volume, nor can any radiation get out. Any radiation attempting to penetrate the secure volume is smoothly guided around by the cloak to emerge traveling in the same direction as if it had passed through the empty volume of space. An observer concludes that the secure volume is empty, but we are free to hide an object in the secure space. An alternative scheme has been recently investigated for the concealment of objects (*17*), but it relies on a specific knowledge of the shape and the material properties of the object being hidden. The electromagnetic cloak and the object concealed thus form a composite whose scattering properties can be reduced in the lowest order approximation: If the object changes, the cloak must change, too. In the scheme described here, an arbitrary object may be hidden because it remains untouched by external radiation. The method leads, in principle, to a perfect electromagnetic shield, excluding both propagating waves and near-fields from the concealed region.

For simplicity, we choose the hidden object to be a sphere of radius R_1 and the cloaking region to be contained within the annulus $R_1 < r < R_2$. A simple transformation that achieves the desired result can be found by taking all fields in the region $r < R_2$ and compressing them into the region $R_1 < r < R_2$,

$$r' = R_1 + r(R_2 - R_1)/R_2,$$
$$\theta' = \theta,$$
$$\phi' = \phi \qquad (6)$$

Applying the transformation rules (*15*) gives the following values: for $r < R_1$, ε' and μ' are free to take any value without restriction and do not contribute to electromagnetic scattering; for $R_1 < r < R_2$

$$\varepsilon'_{r'} = \mu'_{r'} = \frac{R_2}{R_2 - R_1}\frac{(r' - R_1)^2}{r'},$$
$$\varepsilon'_{\theta'} = \mu'_{\theta'} = \frac{R_2}{R_2 - R_1},$$
$$\varepsilon'_{\phi'} = \mu'_{\phi'} = \frac{R_2}{R_2 - R_1} \qquad (7)$$

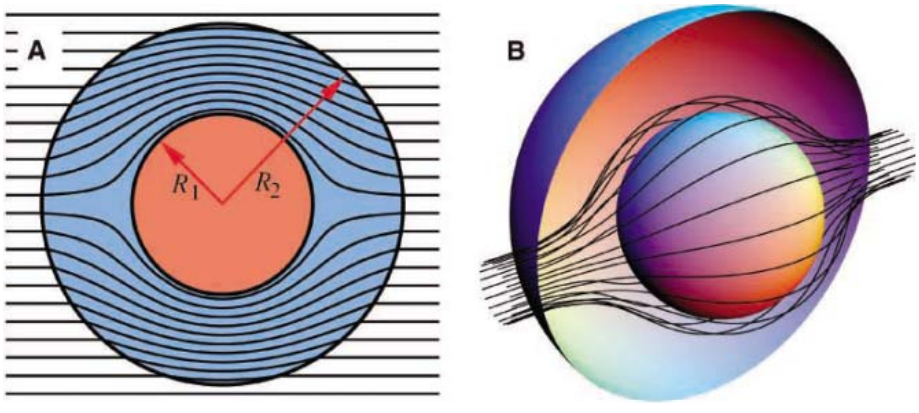

Fig. 2. A ray-tracing program has been used to calculate ray trajectories in the cloak, assuming that $R_2 \gg \lambda$. The rays essentially following the Poynting vector. (**A**) A two-dimensional (2D) cross section of rays striking our system, diverted within the annulus of cloaking material contained within $R_1 < r < R_2$ to emerge on the far side undeviated from their original course. (**B**) A 3D view of the same process.

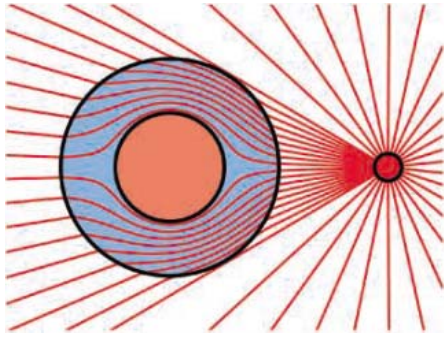

Fig. 3. A point charge located near the cloaked sphere. We assume that $R_2 \ll \lambda$, the near-field limit, and plot the electric displacement field. The field is excluded from the cloaked region, but emerges from the cloaking sphere undisturbed. We plot field lines closer together near the sphere to emphasize the screening effect.

for $r > R_2$

$$\varepsilon'_{r'} = \mu'_{r'} = \varepsilon'_{\theta'} = \mu'_{\theta'} = \varepsilon'_{\phi'} = \mu'_{\phi'} = 1 \quad (8)$$

We stress that this prescription will exclude all fields from the central region. Conversely, no fields may escape from this region. At the outer surface of the cloak ($r = R_2$), we have $\varepsilon'_{\theta'} = \varepsilon'_{\phi'} = 1/\varepsilon'_{r'}$ and $\mu'_{\theta'} = \mu'_{\phi'} = 1/\mu'_{r'}$, which are the conditions for a perfectly matched layer (PML). Thus we can make the connection between this cloak, which is reflectionless by construction, and a well-studied reflectionless interface (*18*).

For purposes of illustration, suppose that $R_2 \gg \lambda$, where λ is the wavelength, so that we can use the ray approximation to plot the Poynting vector. If our system is then exposed to a source of radiation at infinity, we can perform the ray-tracing exercise shown in Fig. 2. Rays in this figure result from numerical integration of a set of Hamilton's equations obtained by taking the geometric limit of Maxwell's equations with anisotropic, inhomogeneous media. This integration provides independent confirmation that the configuration specified by Eqs. 6 and 7 excludes rays from the interior region. Alternatively, if $R_2 \ll \lambda$ and we locate a point charge nearby, the electrostatic (or magnetostatic) approximation applies. A plot of the local electrostatic displacement field is shown in Fig. 3.

Next we discuss the characteristics of the cloaking material. There is an unavoidable singularity in the ray tracing, as can be seen by considering a ray headed directly toward the center of the sphere (Fig. 2). This ray does not know whether to be deviated up or down, left or right. Neighboring rays are bent around in tighter and tighter arcs the closer to the critical ray they are. This in turn implies very rapid changes in ε' and μ', as sensed by the ray. These rapid changes are due (in a self-consistent way) to the tight turn of the ray and the anisotropy of ε' and μ'. Anisotropy of the medium is necessary because we have compressed space anisotropically.

Although anisotropy and even continuous variation of the parameters is not a problem for metamaterials (*19*–*21*), achieving very large or very small values of ε' and μ' can be. In practice, cloaking will be imperfect to the degree that we fail to satisfy Eq. 7. However, very considerable reductions in the cross section of the object can be achieved.

A further issue is whether the cloaking effect is broadband or specific to a single frequency. In the example we have given, the effect is only achieved at one frequency. This can easily be seen from the ray picture (Fig. 2). Each of the rays intersecting the large sphere is required to follow a curved, and therefore longer, trajectory than it would have done in free space, and yet we are requiring the ray to arrive on the far side of the sphere with the same phase. This implies a phase velocity greater that the velocity of light in vacuum which violates no physical law. However, if we also require absence of dispersion, the group and phase velocities will be identical, and the group velocity can never exceed the velocity of light. Hence, in this instance the cloaking parameters must disperse with frequency and therefore can only be fully effective at a single frequency. We mention in passing that the group velocity may sometimes exceed the velocity of light (*22*) but only in the presence of strong dispersion. On the other hand, if the system is embedded in a medium having a large refractive index, dispersion may in principle be avoided and the cloaking operate over a broad bandwidth.

We have shown how electromagnetic fields can be dragged into almost any desired configuration. The distortion of the fields is represented as a coordinate transformation, which is then used to generate values of electrical permittivity and magnetic permeability ensuring that Maxwell's equations are still satisfied. The new concept of metamaterials is invoked, making realization of these designs a practical possibility.

References and Notes

1. J. B. Pendry, A. J. Holden, W. J. Stewart, I. Youngs, *Phys. Rev. Lett.* **76**, 4773 (1996).
2. J. B. Pendry, A. J. Holden, D. J. Robbins, W. J. Stewart, *IEEE Trans. Micr. Theory Techniques* **47**, 2075 (1999).
3. V. G. Veselago, *Soviet Physics USPEKI* **10**, 509 (1968).
4. D. R. Smith, W. J. Padilla, D. C. Vier, S. C. Nemat-Nasser, S. Schultz, *Phys. Rev. Lett.* **84**, 4184 (2000).
5. R. A. Shelby, D. R. Smith, S. Schultz, *Science* **292**, 77 (2001).
6. A. A. Houck, J. B. Brock, I. L. Chuang, *Phys. Rev. Lett.* **90**, 137401 (2003).
7. A. Grbic, G. V. Eleftheriades, *Phys. Rev. Lett.* **92**, 117403 (2004).
8. V. M. Shalaev *et al.*, *Opt. Lett.* **30**, 3356 (2005).
9. D. R. Smith, J. B. Pendry, M. C. K. Wiltshire, *Science* **305**, 788 (2004).
10. E. Cubukcu, K. Aydin, E. Ozbay, S. Foteinopoulou, C. M. Soukoulis, *Nature* **423**, 604 (2003).
11. E. Cubukcu, K. Aydin, E. Ozbay, S. Foteinopolou, C. M. Soukoulis, *Phys. Rev. Lett.* **91**, 207401 (2003).
12. T. J. Yen *et al.*, *Science* **303**, 1494 (2004).
13. S. Linden *et al.*, *Science* **306**, 1351 (2004).
14. A. J. Ward, J. B. Pendry, *J. Mod. Opt.* **43**, 773 (1996).
15. Methods are available as supporting material on *Science* Online.
16. U. Leonhardt, *IEEE J. Selected Topics Quantum Electronics* **9**, 102 (2003).
17. A. Alu, N. Engheta, *Phys. Rev.* **E95**, 016623 (2005).
18. J.-P. Berenger, *J. Comput. Phys.* **114**, 185 (1994).
19. D. R. Smith, J. J. Mock, A. F. Starr, D. Schurig, *Phys. Rev. E* **71**, 036617 (2005).
20. T. Driscoll *et al.*, *Appl. Phys. Lett.* **88**, 081101 (2006).
21. R. B. Greegor *et al.*, *Appl. Phys. Lett.* **87**, 091114 (2005).
22. R. Y. Chiao, P. W. Milonni, *Optics and Photonics News*, June (2002).

23. J.B.P. thanks the Engineering and Physical Sciences Research Council (EPSRC) for a Senior Fellowship, the European Community (EC) under project FP6-NMP4-CT-2003-505699, Department of Defense Office of Naval Research (DOD/ONR) Multidisciplinary Research Program of the University Research Institute (MURI) grant N00014-01-1-0803, DOD/ONR grant N00014-05-1-0861, and the EC Information Societies Technology (IST) program Development and Analysis of Left-Handed Materials (DALHM), project number IST-2001-35511, for financial support. D. Schurig acknowledges support from the Intelligence Community (IC) Postdoctoral Fellowship Program.

Supporting Online Material

www.sciencemag.org/cgi/content/full/1125907/DC1
SOM Text
Figs. S1 to S3

7 February 2006; accepted 26 April 2006
Published online 25 May 2006;
10.1126/science.1125907
Include this information when citing this paper.

Nanoassembly of a Fractal Polymer: A Molecular "Sierpinski Hexagonal Gasket"

George R. Newkome,[1,2]* Pingshan Wang,[1] Charles N. Moorefield,[1] Tae Joon Cho,[1] Prabhu P. Mohapatra,[1] Sinan Li,[3] Seok-Ho Hwang,[1] Olena Lukoyanova,[5] Luis Echegoyen,[5] Judith A. Palagallo,[4] Violeta Iancu,[6] Saw-Wai Hla[6]

Mathematics and art converge in the fractal forms that also abound in nature. We used molecular self-assembly to create a synthetic, nanometer-scale, Sierpinski hexagonal gasket. This nondendritic, perfectly self-similar fractal macromolecule is composed of *bis*-terpyridine building blocks that are bound together by coordination to 36 Ru and 6 Fe ions to form a nearly planar array of increasingly larger hexagons around a hollow center.

Fractal constructs are based on the incorporation of identical motifs that repeat on differing size scales (*1*). Examples of fractal shapes in nature include clouds, trees, waves on a lake, the human circulatory system, and mountains, to mention but a few. The study of fractals has moved from the field of pure mathematics to descriptions of nature that, in turn, have inspired artistic design. More recently, chemists have incorporated the fractal form in molecular synthesis. Since 1985, molecular trees, which generally branch in a binary (*2*) or ternary (*3*) pattern, have been synthesized with increasing size and structural complexity. Beyond their aesthetics, these dendrimers and hyperbranched materials (*4*) are now under study for use in a wide range of practical applications. However, treelike patterns are but one type of fractal composed of repeating geometrical figures. A porphyrin-based dendrimer (*5*) that uses porphyrins as branching centers has been prepared that incorporates the snakelike "kolam" fractal pattern described by Ascher (*6*).

Nonetheless, most mathematically defined fractals have yet to be produced in the laboratory.

The first mathematically defined fractal was derived in 1915 (*7*), when the Polish mathematician Vacław Sierpinski described a series of interrelated equilateral triangles, later called the "Sierpinski gasket" by Mandelbrot (*1*). The original equation has been expanded into other fractal constructs called Sierpinski "n-gons," including the beautiful hexagonal gasket. Mathematically, such fractal hexagonal structures result by operating on the points in a hexagon H_0 with six functions

$$f_j(x, y) = \begin{bmatrix} 1/3 & 0 \\ 0 & 1/3 \end{bmatrix} \left(\begin{bmatrix} x \\ y \end{bmatrix} \right) + P_j$$
$$J = 1,\ldots, 6$$

where P_j are the vertices of H_0. Iteratively, this relation leads to $H_{j+1} = f_1(H_j) + f_2(H_j) + f_3(H_j) + f_4(H_j) + f_5(H_j) + f_6(H_j)$, and the sequence $\{H_j\}$ converges to the hexagonal gasket shown in Fig. 1. This mathematically defined fractal pattern—the "Sierpinski hexagonal gasket"—offers a substantial synthetic challenge for chemical self-assembly (*8*–*11*), given the size and complexity of the target.

Here we report the chemical synthesis of a nondendritic fractal construct based on Sierpinski's hexagonal gasket (incorporating both the Star of David and a Koch snowflake), where the term "nondendritic" refers to repeat units that do not branch in the typical treelike pattern. To create the desired repeat unit, we built on our recent studies of metallohexamer formation (*12*–*14*), in which the facile self-assembly of a *meta*(*bis*-terpyridinyl)benzene (*12*, *13*, *15*) in the presence of one equivalent (1 equiv.) of a metal ion, such as Fe(II), affords a high yield of the desired hexagonal product (*14*).

Initially, 1 equiv. of *bis*-[Ru(III)] monomer **1** was heated with 4.5 equiv. of *tris*-terpyridine (*16*) **2** in refluxing $CHCl_3/CH_3OH$ for 20 hours under reducing conditions (added *N*-ethylmorpholine) to give the pivotal heterotrimer **3**, as deep red microcrystals in 35% yield (Fig. 2). Its ^{1}H nuclear magnetic resonance (NMR) spectrum exhibited two singlets at 9.32 and 9.28 parts per million (ppm) in a 1:1 ratio, attributed to the four inner and outer 3′,5′-tpy-*H*s (tpy, terpyridine) of the complexed ligands, as well as a resonance at 9.08 ppm assigned to the eight remaining 3′,5′-tpy-*H*s of the uncomplexed terpyridines, which integrated in a 2:1 ratio to the former downfield peaks; also, a singlet was observed at 2.89 ppm for the methyl groups. Electrospray ionization mass spectroscopy (ESI-MS) [$C_{139}H_{92}F_{24}N_{24}P_{12}Ru_2$ (2880.38); observed peaks at mass/charge (*m*/*z*) ratios 2736.6 $(M - PF_6)^+$ and 1295.9 $(M - 2PF_6)^{2+}$] gave further evidence for the desired structure. After the chromatography of building blocks **3**, **4**, and **5** using a mixture of H_2O:KNO_3:CH_3CN, the counterions were converted to PF_6^- to facilitate a homogeneous ionic environment for ESI-MS analysis.

Treatment of **3** with homotrimer **4** in the presence of *N*-ethylmorpholine produced the desired red microcrystalline hexamer **5** in 31% yield; this structure was also confirmed by the ratio of the proton resonances (measured by NMR) for the complexed and uncomplexed 3′,5′-tpy-*H*s. The ESI-MS (expected mass for the $C_{250}H_{170}F_{72}N_{42}P_{12}Ru_6$ cationic core and counterions = 6108.30) definitively showed the multiple-charged signals ranging from *m*/*z* at 1077.8 $(M - 5\ PF_6)^{5+}$ to 364.2 $(M - 12\ PF_6)^{12+}$ for the expected charge states. Treatment of hexamer **5** with 1 equiv. of $FeCl_2$ in refluxing CH_3OH resulted in the one-step self-assembly of the desired fractal gasket **6**, isolated in 35% yield, as a deep red solid. Column chromatography and dialysis removed the low-molecular-weight monomers as well as the linear oligomeric materials. This material, isolated as the polyCl$^-$ salt, showed good solubility in CH_3OH, EtOH, *N*,*N*′-dimethylformamide (DMF), and dimethyl sulfoxide (DMSO) and poor solubility in H_2O, CH_2Cl_2, and CH_3CN, whereas after counterion exchange to the polyPF$_6^-$ salt, changes occur that make it soluble in CH_3CN, DMF, and DMSO and insoluble in CH_3OH, EtOH, and CH_2Cl_2.

The characterization of gasket **6** involved a considerable range of spectroscopic and electron microscopy (EM) techniques. Taken together, the data offered strong support for the proposed structure.

The use of a different metal in the last assembly step was planned, because different spectral properties using Fe(II) versus Ru(II) connectivity would aid in the molecular characterization; notably, the all-Ru(II) counterpart was easily formed by the use of $[Ru(DMSO)_4Cl_2]$ in the final macrocyclization. In the case of the Fe-Ru construct, there should be a 1:6 Fe:Ru ratio observed for all cyclic macromolecules generated. Formation of the heterodinuclear construct was initially confirmed by ^{1}H NMR measurements that showed two characteristic 3′,5′-tpy-*H* peaks: one at 9.45 ppm attributed to the tpy-*Fe*-tpy complex and the other at 9.20 ppm attributed to the tpy-*Ru*-tpy complex, displaying the requisite 1:6 integration; a distinct singlet at 2.98 ppm for the methyl groups was also present. Ultraviolet visible (UV-vis) spectroscopy in CH_3CN (for PF_6^-) or CH_3OH (for Cl^-) showed the expected absorbance pattern at 575 and 495 nm with a 1:6 ratio for the tpy-*Fe*-tpy and tpy-*Ru*-tpy units, respectively. These results are consistent with that observed in a previous study (*17*), where a hexagonal metallomacrocycle possessing 3 Fe and 3 Ru ions was prepared in an alternating pattern. As well, the individual $(tpy)_2Fe$ (*18*) and $(CH_3C_6H_4tpy)_2Ru$ (*19*) complexes were shown to have absorptions at 562 and 490, respectively; thus few or no cooperative effects can be attributed to the larger structures. Because of the overall 84^+ molecular charge, matrix-assisted laser desorption ionization time-of-flight mass spectroscopy (MALDI-TOF MS) measurements failed to provide definitive structural information; however, the ESI-MS spectrum showed a broad peak range from *m*/*z* at 310 to 970 attributed to the multicharged stages *m*/*z* = 35^+ to 84^+. A recent investigation (*20*) concerning *bis*-(tpy)Ru(II)-based macrocycles has determined the ESI technique to be superior to the MALDI technique because it has the advantage of direct detection of multiply charged ions, it does not change the complex connectivity through disassembly and reassembly processes, and it effects very little or no fragmentation.

The cyclic voltammogram (CV) of gasket **6** (see supporting online material) exhibits two reductive couples and one oxidative couple. The first and second reductive couples are not reversible, and the first has a sharp oxidative peak that

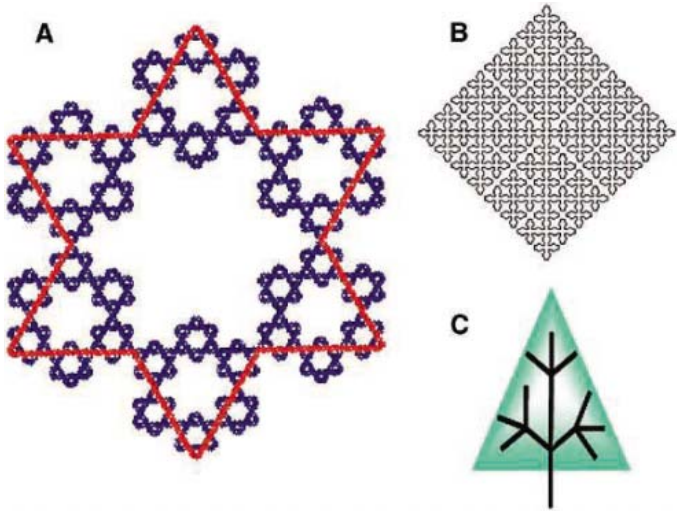

Fig. 1. Sierpinski's hexagonal gasket (**A**) incorporating the Star of David and the Koch snowflake motifs. Images of the snakelike "kolam" pattern (**B**) and (**C**) the 1 → 3 branching pattern of a tree.

[1]Department of Polymer Science, [2]Department of Chemistry, [3]Department of Polymer Engineering, [4]Department of Theoretical and Applied Mathematics, The University of Akron, Akron, OH 44325–4717, USA. [5]Department of Chemistry, Clemson University, Clemson, SC 29634, USA. [6]Department of Physics and Astronomy, Ohio University, Athens, OH 45701, USA.

*To whom correspondence should be addressed. E-mail: newkome@uakron.edu

grows with each successive scan because of adsorption on the electrode surface. The third redox couple observed around 1 V corresponds to the oxidation of Ru(II); however, the oxidation potential of Fe(II) is very close to this value, and thus it is impossible to establish the relative currents derived from Fe versus Ru for stoichiometric quantification. Because these metal terpyridine centers are redox-independent, the electrochemical data cannot be used to confirm the structure of the fractal **6**; however, the data are entirely consistent with the proposed structure.

X-ray photoelectron spectroscopy (XPS, using monochromatic Mg Kα radiation at a power of 250 W) was undertaken in order to verify the presence of the coordinated metals and to gain more data in support of cyclic structure. This technique uses x-ray radiation to measure the characteristic electron binding energies of the elements, and the intensity of the recorded peaks is related to elemental concentration. The XPS spectrum showed binding energy peaks at 398 and 285 eV attributed to the N1s and C1s electrons of the terpyridine ligands, respectively, as well as peaks assigned to Ru ($3d^{1/2}$ at 284 eV and $3d^{5/2}$ at 280 eV) and Fe ($2p^{1/2}$ at 706 eV and $2p^{3/2}$ at 709 eV), thus confirming the presence of Fe and Ru complexes. The exact atomic Ru:Fe ratio of 6:1 afforded further support for the macrocyclization of monomer **5**.

Energy minimization calculations for the desired fractal **6**, performed using molecular modeling software (see supporting online material), indicated that the predicted structure would be 12.3 nm in diameter and 0.7 nm in height; the modeled structure of fractal **6** on a mica surface possessed a slight chairlike or bent geometry rather than strict planarity. Dynamic light scattering (DLS) experiments (see supporting online material) determined the average particle size of fractal **6** to be 12.5 nm, which is the intensity-averaged hydrodynamic diameter (*21*).

Because this fractal construct possesses a uniform internal repeating (polymeric) architecture that is highly symmetrical, the NMR, UV, XPS, CV, and DLS data confirm the repeat units but do not definitively establish the overall architecture of this nanoscopic hexagonal gasket; therefore, it was necessary to undertake single-molecule imaging studies. In order to visually confirm the hexagonal structure, a droplet of an acetonitrile solution of **6** (100 μg of **6** in 500 ml) was deposited on the surface of freshly cleaved mica or Au(111), dried under ambient conditions, and subjected to atomic force microscopy (AFM). This technique allows the mapping of a surface with a tip on a cantilever that results in a topographic image of a surface; the size and sharpness of the tip determine the size of the objects that can be mapped with good resolution. AFM provides data on a sample's dimensions, including height. The AFM images of individual fractal constructs reveal an average diameter of 20 ± 2 nm, relative to the ~4-nm radius of curvature of the silicone tip used in the AFM measurements (Fig. 3A), thereby supporting the modeled diameter of ~12 ± 2 nm (*22*). The higher-magnification images exhibited clear patterns in which the six ruthenium hexamers and the central hole were clearly discernible.

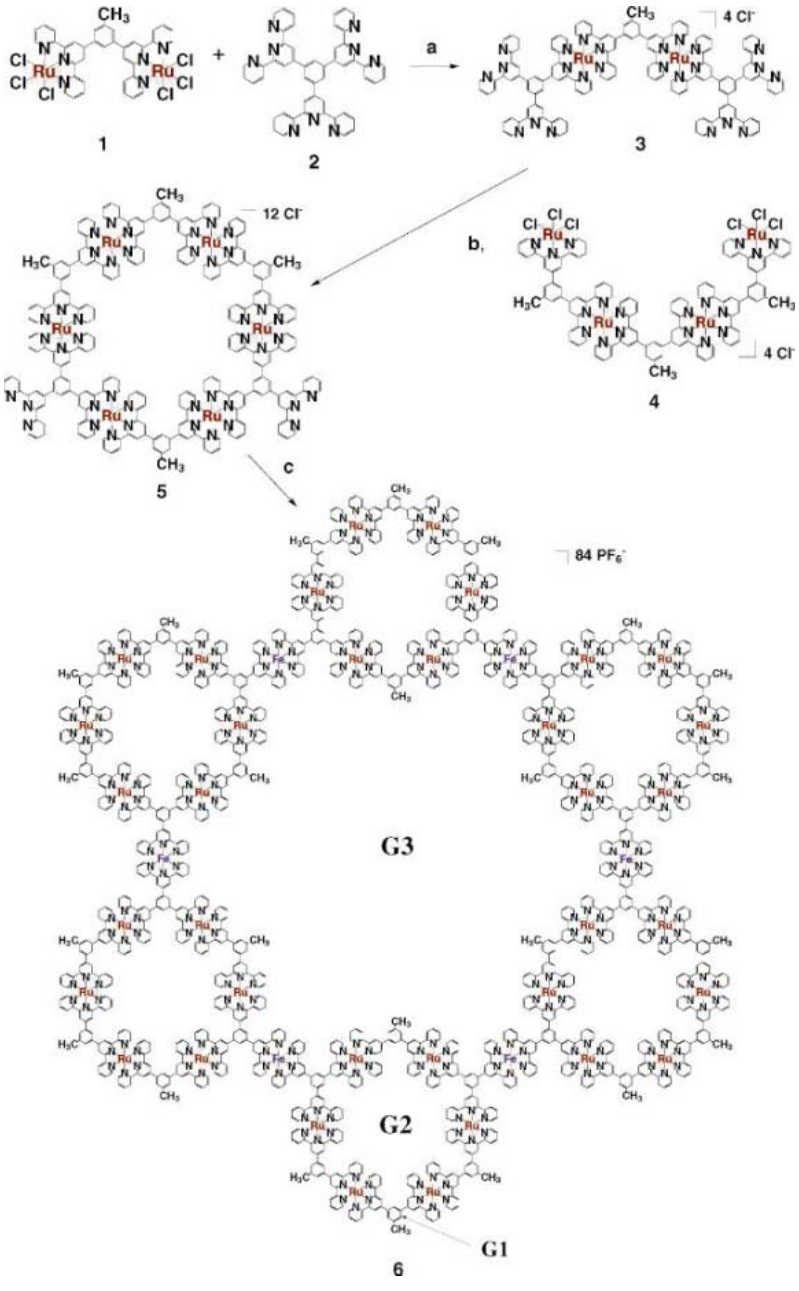

Fig. 2. Reaction scheme for the synthesis of trimer **3**, hexamer **5**, and the fractal gasket **6**. Reaction conditions were as follows: (a) **1** and **2** were mixed with *N*-ethylmorpholine in refluxing $CH_3OH/CHCl_3$ (2:1 v/v), for 20 hours. (b) **3** and **4** were stirred in refluxing CH_3OH with added *N*-ethylmorpholine for 12 hours. (c) First, hexamer **5** was refluxed in CH_3OH in the presence of 1 equiv. of $FeCl_2 \cdot 6H_2O$ for 20 hours. Then, to a CH_3OH solution of $\mathbf{5}(Cl^-)_m(NO_3^-)_n$ was added a solution of NH_4PF_6 to obtain the desired gasket **6** as a precipitate. G1 to G3 indicate generations 1 to 3 that can be envisioned for this fractal-based construct.

Transmission electron microscopy (TEM) (Fig. 3B) was also used for characterization. TEM analysis provides the size, shape, and arrangement of a specimen and in some cases can provide crystallographic information. After casting a dilute methanol solution of **6** (250 μg in 100 ml) on carbon-coated grids (Cu and Ni, 400 mesh), the resultant analysis showed the predicted fractal-like pattern (Fig. 3B) possessing an average diameter of 11 ± 1 nm for the single molecule, which gives direct evidence for the macrocyclization. Study of a higher-magnification TEM image (Fig. 3B, insert) reveals individual hexagonal gaskets lying flat or slightly tilted.

Ultrahigh-vacuum low-temperature scanning tunneling microscopy (UHV-LT-STM) (*23*) was

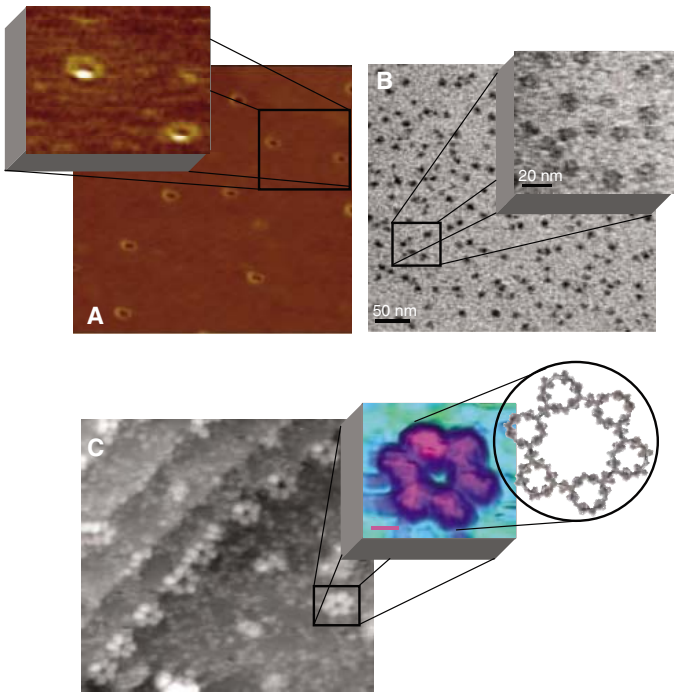

Fig. 3. Images of gasket **6**. (**A**) AFM images at 1.12 × 1.12 μm and 100 × 100 nm. (**B**) TEM pictures with 50- and 20-nm scale bars for the lower- and higher-resolution images, respectively (all images were obtained unstained). (**C**) UHV-STM images (100 × 100 nm) on a Au(111) surface at 6 K, revealing a line of gaskets settled on a ridge on the gold surface and a color-enhanced and magnified image of a single molecule (scale bar, 3 nm).

also used to image the structure. This apparatus can generate images with atomic resolution by directly measuring electronic states. UHV allows clean, controlled surface preparation and cryogenic temperatures to help reduce electronic noise and slow molecular motion. Using the same dilution as for the TEM sample preparation, fractal construct **6** in acetonitrile was cast onto a freshly cleaned Au(111) surface. STM images acquired at 6 K (Fig. 3C) verified a hexagonal pattern of the molecule (12 ± 1 nm diameter, and ~0.8 nm in height), which was consistent with the computer-generated model of the structure. Tunneling conductance spectra determined for single molecules at 6 K showed a 1-eV energy gap. Traces of linear oligomeric as well as larger macrocyclic assemblies (fractoids) were also observed on the STM images (see supporting online material).

References and Notes

1. B. B. Mandelbrot, *The Fractal Geometry of Nature* (Freeman, San Francisco, CA, 1982).
2. D. A. Tomalia *et al.*, *Polym. J. (Tokyo)* **17**, 117 (1985).
3. G. R. Newkome, Z. Yao, G. R. Baker, V. K. Gupta, *J. Org. Chem.* **50**, 2003 (1985).
4. G. R. Newkome, C. N. Moorefield, F. Vögtle, *Dendrimers and Dendrons: Concepts, Syntheses, Applications* (Wiley-VCH, Weinheim, Germany, 2001).
5. K.-i. Sugiura, H. Tanaka, T. Matsumoto, T. Kawai, Y. Sakata, *Chem. Lett. (Jpn.)* **1999** (no. 11), 1193 (1999).
6. M. Ascher, *Am. Sci.* **90**, 56 (2001).
7. W. Sierpinski, *Comptes Rendus (Paris)* **160**, 302 (1915).
8. S. R. Seidel, P. J. Stang, *Acc. Chem. Res.* **35**, 972 (2002).
9. M. Fujita *et al.*, *Chem. Commun.* **2001**, 509 (2001).
10. D. L. Caulder *et al.*, *J. Am. Chem. Soc.* **123**, 8923 (2003).
11. J. L. Atwood, L. J. Barbour, *Cryst. Growth Design* **3**, 3 (2003).
12. G. R. Newkome *et al.*, *Angew. Chem. Int. Ed. Engl.* **38**, 3717 (1999).
13. G. R. Newkome *et al.*, *Chem. Eur. J.* **8**, 2946 (2002).
14. P. Wang, C. N. Moorefield, G. R. Newkome, *Angew. Chem. Int. Ed. Engl.* **44**, 1679 (2005).
15. P. Wang, C. N. Moorefield, G. R. Newkome, *Org. Lett.* **6**, 1197 (2004).
16. E. C. Constable, A. M. W. C. Thompson, *J. Chem. Soc. Chem. Commun.* **1992** (no. 8), 617 (1992).
17. G. R. Newkome, T. J. Cho, C. N. Moorefield, P. P. Mohapatra, L. A. Godínez, *Chem. Eur. J.* **10**, 1493 (2004).
18. P. S. Braterman, J.-I. Song, R. D. Peacock, *Inorg. Chem.* **31**, 555 (1992).
19. J.-P. Sauvage *et al.*, *Chem. Rev.* **94**, 993 (1994).
20. P. Wang, G. R. Newkome, C. Wesdemiotis, *Int. J. Mass Spectrom.*, 10.1016/j.ijms.2006.03.006.
21. D. E. Koppel, *J. Chem. Phys.* **57**, 4814 (1972).
22. C. V. Nguyen *et al.*, *J. Phys. Chem. B* **108**, 2816 (2004).
23. K.-F. Braun, S.-W. Hla, *Nano Lett.* **5**, 73 (2005).

24. Supported by NSF [grants DMR-0196231, DMR-0401780, CHE-0116041 (G.R.N.), and CHE-0509989 (L.E.)]; the Air Force Office of Scientific Research [grant F49620-02-1-0428, 02 (G.R.N.)]; the U.S. Department of Energy [grant DE-FG02-02ER46012 (S.-W.H.)]; and the Ohio Board of Regents. The authors also thank S. Z. D. Cheng, B. Wang, S. F. Lyuksyutov, A. Dhinojwala, and C. Wesdemiotis from The University of Akron and M. J. Saunders from Cleveland State University for their valuable discussions about TEM, STM, AFM, and XPS measurements, as well as F. Ernst and W. D. Jennings from Case Western University for their assistance with the TEM and XPS measurements.

Supporting Online Material

www.sciencemag.org/cgi/content/full/1125894/DC1
SOM Text
Figs. S1 to S7
References

7 February 2006; accepted 17 April 2006
Published online 11 May 2006;
10.1126/science.1125894
Include this information when citing this paper.

Middle Paleolithic Shell Beads in Israel and Algeria

Marian Vanhaeren,[1*] Francesco d'Errico,[2*] Chris Stringer,[3] Sarah L. James,[4] Jonathan A. Todd,[3] Henk K. Mienis[5]

Perforated marine gastropod shells at the western Asian site of Skhul and the North African site of Oued Djebbana indicate the early use of beads by modern humans in these regions. The remoteness of these sites from the seashore and a comparison of the shells to natural shell assemblages indicate deliberate selection and transport by humans for symbolic use. Elemental and chemical analyses of sediment matrix adhered to one *Nassarius gibbosulus* from Skhul indicate that the shell bead comes from a layer containing 10 human fossils and dating to 100,000 to 135,000 years ago, about 25,000 years earlier than previous evidence for personal decoration by modern humans in South Africa.

Early evidence for beads and symbolic behavior by modern humans comes from Blombos Cave, Cape Province, South Africa, where 41 *Nassarius kraussianus* marine shell beads bearing human-made perforations and traces of use are associated with a Still Bay assemblage dated by optically stimulated luminescence (OSL) and thermoluminescence (TL) at ~75 thousand years ago (ka) (*1*–*3*). No other compelling evidence for bead use exists before about 40 ka, when beads appear at African, Eurasian, and Australian sites (*2*, *4*). Other suggested early beads lack reliable cultural and chronological context or evidence of human manufacture. Four *Glycymeris* sp. shells with perforations on the umbo come from the Mousterian layers of Qafzeh Cave, Israel (*5*), dated by TL between ~90 and 100 ka (*6*). However, no anthropogenic traces were detected on the perforations, which are known to occur naturally on the umbo of bivalves. Also, the large size of the shells and the presence of pigment on one specimen indicate that they may have been used as ochre containers rather than as ornaments. Here we identify as beads three marine gastropod shells (Fig. 1), two of which come from the Middle Paleolithic site at Es-Skhul, Mount Carmel, and one from the type site of the Aterian industry, Oued Djebbana, Bir-el-Ater, Algeria.

The shelter of Es-Skhul is located at Mount Carmel, Israel, 3 km south of Haifa, in the canyon of Nahal Me'arot (Wadi el-Mughara), and 3.5 km from the Mediterranean shore (*7*). Excavations in 1931 and 1932 identified three main layers (*8*, *9*): Layer A (20 to 50 cm of soft

sediment) contained a mixture of Natufian, Aurignacian, and Middle Paleolithic stone tools; layer B (about 200 cm thick and bearing all the human remains) contained Middle Paleolithic stone tools; and layer C (shallow sandy deposits at the base of the sedimentary sequence) yielded only a sparse lithic industry and no faunal remains. Layer B was subdivided into two subunits mainly distinguished by their hardness. The upper hard earth unit B1 resembled plaster of Paris, whereas the lower breccia B2 was similar to concrete. The lithics of Skhul Layer B were attributed to the Levantine Mousterian and have been compared with those of Tabun C and Qafzeh (*7*, *10*), whereas the macrofaunal remains in layer B appeared to correspond with those of Tabun C to D (*11*). Ten individuals (Skhul I to Skhul X), some apparently intentionally buried, were recovered from layer B. They are generally attributed to anatomically modern humans (*12*–*14*), albeit with some archaic characteristics. A large boar mandible was enclosed in the arms of Skhul V, interpreted as possible grave goods (*8*). Dates obtained for layer B from the use of electron spin resonance (ESR), U-series analysis, and TL on mammalian fossils or burnt flint range from about 43 to 134 ka (*15*–*17*), but recent ESR and U-series analyses, including direct dating with both techniques of a molar from the Skhul II skeleton, indicate ages between 100 and 135 ka (*18*). Garrod and Bate reported the presence of four marine shell species (*Acanthocardia deshayesii*, *Laevicardium crassum*, *Nassarius gibbosulus*, and *Pecten jacobaeus*), without indicating the number of specimens recovered or their stratigraphic provenance (*7*).

Oued Djebbana is an open-air site, located at Bir-el-Ater, 97 km south of Tebassa, Algeria, close to the Tunisian border and 200 km from the Mediterranean Sea (*19*, *20*). The site contained a 36-m-long by 80- to 100-cm-thick archaeological layer under 3.9 m of sterile alluvial deposits. This layer yielded a lithic assemblage that associates typical Aterian pedunculates with Middle Paleolithic tool types produced in some cases with the Levallois technique. The faunal remains, including *Equus*, *Bubalis boselaphus*, *Bos primigenius*, and *Connochoetes taurinus*, indicate a more humid savannah environment than that at present. The central area of the site, rich in ashes, contained one perforated *N. gibbosulus*. A single infinite conventional radiocarbon date of >35,000 years before the present (MC 657) is available for this site (*21*).

We located the marine shells from Skhul in the Department of Palaeontology, Natural History Museum (NHM), London, and the specimen from Oued Djebbana in the Department of Prehistory, Musée de l'Homme, Paris. The Skhul material includes two perforated *N. gibbosulus*, a valve of *A. deshayesii*, a fragment of *L. crassum*, a fragment of an undetermined shell, and a fragment of a cypraeid. The *P. jacobaeus* mentioned by Garrod and Bate is missing. Only the *N. gibbosulus* bear perforations that could have been used for suspension in a beadwork. However, nonhuman taphonomic processes are known to produce pseudo personal ornaments that can mimic humanly modified and used beads. Ideally, to determine whether purported ancient beads were used as such requires evidence of human involvement in their selection, transport, manufacture, and use. In the case of the multilayered Skhul site, the stratigraphic origin of the *Nassarius* shells also needs to be established. To address these issues, we analyzed sediment matrix adherent to one *N. gibbosulus* from Skhul (Fig. 1A) and sediment samples from layers A, B1, and B2 kept at the NHM (*22*), and compared the specimens from Skhul and Oued Djebbana to modern reference collections of *N. gibbosulus* shells (*22*).

Sediment samples from layers B1 and B2 cannot be distinguished from one another. The difference in their composition (table S1) appears to be controlled by the varying amounts of silica (predominantly from quartz) and calcium (predominantly from calcite). Rare earth elements (REEs) are essentially parallel. Layer A, in contrast, shows a high concentration of apatite (25% as opposed to 4%) that makes it distinct from layers B1 and B2. Phosphorus in apatite is scattered throughout the sample in the cement rather than being concentrated into discrete grains or bone fragments. This is not the case in samples from B1 and B2. Layer A also has elevated levels of Fe_2O_3, MnO, As, Cu, Mo, Ni, U, and Zn, and to a lesser extent, Al_2O_3, Ba, Li, Rb, and the REEs. The higher Al_2O_3 concentration indicates that layer A is richer in clay. Some of the elevated trace elements correlate independently with Al_2O_3 content (such as Fe_2O_3, Ba, Rb, and the REEs) and are probably contained in the clay minerals.

The hardness and the chemical composition of the sediment adherent to the pierced shell fit in well with samples from B1, B2, and a land snail recorded as coming from the Middle Paleolithic breccia (Fig. 2). This similarity with layer B and difference from layer A are shown in many of the major and trace elements as

[1]Centre for the Evolution of Cultural Diversity, University College London, 31–34 Gordon Square, London WC1H OPY, UK. Ethnologie Préhistorique, CNRS UMR 7041, 21 Allée de l'Université, F-92023 Nanterre, France. [2]Institut de Préhistoire et de Géologie du Quaternaire, CNRS UMR 5199, Avenue des Facultés, 33405 Talence, France; and Department of Anthropology, George Washington University, Washington, DC. [3]Department of Palaeontology, [4]Department of Mineralogy, The Natural History Museum, London SW7 5BD, UK. [5]Department of Zoology, Tel Aviv University, 69978 Tel Aviv, Israel.

*To whom correspondence should be addressed. E-mail: m.vanhaeren@ucl.ac.uk (M.V.); f.derrico@ipgq.u-bordeaux1.fr (F.D.)

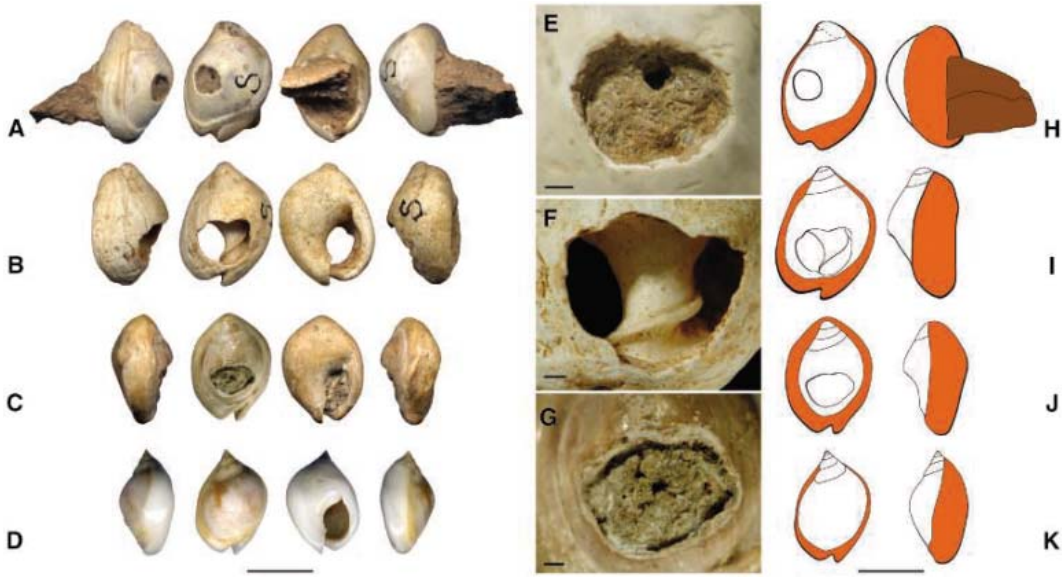

Fig. 1. *N. gibbosulus* shell beads from Es-Skhul (**A** and **B**), Oued Djebbana (**C**), and a present-day shore (**D**). (**E** to **G**) Macrophotos of the perforations on the archaeological specimens. (**H** to **K**) Extent of the ventral shield. Scale bar, 1 cm for (A) to (D), 1 mm for (E) to (G), and 1 cm for (H) to (K).

demonstrated in Fig. 2 (*22*). *N. gibbosulus* dated to the last interglacial bear a more developed and thicker parietal shield (*23*), which makes them wider than modern representatives of the species. This feature is observed on the Skhul and Oued Djebbana specimens (Fig. 1) and is particularly evident on the former, showing a width falling outside the modern range (Fig. 3), thus supporting its attribution to marine isotope stage 5.

Nassarius (*Plicarcularia*) *gibbosulus* (Linnaeus, 1758) is a scavenging marine gastropod that lives in shallow waters on pure sand (*24*) and is now confined to the central-eastern Mediterranean. The presence of these shells at Skhul and Oued Djebbana cannot be explained by natural causes. This species, and other closely related species of *Nassarius* (*Plicarcularia*), originated in the Middle Miocene (*25*), so we can discount derivation of the specimens as fossils from the Cretaceous strata of Mount Carmel or the Eocene rocks of the Nementcha Mountains that are drained by Oued Djebbana. During the accumulation of layers B1 and B2 (100 to 135 ka), the distance of Skhul from the sea varied between 3 and 20 km (*26*, *27*). Oued Djebbana was never, during the whole Upper Pleistocene, closer than 190 km to the sea. The altitude of Skhul (65 m at present and 45 to 150 m between 100 and 135 ka), the good state of preservation of the archaeological shells, their small number, and reduced species spectrum excludes storms as transporting agents (*28*). No known animal predators of *N. gibbosulus* transport these shells into caves or far inland. They can hardly be interpreted as leftovers from human food, because 100 specimens only provide 4.84 g of dry soft tissue (~20 kcal) and require 30 min to extract (*22*). The *N. gibbosulus* from Skhul do not seem to represent a random sample from a natural living or dead population. Both show a single perforation located in the center of the dorsal side (fig. S1), a feature observed in only 3.5% of modern thanatocoenoses. The Djebbana specimen presents the same rare perforation pattern. Microscopic analysis indicates that the agent responsible for the perforations on the Skhul specimens punched the shell body whorl from the outer dorsal side (Fig. 1). The probability of finding two *N. gibbosulus* with a similar perforation type as those from Skhul in a modern thanatocoenosis is very low (P = 0.001). This suggests that the shells were either purposely perforated or deliberately picked out of thanatocoenoses by Skhul inhabitants. We produced perforations similar in size and shape to those on the archaeological specimens by indirect percussion using a flint point as punch and regularizing the resulting hole by rotation. Such perforations are also documented on *N. gibbosulus* used as beads at Upper Paleolithic sites (*29*, *30*). However, considering that natural agents can perforate the shell in the same way, we cannot consider the hole morphology alone as compelling evidence for human agency.

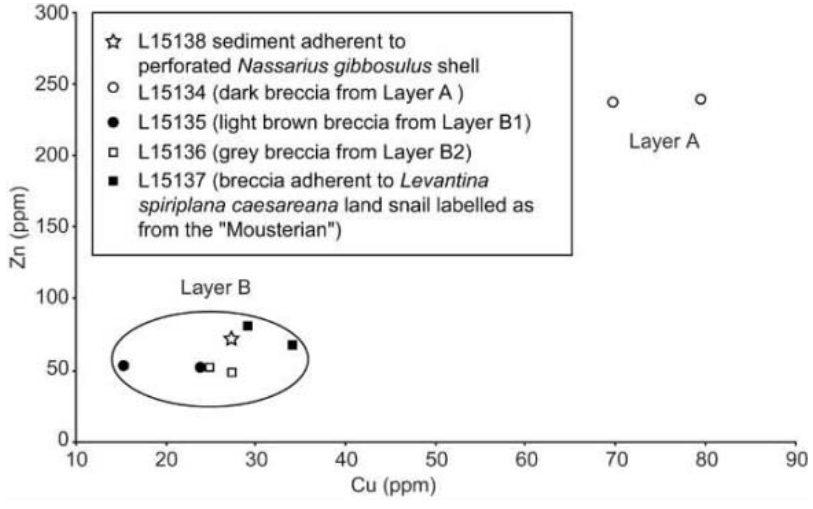

Fig. 2. Variation of Cu and Zn concentrations in Skhul breccias and sediment adherent to the pierced shell. All samples were in duplicate, except for pierced shell sediment, where sample size was insufficient.

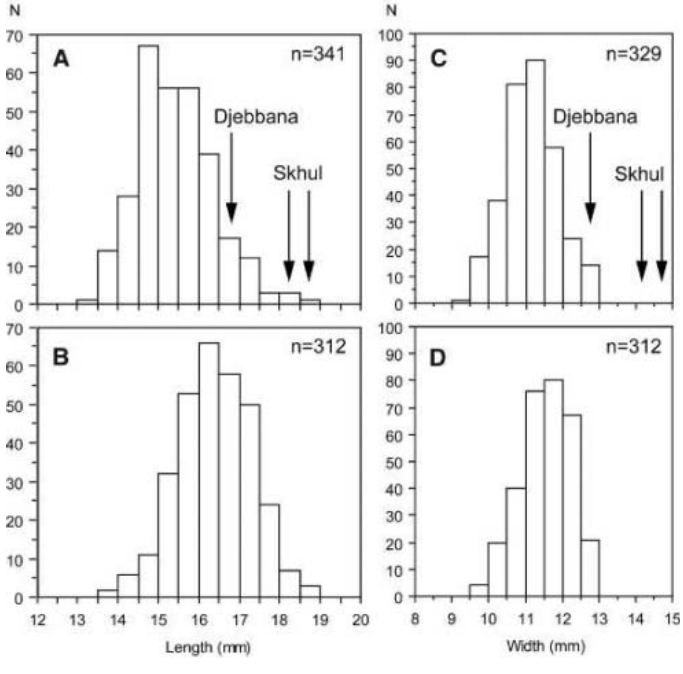

Fig. 3. Length and width distributions of *N. gibbosulus* shells collected from modern bio- and thanatocoenoses at Djerba Island, Tunisia (**A** and **C**) and Haifa Bay, Israel (**B** and **D**). Arrows indicate the length and width of the *N. gibbosulus* from Skhul and Oued Djebbana.

The length of the Skhul specimens (Fig. 3) is significantly larger than that recorded on both reference collections ($P < 0.01$), including the one from the shore close to the site. This does not necessarily imply a preference for large shells, because the variability of size of *N. gibbosulus* shells through time and their size contemporaneous with Skhul layer B is unknown. Our argument for these shells being used as beads relies on the remoteness of the sites from the sea and the rarity of their perforation type in modern thanatocoenoses.

There is substantial uncertainty about the age of the Aterian. Its traditional assignment to a period between 40 and 20 ka (*31*), based on conventional radiocarbon dates from bulk samples of material particularly susceptible to contamination, is now challenged by TL, OSL, and ESR dates, which point to an age of 90 ka to 35 ka (*32*, *33*). This range implies that the age of the Oued Djebbana site, for which only an infinite conventional radiocarbon date is available, could be close to that of Skhul layer B. The shell beads from Skhul and Oued Djebbana belong to the same species as the previous oldest known personal ornaments found in western Eurasia, discovered in the Ahmarian layers of Uçagizli, Turkey, dated to ~40 ka (*34*), and are morphologically similar and belong to the same genus as those from Blombos Cave. The few human remains associated with the Aterian suggest (*35*) that this culture was produced by early anatomically modern human populations, as was the Still Bay culture at Blombos (*36*) and the Ahmarian

culture at Uçagizli [from correlation with K'sar Akil (*37*)]. Genetic (*38*) and paleoanthropological (*39*) data point to an origin of anatomically modern humans in Africa at ~200 ka. However, evidence for cultural modernity before 40 ka has for long remained limited (*40*). These beads support the hypothesis that a long-lasting and widespread beadworking tradition existed in Africa and the Levant well before the arrival of anatomically modern humans in Europe.

References and Notes

1. C. S. Henshilwood, F. d'Errico, M. Vanhaeren, K. van Niekerk, Z. Jacobs, *Science* **304**, 403 (2004).
2. F. d'Errico, C. Henshilwood, M. Vanhaeren, K. van Niekerk, *J. Hum. Evol.* **48**, 3 (2005).
3. C. S. Henshilwood *et al.*, *Science* **295**, 1278 (2002).
4. M. Vanhaeren, in *From Tools to Symbols*, F. d'Errico, L. Backwell, Eds. (Wits Univ. Press, Johannesburg, South Africa, 2005), pp. 525–553.
5. Y. Taborin, in *Echanges et Diffusion dans la Préhistoire Méditerranéenne*, B. Vandermeersch, Ed. (Editions du Comité des Travaux Historiques et Scientifiques, Paris, 2003), pp. 113–122.
6. H. Valladas *et al.*, *Nature* **331**, 614 (1988).
7. D. A. Garrod, D. M. A. Bate, Eds., *The Stone Age of Mount Carmel. Volume 1: Excavations at the Wady El-Mughara* (Clarendon Press, Oxford, 1937).
8. T. D. McCown, in *The Stone Age of Mount Carmel. Volume I: Excavations at the Wady El-Mughara*, D. A. Garrod, D. M. A. Bate, Eds. (Clarendon Press, Oxford, 1937), pp. 91–107.
9. T. D. McCown, A. Keith, *The Stone Age of Mount Carmel II: The Fossil Human Remains from the Levalloiso-Mousterian* (Clarendon Press, Oxford, 1939).
10. O. Bar-Yosef, L. Meignen, in *The Middle Paleolithic: Adaptation, Behavior, and Variability*, H. Dibble, P. Mellars, Eds. (University Museum of the University of Pennsylvania, Philadelphia, PA, 1992), pp. 163–182.
11. D. Bate, in (*7*), pp. 134–233.
12. B. Vandermeersch, in *The Human Revolution*, P. Mellars, C. Stringer, Eds. (Edinburgh Univ. Press, Edinburgh, 1989), pp. 155–164.
13. C. B. Stringer, *Philos. Trans. R. Soc. London Ser. B* **337**, 217 (1992).
14. E. Trinkaus, *Annu. Rev. Anthropol.* **34**, 207 (2005).
15. C. B. Stringer, R. Grün, H. P. Schwarcz, P. Goldberg, *Nature* **338**, 756 (1989).
16. F. McDermott, R. Grün, C. B. Stringer, C. J. Hawkesworth, *Nature* **363**, 252 (1993).
17. N. Mercier *et al.*, *J. Archaeol. Sci.* **20**, 169 (1993).
18. R. Grün *et al.*, *J. Hum. Evol.* **49**, 316 (2005).
19. M. Reygasse, *Recl. Notes Mém. Soc. Archéolog. Constantine* **52-53**, 513, 204 (1919–1922).
20. J. Morel, *L'Anthropologie* **78**, 53 (1974).
21. J. Morel, *Bull. Soc. Préhistorique Française* **71**, 103 (1974).
22. Materials and methods are available as supporting material on *Science* Online.
23. S. Moshkovitz, thesis, Hebrew University of Jerusalem (1968).
24. W. O. Cernohorsky, *Systematics of the Family Nassariidae (Mollusca: Gastropoda)* (Bulletin of the Auckland Institute and Museum 14, Auckland, New Zealand, 1984).
25. C. Gili, J. Martinell, *Lethaia* **33**, 236 (2000).
26. M. Siddall *et al.*, *Nature* **423**, 853 (2003).
27. L. Ferranti *et al.*, *Quat. Int.* **145-146**, 30 (2006).
28. C. Claassen, *Shells* (Cambridge Univ. Press, Cambridge, 1998).
29. Y. Taborin, *La Parure en Coquillage au Paléolithique* (CNRS, Paris, 1993).
30. M. C. Stiner, in *The Chronology of the Aurignacian and the Transitional Technocomplexes*, J. Zilhao, F. d'Errico, Eds. (Instituto Português de Arqueologia, Trabalhos de Arqueologia 33, Lisbon, Portugal, 2003), pp. 49–59.
31. A. Debénath, *L'Anthropologie* **96**, 711 (1992).
32. M. Cremaschi, S. Di Lernia, E. A. A. Garcea, *Afr. Archaeol. Rev.* **15**, 261 (1998).
33. P. J. Wrinn, W. J. Rink, *J. Archaeol. Sci.* **30**, 123 (2003).
34. S. L. Kuhn, M. C. Stiner, D. S. Reese, E. Güleç, *Proc. Natl. Acad. Sci. U.S.A.* **98**, 7641 (2001).
35. J.-J. Hublin, in *Human Roots: Africa and Asia in the Middle Pleistocene*, L. Barham, K. Robson-Brown, Eds. (Western Academic and Specialist Press, Bristol, UK, 2001), pp. 99–121.
36. F. E. Grine, C. S. Henshilwood, J. C. Sealy, *J. Hum. Evol.* **37**, 755 (2000).
37. C. A. Bergman, C. B. Stringer, *Paléorient* **15**, 99 (1989).
38. M. Ingman, H. Kaessmann, S. Pääbo, U. Gyllensten, *Nature* **408**, 708 (2000).
39. C. B. Stringer, *Philos. Trans. R. Soc. London Ser. B* **357**, 653 (2002).
40. S. McBrearty, A. S. Brooks, *J. Hum. Evol.* **39**, 453 (2000).

41. We thank F. Sémah and O. Romain for access to the Oued Djebbana material kept at the Musée de l'Homme, Paris; C. Barbera, B. Cahuzac, L. Charles, C. Claes, L. Ferranti, P. Lozouet, G. Mastronuzzi, I. Nofroni, R. Sablon, J.-P. Tastet, M. Taviani, and J. Van Goethem for information on modern and fossil *N. gibbosulus*; and D. Bar-Yosef Mayer, G. Slabodsky, and W. Banks for discussion. This work was funded by the Origin of Man, Language and Languages program of the European Science Foundation; the French Ministry of Research; and postdoctoral grants from the French Centre National de la Recherche Scientifique and Fyssen Foundation.

Supporting Online Material

www.sciencemag.org/cgi/content/full/312/5781/1785/DC1
Materials and Methods
Fig. S1
Table S1
Reference

30 March 2006; accepted 15 May 2006
10.1126/science.1128139

Phosphorus in Cold-Water Corals as a Proxy for Seawater Nutrient Chemistry

Paolo Montagna,[1]* Malcolm McCulloch,[2] Marco Taviani,[3] Claudio Mazzoli,[4,5] Begoña Vendrell[6]

Phosphorus is a key macronutrient being strongly enriched in the deep ocean as a result of continuous export and remineralization of biomass from primary production. We show that phosphorus incorporated within the skeletons of the cosmopolitan cold-water coral *Desmophyllum dianthus* is directly proportional to the ambient seawater phosphorus concentration and thus may serve as a paleo-oceanographic proxy for variations in ocean productivity as well as changes in the residence times and sources of deep-water masses. The application of this tool to fossil specimens from the Mediterranean reveals phosphorus-enriched bottom waters at the end of the Younger Dryas period.

Phosphorus is a major biolimiting nutrient (*1*–*3*) that plays a key role in sustaining the biological productivity of the world's oceans. It is rapidly used by marine phytoplankton and exhibits a characteristic depletion in the uppermost surface oceans as a result of export of biomass to the deep oceans. This mechanism may be so efficient that changes in nutrient use in the Southern Ocean are considered to have played an important role in CO_2 sequestration and hence the lower levels of atmospheric CO_2 present during glacial cycles (*4*). Therefore, evaluating and quantifying past changes in the export of biological production to deep waters is a major issue, not only to understand past changes in atmospheric CO_2 but also to help predict how the ocean may buffer future increases in atmospheric CO_2. The P content of the deep-water masses also shows systematic differences across the major ocean basins, with the older deep-water masses in the North Pacific having ~50% higher P concentration than those formed more recently in the North Atlantic, reflecting ongoing remineralization of organic particles in the deep waters. Thus, changes in the P content of deep waters reflect changes in the biological production and cycling in surface waters as well as changes in the residence time of abyssal water masses.

Despite the importance of P, a straightforward approach for quantifying longer term changes in the concentration of this key paleonutrient in seawater is not yet available. The most commonly used proxies, namely carbon isotopes ($\delta^{13}C$) and Cd/Ca ratios in foraminiferal tests, appear to respond to a variety of additional environmental factors, including carbonate ion concentration, $\delta^{13}C$ of foraminiferal diet, and seawater temperature (*5*, *6*), although the lack of a significant temperature influence on the incorporation of Cd into benthic foraminiferal tests has been reported recently (*7*). Furthermore, although Ba and organic matter accumulation in marine sediments are recognized as potential tracers of marine biological productivity (*8*, *9*), their use as paleoproductivity proxies is dependent on

[1]Istituto Centrale per la Ricerca Scientifica e Technologica Applicata al Mare (ICRAM), Via di Casalotti 300, 00166, Rome, Italy. [2]Research School of Earth Sciences, Australian National University, Canberra, ACT 0200, Australia. [3]Istituto di Scienze Marine (ISMAR), Consiglio Nazionale delle Ricerche (CNR), Via P. Gobetti 101, 40129 Bologna, Italy. [4]Dipartimento Mineralogia e Petrologia, Università di Padova, Corso G. Garibaldi 37, 35137 Padova, Italy. [5]Istituto di Geoscienze e Georisorse, CNR, Corso G. Garibaldi 37, 35137 Padova, Italy. [6]Institut de Ciències del Mar (CSIC), Passeig Marítim de la Barceloneta, 37-49 08003 Barcelona, Spain.

*To whom correspondence should be addressed. E-mail: p.montagna@icram.org

their preservation in the sediment records (*9*, *10*) and their sedimentation rate. Very few studies have tried to explore scleractinian and deep-sea gorgonian corals as potential high-resolution paleonutrient or chemical pollution (phosphorus) archives in seawater (*12*–*17*), and no direct calibrations have yet been reported between nutrient proxies (e.g., P/Ca, Cd/Ca) and environmental parameters (e.g., nutrient content in seawater, surface particulate organic matter). Accordingly, we have investigated whether P incorporated in the aragonite skeleton of the scleractinian coral *Desmophyllum dianthus* can provide a quantitative proxy for the ambient P concentration in deep ocean waters.

D. dianthus is a solitary cold-water coral mainly found at bathyal depths with a cosmopolitan geographic distribution (*18*, *19*). To assess its potential as a proxy for seawater fertility, we have analyzed specimens collected from a range of geographic locations characterized by distinctive P contents: the western (Balearic Islands) and central (Ionian) Mediterranean Sea, the Australian sector of the western Pacific Ocean, and the northern Chilean fjords region (*20*). The Mediterranean Sea primarily displays oligotrophic conditions with some more eutrophic areas, whereas the northern Chilean fjords are characterized by a strongly eutrophic environment (*21*). The Australian sector of the western Pacific Ocean shows intermediate environmental conditions. Furthermore, fossil coral skeletons from the Mediterranean Sea were also analyzed. Both living and fossil samples consist of pristine aragonite, and there is no evidence for secondary aragonite precipitation, micrite cement, and Fe-Mn oxide/hydroxide black crusts (*20*). The mean annual extension rates of the living corals, based on ^{238}U-^{230}Th dating (table S1), are estimated to be ~7 mm/year for the deep-water western Pacific Ocean and ~10 mm/year for shallow water samples from the northern Chilean fjords (*22*). Deep-water corals from the central and western Mediterranean Sea were assumed to grow at ~0.4 mm/year, using a reasonable growth rate for living *D. dianthus* (*23*).

P/Ca ratios were measured in situ along the main septal elements of *D. dianthus* with a high-efficiency ultraviolet (193 nm) excimer laser ablation system coupled to an inductively coupled plasma mass spectrometer (ICP-MS) (*20*). To recover unambiguous environmental signals, analyses were carried out on the aragonite fibers on the outer faces of each septum, avoiding the early mineralizing centers of calcification that make up part of the central midplane of each septum (Fig. 1). This precaution was found to be necessary after reconnaissance studies on different structural elements (i.e., aragonitic fibers versus early mineralizing zones or centers of calcification) revealed that fine-scale geochemical differences are present between these regions (*24*) (fig. S1). Along the mid-plane centers of calcification, there is a strong correlation (~0.9) between P, Ba, and Mg (*24*, *25*), which is attributed to vital effects associated with high organic contents. This is consistent with the presence of similar enrichments in the organic rich tissue zone of shallow-water hermatypic corals (*26*). Alternatively, the strong correlation together with the higher P and Mg contents in the centers of calcification might in part be the trace element signature of transient amorphous calcium carbonate, which may contain considerable quantities of Mg and/or P (*27*). The mechanism whereby P is incorporated in the outer fibrous portion of the septal elements is, however, still uncertain. Unlike with zooxanthellate shallow-water corals (*26*), there is no evidence for P-enriched organic matter, and P is weakly correlated with Ba variations (~0.3). In addition, petrographic studies have revealed the lack of prominent organic-enriched layers in the outer fibrous portion of azooxanthellate corals (*28*). This, together with the relatively uniform pattern of P uptake, suggests that a considerable proportion of P may be stoichiometrically incorporated within the skeletal aragonite of *D. dianthus* during crystal growth rather than by adsorption on crystal surfaces. It is also possible that a relatively fast (~1 week, depending on growth rate) mechanism of P incorporation into the crystal lattice exists once P is adsorbed on crystal surfaces (supporting online text). Reliability and long-term reproducibility of the data were tested by comparing two parallel tracks within the same septum (living sample 7a) together with values obtained from an adjacent septum of the same specimen (living sample 7a) and from an additional septum of a nearby specimen of the same age (living sample 7b). In addition, tracks acquired 2 weeks apart were replicated in living sample SML. Adjacent and replicated tracks on the same septa, as well as tracks in different septa of the same age, produced similar patterns, with differences being well within analytical error (fig. S2).

For modern corals from the Mediterranean and the western Pacific Ocean, P concentrations obtained from two adjacent analytical tracks along the outer septal walls were averaged relative to the last 3 months of coral

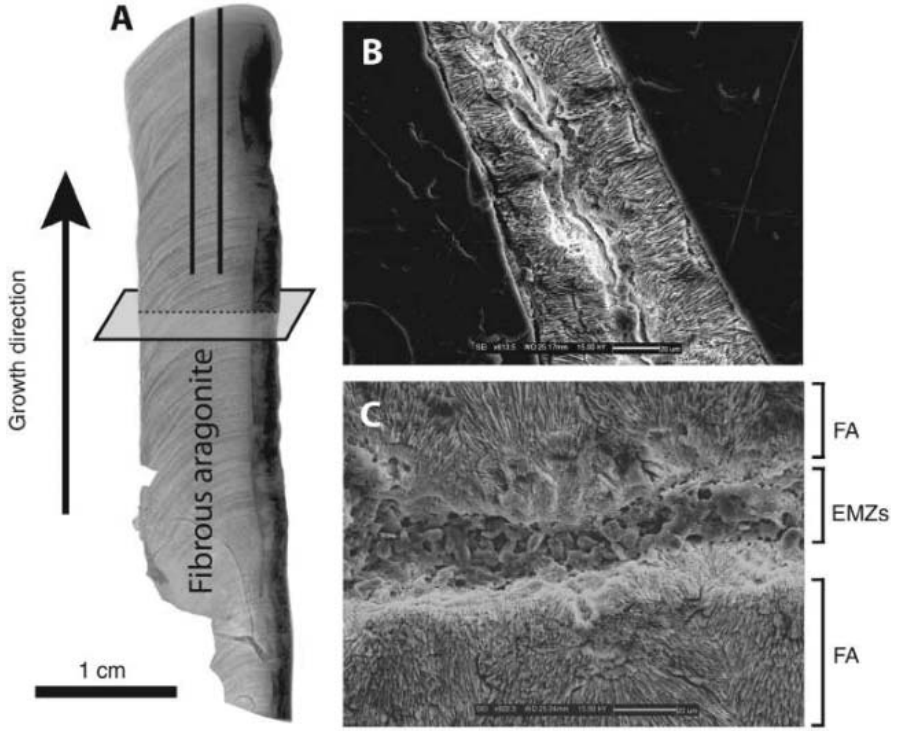

Fig. 1. Photomicrographs of the cold-water coral *D. dianthus*. (**A**) Transmitted light image of the main septum (S1). The density banding is clearly visible throughout the septum with alternating white and dark microbands (~10-μm wide). The outer face of the S1 septum is smooth and mainly composed of bundles of aragonitic fibers, with occasionally some small portions of early mineralization zones (EMZs) developed as granulations. As indicated in (A), the septum was transversely sectioned to reveal the midplane microstructures. The black lines in (A) represent two adjacent laser ablation tracks. (**B**) Scanning electron microscopy (SEM) image of a transverse, polished, and etched septum, showing the chain of EMZs surrounded by radiating fibers. (**C**) SEM enlargement of (B) showing fine-grained crystals (EMZs) and adjacent bundles of acicular crystals. EMZs are composed of apparently non-crystalline, "blurry" material. FA, fibrous aragonite.

growth and compared with direct in situ seawater measurements of dissolved inorganic phosphorus (DIP) (*20*). For modern coral NCF 7a, we used both the mean value relative to 1 year and the average of 3 months of coral growth corresponding to the spring period. With this approach, P uptake in *D. dianthus* is shown to be linearly dependent on the dissolved inorganic P of ambient

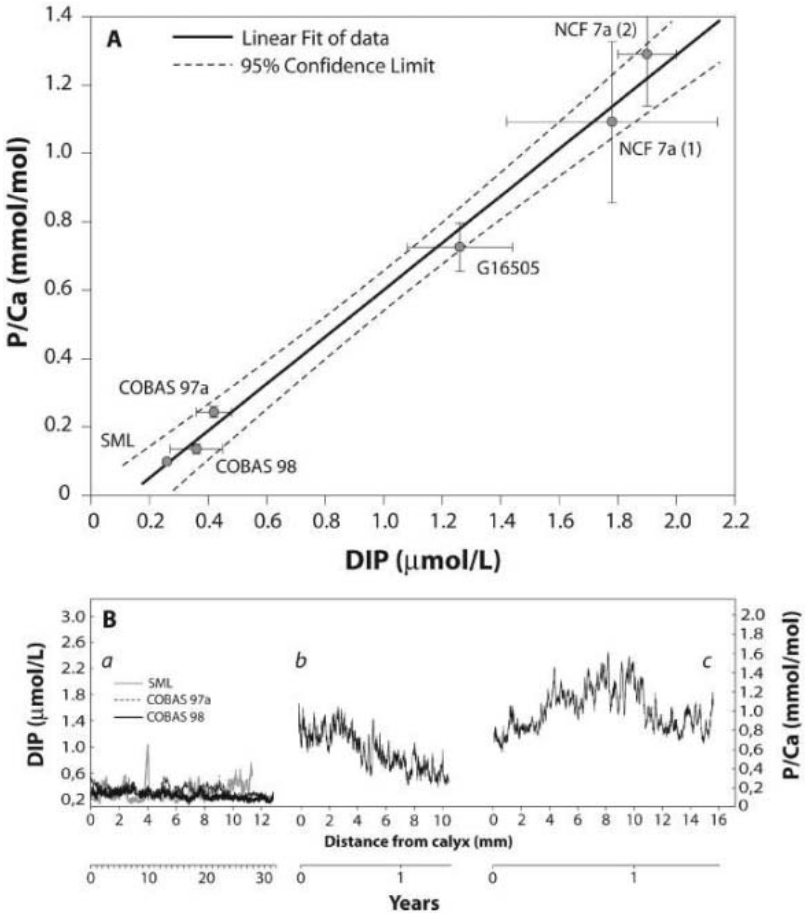

Fig. 2. (**A**) Linear regression of coralline P/Ca ratios (mmol/mol) versus in situ measured dissolved inorganic phosphorus (μmol/L). P/Ca values for modern corals from the Mediterranean and the western Pacific Ocean represent an average of the last 3 months of coral growth. Regarding the Chilean coral NCF 7a, the average of 1 year (1) and the average of 3 months of coral growth corresponding to the spring period (2) were used. For each of the considered samples, two adjacent analytical tracks were averaged. Error bars represent 1 SD. DIP values used for the linear regression are explained in (*20*). Coral P/Ca ratios are linearly dependent on the DIP values. (**B**) P/Ca-derived DIP values and P/Ca ratios versus distance from calyx and time for the modern corals used to obtain the calibration. *a*, SML, COBAS 97a, and COBAS 98 corals. *b*, G16505 coral. The P/Ca-derived DIP varies between ~0.7 and 1.5 μmol/L, which is comparable with the variability of the DIP concentration measured in the seawater (*19*). *c*, NCF 7a coral. The bell-shaped pattern of the P/Ca ratios represents an annual cycle, and variability of the corresponding P/Ca-derived DIP is comparable with seasonal DIP variations in the northern Chilean fjords (*20*).

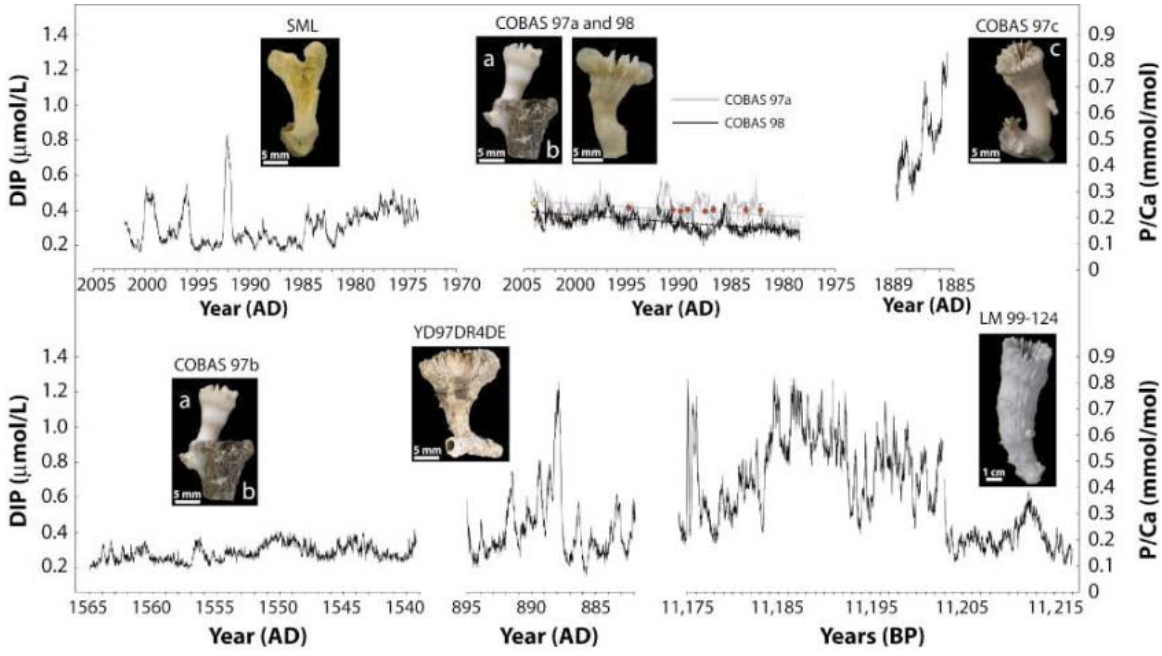

Fig. 3. P/Ca-derived DIP values, obtained using Eq. 1, and P/Ca ratios for living and fossil Mediterranean samples. COBAS 97a was dredged at deeper water depth (1163 to 685 m) compared with COBAS 98 (369 to 301.5 m) and shows higher DIP values, associated with the vertical transfer of phosphate from biological activity. Both P/Ca-derived DIP time series follow an increasing trend since the 1970s, consistent with historical values for nutrients in the western Mediterranean, acquired in the 400-m bottom layer (red dots) (*28*). DIP value in 2004 was calculated using water samples during COBAS cruise (yellow dot). The gray and the black dotted lines represent the linear trend model for COBAS 97a and COBAS 98, respectively. COBAS 97c and LM 99-124 reveal high DIP values, suggesting more nutrient-rich waters during the end of the 19th century and at ~11,190 yr B.P.

seawater (Fig. 2), according to the following relationship.

$$\begin{aligned} \text{DIP } (\mu\text{mol/L}) &= 1.43\ (\pm 0.07) \\ &\times \text{P/Ca } (\text{mmol/mol}) + \\ &0.13\ (\pm 0.05) \qquad (1) \\ r^2 = 0.99, P &= 0.0001 \end{aligned}$$

Errors on the regression are calculated with respect to the dispersion on the y axis and are given at 1 SE.

To test the robustness of the phosphorus calibration based on modern global data sets, Eq. 1 was applied to long-lived modern specimens (COBAS 97a and COBAS 98) from the western Mediterranean Sea, with growth encompassing about the past 30 years. Both coral samples show an increase in P/Ca ratio of ~1.2% per year over this period (Fig. 3), in agreement with direct measurements of nutrients, reflecting the effects of increasing agricultural, industrial, and urban activities in the Mediterranean countries since the 1960s (*29*). In addition to the general positive trend in the nutrient content for the past 30 years, P content within *D. dianthus* also reveals decadal-scale variations within the water column and an almost constant offset between the two specimens over the growth period, suggesting a connected evolution at different water depths.

To further demonstrate the utility of this new proxy, we have examined premodern and fossil *D. dianthus* samples dredged from submerged coral assemblages in the western Mediterranean Sea. The most striking feature of these samples, which have ages within ~120 to ~11,190 years before the present (yr B.P.) (^{230}Th-^{238}U ages) (table S1), is their high P/Ca ratios (Fig. 3), which indicate the presence of more nutrient-rich deep waters. In particular the P content of the submodern coral COBAS 97c is almost twice that of present-day values, with even higher levels being found in a 11,230-year-old coral (LM 99-124), indicating nutrient-rich seawater similar to the present-day Chilean eutrophic environment.

These results are also consistent with phytoliths and freshwater diatom records from sediment cores in the western Mediterranean Sea, which suggest the establishment of humid conditions at the end of the Younger Dryas event, related to an intensification of the African monsoon (*30*). This might have led to an increase of phosphate availability, which in the Mediterranean is mainly related to river runoff (*29*). These results confirm the utility of cold-water coral *D. dianthus* as a proxy for seawater P, providing a new tool for reconstructing changes in the nutrient status of the oceans.

References and Notes

1. C. R. Benitez-Nelson, *Earth Sci. Rev.* **51**, 109 (2000).
2. T. Tyrrell, *Nature* **400**, 525 (1999).
3. M. L. Delaney, *Global Biogeochem. Cycles* **12**, 563 (1998).
4. D. M. Sigman, E. A. Boyle, *Nature* **407**, 859 (2000).
5. H. J. Spero, J. Bijma, D. W. Lea, B. E. Bemis, *Nature* **390**, 497 (1997).
6. R. E. M. Rickaby, H. Elderfield, *Paleoceanography* **14**, 293 (1999).
7. T. M. Marchitto, *Geochem. Geophys. Geosyst.* **5**, Q10D11 (2004).
8. J. Dymond, E. Suess, M. Lyle, *Paleoceanography* **7**, 163 (1992).
9. P. Bertrand, E. Lallier-Vergès, *Nature* **364**, 786 (1993).
10. J. McManus *et al.*, *Geochim. Cosmochim. Acta* **62**, 3453 (1998).
11. S. G. Wakeham, C. Lee, in *Organic Geochemistry*, M. Engel, S. Macko, Eds. (Plenum, New York, 1993), pp. 145–169.
12. R. E. Dodge, T. D. Jickells, A. H. Knap, S. Boyd, R. P. M. Bak, *Mar. Pollut. Bull.* **15**, 178 (1984).
13. W. Shotyk, I. Immenhauser-Potthast, H. A. Vogel, *J. Chromatogr.* **706**, 209 (1995).
14. C. E. Rasmussen, C. Cuff, *Proc. Fourth Pacific Congress on Marine Science and Technology* **1**, 13 (1990).
15. J. F. Adkins, H. Cheng, E. A. Boyle, E. R. M. Druffel, R. L. Edwards, *Science* **280**, 725 (1998).
16. J. M. Heikoop, D. D. Hickmott, M. J. Risk, C. K. Shearer, V. Atudorei, *Hydrobiologia* **471**, 117 (2002).
17. O. A. Sherwood *et al.*, *Mar. Ecol. Prog. Ser.* **301**, 135 (2005).
18. S. D. Cairns, G. D. Stanley Jr., *Proc. Fourth Internatl. Coral Reef Symposium* **1**, 611 (1981).
19. G. Försterra, V. Häussermann, *Zool. Verth. Leiden* **345**, 117 (2003).
20. Materials and methods are available as supporting material on *Science* Online.
21. F. Norambuena, thesis, Universidad Austral de Chile (2002).
22. M. McCulloch *et al.*, *Program and Abstract Book of the Third Internatl. Symposium on Deep-Sea Corals*, Miami 191 (2005).
23. H. Cheng, J. Adkins, R. L. Edwards, E. A. Boyle, *Geochim. Cosmochim. Acta* **64**, 2401 (2000).
24. P. Montagna, M. T. McCulloch, M. Taviani, A. Remia, C. Mazzoli, *Program and Abstract Book of the Third Internatl. Symposium on Deep-Sea Corals*, Miami 193 (2005).
25. P. Montagna, M. T. McCulloch, T. Taviani, A. Remia, G. Rouse, in *Cold-Water Corals and Ecosystems*, A. Freiwald, J. M. Roberts, Eds. (Springer-Verlag, Berlin, Heidelberg, 2005), pp. 671–688.
26. C. Alibert *et al.*, *Geochim. Cosmochim. Acta* **67**, 231 (2003).
27. Y. L. Addadi, S. Raz, S. Weiner, *Adv. Mater.* **15**, 959 (2003).
28. J. Stolarski, *Acta Palaeontol. Pol.* **48**, 497 (2003).
29. J. P. Béthoux *et al.*, *Mar. Chem.* **63**, 155 (1998).
30. M. A. Bárcena *et al.*, *Palaeogeogr. Palaeoclimatol. Palaeoecol.* **167**, 337 (2001).

31. We thank G. Mortimer and L. Kinsley for U-series dating and technical assistance with laser ablation analysis, respectively. We are grateful to S. Castelli for technical photographic support, S. Frisia and M. Prieto for suggestions on the P incorporation into aragonite, and S. Russo for helping on the moving correlation analysis. We are also grateful to C. Ianni, V. Brando, and J. Sepulveda for helping in the acquisition of the DIP data from the Ionian Sea, the Australian sector of the western Pacific Ocean, and the Chilean fjords, respectively; G. Forsterra for sampling the Chilean corals; and the Australian Museum for access to their collections. The work by P.M. was supported by a Ph.D. scholarship of the University of Padova and by the Ermenegildo Zegna Foundation. Support from the Australian Research Council Centre of Excellence for Coral Reef Studies and grant DP0559042 to M.Mc. is gratefully acknowledged, as well as partial funding to M.T. by European Science Foundation Moundforce and European Union Hermes programs and Ismar-Bologna contribution 1506.

Supporting Online Material

www.sciencemag.org/cgi/content/full/312/5781/1788/DC1
Materials and Methods
SOM Text
Figs. S1 to S4
Table S1
References

3 February 2006; accepted 11 May 2006
10.1126/science.1125781

The Structure of an Infectious P22 Virion Shows the Signal for Headful DNA Packaging

Gabriel C. Lander,[1,2] Liang Tang,[1] Sherwood R. Casjens,[3] Eddie B. Gilcrease,[3] Peter Prevelige,[4] Anton Poliakov,[4] Clinton S. Potter,[2] Bridget Carragher,[2] John E. Johnson[1]*

Bacteriophages, herpesviruses, and other large double-stranded DNA (dsDNA) viruses contain molecular machines that pump DNA into preassembled procapsids, generating internal capsid pressures exceeding, by 10-fold, that of bottled champagne. A 17 angstrom resolution asymmetric reconstruction of the infectious P22 virion reveals that tightly spooled DNA about the portal dodecamer forces a conformation that is significantly different from that observed in isolated portals assembled from ectopically expressed protein. We propose that the tight dsDNA spooling activates the switch that signals the headful chromosome packing density to the particle exterior.

Since its discovery in 1952, the bacteriophage P22, which infects *Salmonella enterica*, has been an intensely studied model for virus assembly (*1*, *2*). The assembly pathway of P22, illustrating the role of the portal protein (gp1) as a conduit for DNA packaging, is shown in Fig. 1. As in many other dsDNA viruses, a sensor that detects chromosome density within the capsid independently of DNA sequence controls termination of genome packaging. Genetic studies showed that the portal plays this role, but how events occurring within the particle are detected and signaled to exterior packaging machinery remains unclear. Here we show a three-dimensional reconstruction of infectious P22 particles determined without applying icosahedral symmetry, revealing the portal switch in an activated state, presumably triggered by close contact with spooled dsDNA. Comparison of this structure with the previously determined free portal

structure indicates a large-scale reorganization of the portal, which can explain the signal transduction pathway from inside to outside of the particle.

The validation of the asymmetric reconstruction depends on previous studies in which several components of the P22 virion machinery were isolated and their structures determined by x-ray crystallography or cryo–electron microscopy (cryo-EM). The crystal structure of the gp9 tail spike (an endorhamnosidase that binds to and cuts the O-antigen polysaccharide receptor on the bacteria) was solved as two separate fragments, the virion-binding domain (residues 1 to 124) at 2.3 Å resolution and the receptor-binding domain (residues 109 to 666) at 1.6 Å (*3*, *4*). Cryo-EM was used to determine the structure of the entire tail machine structure (gp1, 4, 9, 10, and 26), isolated from virions, at 25 Å (*5*). P22 coat protein shell structures before and after expansion were determined at subnanometer resolution by cryo-EM and icosahedral averaging (*6*). Such averaging ignores the fact that one pentameric vertex is occupied by the portal ring in the procapsid and the whole tail machine in the virion. At this resolution some secondary structural elements of the coat protein subunit and conformational changes undergone during capsid expansion were observed, but icosahedral averaging eliminates the density for any non-icosahedral structural features. Cryo-EM reconstructions of bacteriophages T7 (*7*, *8*), T4 (*9*), and ϕ29 (*10*–*12*) have been determined without icosahedral averaging (asymmetric reconstructions) and supplied qualitative insight into the organization of these capsids; however, these lower-resolution reconstructions did not reveal details of the packaging machinery. Recently the structure of phage epsilon 15 was determined as an asymmetric reconstruction (*13*), with packaged DNA and details of the portal visible as well. However, crystal structures are not available for any of the viral components, nor is there any genetic or biochemical information about the function or location of gene products.

The asymmetric reconstruction of the P22 virion electron density exhibited the expected $T = 7l$ coat protein lattice (a left-handed lattice containing seven subunits in an icosahedral asymetric unit) observed in the icosahedrally averaged reconstruction, with a hexameric tail assembly replacing one pentamer vertex (Fig. 2). The color-coded location of the P22 gene products in the particle is shown in Fig. 3A. The portal can be readily identified within the interior of the capsid by its 12-fold symmetry (Fig. 3, B and C). The overall organization of the viral tail machine was in excellent agreement with the earlier reconstruction of the isolated tail complex (*5*). Furthermore, the virion density of the individual tail spike gp9 trimers envelopes the x-ray model (*3*) of the receptor-binding portion of gp9 with exceptional accuracy (Fig. 4A). Attachment of gp9 to the tail-machine tube occurs in two places on each tail-spike trimer, which suggests that it interacts with both gp4 and gp10. The close similarities of the coat protein lattice, the tail machine, and the isolated tail-spike portions of the asymmetric reconstruction of the P22 virion to independently determined substructures indicate that the reconstruction strategy accurately reproduces the native structure of the virion [see supporting online material (SOM)].

All tailed phages have a symmetry mismatch between the tail machine's 12-fold symmetric portal and a 5-fold axis of the coat protein shell (Fig. 4B). Such a mismatch has been postulated to facilitate rotational movements during the packaging of DNA (*14*–*16*). Although this reconstruction neither proves nor disproves the possibility of portal rotation upon DNA packaging, the precision of the tail machine density in the reconstruction requires that it must always be aligned in a particular spatial orientation with respect to the pentavalent coat lattice opening. Thus, the portal in the infectious particle must always occupy one of five equivalent registers within the capsid opening.

Ectopically expressed gp1 assembles into ringlike structures in vitro (*5*). The plasmid expressed protein used for crystallography (102 amino acids were removed from its C terminus to increase its solubility in vitro) was analyzed by cryo-EM, and two populations of rings were identified, ~80% with 11-fold symmetry and 20% with 12-fold symmetry. These populations could be computationally segregated, and the highest-resolution reconstruction was obtained of the 11-fold portal structure. Comparison of this

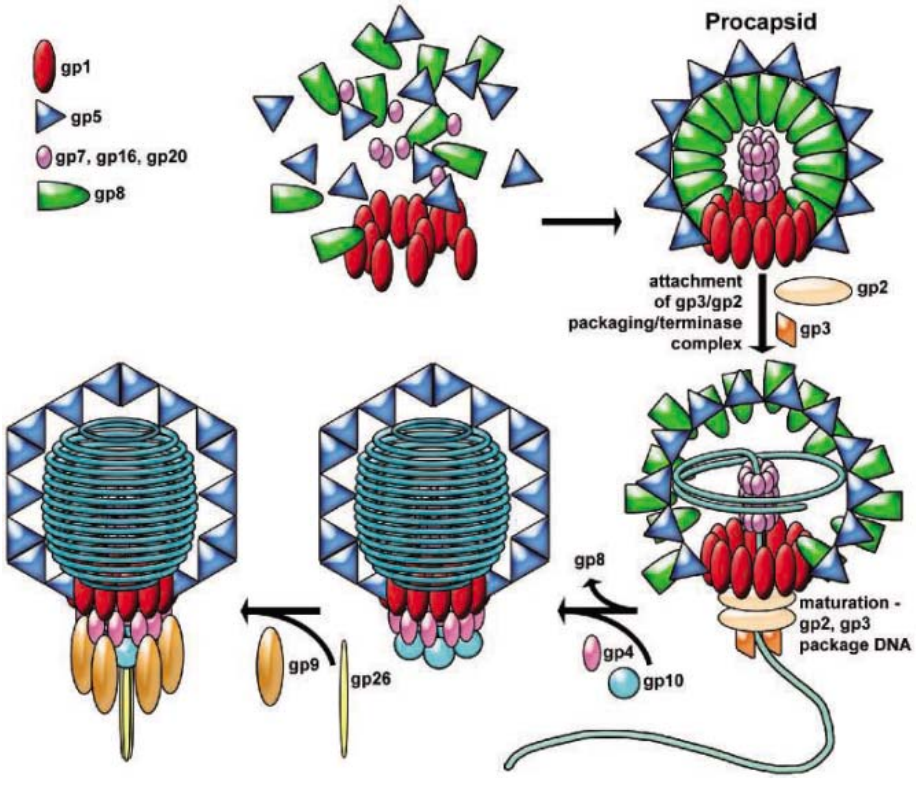

Fig. 1. The bacteriophage P22 assembly pathway. P22 assembles a protein precursor particle called a procapsid, which is the receptacle into which its 43.5 thousand base pairs (kbp) DNA chromosome is packaged. P22 procapsid shells are built from two major components, 415 molecules of coat protein (gp5, the product of gene *5*) arranged in a $T = 7l$ icosahedral shell and roughly 250 molecules of scaffolding protein (gp8) within the coat protein shell. In addition, smaller numbers of four other proteins are present in the procapsid. A dodecamer of 84-kD proteins (gp1) is present at a single unique icosahedral vertex. Six to 20 intravirion molecules of the products of genes *7*, *16*, and *20* are required for successful DNA injection into susceptible cells and are released from the virion during the injection process. As DNA is packaged, the thick procapsid shell expands from a radius of about 55 nm to a thinner, more angular shell 65 nm in diameter. Despite having a genome 41.7 kbp in length, P22 packages DNA until the capacity of the capsid is reached, ~43.5 kbp, a strategy referred to as "headful" DNA packaging. Termination of packaging by cleavage of the concatemeric DNA is initiated not by sequence, but when the chromosome is at a defined packing density that is sensed by portal protein. After DNA is packaged, the tail assembly is constructed by the sequential addition of multiple copies of four gene products (gp4, gp10, gp26, and gp9) to the vertex occupied by the portal ring [for further details see references (*1*, *2*, *5*) and references therein].

[1]Department of Molecular Biology, The Scripps Research Institute, 10550 North Torrey Pines Road, La Jolla, CA 92037, USA. [2]National Resource for Automated Molecular Microscopy, Department of Cell Biology, The Scripps Research Institute, 10550 North Torrey Pines Road, La Jolla, CA 92037, USA. [3]Department of Pathology, University of Utah School of Medicine, Salt Lake City, UT 84112, USA. [4]Department of Microbiology, University of Alabama at Birmingham, Birmingham, AL 35294, USA.

*To whom correspondence should be addressed. E-mail: jackj@scripps.edu

structure of the isolated P22 portal with the portal in the virion reconstruction revealed a significant reorganization during assembly and maturation of the virion (Fig. 4C). Part of this apparent change in conformation may be due to the missing 102 amino acids at the C terminus of the isolated protein; however, the extensive differences between the two structures imply that portions of the portal adopt a different conformation in the virion than when it is isolated in solution.

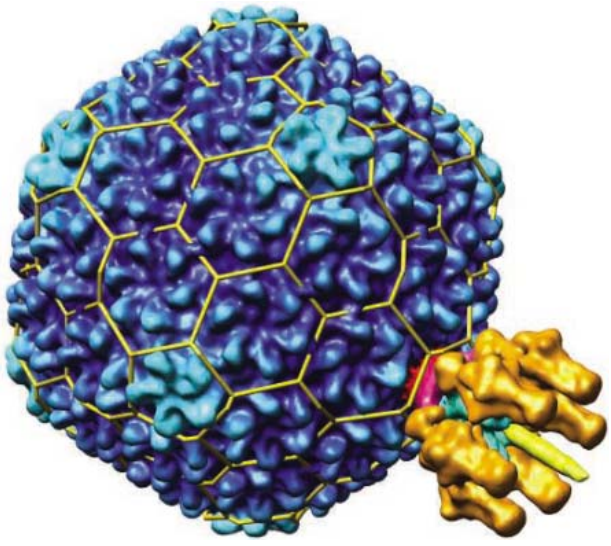

Fig. 2. Surface volume representation of the P22 bacteriophage infectious virion at 17 Å resolution. A three-dimensional reconstruction of the P22 virion resulting from the superposition of 26442 particles is shown with the same coloring scheme as in Fig. 1. The $T = 7l$ organization (indicated by the yellow lattice cage) of the coat proteins (blue) is clearly visible in the reconstruction without the imposition of icosahedral symmetry. The tail machinery, which exhibits 6- and 12-fold symmetry at different distances from the virion center, is situated at a single five-fold vertex of the capsid and replaces five coat subunits there.

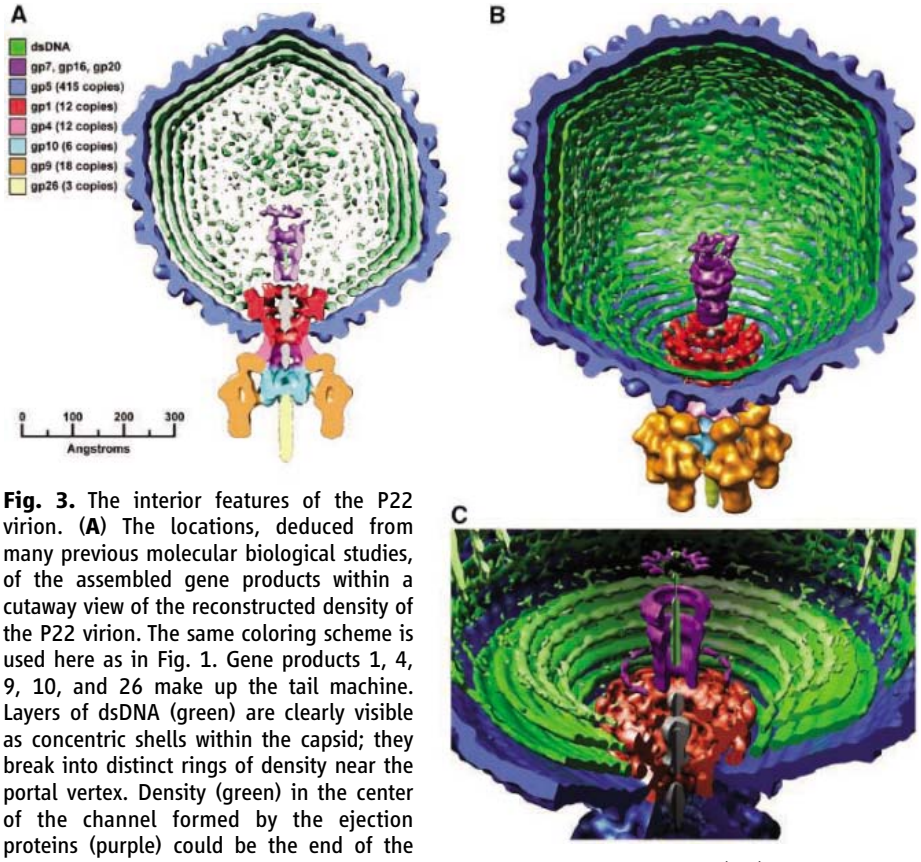

Fig. 3. The interior features of the P22 virion. (**A**) The locations, deduced from many previous molecular biological studies, of the assembled gene products within a cutaway view of the reconstructed density of the P22 virion. The same coloring scheme is used here as in Fig. 1. Gene products 1, 4, 9, 10, and 26 make up the tail machine. Layers of dsDNA (green) are clearly visible as concentric shells within the capsid; they break into distinct rings of density near the portal vertex. Density (green) in the center of the channel formed by the ejection proteins (purple) could be the end of the P22 chromosome; however, density on this axis within the portal protein ring (red) does not appear to be consistent with DNA. (**B**) A cutaway view of the internal portion of the asymmetrically reconstructed particle contoured at 3 σ, showing the 12-fold symmetry of the portal (red), the putative ejection proteins (purple), and individual strands of dsDNA (green). (**C**) Close-up view of the packaged interior upon 12-fold averaging along the tail tube axis. Although the E-proteins (purple) themselves in reality may or may not exhibit 12-fold symmetry, this view demonstrates the channel-like nature of the structure they form in the virion, as well as the dsDNA (green) that may be seated within their channel. Three concentric shells of spooled DNA are clearly visible.

Termination of DNA packaging when the P22 head is full implies a pressure sensor that conveys a signal from within the particle to the exterior, which initiates a program of cutting the DNA (by the gp2/gp3 terminase complex), release of gp2 and gp3, and attachment of the other components of the tail machine (gp4, 10, 9, and 26) to the portal (Fig. 1). The reconstruction shows that the portal ring extends from the capsid interior (where it makes direct contact with packaged DNA) to the outside (where it must make direct contact with the DNA gp2/gp3 packaging-terminase complex, during the DNA filling process). The structural change of the portal from a "low-pressure" free state to a "high-pressure" assembled state is consistent with the portal as the signal transducer of a full head of DNA. Indeed, Casjens *et al*. (*17*) proposed a role for the portal in headful sensing when they found that two different single–amino acid changes (near the N terminus and the middle of the protein) each caused 2000 extra base pairs to be encapsidated before the packaged DNA was cleaved from the remaining concatemeric DNA. Examination of the intravirion portal shows a tightly wound ring of dsDNA (resulting from averaging many particles with different start points for the duplex spiral into the next ring) surrounding a region of the portal that has undergone a conformational change (Fig. 4C) relative to the free form. We suggest, therefore, that the portal is in the isolated form within the procapsid as packaging of the DNA commences. As the DNA continues to enter and is spooled into the capsid, the resulting increase in pressure forces DNA to tighten around the portal. At a critical point in the packaging process, when the capsid has fully expanded and with the chromosome at the headful density, the surrounding ring of DNA exerts such a force on the portal that it changes conformation, signaling the packaging motor to cease and the packaging-terminase complex to cut the packaged chromosome from the remaining concatemeric DNA. The new portal conformation can bind the remaining gene products that form the tail machinery required for infection. Although it was not discussed in detail, a similar ring of apparent DNA density was seen in the asymmetric reconstructions of T7 and epsilon 15 virions (*7*, *13*), suggesting that such a portal-DNA interaction may be a general feature of the tailed-phage virions.

Further support for this hypothesis is evidenced by a comparison of the P22 portal to the crystal structure of the phage ϕ29 portal. Although it does not use the headful packaging mechanism, ϕ29 uses a DNA translocase that is similar to other tailed phages (*18*). Docking of the ϕ29 portal crystal structure (*15*) into the P22 portal density reveals an exceptionally good fit to the lower stalk region that extends outside of the particle and to the lower portion of the wing region that makes contact with the capsid protein. However,

the model of P22 does not extend to the density that is in the upper part of the wing and above the wing in the high-pressure form (fig. S4). This comparison suggests that the additional 416 residues per subunit in the P22 portal are required for pressure sensing, while a structural core of similar size to the ϕ29 portal (307 residues) participates in DNA packaging.

In addition to the tail machine and packaging proteins discussed above, multiple molecules of the products of genes *7*, *16*, and *20* are also present in the infectious virion (*19*). They are not essential for assembly of virion-like particles that contain DNA (*19*–*21*), but are ejected from the virion during DNA injection (*22*) and are required for successful DNA injection into the host cell (*20*, *23*). One or more of these ejection proteins are likely to form the tubular set of electron densities above the portal and around the central axis of the tail machine. This density is not dsDNA (Fig. 3B), because of its size and morphology, as well as the fact that the inner channel is occupied with density that is probably dsDNA aligned with the tail-machine tube. Another candidate for an ejection protein is density within the portal and tail machine that is clearly not dsDNA, but rather a plug-like density (colored gray in Fig. 3C) that probably aids in maintaining the highly pressurized DNA within the capsid.

The virion structure reported here is valuable for understanding the P22 assembly program as well as the mechanism of injection of DNA into susceptible cells. All of the major components of P22 were recognized in the reconstruction (Fig. 3A), and candidates for minor components were identified, and DNA is clearly recognizable in the particle's interior. There are no proteins in tailed-phage virions that hold the DNA in place (*14*), so the internal rings of density must be the packaged DNA. The observed dsDNA density is consistent with DNA spooling about the central axis of the particle (defined by extending the 12-fold axis of the portal to the coat pentamer on the opposite side of the particle), initially laying down a layer of coaxial rings adjacent to the protein capsid. This spool orientation is similar to that seen in T7 and epsilon 15 and so may be general, at least among the *Podoviridae* (*7*, *13*). It is impossible to discern from the structure, however, whether the first DNA rings deposited during packaging are adjacent to the portal or at the vertex opposite the portal. The structure is clearly a coaxial spool of DNA in contrast to concentric spool, "ball of twine" or folded DNA models. The icosahedrally averaged structure of P22 could not distinguish among these models, but the asymmetric reconstruction does.

Layers closest to the portal display the highest degree of order with individual rings of dsDNA clearly defined in the first and second layers when contoured at 2.5 times the standard deviation of the density (Fig. 3, B and C). At lower contour levels, five coaxial layers of DNA can be seen; the innermost is marginally discernible as a layer. Internal to this layer, the persistence length of the DNA cannot be accommodated in smooth rings, and more chaotic packing results. The DNA that occupies the central tube above the portal is most likely the last to enter during packaging, so that the vectorial injection of the DNA can proceed with the proper orientation (last base pairs in are the first base pairs out). No matter whether it is laid down first or last, the increasing disorder with distance from the portal suggests that it is the interaction with the portal that determines the overall orientation of the spool and arrangement of DNA within the virion. The exceptional order of the ring of DNA closest to the portal indicates that it is squeezed tightly against the portal in the infectious particle so that the portal pressure sensor is in the "on" position.

Our understanding of the P22 assembly pathway and the availability of a rich variety of mutant P22 particles, including those that lack ejection proteins or DNA, will allow further understanding of the structure described and definitive assignment of density to those gene products that are speculative at this time.

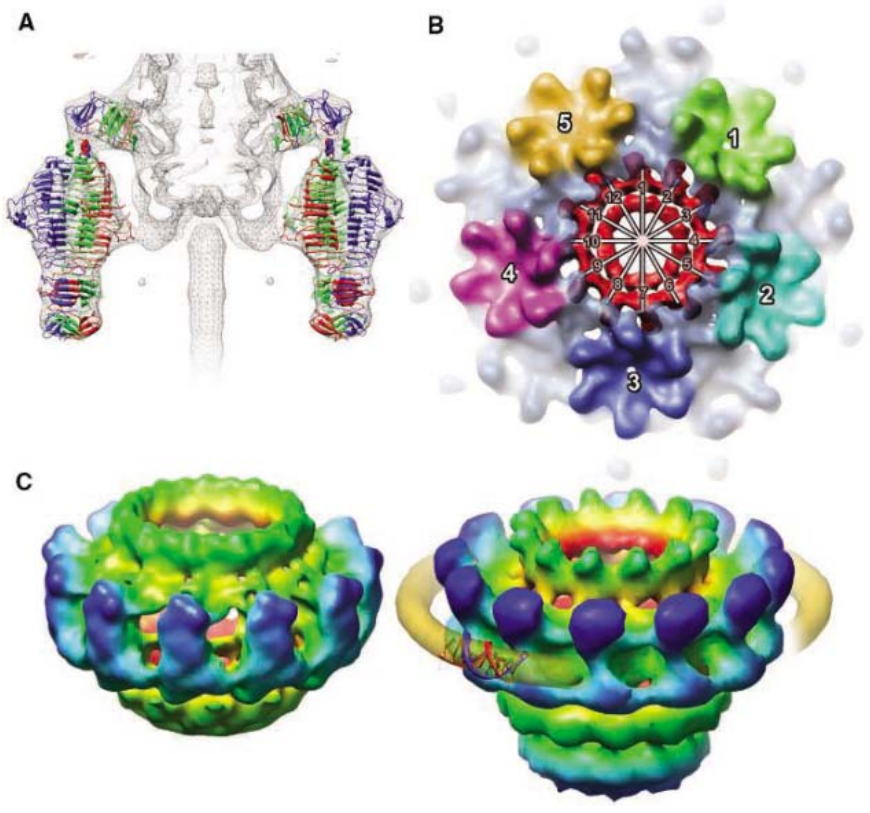

Fig. 4. P22 virion substructures. (**A**) Docking of tail-spike crystal structures. The crystal structure of the tail spike was solved as two separate parts, the virion-binding domain and the receptor-binding domain (*3*, *4*), and they fit into the six-fold averaged reconstruction density with exceptional accuracy. The reconstruction depicts the head-binding domain of the tail spike at an angle of 20° relative to the receptor-binding domain, indicating that there is a hinge between the two domains. This fitting also shows that the spike is in contact with gp4 and gp10 proteins in the tail tube at two distinct locations, one with the head-binding domain and a smaller one with the receptor-binding domain. (**B**) The coat-portal symmetry mismatch. The symmetry mismatch between the 12-fold portal (red) and the 5-fold opening in the $T = 7l$ coat protein surface lattice is shown with each hexamer of the capsid colored uniquely to emphasize the different units that form the 5-fold symmetric vertex. (**C**) Two P22 portal protein states. On the left is the 20 Å reconstruction of the free portal ring in solution (built from assembly of naïve gp1 subunits in vitro), and on the right is the portal ring that was virtually extracted from the asymmetric reconstruction of the P22 virion. The portal rings are colored radially such that density closest to the central axis is red, intermediate distance density is green, and the density farthest away is blue. Surrounding the intravirion portal is the first ring of dsDNA seen in the reconstruction (yellow) with a short segment of B-form dsDNA (PDB ID:1bna) arbitrarily docked into the density.

References and Notes

1. S. Casjens, P. Weigele, in *Viral Genome Packaging*, C. Catalano, Ed. (Landes Publishing, 2005), pp. 80–88.
2. P. E. Prevelige Jr., in *The Bacteriophages*, R. Calendar, Ed. (Oxford Univ. Press, New York, ed. 2, 2005), pp. 457–468.
3. S. Steinbacher *et al.*, *Proc. Natl. Acad. Sci. U.S.A.* **93**, 10584 (1996).
4. S. Steinbacher *et al.*, *J. Mol. Biol.* **267**, 865 (1997).
5. L. Tang, W. R. Marion, G. Cingolani, P. E. Prevelige, J. E. Johnson, *EMBO J.* **24**, 2087 (2005).
6. W. Jiang *et al.*, *Nat. Struct. Biol.* **10**, 131 (2003).
7. X. Agirrezabala *et al.*, *EMBO J.* **24**, 3820 (2005).
8. X. Agirrezabala *et al.*, *J. Mol. Biol.* **347**, 895 (2005).
9. A. Fokine *et al.*, *Proc. Natl. Acad. Sci. U.S.A.* **101**, 6003 (2004).
10. M. C. Morais *et al.*, *J. Struct. Biol.* **135**, 38 (2001).
11. Y. Tao *et al.*, *Cell* **95**, 431 (1998).
12. M. C. Morais *et al.*, *Mol. Cell* **18**, 149 (2005).

13. W. Jiang *et al.*, *Nature* **439**, 612 (2006).
14. S. Casjens, R. Hendrix, in *The Bacteriophages*, R. Calendar, Ed. (Plenum Press, New York, 1988), vol. 1, pp. 15–91.
15. A. A. Simpson *et al.*, *Nature* **408**, 745 (2000).
16. R. W. Hendrix, *Proc. Natl. Acad. Sci. U.S.A.* **75**, 4779 (1978).
17. S. Casjens *et al.*, *J. Mol. Biol.* **224**, 1055 (1992).
18. D. Anderson, S. Grimes, in *Viral Genome Packaging*, C. Catalano, Ed. (Landes Publishing, 2005), pp. 102–116.
19. S. Casjens, J. King, *J. Supramol. Struct.* **2**, 202 (1974).
20. D. Botstein, C. H. Waddell, J. King, *J. Mol. Biol.* **80**, 669 (1973).
21. J. King, E. V. Lenk, D. Botstein, *J. Mol. Biol.* **80**, 697 (1973).
22. V. Israel, *J. Virol.* **23**, 91 (1977).
23. B. Hoffman, M. Levine, *J. Virol.* **16**, 1547 (1975).
24. This work was supported by grants from the NIH and the NSF. The cryo-EM was conducted at the National Resource for Automated Molecular Microscopy, which is supported by the NIH through the National Center for Research Resources' P41 program (RR17573).

Supporting Online Material
www.sciencemag.org/cgi/content/full/1127981/DC1
Material and Methods
Figs. S1 to S4
References

28 March 2006; accepted 5 May 2006
Published online 18 May 2006;
10.1126/science.1127981
Include this information when citing this paper.

Metagenomic Analysis of Coastal RNA Virus Communities

Alexander I. Culley,[1] Andrew S. Lang,[2] Curtis A. Suttle[3]*

RNA viruses infect marine organisms from bacteria to whales, but RNA virus communities in the sea remain essentially unknown. Reverse-transcribed whole-genome shotgun sequencing was used to characterize the diversity of uncultivated marine RNA virus assemblages. A diverse assemblage of RNA viruses, including a broad group of marine picorna-like viruses, and distant relatives of viruses infecting arthropods and higher plants were found. Communities were dominated by distinct genotypes with small genome sizes, and we completely assembled the genomes of several hitherto undiscovered viruses. Our results show that the oceans are a reservoir of previously unknown RNA viruses.

High mutation rates and short generation times cause RNA viruses to exist as dynamic populations of genetic variants that are capable of using multiple host species (*1*). In the oceans, the largest ecosystem on Earth, RNA viruses infect ecologically and economically important organisms at all trophic levels, including heterotrophic bacteria (*2*), fish (*3*), crustaceans (*4*), and marine mammals (*5*). Recently, a series of previously unknown RNA viruses have been characterized that infect marine phytoplankton. These include positive-sense single-stranded (ss) RNA viruses (HaRNAV and HcRNAV) that lyse the toxic-bloom formers *Heterosigma akashiwo* and *Heterocapsa circularisquama* (*6*, *7*), a positive-sense ssRNA virus (RsRNAV) that infects the diatom *Rhizosolenia setigera* (*8*), and a double-stranded (ds) RNA virus (MpRNAV) with a genome organization similar to reoviruses that infects the cosmopolitan species *Micromonas pusilla* (*9*).

Despite the apparent importance of RNA viruses to marine organisms, almost nothing is known about natural communities of RNA viruses in the sea. The most tantalizing evidence that the diversity of RNA viruses in the sea extends well beyond what has been revealed in culture comes from a study that used gene-specific primers to target a subset of picorna-like viruses (*10*). The work showed that these positive-sense ssRNA viruses are persistent, widespread, and diverse members of marine virus communities.

Cultivation-independent genomic approaches have recently been used to characterize entire microbial (*11*, *12*) and bacteriophage (*13*, *14*) assemblages from a diversity of ecosystems. This approach does not require prior assumptions of the composition of the target community and produces data that can be used to estimate community structure. For this study we used randomly reverse-transcribed whole-genome shotgun sequencing to characterize the diversity of uncultivated marine RNA virus assemblages.

Natural virus communities were concentrated from English Bay at Jericho Pier (JP) and the Strait of Georgia (SOG), British Columbia, Canada (table S1). RNA was extracted from the purified virus fraction, reverse-transcribed into cDNA, and used to construct libraries representative of the natural RNA virus communities (*15*). Few sequence fragments [37 and 19% for JP and SOG, respectively (Fig. 1)] showed significant similarity [tBLASTx (*16*) expect value (E) < 0.001] to sequences in the National Center for Biotechnology Information (NCBI) database and no similarity to sequences from the Sargasso Sea microbial metagenome (*17*). In contrast, ~90% of Sargasso Sea microbial sequence fragments are notably similar to sequences in the NCBI database (*18*). These results imply that most RNA viruses in the sea are distantly related to known viruses and that their genetic diversity is much less explored relative to that of the prokaryotic community.

Sequence similarity (tBLASTx E < 0.001) in our samples revealed 98% of sequences belonged to positive-sense ssRNA viruses. The one exception was a sequence with similarity to a dsRNA virus. No RNA phage were detected, supporting arguments that most marine phages have DNA genomes (*19*) and that the predominate hosts of marine RNA viruses are eukaryotes. In addition, no sequences were similar to retroviral or negative-sense ssRNA viruses. Our results are minimum estimates of the richness of marine viral communities, because some viruses may have been excluded by our sam-

Table 1. Classification of significant tBLASTx matches (E value < 0.001, n = 92) to viral sequences into protein categories.

Protein classification	% of total viral hits
RNA-dependent RNA polymerase	39
Capsid	33
Unidentified structural	16
Unidentified nonstructural	7
Helicase	3
RNA binding protein	1
Replication initiator protein	1

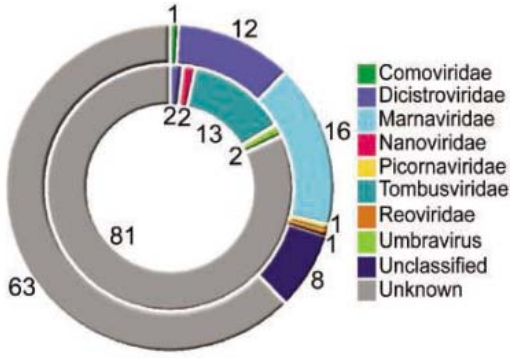

Fig. 1. Composition of the JP (outer circle, n = 216) and the SOG (inner circle, n = 61) libraries. The top tBLASTx matches of sequences from JP and SOG with the GenBank nonredundant database (E value < 0.001) are categorized by taxonomic group. Virus families or genera are color coded. The *Comoviridae*, *Dicistroviridae*, *Marnaviridae*, and *Picornaviridae* are families in the proposed order *Picornavirales* (*25*). The percent values for each virus group in each library are shown. The identification of the individual viruses from each taxonomic group can be found in table S1.

[1]Department of Botany, University of British Columbia, 3529-6270 University Boulevard, Vancouver, BC V6T 1Z4, Canada. [2]Institute of Marine Science, University of Alaska Fairbanks, 905 North Koyukuk Drive, Fairbanks, AK 99775, USA. [3]Department of Earth and Ocean Sciences, Department of Microbiology and Immunology, Department of Botany, University of British Columbia, 1461-6270 University Boulevard, Vancouver, BC V6T 1Z4, Canada.

*To whom correspondence should be addressed. E-mail: csuttle@eos.ubc.ca

pling methods. Nonetheless, we observed sequences resembling those of tombusviruses (*20*), umbraviruses (*21*), and nanoviruses (*22*), all of which are RNA viruses that have not previously been reported from aquatic environments (Fig. 1 and table S2). Most sequences with significant matches to known sequences (77%) were similar to viral genes with known functions, which is not surprising given the limited number of genes encoded by RNA viruses and their relatively small average genome size (Table 1).

The sequence fragments from the two aquatic viral communities were assembled by using a minimal mismatch percentage of 98% and an overlap of 20 base pairs (bp), the most stringent settings given the total introduced error of the RNA virus shotgun library construction method (*15*). Simulations demonstrated that these parameters correctly reassembled the genomes of different strains of the same species of RNA viruses from a random assortment of sequence fragments. After assembly, 50% of JP and 36% of SOG sequence fragments overlapped with other sequence fragments and formed contiguous segments (contigs) of overlapping sequence fragments. In the JP library, 66% of the overlapping sequence fell within four large contigs, which were subsequently assembled into two complete viral genomes that are similar in structure to each other but that differ from most other known picorna-like viruses (Fig. 2A). In contrast, over 90% of the remaining 14 contigs were formed from three sequence fragments or fewer, indicating that the JP RNA virioplankton is composed of two very abundant genotypes and others that were relatively rare. Similarly, the genotypic composition of the SOG library was also uneven, with 59% of the sequence fragments forming a single contig that contained most of a novel viral genome, including the 3′ untranslated region (UTR), the structural proteins, and all eight conserved regions of the replicase (*23*) (Fig. 2B). All the remaining sequences fell into contigs composed of two or fewer fragments. Attempts to quantify the structure and diversity of the two RNA virus communities with Phage Communities from Contig Spectrum (PHACCS) (*24*), an online tool designed to estimate the diversity of phage communities on the basis of the frequency of overlapping sequence fragments from whole-genome shotgun libraries, failed primarily owing to the disproportionate contribution of sequence fragments from a small number of dominant genotypes to the total number of contigs in both RNA virus libraries. Nevertheless, marine RNA virus communities appear to be dominated by even fewer genotypes than the dsDNA phage communities, which are also quite uneven (*14*).

The complete genomes assembled from the JP and SOG genomic libraries do not fall within any of the established families of RNA viruses. The JP genomes appear to be dicistronic single molecules of positive-sense ssRNA about 9 kb in size (Fig. 2A). The JP genomes have characteristics similar to viruses in the proposed order *Picornavirales* (*25*), including synteny of putative nonstructural genes, a polyadenylate [poly(A)] tail, a similar G + C content, and core regions of sequence similarity. However, phylogenetic analysis based on aligned RNA-dependent RNA polymerase (RdRp) amino acid sequences placed the JP genomes definitively outside the family *Dicistroviridae* (Fig. 3A), the only dicistronic family of viruses in the proposed order *Picornavirales*. Instead, the sequences fell within a well-supported clade that included HaRNAV, RsRNAV, and SssRNAV, suggesting that they share a common ancestry with viruses that infect marine protists (Fig. 3A). Phylogenies based on alignments of RdRp sequences from RNA viruses were congruent with established family assignments (*10*, *23*) and hence provided a means of classifying unknown RNA virus sequences from the environment. Like the JP genomes, the SOG genome appears to be from a positive-sense ssRNA virus. BLASTp searches and phylogenetic analyses (Fig. 3B), as well as genomic features such as a putative polymerase domain interrupted by an in-frame termination codon and the absence of obvious helicase motifs (Fig.2B) (*20*), indicated similarity to viruses in the family *Tombusviridae* and the unassigned *Umbravirus* genus, which infect flowering plants. However, unlike these viruses, the SOG genome had no detectable movement protein (on the basis of sequence similarity) and is therefore unlikely to be from a virus that infects a terrestrial plant.

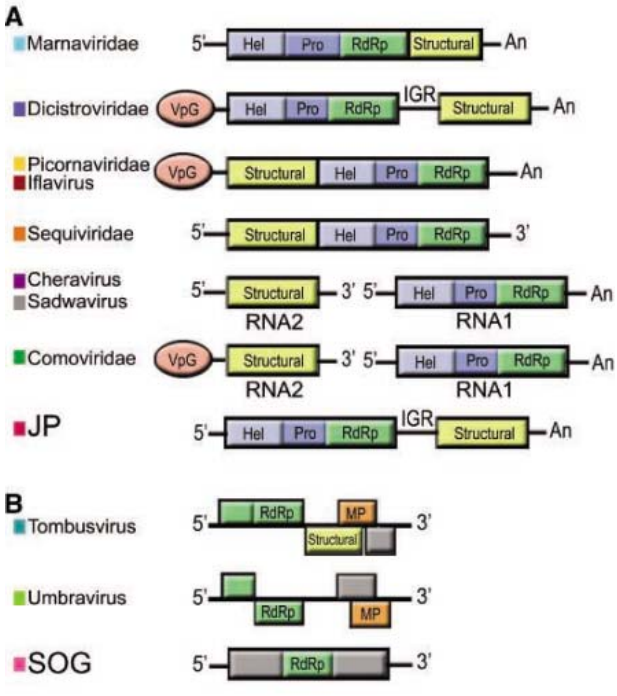

Fig. 2. Comparison of the general genomic organization of the RNA virus genomes assembled from the JP and SOG libraries with representative viruses from the (**A**) proposed order *Picornavirales* (*25*) and the (**B**) family *Tombusviridae* and genus *Umbravirus*. Genomes are shown from 5′ to 3′, where conserved RNA virus protein domains are labeled as Hel for helicase; Pro, protease; RdRp, RNA-dependent RNA polymerase; IGR, intergenic region; MP, movement protein; and An, the presence of a poly(A) tail. The characteristic read-through stop codon of the *Tombusviridae* replicase (represented by a divided RdRp) and the −1 frame shift of the *Umbravirus* replicase (represented by a staggered RdRp) are also shown (B). Regions in gray refer to sequences that code for protein of unknown function. The colors adjacent to each virus genome correspond to the colors used in Figs. 1 and 3.

In the JP sample, 97% of the significant sequence matches were to viruses in the proposed order *Picornavirales* (*25*) (Fig. 1 and table S2). Of these, 43% were most similar to HaRNAV, which was first isolated from British Columbia waters (*26*) and which is the lone genome in the database for a picorna-like, phytoplankton-infecting RNA virus. Although the sequences were divergent from HaRNAV, the results suggest that related viruses were important members of the RNA virus community at the JP site. The second most frequent top scoring matches were to picorna-like virus RdRp sequence fragments amplified from the coastal waters of British Columbia (*10*), followed by matches to an array of *Picornavirales* sequences, including viruses infecting higher plants (apple latent spherical virus), arthropods (Taura syndrome virus), and mammals (foot-and-mouth disease virus) (table S2). Nonetheless, the sequences were notably divergent from others in the database, showing that the marine viruses were distantly related to known RNA viruses. One sequence fragment was most similar to a rotavirus sequence, indicating that dsRNA viruses were also likely present, although rare. A significant match (tBLASTx e value = 3×10^{-20}) to the RdRp of *Sclerophthora macrospora* virus A, an unclassified positive-sense ssRNA mycovirus with a unique genome organization (*27*), further illustrates the genetic novelty of marine RNA viruses.

In contrast, in the SOG sample, 73% of the significant sequence matches and the largest contig containing the highest number of sequence fragments were similar to sequences from the *Tombusviridae* (Fig. 1 and table S2). Known members of this family

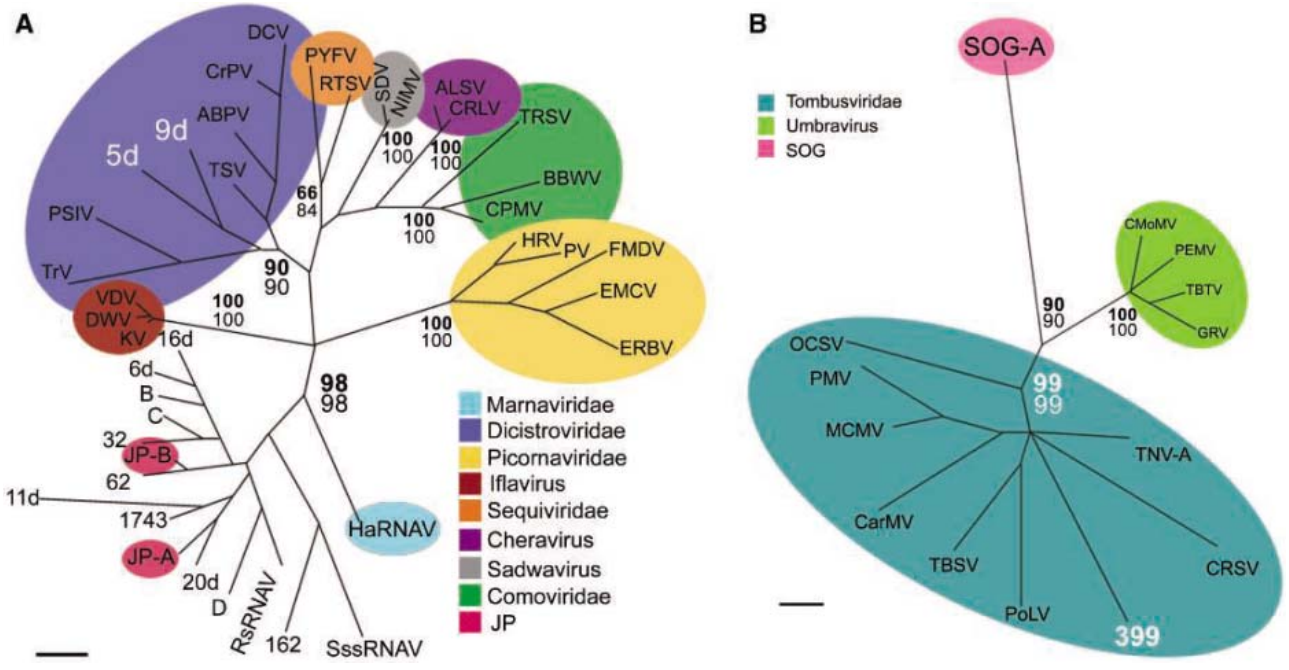

Fig. 3. Bayesian maximum likelihood trees of aligned RdRp amino acid sequences from (**A**) the JP RNA virus community and representative members of the proposed order *Picornavirales* (*25*) and from (**B**) the SOG virus library and representative viruses from the *Tombusviridae* and *Umbravirus* genus (see table S3 for complete virus names and sequence accession numbers). Bayesian clade credibility values are shown for relevant nodes in boldface followed by bootstrap values based on neighbor-joining analysis. JP-A, JP-B, and SOG-A are from the assembled environmental genomes. The Bayesian scale bar indicates a distance of 0.1. Environmental sequence numbers followed by a "d" are from excised denaturing gradient gel electrophoresis bands (*15*).

infect higher plants and have positive-sense ssRNA genomes greater than 5.5 kb in size (*20*). These data suggest that another unknown group of viruses related to the *Tombusviridae* can dominate the RNA virus community in temperate coastal waters. Also present in the community were sequences similar to viruses in the genera *Umbravirus* and *Nanovirus* (Fig. 1 and table S2).

Although the population structures of the SOG and JP assemblages were similar, there was little similarity in community composition. Picorna-like virus RdRp sequences were amplified from the JP site but not the SOG sample (*10*). tBLASTx searches among sequence fragments from both libraries resulted in 7% of SOG and 8% of JP having significant similarity (e value < 0.001) with each other. Numerous factors may have affected the composition of the JP and SOG virus communities, including salinity [12 parts per thousand (ppt) for JP versus 27 ppt for SOG], interannual variability (JP and SOG samples were collected in 2000 and 2004, respectively), and depth of sampling (JP is a surface sample whereas SOG was collected at 11 m; see table S1 for additional station characteristics). An indirectly shared characteristic between the samples was that 4% of JP and 9% of SOG sequence fragments had significant similarity to the same cripavirus (KBV), although these sequences had no demonstrable homology. Even though the JP and SOG communities were very different, they showed the same pattern of unevenness dominated by a few genotypes, consistent with the "boom or bust" oscillations (*28*) of virus-host dynamics.

Our results demonstrate that marine RNA virus communities are diverse and that their dominant members are distantly related to established groups of viruses. Both Bayesian (*29*) and neighbor-joining (*30*) phylogenetic analyses of RdRp sequences strongly supported the occurrence of a distinct clade of marine picorna-like viruses. The only known viruses in this clade are HaRNAV, RsRNAV, and SssRNAV (Fig. 3A), all of which infect marine photosynthetic protists; hence, it seems likely that the environmental sequences were also from viruses that infect phytoplankton. Moreover, the large differences between the communities show that the RNA virus populations can differ greatly between two locations (i.e., they are not the same everywhere).

The congruence between RdRp sequences and the established taxonomy of picorna-like viruses (Fig. 3A) suggests that the environmental RdRp sequences likely originate from 10 previously unknown genera of positive-sense ssRNA viruses. A second well-supported clade included two sequences that were related to sequences from viruses in the genus *Cripavirus* (Fig. 3A), a group of viruses known only to infect arthropods. This suggests these environmental sequences may have originated from viruses that infect marine arthropods. Phylogenetic analyses of RdRp sequences from the SOG library and representative members of the family *Tombusviridae* and genus *Umbravirus* indicated that the environmental sequences did not belong within established genera (Fig. 3B) and clearly supported the existence of other marine RNA viruses that are only distantly related to extant taxa.

Our analyses suggest the existence of a diverse group of RNA viruses that includes sequences related to viruses known to infect marine protists. Compared with the intensive sequencing required to characterize marine prokaryotic communities (*17*), the relatively small genome size of RNA viruses makes the construction of whole-genome shotgun libraries a realistic approach to rapidly survey the diversity of RNA virus communities. In conjunction with the isolation and the sequencing of individual RNA viruses, genomic surveys of RNA virus assemblages is an important step toward a greater understanding of the diversity and ecological impact of these pathogens in the ocean.

References and Notes

1. J. W. Drake, J. J. Holland, *Proc. Natl. Acad. Sci. U.S.A.* **96**, 13910 (1999).
2. K. Y. Børsheim, *FEMS Microbiol. Ecol.* **102**, 141 (1993).
3. D. H. Kim *et al.*, *Virus Res.* **107**, 1 (2005).
4. J. Mari *et al.*, *J. Gen. Virol.* **83**, 915 (2002).
5. B. K. Rima *et al.*, *Virus Genes* **30**, 113 (2005).
6. A. S. Lang *et al.*, *Virology* **320**, 206 (2004).

7. K. Nagasaki *et al.*, *Appl. Environ. Microbiol.* **71**, 8888 (2005).
8. K. Nagasaki *et al.*, *Appl. Environ. Microbiol.* **70**, 704 (2004).
9. C. P. D. Brussaard *et al.*, *Virology* **319**, 280 (2004).
10. A. I. Culley *et al.*, *Nature* **424**, 1054 (2003).
11. E. F. DeLong, D. M. Karl, *Nature* **437**, 336 (2005).
12. E. F. DeLong *et al.*, *Science* **311**, 496 (2006).
13. M. Breitbart *et al.*, *Proc. Natl. Acad. Sci. U.S.A.* **99**, 14250 (2002).
14. M. Breitbart *et al.*, *Proc. R. Soc. London Ser. B* **271**, 565 (2004).
15. Materials and methods are available as supporting material on *Science* Online.
16. S. F. Altschul *et al.*, *Nucleic Acids Res.* **25**, 3389 (1997).
17. J. C. Venter *et al.*, *Science* **304**, 66 (2004); published online 4 March 2004 (10.1126/science.1093857).
18. R. A. Edwards, F. Rohwer, *Nat. Rev. Microbiol.* **3**, 504 (2005).
19. M. G. Weinbauer, *FEMS Microbiol. Rev.* **28**, 127 (2004).
20. S. A. Lommel *et al.*, in *Virus Taxonomy: Eighth Report of the International Committee on Taxonomy of Viruses*, C. M. Fauquet, Ed. (Elsevier, San Diego, 2004), pp. 907–936.
21. M. E. Taliansky *et al.*, in *Virus Taxonomy: Eighth Report of the International Committee on Taxonomy of Viruses*, C. M. Fauquet, Ed. (Elsevier, San Diego, 2004), pp. 901–906.
22. H. J. Vetten *et al.*, in *Virus Taxonomy: Eighth Report of the International Committee on Taxonomy of Viruses*, C. M. Fauquet, Ed. (Elsevier, San Diego, 2004), pp. 343–352.
23. E. V. Koonin, V. V. Dolja, *Crit. Rev. Biochem. Mol. Biol.* **28**, 375 (1993).
24. F. Angly *et al.*, *BMC Bioinformatics* **6**, 41 (2005).
25. P. Christian *et al.*, paper presented at the Microbes in a Changing World meeting of the International Union of Microbiology Societies, San Francisco, CA, 23 July 2005.
26. V. Tai *et al.*, *J. Phycol.* **39**, 343 (2003).
27. T. Yokoi *et al.*, *Virology* **311**, 394 (2003).
28. K. E. Wommack *et al.*, *Appl. Environ. Microbiol.* **65**, 241 (1999).
29. G. Altekar *et al.*, *Bioinformatics* **20**, 407 (2004).
30. D. L. Swofford, PAUP* 4.0b10 (Sinauer, Sunderland, MA, 2002).

31. We thank A. Toperoff for aid with the figures, the officers and crew of the Canadian Coast Guard Ship *Vector*, past and present members of the Suttle laboratory for assistance throughout this work, and K. Nagasaki for the RsRNAV sequence. Sequences have been deposited in GenBank with accession numbers DX420985-DX421142 and DQ439712-DQ439732. This work was supported by grants from the Natural Science and Engineering Research Council of Canada.

Supporting Online Material

www.sciencemag.org/cgi/content/full/312/5781/1795/DC1
Materials and Methods
SOM Text
Tables S1 to S3
References

14 March 2006; accepted 19 May 2006
10.1126/science.1127404

A Topoisomerase IIβ–Mediated dsDNA Break Required for Regulated Transcription

Bong-Gun Ju,[1] Victoria V. Lunyak,[2] Valentina Perissi,[1] Ivan Garcia-Bassets,[1] David W. Rose,[2] Christopher K. Glass,[3] Michael G. Rosenfeld[1]*

Multiple enzymatic activities are required for transcriptional initiation. The enzyme DNA topoisomerase II associates with gene promoter regions and can generate breaks in double-stranded DNA (dsDNA). Therefore, it is of interest to know whether this enzyme is critical for regulated gene activation. We report that the signal-dependent activation of gene transcription by nuclear receptors and other classes of DNA binding transcription factors, including activating protein 1, requires DNA topoisomerase IIβ-dependent, transient, site-specific dsDNA break formation. Subsequent to the break, poly(adenosine diphosphate–ribose) polymerase–1 enzymatic activity is induced, which is required for a nucleosome-specific histone H1–high-mobility group B exchange event and for local changes of chromatin architecture. Our data mechanistically link DNA topoisomerase IIβ–dependent dsDNA breaks and the components of the DNA damage and repair machinery in regulated gene transcription.

Regulated activation of gene transcription requires a network of sequentially exchanged cofactor complexes (*1*–*3*). Recently, a signal-inducible exchange of coregulator complex and poly[adenosine diphosphate (ADP)–ribose] polymerase–1 (PARP-1), a nicotinamide adenine dinucleotide (NAD^+)–dependent enzyme that detects and repairs damage to DNA, has been linked to these multistep events for regulated activation of gene transcription (*4*–*7*). Therefore, we explored whether the components of the DNA damage and repair apparatus and the enzymatic activity of DNA topoisomerase IIβ (TopoIIβ) might be critical to the multistep events required for regulated gene expression, in response to ligand- or signal-dependent stimuli.

Using chromatin immunoprecipitation (ChIP) analysis, we examined the time course of cofactor exchange on the *pS2* promoter in 17β-estradiol (E_2)–treated Michigan Cancer Foundation (MCF)–7 cells. We observed basal levels of PARP-1 and TopoIIβ along with nuclear receptor corepressor (N-CoR) and histone deacetylase 3 (HDAC3) components of the corepressor complex but no detectable changes in that of the adenosine 3′,5′-monophosphate response element–binding protein (CBP) coactivator and RNA polymerase II (Pol II) in the absence of the ligand (Fig. 1A and fig. S1A). Previously identified components of the PARP-1 corepressor complex, including nucleolin, nucleophosmin, and human heat shock protein 70 (HSP70) (*7*), were present on the *pS2* promoter in unstimulated cells but were rapidly depleted in E_2-treated cells (Fig. 1A). There was a rapid increase of TopoIIβ and PARP-1 recruitment together with the CBP coactivator and subsequent recruitment of Pol II and the elimination of N-CoR and HDAC3 corepressors in response to E_2 (Fig. 1A and fig. S1A). PARP-1 was detected with the components of DNA damage and repair machinery (*8*, *9*), and Western blot analyses revealed that TopoIIβ, DNA-dependent protein kinase (DNA-PK), and Ku86 and Ku70 were copurified with PARP-1 (fig. S1B). DNA-PK is a nuclear serine-threonine protein kinase that forms a complex with the regulatory DNA binding subunits Ku86 and Ku70 in DNA damage and repair (*9*). After E_2 treatment, all components of the TopoIIβ/DNA-PK/Ku86/Ku70 complex were stably recruited to the *pS2* promoter but not to the coding region of the *pS2* gene (*10*) (Fig. 1B and fig. S1C). No increased recruitment of TopoIIα was detected on promoter region (Fig. 1B). After an initial ChIP with an antibody to TopoIIβ, we performed a second step of ChIP analysis to confirm the mutual presence of all of the components of this TopoIIβ/PARP-1 complex on the *pS2* promoter in E_2-treated MCF-7 cells (Fig. 1C).

We next tested the hypothesis that the enzymatic activity of TopoIIβ that alters the topology of the DNA (*11*) might be a required component for signal-dependent activation of gene transcription. We developed a protocol that detects DNA break formation in the promoter region using a combination of biotin-11–deoxyuridine triphosphate (dUTP) labeling by terminal deoxynucleotide transferase (TdT) and subsequent ChIP analysis. In MCF-7 cells stimulated with E_2 for 10 min, we detected putative DNA breaks in the *pS2* promoter but no signal in the coding region of the *pS2* gene (Fig. 1D). In contrast to the strong signal in the *pS2* promoter, no increased enrichment of biotin incorporation was observed either at the promoter region of a gene encoding the ribosomal protein L13a, which is expressed in MCF-7 cells in an E_2-independent fashion, or at the promoter of the neuronal-specific sodium

[1]Howard Hughes Medical Institute, Department of Medicine, [2]Department of Medicine, Division of Endocrinology, [3]Department of Cellular and Molecular Medicine, School of Medicine, 9500 Gilman Drive, University of California, San Diego, La Jolla, CA 92093–0648, USA.

*To whom correspondence should be addressed. E-mail: mrosenfeld@ucsd.edu

channel II (*NaChII*), which is not transcribed in MCF-7 cells (fig. S1D). We did not detect breaks in the DNA on the *pS2* promoter in the E_2 antagonist, 4-hydroxytamoxifen (4-OHT)–treated MCF-7 cells (fig. S1E).

Evidence that the regulated DNA breaks occur only in a transient fashion in the *pS2* promoter region was obtained by performing a time course of DNA break–labeling ChIP assay in E_2-stimulated MCF-7 cells, after the release from α-amanitin treatment to achieve transcriptional synchronization of cells (Fig. 1E). These results suggest that transcriptional activation can be triggered, at least in part, by the same molecular machinery responsible for the relief of torsional tension on the DNA by creating transient double-stranded breaks in response to signals for transcriptional gene activation.

Conversely, a two-step ChIP assay using an antibody against biotin as a mark of DNA breaks revealed the presence of the TopoIIβ/PARP-1 complex in the vicinity of the DNA break formation within the *pS2* promoter region (Fig. 2A). These data suggest that specific components of the DNA repair machinery may also participate in nuclear receptor–dependent transcriptional activation in the vicinity of DNA break sites upon ligand treatment. This finding is consistent with several reports of the presence of Ku86 and Ku70 subunits and DNA-PK on the Pol II transcription units (*12*–*15*).

To test whether TopoII is mediating the formation of DNA breaks in the *pS2* promoter region, we treated cells with the TopoII inhibitor merbarone (Mer) (5-*N*-phenylcarboxamido-2-thiobarbituric acid), which inhibits the cleavage activity of TopoII without damaging the DNA or the stabilizing DNA-TopoII cleavable complexes. Treatment with Mer prevented the DNA breaks on the stimulated *pS2* promoter and blocked *pS2* transcriptional activation (Fig. 2B). These results are consistent with the observation that the inhibitor of TopoII ultimately blocked recruitment of coactivators such as CBP and Pol II in E_2-treated MCF-7 cells (Fig. 2C). To further clarify the requirement of enzyme activity of TopoIIβ, we performed transient transfection assays using enzymatically inactive mutant mouse TopoIIβ ($Pro^{723} \rightarrow Leu^{723}$) (*16*) with human-specific TopoIIβ small interfering RNA (siRNA) (Fig. 2D and fig. S2A). Consistent with the results of the specific inhibitor, enzymatic activity of TopoIIβ

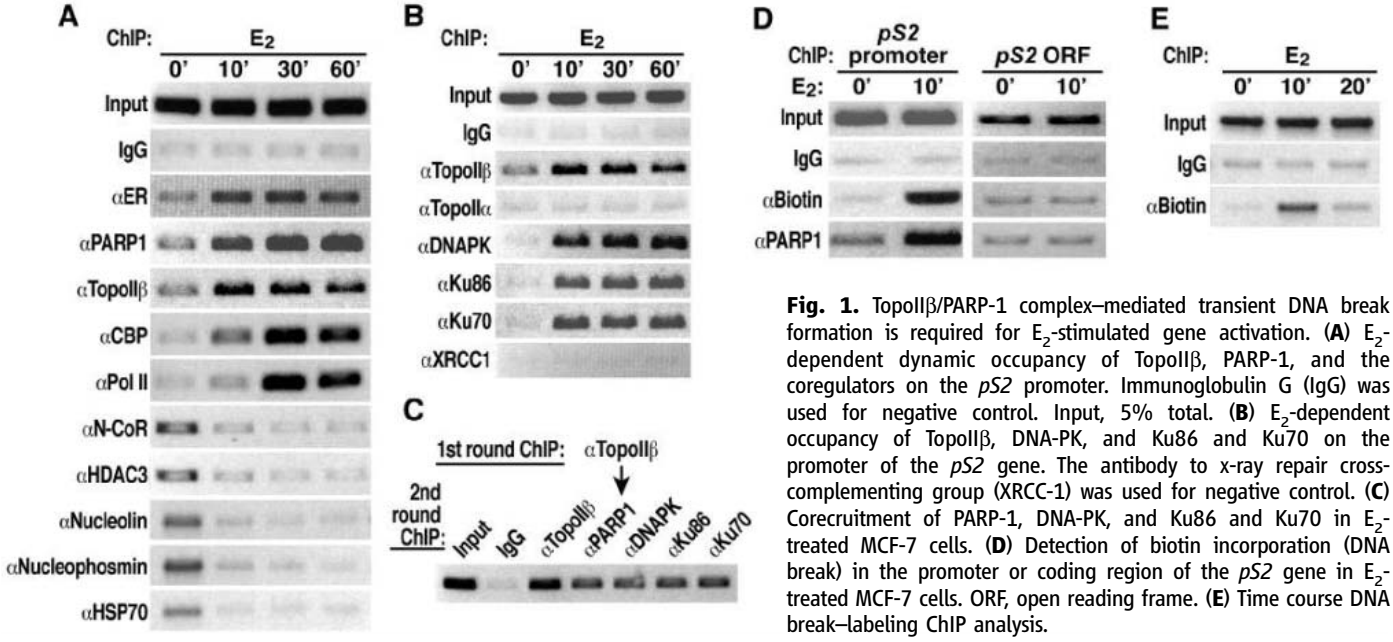

Fig. 1. TopoIIβ/PARP-1 complex–mediated transient DNA break formation is required for E_2-stimulated gene activation. (**A**) E_2-dependent dynamic occupancy of TopoIIβ, PARP-1, and the coregulators on the *pS2* promoter. Immunoglobulin G (IgG) was used for negative control. Input, 5% total. (**B**) E_2-dependent occupancy of TopoIIβ, DNA-PK, and Ku86 and Ku70 on the promoter of the *pS2* gene. The antibody to x-ray repair cross-complementing group (XRCC-1) was used for negative control. (**C**) Corecruitment of PARP-1, DNA-PK, and Ku86 and Ku70 in E_2-treated MCF-7 cells. (**D**) Detection of biotin incorporation (DNA break) in the promoter or coding region of the *pS2* gene in E_2-treated MCF-7 cells. ORF, open reading frame. (**E**) Time course DNA break–labeling ChIP analysis.

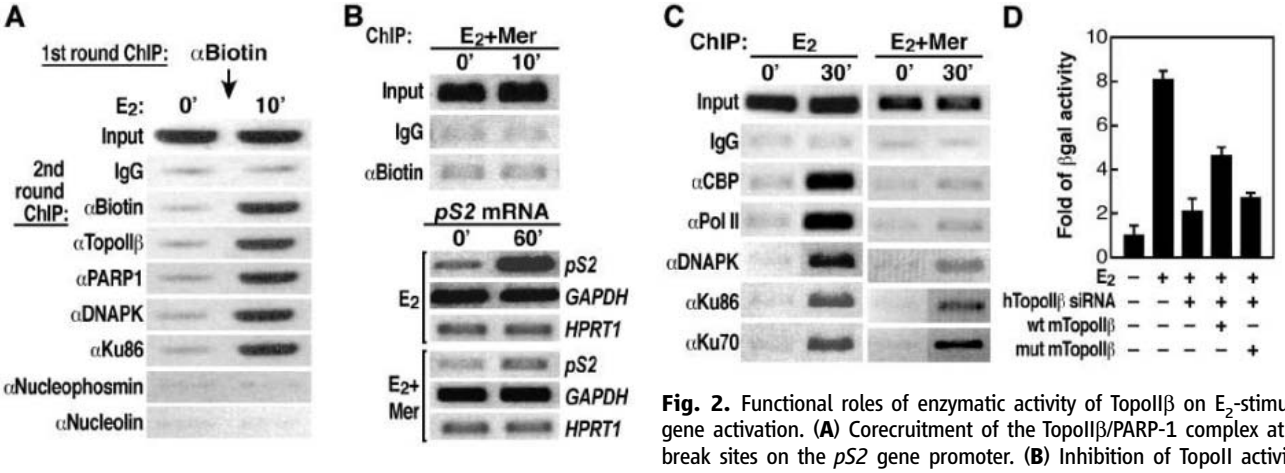

Fig. 2. Functional roles of enzymatic activity of TopoIIβ on E_2-stimulated gene activation. (**A**) Corecruitment of the TopoIIβ/PARP-1 complex at DNA break sites on the *pS2* gene promoter. (**B**) Inhibition of TopoII activity by 100 μM Mer blocked DNA break formation (top section) and blocked E_2-stimulated *pS2* transcription (bottom section). GAPDH, glyceraldehyde-3-phosphate dehydrogenase; HPRT1, hypoxanthine-guanine phosphoribosyltransferase 1. (**C**) Mer inhibits E_2-dependent recruitments of CBP coactivator and Pol II on the *pS2* gene promoter. (**D**) Requirement of enzymatic activity of TopoIIβ for ERα reporter activation. β-Gal, β-galactosidase; wt, wild type; mut, mutant. Error bars indicate SEM.

was required for transcriptional activation in response to ligand treatment.

To further examine the mechanisms of TopoIIβ/PARP-1–dependent *pS2* gene activation events, we refined our analysis to the level of single nucleosomes by examining the area of the surrounding estrogen response element (ERE) present in the *pS2* promoter. Chromatin was digested to mononucleosomes and examined by ChIP analysis (nucleosome-ChIP assay). Occupancy on individual nucleosomes was assessed by means of nucleosome-specific polymerase chain reaction (PCR) primers (*17*). After treatment with E_2, PARP-1 localized to the nucleosome containing the cognate estrogen receptor binding site (NucE) of the *pS2* promoter, whereas the adjacent nucleosomes (NucU and NucT) exhibited a decrease of PARP-1 occupancy (Fig. 3A). In contrast, TATA-binding protein (TBP) was associated with the TATA box–containing NucT (Fig. 3A). Therefore, PARP-1 binds weakly to all three nucleosomes as a corepressor complex in the unstimulated *pS2* promoter region but, after treatment with E_2, becomes localized to NucE alone. Similar results were found for TopoIIβ localization (fig. S3A).

These data suggest that recruitment of the TopoIIβ/PARP-1 complex in the NucE might reflect the actions of a specific coactivator complex recruited to the liganded receptor. Indeed, PARP-1, DNA-PK, and Ku86 and Ku70 have been noted to be able to bind to the C terminus of an Leu-X-X-Leu-Leu–containing thyroid hormone receptor-binding coactivator, alternatively referred to as protein-activating signal coregulator 2 (ASC2) (*18*). ASC2 is also capable of interacting with many liganded nuclear receptors and other classes of transcription factors (*18*, *19*). ASC2, TopoIIβ, PARP-1, DNA-PK, and Ku86 and Ku70 coimmunoprecipitate from the total extract of E_2-treated MCF-7 cells with an antibody to estrogen receptor α (ERα) (Fig. 3B). Consistent with this observation, the nucleosome-ChIP assay revealed selective recruitment of ASC2 to NucE (Fig. 3C). siRNA-mediated reduction of ASC2 abrogated the E_2-dependent activation of ERα reporter activity (fig. S3B).

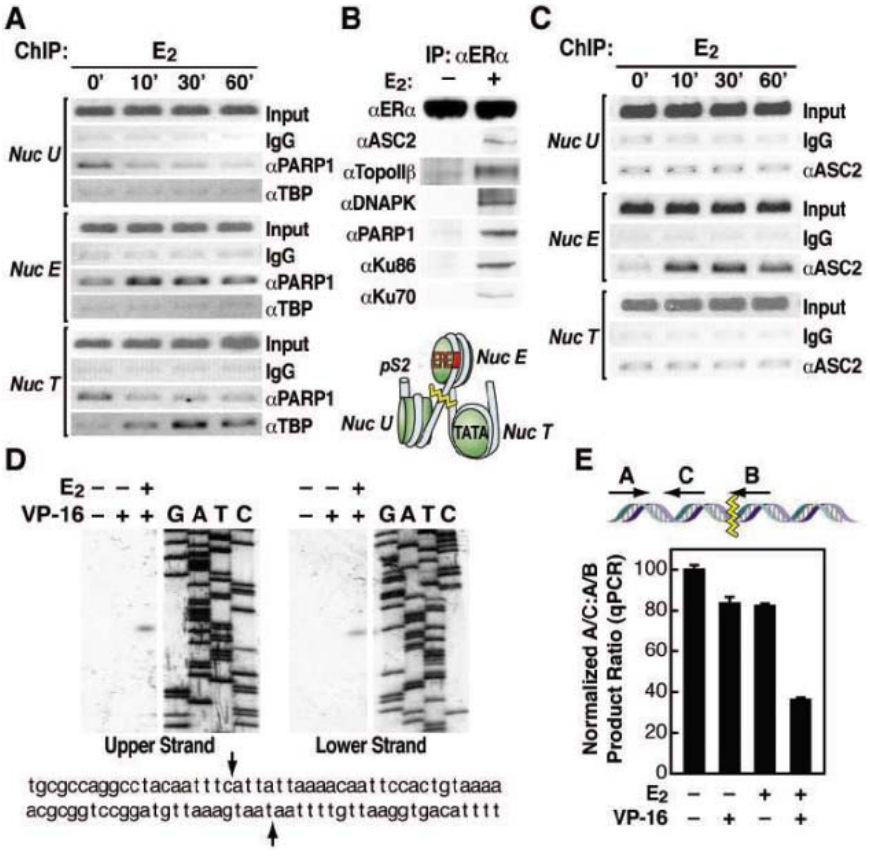

Fig. 3. Nucleosome-specific recruitment of the TopoIIβ/PARP-1 complex to the *pS2* promoter. (**A**) Decreased recruitment in PARP-1 on NucU and NucT but increased recruitment on NucE in response to E_2. (**B**) Antibody to ERα immunoprecipitated material from E_2-treated MCF-7 cells as assessed by Western blot analysis. (**C**) NucE-selective recruitment of ASC2 coactivator in E_2-treated MCF-7 cells. (**D**) Identification of TopoII-mediated DNA break site (arrows) upon E_2 stimulation in MCF-7 cells. Dideoxy-terminated sequence ladders were generated with the same primers. (**E**) Proportion of the *pS2* promoter that contains dsDNA breaks in E_2-treated MCF-7 cells. qPCR, quantitative real-time PCR. Error bars indicate SEM.

Overexpression of an activation function 2 helix-deleted ERα mutant that cannot bind Leu-X-X-Leu-Leu motif–containing coactivators (*20*) similarly blocked E_2-dependent DNA break formation of the *pS2* promoter in HeLa cells (fig. S3C). Taken together, these data indicate a nucleosome-specific recruitment of a TopoIIβ/PARP-1 complex to the *pS2* promoter by liganded ERα and its associated coactivators. In addition, we observed reduced recruitment of TopoIIβ/ASC2 in 4-OHT–treated MCF-7 cells (fig. S3D), consistent with a failure of TopoII-mediated DNA break formation in response to 4-OHT (fig. S1E).

To identify endogenous TopoII-mediated DNA cleavage sites on the *pS2* promoter region upon E_2 treatment, we stabilized the transient covalent TopoII-DNA intermediate (a cleavage complex) by using etoposide (VP-16), which is capable of blocking TopoII ligase activity, and sequenced the cleavage sites by primer extension of genomic DNA (*21*). This strategy revealed that the position of the DNA break within *pS2* promoter was centered at an adenine-thymine–rich linker region between NucU and NucE; no extension products were detected in unstimulated MCF-7 cells (Fig. 3D). These data suggest that TopoII is required for transient, site-specific dsDNA break formation during nuclear receptor-mediated transcriptional activation. To investigate the proportion of *pS2* promoters in E_2-stimulated MCF-7 cells that harbored the specific dsDNA break, we stabilized the transient covalent TopoII-DNA intermediate by using VP-16 and performed PCR using specific primer pairs around the cleavage site. The quantitative PCR data showed that >50% of the *pS2* promoters exhibited the specific dsDNA break in response to E_2 (Fig. 3E).

Despite the several lines of evidence indicating that PARP-1 may exert its function in transcriptional regulation, the molecular determinants for PARP-1 recruitment and function in the absence of genotoxic stress have remained obscure (*4*–*7*, *22*–*26*). To further define the potential molecular mechanisms by which PARP-1 may function as a coregulator for nuclear receptors, we measured the *pS2* transcript. The presence of PARP inhibitors (3-AB or PJ-34) blocked ERα-dependent gene activation (Fig. 4A and fig. S4, A and B). Single-cell microinjection of either an antibody to PARP-1 or specific *PARP-1* siRNA (fig. S2B) similarly blocked ERα-dependent reporter gene activation (fig. S4C). Inhibition of ERα-dependent gene expression by human *PARP-1* siRNA could be efficiently restored by expression of wild-type murine *PARP-1* (fig. S4D). However, a catalytic mutant ($Glu^{988} \rightarrow Ala^{988}$) of PARP-1 did not rescue the activation of ERα-dependent reporter (fig. S4D). These data confirm that

the catalytic activity of PARP-1 is required for transcriptional activation by the ER.

Because PARP-1 can use histone H1 as a substrate for poly(ADP-ribosyl)ation (*6*, *27*) and because histone H1 is widely viewed as a repressor of transcription (*28*), we investigated whether the poly(ADP-ribosyl)ation activity of PARP-1 regulates histone H1 modification in a nucleosome-specific fashion during ligand-dependent transcriptional activation. A nucleosome-ChIP analysis indicated that histone H1 dismissal may occur locally on the single nucleosome containing ERE upon E_2 treatment, whereas the two adjacent nucleosomes did not exhibit a decrease of histone H1 occupancy (Fig. 4B). In contrast to dismissal of histone H1, ChIP analysis revealed that high mobility group B 1/2 (HMGB1/2) (formerly known as HMG1/2) was recruited on the NucE after E_2 treatment, suggesting that histone H1 is replaced by HMGB1/2 upon E_2 stimulation (Fig. 4C and fig. S4E). These results suggest that the replacement of histone H1 by HMGB1/2 on the single ERE-containing nucleosome may be part of the ERα-mediated transcriptional activation of the *pS2* gene, because HMGB1/2 has been viewed as an activator (*29*), and may even stabilize the binding of ERα to cognate DNA sites (*30*, *31*). Inhibitors of either PARP-1 (3-AB) or TopoII (Mer) enzymatic activity blocked exchange of histone H1 for HMGB1/2 on NucE, which is consistent with suppression of the *pS2* gene expression (Fig. 4D and fig. S4F).

Events analogous to those observed for ERα-dependent promoters were also observed for androgen receptor (AR), retinoic acid receptor (RAR), thyroid receptor (T_3R), and activating protein 1 (AP-1)–dependent transcriptional activation, all of which recruited the TopoIIβ/PARP-1 complex that caused the DNA break–dependent activation of PARP-1 and histone H1-HMGB exchange (fig. S5). Consistent with suggestions that the TopoIIβ-dependent DNA break represented a widespread strategy for regulated gene transcription, DNA break–labeling ChIP assays in AR-, RAR-, T_3R-, and AP-1–dependent transcription events revealed increased incorporation of biotin in their promoters in response to the signal and ligand (Fig. 5A).

To address whether identical molecular events operated in response to different signaling pathways targeting the same nucleosome, we investigated the actions of AP-1, which binds to a site that is also located in NucE (*32*, *33*). In addition to E_2, AP-1 can mediate *pS2* gene activation in 12-*O*-tetradecanoylphorbol 13-acetate (TPA)–stimulated MCF-7 cells (Fig. 5B). Analogous to the effects imposed by estrogen treatment, TPA-treated MCF-7 cells also exhibited a transient DNA break in the *pS2* promoter region (Fig. 5B).

Taken together, these data suggest that the transient TopoIIβ-mediated dsDNA break formation creates the signal that, either directly or indirectly, results in the activation of a PARP-1 enzymatic function, underlying a nucleosome-specific histone H1-HMGB exchange and is likely to serve as a general mechanism for regulated initiation of gene transcription upon ligand- or signal-dependent stimulation (Fig. 5C).

The TopoIIβ-containing complex functions as an additional component of the cascade of coactivator complexes required for regulated gene transcription. Thus, a component of the genome-wide DNA-damage surveillance machinery also serves in the multistep process of regulated, gene-specific transcription, functioning to facilitate dynamic changes in chromatin organization in a localized fashion with the precision of a single nucleosome. Our data are consistent with the report that TopoII inhibitor treatment caused notable

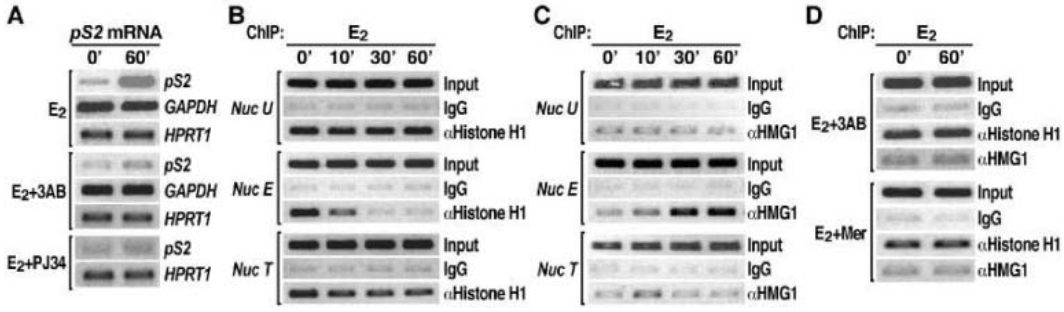

Fig. 4. TopoIIβ/PARP-1–dependent exchange of histone H1 for HMGB 1 on NucE in E_2-treated MCF-7 cells. (**A**) PARP inhibitor (3-AB or PJ-34) blocked activation of *pS2* transcription. (**B**) Loss of histone H1 in E_2-treated MCF-7 cells on NucE. (**C**) E_2-dependent recruitment of HMGB1 on NucE. (**D**) Inhibition of E_2-dependent exchange of histone H1 for HMGB1 on NucE by 3-AB– or Mer-treated MCF-7 cells.

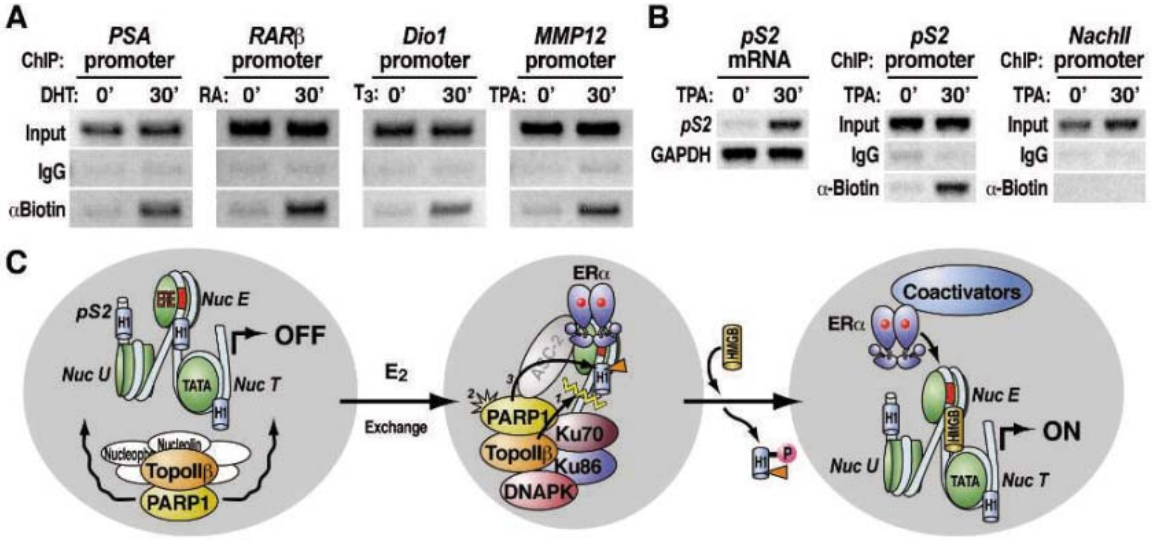

Fig. 5. The general roles of the TopoIIβ/PARP-1 complex in nuclear receptor-mediated gene regulation. (**A**) TopoIIβ-mediated transient dsDNA breaks occurred on endogenous promoters of AR [*prostate-specific antigen* (*PSA*)], RAR (*RAR*β), T_3R (*Dio1*), and AP-1 [*matrix metalloprotease 12* (*MMP12*)]. (**B**) TPA-dependent activation of AP-1-mediated *pS2* gene expression in MCF-7 cells (left). TPA-induced DNA break formation was observed on *pS2* promoter (middle) but not on the silent *NaChII* promoter (right). (**C**) Molecular mechanism of TopoIIβ/PARP-1–dependent regulated gene transcription. *DHT*, *dihydrotestosterone*.

changes at or near promoters, whereas TopoI inhibitors caused transcription complexes to stall in the midst of transcription units (*34*).

Collectively, our data reveal that a transient dsDNA break occurs at multiple regulated transcription units. This raises questions regarding the interplay between molecular machineries that are involved in the repair of dsDNA breaks and the activation of the gene transcription.

References and Notes

1. C. K. Glass, M. G. Rosenfeld, *Genes Dev.* **14**, 121 (2000).
2. B. M. Spiegelman, R. Heinrich, *Cell* **119**, 157 (2004).
3. V. Perissi, M. G. Rosenfeld, *Nat. Rev. Mol. Cell Biol.* **6**, 542 (2005).
4. A. Tulin, D. Stewart, A. C. Spradling, *Genes Dev.* **16**, 2108 (2002).
5. R. Pavri *et al.*, *Mol. Cell* **18**, 83 (2005).
6. M. Y. Kim, S. Mauro, N. Gevry, J. T. Lis, W. L. Kraus, *Cell* **119**, 803 (2004).
7. B. G. Ju *et al.*, *Cell* **119**, 815 (2004).
8. M. Malanga, F. R. Althaus, *Biochem. Cell Biol.* **83**, 354 (2005).
9. S. Burma, D. J. Chen, *DNA Repair* **3**, 909 (2004).
10. J. M. Jeltsch *et al.*, *Nucleic Acids Res.* **15**, 1401 (1987).
11. J. C. Wang, *Nat. Rev. Mol. Cell Biol.* **3**, 430 (2002).
12. A. Dvir, S. R. Peterson, M. W. Knuth, H. Lu, W. S. Dynan, *Proc. Natl. Acad. Sci. U.S.A.* **89**, 11920 (1992).
13. T. Chibazakura *et al.*, *Eur. J. Biochem.* **247**, 1166 (1997).
14. C. A. Sartorius, G. S. Takimoto, J. K. Richer, L. Tung, K. B. Horwitz, *J. Mol. Endocrinol.* **24**, 165 (2000).
15. G. L. Mayeur *et al.*, *J. Biol. Chem.* **280**, 10827 (2005).
16. C. Leontiou, J. H. Lakey, R. Lightowlers, R. M. Turnbull, C. A. Austin, *Mol. Pharmacol.* **69**, 130 (2006).
17. R. Metivier *et al.*, *Cell* **115**, 751 (2003).
18. L. Ko, G. R. Cardona, W. W. Chin, *Proc. Natl. Acad. Sci. U.S.A.* **97**, 6212 (2000).
19. S. K. Lee *et al.*, *Mol. Endocrinol.* **14**, 915 (2000).
20. J. Torchia *et al.*, *Nature* **387**, 677 (1997).
21. M. Binaschi, R. Farinosi, M. E. Borgnetto, G. Capranico, *Cancer Res.* **60**, 3770 (2000).
22. M. N. Cervellera, A. Sala, *J. Biol. Chem.* **275**, 10692 (2000).
23. P. O. Hassa, M. Covic, S. Hasan, R. Imhof, M. O. Hottiger, *J. Biol. Chem.* **276**, 45588 (2001).
24. C. Le Page, J. Sanceau, J. C. Drapier, J. Wietzerbin, *Biochem. Biophys. Res. Commun.* **243**, 451 (1998).
25. A. J. Butler, C. P. Ordahl, *Mol. Cell. Biol.* **19**, 296 (1999).
26. M. Ku, S. Stewart, A. Hata, *Biochem. Biophys. Res. Commun.* **311**, 702 (2003).
27. F. R. Althaus *et al.*, *Mol. Cell. Biochem.* **138**, 53 (1994).
28. D. T. Brown, *Biochem. Cell Biol.* **81**, 221 (2003).
29. J. O. Thomas, *Biochem. Soc. Trans.* **29**, 395 (2001).
30. M. F. Ruh, J. C. Chrivia, L. K. Cox, T. S. Ruh, *Mol. Cell. Endocrinol.* **214**, 71 (2004).
31. D. Das, R. C. Peterson, W. M. Scovell, *Mol. Endocrinol.* **18**, 2616 (2004).
32. A. M. Nunez, M. Berry, J. L. Imler, P. Chambon, *EMBO J.* **8**, 823 (1989).
33. T. Barkhem, L. A. Haldosen, J. A. Gustafsson, S. Nilsson, *Mol. Pharmacol.* **61**, 1273 (2002).
34. I. Collins, A. Weber, D. Levens, *Mol. Cell. Biol.* **21**, 8437 (2001).

35. We thank C. Nelson and K. Ohgi for their assistance; S. Ogawa and J. Puc for reagents; and X. Zhu and T. Wang for discussions and advice. We also thank J. Hightower and M. Fisher for assistance in figure and manuscript preparation and M. Gonzalez (Santa Cruz Biotechnology) for advice on reagents. M.G.R. is an investigator with the Howard Hughes Medical Institute and B.J. is supported by the U.S. Army Medical Research and Materiel Command (grant DAMD17-01-1-0184). These studies are supported by NIH and National Cancer Institute grants to M.G.R. and C.K.G.

Supporting Online Material

www.sciencemag.org/cgi/content/full/312/5781/1798/DC1
Materials and Methods
Figs. S1 to S5
References

9 March 2006; accepted 4 May 2006
10.1126/science.1127196

The Muscle Protein Dok-7 Is Essential for Neuromuscular Synaptogenesis

Kumiko Okada,[1]* Akane Inoue,[1]* Momoko Okada,[1] Yoji Murata,[1] Shigeru Kakuta,[3] Takafumi Jigami,[4] Sachiko Kubo,[3] Hirokazu Shiraishi,[5] Katsumi Eguchi,[5] Masakatsu Motomura,[5] Tetsu Akiyama,[4] Yoichiro Iwakura,[3] Osamu Higuchi,[1]† Yuji Yamanashi[1,2]†

The formation of the neuromuscular synapse requires muscle-specific receptor kinase (MuSK) to orchestrate postsynaptic differentiation, including the clustering of receptors for the neurotransmitter acetylcholine. Upon innervation, neural agrin activates MuSK to establish the postsynaptic apparatus, although agrin-independent formation of neuromuscular synapses can also occur experimentally in the absence of neurotransmission. Dok-7, a MuSK-interacting cytoplasmic protein, is essential for MuSK activation in cultured myotubes; in particular, the Dok-7 phosphotyrosine-binding domain and its target in MuSK are indispensable. Mice lacking Dok-7 formed neither acetylcholine receptor clusters nor neuromuscular synapses. Thus, Dok-7 is essential for neuromuscular synaptogenesis through its interaction with MuSK.

Skeletal muscle is controlled by motor neurons, which contact the muscle at the neuromuscular junction, a synapse that uses the neurotransmitter acetylcholine (*1*, *2*). To achieve sufficient sensitivity to the neurotransmitter, acetylcholine receptors (AChRs) on the muscle must be densely clustered on the postsynaptic side of the neuromuscular junction (*1*, *2*). Failure of AChR clustering is associated with disorders in neuromuscular transmission, including congenital myasthenic syndrome and myasthenia gravis (*3*, *4*). The presynaptic motor-nerve terminal secretes the glycoprotein agrin to activate postsynaptic MuSK (*5*). This agrin-dependent activation of MuSK is essential to establish the postsynaptic apparatus, including the clustering of AChRs, via the AChR-associated protein Rapsyn (*6*–*8*). Nevertheless, before innervation, MuSK-dependent AChR clusters can form at the endplate area of myotubes, suggesting a mechanism of postsynaptic specialization that is independent of agrin and innervation (*9*–*11*). Furthermore, neuromuscular synapses can form independently of agrin in mice that lack acetylcholine, which appears to antagonize postsynaptic differentiation (*12*, *13*). Thus, in addition to agrin, there may be another element that can achieve MuSK activation and trigger postsynaptic specializations at the neuromuscular junction. MuSK contains a phosphotyrosine-binding domain (PTB domain) target motif Asn-Pro-X-Tyr encompassing Tyr^{553} in the juxtamembrane region, which is essential for proper functioning in vivo (*14*). The binding partner for this motif has remained elusive.

By searching databases, including GenBank, the European Molecular Biology Laboratory, and the DNA Data Bank of Japan, for a previously unidentified member of the Dok-family of proteins, each of which has a PTB domain, we identified Dok-7 and cloned human cDNA encoding 504 amino acids. Like other members, Dok-7 has pleckstrin-homology (PH) and PTB domains in the N-terminal portion and Src homology 2 (SH2) domain target motifs in the C-terminal region (fig. S1) (*15*–*17*). Cloning of mouse (*Mus musculus*) and puffer fish (*Takifugu rubripes*) Dok-7 cDNA revealed a highly conserved structure (fig. S2). Like agrin and MuSK, no ortholog was found in invertebrates such as the fruit fly (*Drosophila melanogaster*) and nematode (*Caenorhabditis elegans*). Northern blot analysis of human tissues showed that Dok-7 mRNA is preferentially expressed in skeletal muscle and in the heart (fig. S3A), and immunoblot analysis identified a 55-kD Dok-7 protein in the thigh muscle, diaphragm, and heart but not in the liver or spleen (fig. S3B). Furthermore, immunostaining of mouse skeletal muscles, including the sternocleidomas-

[1]Department of Cell Regulation, Medical Research Institute, [2]School of Biomedical Science, Tokyo Medical and Dental University, Tokyo 113–8510, Japan. [3]Center for Experimental Medicine, Institute of Medical Science, University of Tokyo, Tokyo 108–8639, Japan. [4]Laboratory of Molecular and Genetic Information, Institute of Molecular and Cellular Biosciences, University of Tokyo, Tokyo 113–0032, Japan. [5]The First Department of Internal Medicine, Graduate School of Biomedical Sciences, Nagasaki University, Nagasaki 852–8501, Japan.

*These authors contributed equally to this work.
†To whom correspondence should be addressed. E-mail: yamanashi.creg@mri.tmd.ac.jp (Y.Y.); higuchi.creg@mri.tmd.ac.jp (O.H.)

toid, extensor digitorum longus, and gastrocnemius, with antiserum to Dok-7 highlighted the accumulation of Dok-7 at neuromuscular junctions (Fig. 1, A to C), which are composed of the postsynaptic membrane with its densely clustered AChRs in close juxtaposition with the presynaptic nerve terminal. Therefore, we denervated a mouse gastrocnemius muscle by sciatic nerve resection to confirm the muscular, and thus postsynaptic, localization of Dok-7. One week after the operation, synaptophysin, a component of the presynaptic vesicle, was completely abolished in denervated muscles (fig. S4). However, the muscular localization of Dok-7 and AChRs remained intact, indicating a postsynaptic localization of Dok-7 at neuromuscular junctions (Fig. 1, D to F). Because postsynaptic differentiation and neuromuscular synapse formation are initiated at the endplate zone of skeletal muscle during embryogenesis (*9*–*11*), we performed a whole-mount in situ hybridization and found that Dok-7 transcripts are expressed in the central region encompassing the endplate area of the diaphragm muscles at day 14.5 of embryonic development (E14.5), when AChRs cluster in a nerve- and agrin-independent manner (fig. S5). Together, these results suggest that Dok-7 has the appropriate distribution to be involved in the neuromuscular junction.

Given the requirement for MuSK's PTB target motif and presumably its binding partner in postsynaptic specialization (*14*, *18*, *19*), we next examined the interaction of MuSK with Dok-7, which has a PTB domain, in 293T cells. These heterologous cells do not express either protein detectably, and forced expression of MuSK in these cells induced weak

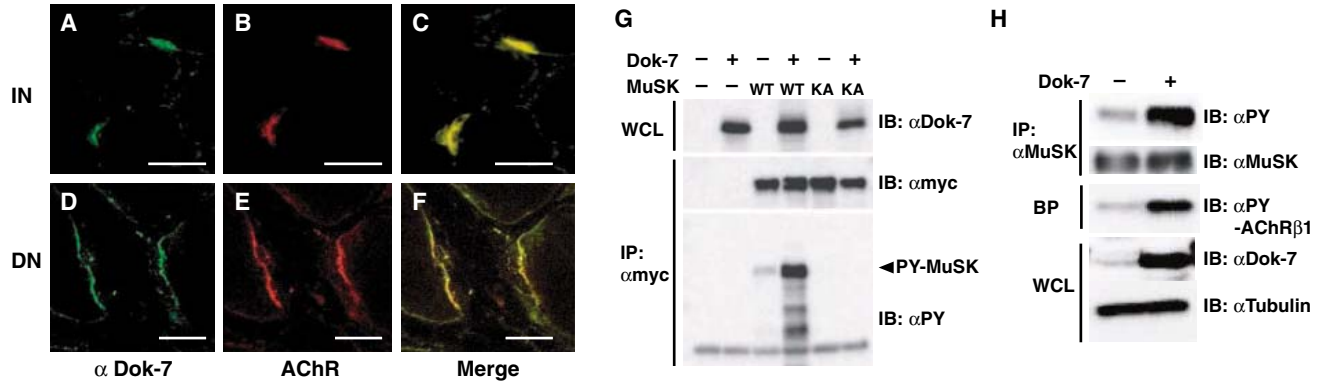

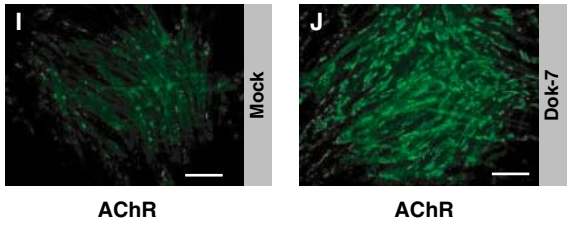

Fig. 1. Forced expression of the muscle protein Dok-7 activates MuSK and induces AChR clustering. (**A** to **F**) Postsynaptic localization of Dok-7 at neuromuscular junction. Dok-7 and AChR were visualized with antibodies (αDok-7) and α-bungarotoxin, respectively, at an innervated (IN) or denervated (DN) neuromuscular junction. Scale bars, 20 μm. (**G**) Dok-7 induces autophosphorylation of MuSK. Whole-cell lysates (WCL) or anti-Myc immunoprecipitates (IP: αmyc) prepared from 293T cells transfected with plasmids expressing Dok-7 and either Myc-tagged MuSK (WT) or MuSK-KA (KA) were subjected to immunoblotting (IB). PY, phosphotyrosine. (**H**) Forced expression of Dok-7 activates the MuSK pathway. Anti-MuSK IP, α-bungarotoxin precipitates (BP), or WCL from C2 myotubes transfected with plasmids for Dok-7 were subjected to IB. (**I** and **J**) Forced expression of Dok-7 induces aneural AChR clustering in C2 myotubes. Abundant clusters of AChRs formed in C2 myotubes transfected with Dok-7 expression plasmids (J), but only a few small clusters formed in the control (Mock) (I). Scale bars, 200 μm.

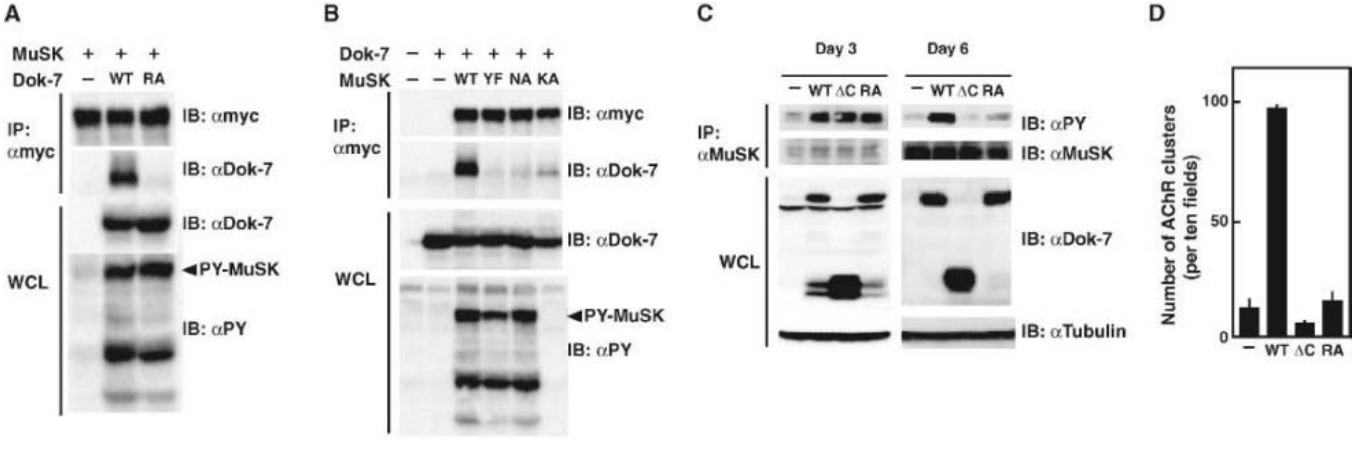

Fig. 2. Dok-7 interacts with MuSK by way of the PTB domain. (**A** and **B**) The PTB domain, its target, and kinase activity are essential for Dok-7 binding to MuSK. Anti-Myc IP or WCL from 293T cells transfected with plasmids for Dok-7 and Myc-tagged MuSK or their mutants, including MuSK-KA, were subjected to IB. (**C** and **D**) The PTB domain and C-terminal region are indispensable for the Dok-7–induced activation of MuSK and AChR clustering in fully differentiated C2 myotubes. Anti-MuSK IP or WCL from C2 cells transfected with expression plasmids for Dok-7 (WT), Dok-7–ΔC (ΔC), or Dok-7–RA (RA) were prepared at day 3 or 6 upon differentiation into myotubes and subjected to IB (C). The number of AChR clusters (mean ± SD) counted at day 7 is shown (D). Differentiation was achieved by day 6, whereas only a few myotubes had formed by day 3.

autophosphorylation (*20*, *21*). Forced expression of Dok-7 induced an intense tyrosine phosphorylation of MuSK but not the kinase-inactive mutant with a Lys/Ala substitution (MuSK-KA), indicating that Dok-7 induced the autophosphorylation of MuSK (Fig. 1G). This activity was unique to Dok-7; no other mammalian Dok-family proteins induced phosphorylation of MuSK (fig. S6). It was also conserved; Dok-7 from puffer fish was able to activate even mammalian MuSK. Also, in C2 myotubes, the forced expression of Dok-7 induced tyrosine phosphorylation of MuSK and the β subunit (AChRβ1) of the AChR complex, which is known to be tyrosine-phosphorylated upon activation of MuSK (*22*) (Fig. 1H). Furthermore, this forced expression induced numerous clusters of AChRs, and the number of AChR clusters correlated with the amount of Dok-7 expression plasmid (Fig. 1, I and J; fig. S7A and supporting online material). The exogenous Dok-7–induced AChR clusters were elaborately branched, and their complicated architecture resembled the differentiated "pretzel-like" AChR clusters formed in vivo (fig. S7, B and C). In addition, forced expression in myotubes of Dok-7 that had been fused with enhanced green fluorescent protein (EGFP) induced Dok-7 and AChR coclustering (fig. S7, D to I), as observed at postsynaptic areas in vivo (Fig. 1, C and F).

Because the regulatory interaction of Dok-7 with MuSK as described above implies their physical interaction, we examined whether Dok-7 binds to MuSK by way of the PTB domain in 293T cells. MuSK was coimmunoprecipitated with Dok-7 but not with Dok-7 carrying three Arg/Ala substitutions (Dok-7–RA) in the PTB domain (Fig. 2A). Consistently, the mutant MuSK carrying either a Tyr/Phe substitution at Tyr^{553} (MuSK-YF) or an Asn/Ala substitution at Asn^{550} (MuSK-NA) in the PTB target motif was not coimmunoprecipitated with Dok-7 (fig. S9 and Fig. 2B). The failure of the MuSK-KA kinase-inactive mutant to be coimmunoprecipitated with Dok-7 confirms the requirement of tyrosine phosphorylation for the binding of MuSK with Dok-7 via the PTB domain. These results indicate that Dok-7 binds to MuSK through the PTB domain in a manner dependent on the tyrosine phosphorylation of its target motif in MuSK.

Nevertheless, mutations in the PTB domain (Dok-7–RA) or PTB target motif (MuSK-NA or -YF) did not block activation of MuSK, at least in heterologous cells (Fig. 2, A and B). In addition, the N- and C-terminal deletion mutants of Dok-7 (Dok-7-ΔN and -ΔC) revealed that the C-terminal moiety, but not the PH domain, of Dok-7 is dispensable for MuSK activation in heterologous cells (fig. S10). Also, the forced expression of Dok-7–RA or Dok-7–ΔC induced MuSK activation even in C2 cells at day 3 of differentiation into myotubes (Fig. 2C), when very few myotubes have formed. Unexpectedly, however, the PTB domain and C-terminal portion were indispensable for Dok-7–induced MuSK activation and AChR clustering in fully differentiated C2 myotubes at days 6 and 7 of differentiation (Fig. 2, C and D). In addition, the PH domain, responsible for membrane localization in general, was indispensable for the activation of MuSK in fully differentiated myotubes (fig. S11), as was seen in heterologous cells (fig. S10). Together these findings suggest that a negative regulatory mechanism preventing MuSK activation is established upon differentiation into myotubes, which is accompanied by increased expression of MuSK and Dok-7 (fig. S12). Trace phosphorylation of MuSK in myotubes might allow physical interaction with Dok-7, in turn facilitating dimerization and/or conformational changes in MuSK that are necessary for its sustained activation.

MuSK-deficient myotubes do not form agrin-dependent or -independent clusters of AChRs unless MuSK is reintroduced (*18*, *19*, *23*). To confirm whether Dok-7–mediated AChR clustering is dependent on MuSK, we introduced Dok-7 into MuSK-deficient myotubes. Unlike its effect in C2 myotubes, forced expression of Dok-7 induced no AChR clustering in the MuSK-deficient myotubes; however, additional expression of wild-type MuSK resulted in robust clustering of AChRs in these cells (Fig. 3A). Furthermore, the MuSK-KA and MuSK-YF mutant each failed to complement the MuSK deficiency, regardless of exogenous Dok-7. These findings demonstrate that Dok-7–induced AChR clustering in myotubes depends on Dok-7 interaction with MuSK and subsequent activation of MuSK catalytic activity. Thus, we examined the regulatory interaction of Dok-7 with a MuSK mutant [MuSK-Val/Met (MuSK-VM)] that carries a Val^{790} to Met substitution. This mutation is causally associated with the congenital myasthenic syndrome by way of an as yet unclear mechanism (*24*). As observed with MuSK-YF (Fig. 2B), forced expression of Dok-7 in 293T cells induced the autophosphorylation of MuSK-VM, but its coimmunoprecipitation with Dok-7 was barely detectable in these heterologous cells (fig. S13). Forced expression of Dok-7 with MuSK-VM induced only very weak AChR clustering in MuSK-deficient myotubes (Fig. 3A). Therefore, the congenital myasthenic syndrome–associated Val^{790} to Met mutation impaired interaction of MuSK with Dok-7, suggesting a possible cause of neuromuscular junction dysfunction in these patients.

To examine the effects of Dok-7 down-regulation in myotubes, we used a small interfering RNA (siRNA) designed specifically to block its expression. Inhibition of Dok-7 suppressed the tyrosine phosphorylation of

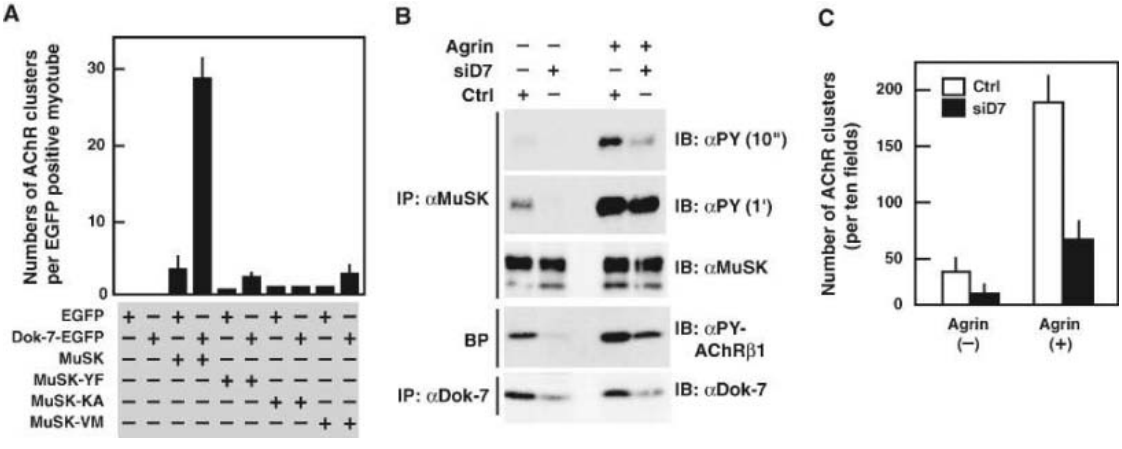

Fig. 3. Dok-7 is essential for activation of the MuSK-pathway to AChR clustering in myotubes. (**A**) MuSK is required for Dok-7–induced AChR clustering. MuSK-deficient myotubes were transfected with the indicated plasmids. The number of AChR clusters (mean ± SD) per EGFP-positive myotube is shown. MuSK-VM is a congenital myasthenic syndrome–associated mutant. (**B**) Activation of the MuSK pathway requires Dok-7. C2 myotubes transfected with Dok-7 siRNA (siD7) or the control (Ctrl) without (–) or with (+) agrin treatment for 15 min were studied as in Fig. 1H. Both short [10 s (10″)] and long [1 min (1′)] exposures are shown for the anti-PY IB of the anti-MuSK IP. (**C**) Dok-7 is essential for AChR clustering. C2 myotubes were transfected with Dok-7 siRNA (siD7) or the control (Ctrl) with or without agrin treatment for 12 hours. The number of AChR clusters (mean ± SD) is shown.

MuSK and AChRβ1 in C2 myotubes, demonstrating its essential role in the aneural, basal catalytic activity of MuSK (Fig. 3B). Indeed, MuSK-dependent spontaneous AChR clustering was suppressed by this siRNA-mediated inhibition (Fig. 3C). Moreover, the inhibition of Dok-7 impaired the agrin-dependent activation of MuSK, the phosphorylation of AChRβ1, and the subsequent formation of AChR clusters (Fig. 3, B and C). Thus, we conclude that Dok-7 is essential for aneural activation of MuSK and AChR clustering in myotubes and is also crucial for agrin-dependent activation of MuSK and AChR clustering. Nonetheless, our results do not exclude the possibility that Dok-7 might also play a role downstream of MuSK. Indeed, Dok-7 and MuSK were synchronously tyrosine phosphorylated upon treatment of myotubes with agrin (fig. S14).

We generated mice lacking Dok-7 to explore its role in vivo (fig. S15). Like mice lacking MuSK or agrin (*6*, *7*), all Dok-7–deficient (Dok-7$^{-/-}$) mice were immobile at birth and died shortly thereafter (26 homozygotes were observed among the first 137 pups), although their wild-type and heterozygous littermates appeared normal. Also, the alveoli of the mutant mice were not expanded at birth (fig. S15D), indicating a failure to breathe and suggesting a severe defect in neuromuscular transmission in the skeletal muscles. Consistently, there were no detectable AChR clusters in the endplate area of the diaphragm muscle in Dok-7$^{-/-}$ embryos at either E14.5 or E18.5 (Fig. 4, E and K). Because nascent AChR clusters are formed in a nerve- and agrin-independent manner at E13.5 to E16.5, whereas most neuromuscular junctions are formed in a nerve- and agrin-dependent manner at E18.5, our findings indicate a requirement for Dok-7 in both types of MuSK-dependent postsynaptic specialization, although we cannot exclude the possibility that nascent AChR clustering is a prerequisite for nerve- and agrin-dependent AChR clustering (*9*–*11*). Consistent with this finding, Dok-7 transcripts were expressed in the endplate area of the diaphragm muscle (fig. S5). In addition, axonal branches extending from the motor nerve trunk were aberrantly long in the endplate area of Dok-7$^{-/-}$ diaphragms at E18.5 and, unlike the controls, did not terminate near the nerve trunk (Fig. 4, G and J). Overall, these pre- and postsynaptic abnormalities are indistinguishable from those found in mice lacking MuSK (*7*), demonstrating an essential role in vivo for Dok-7 in neuromuscular synaptogenesis, a MuSK-dependent vital process.

MuSK-dependent postsynaptic specialization during neuromuscular synaptogenesis appears to be controlled by multiple regulatory mechanisms (*2*, *25*). We have shown that Dok-7 may be a muscle-intrinsic activator of MuSK by demonstrating its essential role in the aneural activation of MuSK and subsequent AChR clustering in cultured myotubes. This conclusion is further supported by our findings that mice lacking Dok-7 showed marked disruption of neuromuscular synaptogenesis that was indistinguishable from the disruption found in MuSK-deficient mice. Thus, neuromuscular synaptogenesis requires Dok-7 within the skeletal muscle. Dok-7 dysfunction may be involved in the pathogenesis of neuromuscular junction disorders.

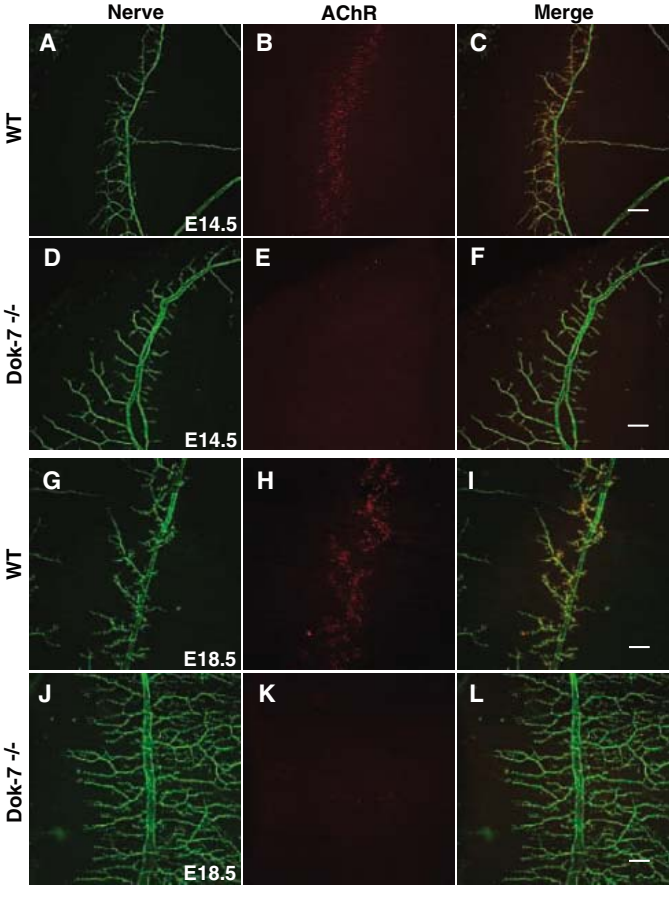

Fig. 4. Dok-7 is essential for neuromuscular synaptogenesis in vivo. Diaphragm muscles were prepared from the wild-type control (WT) or Dok-7$^{-/-}$ embryos at E14.5 (**A** to **F**) or E18.5 (**G** to **L**) and subjected to whole-mount anti-neurofilament and α-bungarotoxin staining, to visualize nerve and AChR, respectively. Scale bars, 100 μm.

References and Notes

1. S. J. Burden, *Genes Dev.* **12**, 133 (1998).
2. J. R. Sanes, J. W. Lichtman, *Nat. Rev. Neurosci.* **2**, 791 (2001).
3. A. G. Engel, K. Ohno, S. M. Sine, *Nat. Rev. Neurosci.* **4**, 339 (2003).
4. A. Vincent *et al.*, *Ann. N. Y. Acad. Sci.* **998**, 324 (2003).
5. D. J. Glass *et al.*, *Cell* **85**, 513 (1996).
6. M. Gautam *et al.*, *Cell* **85**, 525 (1996).
7. T. M. DeChiara *et al.*, *Cell* **85**, 501 (1996).
8. M. Gautam *et al.*, *Nature* **377**, 232 (1995).
9. W. Lin *et al.*, *Nature* **410**, 1057 (2001).
10. X. Yang *et al.*, *Neuron* **30**, 399 (2001).
11. X. Yang, W. Li, E. D. Prescott, S. J. Burden, J. C. Wang, *Science* **287**, 131 (2000).
12. T. Misgeld, T. T. Kummer, J. W. Lichtman, J. R. Sanes, *Proc. Natl. Acad. Sci. U.S.A.* **102**, 11088 (2005).
13. W. Lin *et al.*, *Neuron* **46**, 569 (2005).
14. R. Herbst, E. Avetisova, S. J. Burden, *Development* **129**, 5449 (2002).
15. N. Carpino *et al.*, *Cell* **88**, 197 (1997).
16. Y. Yamanashi, D. Baltimore, *Cell* **88**, 205 (1997).
17. R. J. Crowder, H. Enomoto, M. Yang, E. M. Johnson Jr., J. Milbrandt, *J. Biol. Chem.* **279**, 42072 (2004).
18. H. Zhou, D. J. Glass, G. D. Yancopoulos, J. R. Sanes, *J. Cell Biol.* **146**, 1133 (1999).
19. R. Herbst, S. J. Burden, *EMBO J.* **19**, 67 (2000).
20. A. Watty *et al.*, *Proc. Natl. Acad. Sci. U.S.A.* **97**, 4585 (2000).
21. S. K. H. Gillespie, S. Balasubramanian, E. T. Fung, R. L. Huganir, *Neuron* **16**, 953 (1996).
22. C. Fuhrer, J. E. Sugiyama, R. G. Taylor, Z. W. Hall, *EMBO J.* **16**, 4951 (1997).
23. J. E. Sugiyama, D. J. Glass, G. D. Yancopoulos, Z. W. Hall, *J. Cell Biol.* **139**, 181 (1997).
24. F. Chevessier *et al.*, *Hum. Mol. Genet.* **13**, 3229 (2004).
25. T. T. Kummer, T. Misgeld, J. R. Sanes, *Curr. Opin. Neurobiol.* **16**, 74 (2006).

26. We thank Regeneron Pharmaceuticals for MuSK-deficient cells; K. Manji, J. Hamuro, H. Moriya, and A. Ishii for technical assistance; and M. Shirakata, T. Yasuda, S. Sugano, T. Tezuka, R. F. Whittier, S. Tronick, and T. Yamamoto for discussions. This work was supported by Grants-in-Aid for Scientific Research from the Ministry of Education, Culture, Sports, Science and Technology and by a grant from the Uehara Foundation.

Supporting Online Material

www.sciencemag.org/cgi/content/full/312/5781/1802/DC1
Materials and Methods
SOM Text
Figs. S1 to S15
References

8 March 2006; accepted 19 May 2006
10.1126/science.1127142

Depletion, Degradation, and Recovery Potential of Estuaries and Coastal Seas

Heike K. Lotze,[1*] Hunter S. Lenihan,[2] Bruce J. Bourque,[3] Roger H. Bradbury,[4] Richard G. Cooke,[5] Matthew C. Kay,[2] Susan M. Kidwell,[6] Michael X. Kirby,[7] Charles H. Peterson,[8] Jeremy B. C. Jackson[5,9]

Estuarine and coastal transformation is as old as civilization yet has dramatically accelerated over the past 150 to 300 years. Reconstructed time lines, causes, and consequences of change in 12 once diverse and productive estuaries and coastal seas worldwide show similar patterns: Human impacts have depleted >90% of formerly important species, destroyed >65% of seagrass and wetland habitat, degraded water quality, and accelerated species invasions. Twentieth-century conservation efforts achieved partial recovery of upper trophic levels but have so far failed to restore former ecosystem structure and function. Our results provide detailed historical baselines and quantitative targets for ecosystem-based management and marine conservation.

Estuaries and coastal seas have been focal points of human settlement and marine resource use throughout history. Centuries of overexploitation, habitat transformation, and pollution have obscured the total magnitude of estuarine degradation and biodiversity loss and have undermined their ecological resilience (*1*–*5*). This poses potential for disaster, as demonstrated in numerous fisheries collapses (*1*–*3*) and the recent impacts of the 2004 Asian tsunami and 2005 Hurricane Katrina that were exacerbated by historical losses of mangroves and wetlands (*5*–*7*). With recognition of their essential role for human and marine life, estuaries and coastal zones have become the focus of efforts to develop ecosystem-based management and large-scale restoration strategies. To be successful, these approaches require historical reference points and assessments of the degree and drivers of degradation in an ecosystem context (*8*, *9*).

We reconstructed historical baselines and quantified the magnitude and causes of change in 12 temperate estuarine and coastal ecosystems in Europe, North America, and Australia from the onset of human settlement until today (Table 1). We used paleontologic, archaeological, historical, and ecological records (table S1) to quantify changes in 30 to 80 species per system standardized into 22 guilds and six taxonomic and seven functional groups, as well as seven water-quality parameters and species invasions (*10*). Species were selected for their economic, structural, or functional significance throughout history. We estimated relative abundance of each species over real time and across seven cultural periods reflecting the stage of cultural and market development rather than calendar dates (tables S2 and S3). Relative abundance was quantified as pristine (100%), abundant (90%), depleted (50%), rare (10%), or extinct (0%) (table S4). Recovery was quantified as partial or substantial when increasing from <10% to >10% and >50%, respectively (*10*). Our estimates are conservative compared with available absolute abundance records.

Overall historical change in each study system was tracked by using arithmetic and multivariate means of relative abundance of taxonomic and functional groups (*10*), all of which yielded similar results (Fig. 1 and fig. S1). Despite wide geographic distribution and unique regional histories, all systems showed similar trajectories of long periods of slow decline followed by rapid acceleration over the last 150 to 300 years (Fig. 1A). Severe resource depletion first began during Roman times (2500 years B.P.) in the Adriatic Sea, Medieval times (1000 years B.P.) in the Wadden and Baltic Seas, and in the wake of European colonization in North America and Australia (Fig. 1A). Substituting cultural periods for calendar dates revealed low human impacts during the hunter-gatherer, agricultural, and market-colonial establishment periods (Fig. 1B), when exploitation was mainly for subsistence purposes. However, signs of local resource depletion were evident in some systems such as San Francisco Bay (Fig. 1B), where prehistoric populations depleted highly valued resources such as sea otters (*Enhydra lutris*), large

[1]Biology Department, Dalhousie University, 1355 Oxford Street, Halifax, NS, Canada B3H 4J1. [2]Bren School of Environmental Science and Management, Bren Hall 3428, University of California, Santa Barbara, CA 93106–5131, USA. [3]Department of Anthropology, 155 Pettengill Hall, Bates College, Lewiston, ME 04240, USA. [4]Resource Management in Asia-Pacific Program, Research School of Pacific and Asian Studies, Australian National University, Canberra, ACT 0200, Australia. [5]Center for Tropical Paleoecology and Archeology, Smithsonian Tropical Research Institute, Unit 0948, APO AA 34002–0948, Republic of Panama. [6]Department of Geophysical Sciences, University of Chicago, 5734 South Ellis Avenue, Chicago, IL 60637, USA. [7]Florida Museum of Natural History, University of Florida, Museum Road, P.O. Box 117800, Gainesville, FL 32611–7800, USA. [8]Institute of Marine Sciences, University of North Carolina at Chapel Hill, Morehead City, NC 28557, USA. [9]Center for Marine Biodiversity and Conservation, Scripps Institution of Oceanography, University of California at San Diego, La Jolla, CA 92093–0244, USA.

*To whom correspondence should be addressed. E-mail: hlotze@dal.ca

Table 1. Location and characteristics of study systems. Species richness (SpR, fish richness as proxy for overall richness) and primary productivity (PP) represent regional data for large marine ecosystems [table S1 (*10*)]. Origin indicates the time when the system developed today's size and shape. Impact length and human population growth rate were calculated since beginning of the development period. Human population total and density refer to today's population in provinces and countries bordering the studied systems (*10*).

System	Lat.	Long.	Size (km^2)	SpR (fish)	PP (mg C· m^{-2}·d^{-1})	Origin (years $\times 10^3$ B.P.)	Impact (years)	Human population		
								Growth (*x*-fold)	Total ($\times 10^6$)	Density (km^{-2})
W. Baltic Sea	55 N	16 E	390,077	156	1,804	7.0–9.0	1,000	4	84.94	230
Wadden Sea	54 N	8 E	13,500	189	1,067	7.5	1,000	26	6.50	699
N. Adriatic Sea	44 N	14 E	160,000	606	385	8.0	2,500	21	103.00	746
S. Gulf St. Lawrence	47 N	63 W	65,000	197	1,044	6.4–14.5	240	135	7.41	114
Outer Bay of Fundy	45 N	67 W	148	197	1,044	7.0–15.0	240	18	0.03	260
Massachusetts Bay	42 N	71 W	768	645	1,124	6.3–12.0	320	156	2.50	5,230
Delaware Bay	38 N	75 W	2,070	645	1,124	7.0–8.0	240	95	3.33	2,693
Chesapeake Bay	37 N	76 W	6,974	645	1,124	7.4–8.2	240	19	6.93	1,004
Pamlico Sound	35 N	76 W	4,680	1,170	564	7.2–8.2	300	144	0.22	43
Galveston Bay	29 N	95 W	1,456	972	417	7.7–8.2	180	2,659	3.99	4,482
San Francisco Bay	38 N	123 W	838	803	501	8.5–9.3	180	4,533	6.80	8,200
Moreton Bay	27 S	153 E	1,600	1,239	441	6.5	150	710	2.20	1,375

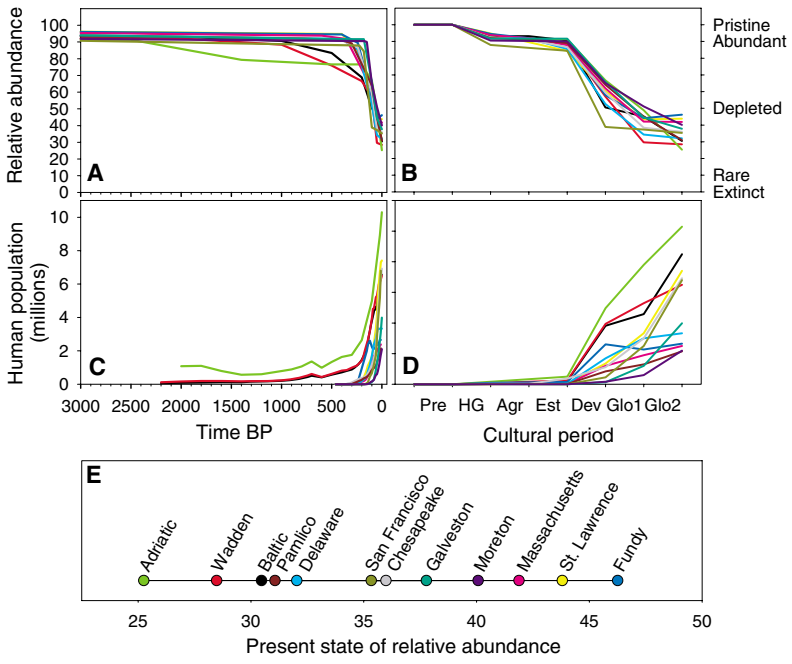

Fig. 1. History and present state of 12 estuarine and coastal ecosystems in North America, Europe, and Australia. (**A**) Relative abundance of six taxonomic groups (as arithmetic means) over real time and (**B**) cultural periods (Pre, prehuman; HG, hunter-gatherer; Agr, agricultural; Est, market–colonial establishment; Dev, market–colonial development; Glo1, global market 1900–1950; and Glo2, global market 1950–2000). (**C**) Human population growth over real time and (**D**) cultural period (Baltic and Adriatic, $\times 10^{-1}$; Fundy, $\times 10$; Pamlico, $\times 10^{2}$ to fit scale). (**E**) Present state of relative abundance. Color codes depict study systems as shown in (E).

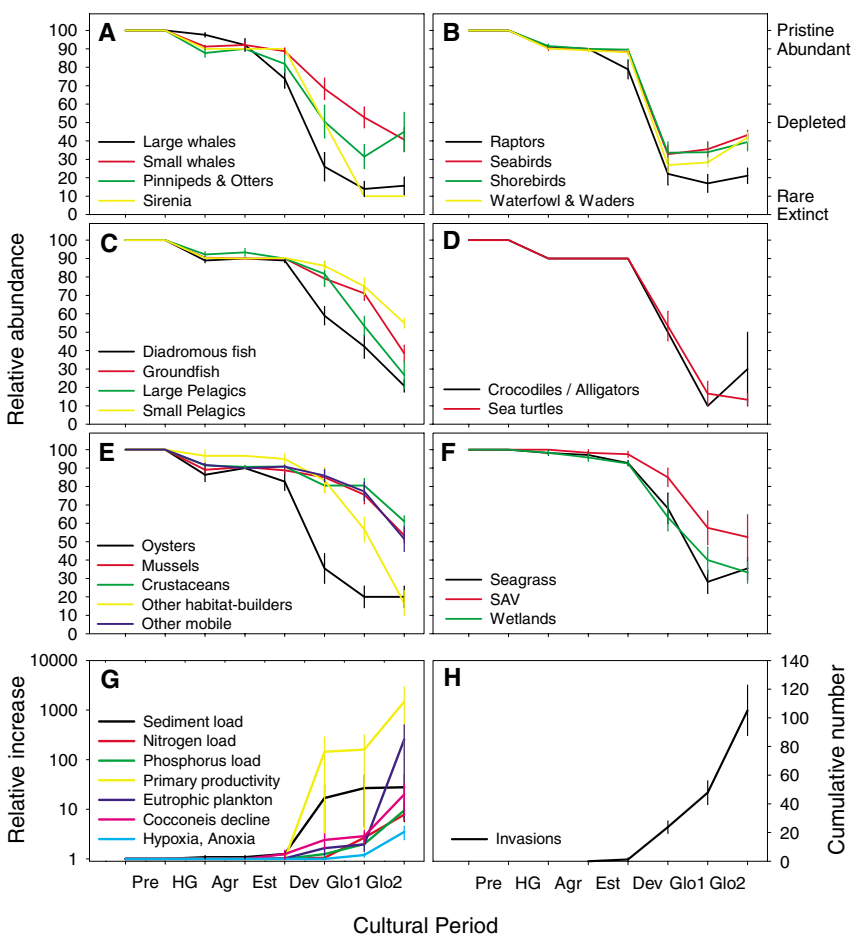

Fig. 2. Common patterns of decline in 22 species guilds averaged over 12 study systems for (**A**) marine mammals, (**B**) coastal birds, (**C**) fish, (**D**) reptiles, (**E**) invertebrates, and (**F**) vegetation. (**G**) Degradation of water quality as indicated by the relative increase in eutrophication parameters [eight systems (*10*)]. (**H**) Cumulative increase in recorded species invasions [five systems (*10*)]. Data are means ± SEM.

geese (*Anser*, *Branta*, *Chen* spp.), white sturgeon (*Acipenser transmontanus*), and native oyster (*Ostreola conchaphila*) (*11*).

Human impacts escalated into rapid resource depletion during the market–colonial development period and continued in the two global market periods, 1900–1950 and 1950–2000, in all systems (Fig. 1B). These were the periods of (i) rapid human population growth (Fig. 1, C and D) and increasing demand, (ii) commercialization of resource use and development of luxury markets, and (iii) industrialization and technological progress toward more efficient but also unselective and destructive gears (table S2). In the two global periods, degradation trends slowed in most and reversed in some systems because of conservation efforts (Fig. 1B). These general trends suggest that rapid degradation was driven by human history rather than natural change and that we may have passed the low point and are on a slow path to recovery—at least in developed countries. In developing countries, however, expected future population growth associated with growing pressures on coastal ecosystems may increase degradation.

The degree of degradation, as indicated by the endpoints of historical trajectories (Fig. 1E), was independent of system size, species richness, primary productivity, and human population density and growth rate (Table 1, linear regressions, $P > 0.05$). Nevertheless, systems with the longest history of intense human impacts and highest total human population were among the most degraded, including the Adriatic, Wadden, and Baltic Seas {Fig. 1E, linear regressions, log[length impact], $F(1,10) = 10.3$, $P = 0.009$, $r^2 = 0.51$; log[total population], $F(1,10) = 5.06$, $P = 0.048$, $r^2 = 0.34$, see fig. S1 for alternative measures}. The outer Bay of Fundy, Southern Gulf of St. Lawrence,

and Massachusetts Bay were consistently ranked as the least degraded systems (Fig. 1E and fig. S1).

Detailed time lines for species guilds, taxonomic and functional groups, water-quality parameters, and species invasions followed similar patterns of degradation across study systems (Fig. 2 and fig. S2). Most mammals, birds, and reptiles (Fig. 2, A, B, and D) were depleted by 1900 and declined further by 1950 because of intense exploitation for food, oil, or luxury items including furs, feathers, and ivory (*2*, *12*). Among fish (Fig. 2C), diadromous species such as salmon and sturgeon were highly desired, easily accessible, and depleted first, successively followed by large pelagics such as tuna and sharks, groundfish such as cod and halibut, and small pelagics such as herring and sardines. Oysters were the first invertebrate suffering depletion (Fig. 2E) because of high value, accessibility, and destructive exploitation methods (*13*). Because of their reef-forming and filtration capacity, depletion of oysters reduced the ecosystem's ability to provide high water quality and complex habitats. Other habitat-building filter-feeders including corals, sponges, and hydrozoans were little affected until the development period, but rapidly declined with expanding seafloor trawling (*12*). Mussels, crustaceans, and other mobile invertebrates have been harvested throughout history, but only recently became targets of expanding low–trophic level fisheries (*2*, *14*). Thus, among mammals, fish, and invertebrates, we see sequential depletion of the most valued and largest species and subsequent replacement with smaller, less valuable ones (*14*).

Over time, 67% of wetlands, 65% of seagrasses, and 48% of other submerged aquatic vegetation (SAV) were lost because of reclamation, eutrophication, disease, destruction, and direct exploitation (Fig. 2F). Declines in coastal vegetation caused substantial losses of nursery habitats, nutrient and sediment sinks, and coastline protection. By the late 20th century, 91% of the recorded species were depleted; 31% were rare; and 7% were extinct. Conservation efforts in the 20th century led to partial recovery of 12% and substantial recovery of 2% of the species, especially among pinnipeds, otters, birds, crocodiles, and alligators (Fig. 2, A, B, and D). Large whales, sirenia, and sea turtles, however, remain at low population levels.

Degradation of water quality occurred in two phases (*10*). During the development period (Fig. 2G), primary productivity and sediment loading strongly increased, mainly driven by deforestation that mobilized sediments and nutrients. These trends stabilized during the first global period (1900–1950) except for increasing nitrogen loading. In the second global period (1950–2000), sediment loads stabilized but strong increases occurred in nitrogen and phosphorus loading, primary productivity, eutrophic plankton, oxygen depletion, and losses of epiphytic diatoms (*Cocconeis* spp.), commonly associated with seagrass. These trends reflect coastal eutrophication driven by nutrient loading from point and nonpoint sources and losses of filtering and buffering capacity of vegetation and suspension feeders (*1*, *15*).

The first identified invasion was by the soft-shelled clam *Mya arenaria*, introduced from North America into the Baltic and North Seas probably by Norse voyagers before 1245 A.D. (*10*, *16*). In the following centuries, invasions were only gradually recorded but increased during the development and accelerated during the global periods (Fig. 2H), driven by increased global navigation and commerce (*17*).

The recorded causes of past changes (*10*) highlight priority targets for ecosystem-based management and marine conservation. Exploitation stands out as the causative agent for 95% of species depletions and 96% of extinctions in our study systems, followed by habitat destruction (Fig. 3A). This is consistent with reported causes of marine (*18*) and terrestrial (*19*) extinctions worldwide. Pollution, disturbance, disease, eutrophication, and introduced land predators were associated with fewer species losses (Fig. 3A) but contributed to declines of habitat-building species and may hinder recovery. In our records, which focused on commercially, structurally, and functionally important species, no depletion or extinction was caused by invasive species or climate change, although such cases have been documented (*3*, *18*, *20*). We caution, however, that the relative importance of these factors may shift in the future with exploitation becoming more restricted, but invasions and climate change accelerating (*21*).

Our results indicate that human impacts do not act in isolation. In 45% of species depletions and 42% of extinctions, multiple human impacts were involved, commonly, exploitation and habitat loss. Such synergistic effects have been significant for terrestrial extinctions (*19*) and estuarine depletions (*22*). Cumulative impacts were even more important for recovery. Although 22% of recoveries resulted from mitigation of a single human impact, mostly exploitation, 78% resulted from reduction of at least two impacts, mostly habitat protection and restricted exploitation but also pollution (Fig. 3A). Reduced

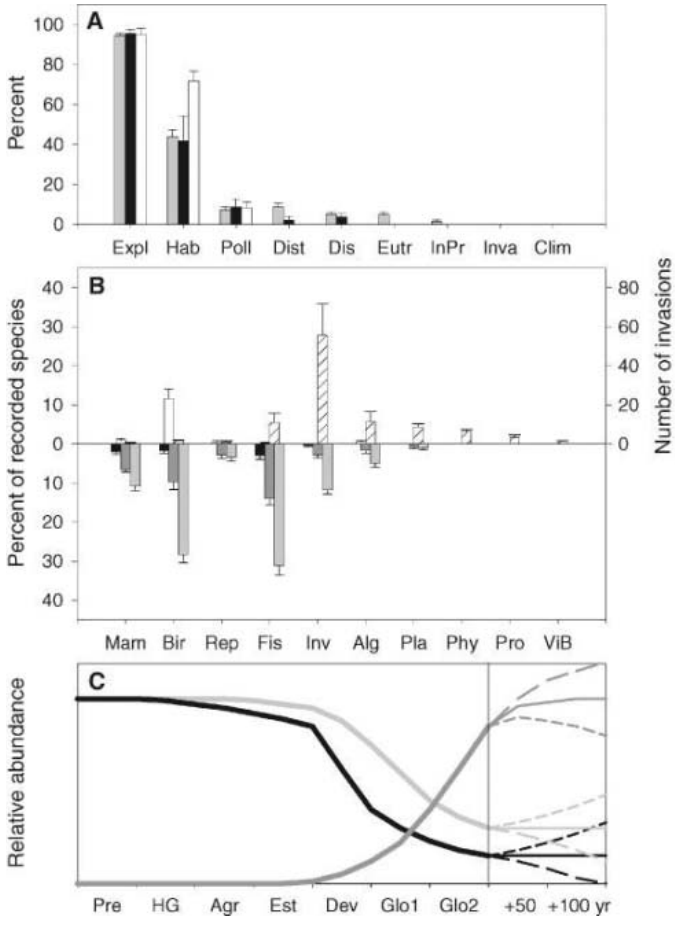

Fig. 3. Causes and consequences of change in 12 study systems (means ± SEM). (**A**) Percent of species depletions (light gray) and extinctions (black) caused by different human impacts (Expl, exploitation; Hab, habitat loss; Poll, pollution; Dist, human disturbance; Dis, disease; Eutr, eutrophication; InPr, introduced land predators; Inva, invasive species; and Cli, climate change), and percent of recoveries (white) resulting from impact reduction. (**B**) Diversity shift due to biased losses and gains across different taxonomic groups (Mam, mammals; Bir, birds; Rep, reptiles; Fis, fish; Inv, invertebrates; Alg, macroalgae; Pla, higher plants; Phy, phytoplankton; Pro, protozoa; and ViB, viruses and bacteria): percent of recorded species currently depleted (light gray), rare (dark gray), extinct (black), or recovering (white), and number of species invasions (cross-hatched; data for seven systems). (**C**) Past, present, and potential future changes in important structural and functional ecosystem components: large consumers (black), habitat and filter organisms (light gray), eutrophication and invasive species (dark gray) [cultural periods as in Fig. 1, adapted from (*28*)]. Future scenarios depict stabilizing (solid lines), improving (short dashed), or worsening (long dashed) trends.

exploitation, habitat protection, and improved water quality need to be considered together, and the cumulative effects of multiple human interventions must be included in both management and conservation strategies (*22*).

Marked shifts in diversity were caused by the taxonomic bias of almost all extinctions (93%) and most depletions (81%) affecting large vertebrates (Fig. 3B) (*10*). This bias was amplified by the high incidence of invasions among invertebrates, plants, and smaller organisms (Fig. 3B) (*10*). Given past trends in depletions, extinctions, and invasions (Fig. 2), this shift in species composition is likely to accelerate in the future, only partly dampened by recent trends in recovery (Figs. 2 and 3B).

The structure and functioning of estuarine and coastal ecosystems has been fundamentally changed by the loss of large predators and herbivores, spawning and nursery habitat, and filtering capacity that sustains water quality (Fig. 3C and fig. S2). The erosion of diversity and complexity has slowly undermined resilience, giving way to undesirable algal blooms, dead zones, disease outbreaks, and invasions, and elevating the potential for disaster (*1*–*7*, *21*). Although declines in large vertebrates and habitat-providing species have slowed in the last 50 to 100 years, trends in small consumers, water quality, and species invasions continue to deteriorate (Figs. 2 and 3C). Together with the historical degradation of coral reefs (*4*), kelp forests (*23*), and an up-welling system (*24*), our results document severe, long-term degradation of near-shore marine systems worldwide. As human impacts spread rapidly from the coast to the shelf, open ocean, and deep sea (*25*–*27*), past trajectories in coastal zones may well forecast future changes in the entire ocean. Strong countermeasures are needed to reverse trends of expanding degradation (Fig. 3C).

Human impacts have pushed estuarine and coastal ecosystems far from their historical baseline of rich, diverse, and productive ecosystems. The severity and synchrony of degradation trends and the commonality of causes and consequences of change provide reference points and quantitative targets for ecosystem-based management and restoration. Overexploitation and habitat destruction have been responsible for the large majority of historical changes, and their reduction should be a major management priority. Eutrophication, although severe in the last phase of estuarine history, largely followed rather than drove observed declines in diversity, structure, and functioning. Despite some extinctions, most species and functional groups persist, albeit in greatly reduced numbers. Thus, the potential for recovery remains, and where human efforts have focused on protection and restoration, recovery has occurred, although often with significant lag times (*2*, *12*). Our study not only provides baselines on the extent of historical degradation, but also a vision for regenerating resilient estuarine and coastal ecosystems that can absorb shocks and disasters in an uncertain future.

References and Notes

1. J. B. C. Jackson *et al.*, *Science* **293**, 629 (2001).
2. H. K. Lotze, I. Milewski, *Ecol. Appl.* **14**, 1428 (2004).
3. H. K. Lotze *et al.*, *Helgol. Mar. Res.* **59**, 84 (2005).
4. J. M. Pandolfi *et al.*, *Science* **301**, 955 (2003).
5. W. N. Adger, T. P. Hughes, C. Folke, S. R. Carpenter, J. Rockström, *Science* **309**, 1036 (2005).
6. F. Danielsen *et al.*, *Science* **310**, 643 (2005).
7. E. Stokstad, *Science* **310**, 1264 (2005).
8. A. Balmford *et al.*, *Science* **307**, 212 (2005).
9. E. K. Pikitch *et al.*, *Science* **305**, 346 (2004).
10. Detailed methods are available as supporting online material on *Science* Online.
11. J. M. Broughton, *World Archaeol.* **34**, 60 (2002).
12. H. K. Lotze, *Helgol. Mar. Res.* **59**, 71 (2005).
13. M. X. Kirby, *Proc. Natl. Acad. Sci. U.S.A.* **101**, 13096 (2004).
14. D. Pauly, V. Christensen, J. Dalsgaard, R. Froese, F. Torres Jr., *Science* **279**, 860 (1998).
15. J. E. Cloern, *Mar. Ecol. Prog. Ser.* **210**, 223 (2001).
16. K. S. Petersen, K. L. Rasmussen, J. Heinemeier, N. Rud, *Nature* **359**, 679 (1992).
17. G. M. Ruiz, J. T. Carlton, E. D. Grosholz, A. H. Hines, *Am. Zool.* **37**, 621 (1997).
18. N. K. Dulvy, Y. Sadovy, J. D. Reynolds, *Fish Fish.* **4**, 25 (2003).
19. D. A. Burney, T. F. Flannery, *Trends Ecol. Evol.* **20**, 395 (2005).
20. J. T. Carlton, J. B. Geller, M. L. Reaka-Kudla, E. A. Norse, *Annu. Rev. Ecol. Syst.* **30**, 515 (1999).
21. C. D. Harvell *et al.*, *Science* **296**, 2158 (2002).
22. H. S. Lenihan, C. H. Peterson, *Ecol. Appl.* **8**, 128 (1998).
23. R. S. Steneck *et al.*, *Environ. Conserv.* **29**, 436 (2002).
24. C. L. Griffiths *et al.*, *Oceanogr. Mar. Biol. Annu. Rev.* **42**, 303 (2004).
25. B. Worm, M. Sandow, A. Oschlies, H. K. Lotze, R. A. Myers, *Science* **309**, 1365 (2005).
26. D. Pauly *et al.*, *Science* **302**, 1359 (2003).
27. M. Pahlow, U. Riebesell, *Science* **287**, 831 (2000).
28. J. B. C. Jackson, *Proc. Natl. Acad. Sci. U.S.A.* **98**, 5411 (2001).

29. We thank all colleagues for sharing data and insight and B. Worm and R. A. Myers for critical discussions. This work was initiated as part of the Long-Term Ecological Records of Marine Environments, Populations and Communities Working Group supported by the National Center for Ecological Analysis and Synthesis (funded by NSF grant DEB-0072909, the University of California, and the University of California, Santa Barbara). Additional funding was granted to H.K.L. by the Alfred-Wegener Institute for Polar and Marine Research, the Sloan Foundation (Census of Marine Life, History of Marine Animal Populations Program), and the Lenfest Ocean Program at the Pew Charitable Trusts.

Supporting Online Material

www.sciencemag.org/cgi/content/full/312/5781/1806/DC1
Materials and Methods
Figs. S1 and S2
Tables S1 to S8
References and Notes

29 March 2006; accepted 3 May 2006
10.1126/science.1128035

JETLAG Resets the *Drosophila* Circadian Clock by Promoting Light-Induced Degradation of TIMELESS

Kyunghee Koh, Xiangzhong Zheng, Amita Sehgal*

Organisms ranging from bacteria to humans synchronize their internal clocks to daily cycles of light and dark. Photic entrainment of the *Drosophila* clock is mediated by proteasomal degradation of the clock protein TIMELESS (TIM). We have identified mutations in *jetlag*—a gene coding for an F-box protein with leucine-rich repeats—that result in reduced light sensitivity of the circadian clock. Mutant flies show rhythmic behavior in constant light, reduced phase shifts in response to light pulses, and reduced light-dependent degradation of TIM. Expression of JET along with the circadian photoreceptor cryptochrome (CRY) in cultured S2R+ cells confers light-dependent degradation onto TIM, thereby reconstituting the acute response of the circadian clock to light in a cell culture system. Our results suggest that JET is essential for resetting the clock by transmitting light signals from CRY to TIM.

Travel across time zones often produces jet lag because it takes some time to resynchronize internal circadian clocks to the new day and night cycle. Although the molecular mechanisms for generating circadian rhythms through interlocking transcriptional feedback loops and posttranslational modifications have been characterized in some detail (*1*), few components of the light entrainment pathway are known (*2*). Photic entrainment in *Drosophila* can be mediated by the visual system and by CRY, a circadian blue-light photoreceptor expressed in clock cells (*3*). When the fly is exposed to light, CRY binds a core clock protein, TIM, which leads to subsequent ubiquitination and degradation of TIM by the proteasome pathway (*4*–*8*). Rapid, light-dependent degradation of TIM underlies the fly's ability to reset the circadian phase to reflect environmental fluctuations in light levels (*9*, *10*). However, the specific signals that drive the TIM response to light are not known.

In the course of characterizing rest:activity rhythms of various fly strains, we discovered a strain with anomalous activity patterns in constant light (LL). Whereas wild-type flies

Howard Hughes Medical Institute, Department of Neuroscience, University of Pennsylvania School of Medicine, Philadelphia, PA 19104, USA.

*To whom correspondence should be addressed. E-mail: amita@mail.med.upenn.edu

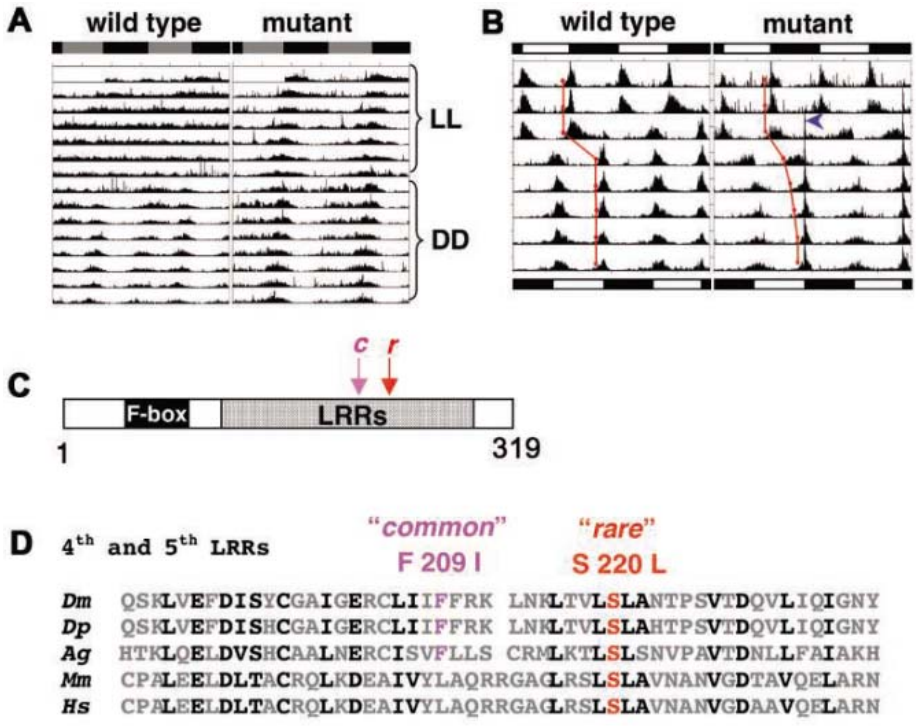

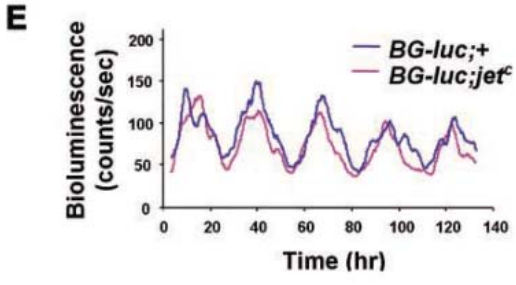

Fig. 1. Mutant phenotypes and mapping of the *jet* mutations. (**A**) Activity records of representative wild-type (*y w*) and mutant flies in LL and DD. The gray and black bars at the top indicate the LD cycle. (**B**) Activity records showing average activity of wild-type and mutant flies (n = 13 and 15, respectively) in a "jet lag" experiment. The flies were transferred from one LD schedule (indicated by the bars at the top) to another with an 8-hour delay (indicated by the bars at the bottom) during the third day. Red dots indicate evening onsets, and the blue arrowhead indicates a startle response at lights-off after the transfer to a new LD schedule. (**C**) Schematic representation of the JET protein. Arrows indicate the Phe → Ile (*c*) and Ser → Leu (*r*) substitutions in the fourth and fifth LRRs, respectively. (**D**) Alignment of the fourth and fifth LRRs of insect, mouse, and human F-box proteins with highest similarity to JET. See supporting online material for GenBank accession numbers. (**E**) Normal circadian expression of *per* in peripheral clocks of *jet*^{c} mutants. Flies (21 control, 22 mutant) carrying a *per*-luciferase (*BG-luc*) transgene were entrained to a 12 hour:12 hour LD cycle and were individually monitored in DD for ~5 days; data are mean numbers of counts per second.

became arrhythmic after a day or two in LL, the mutant flies were rhythmic for more than a week (Fig. 1A and Table 1). Although the mutants could be entrained to light:dark (LD) cycles, they took longer to be re-entrained to a new schedule than wild-type flies (Fig. 1B), and so we named the mutation *jetlag* (*jet*). The behavior of *jet* flies in LD and in constant darkness (DD) conditions was normal (Fig. 1 and Table 1). These phenotypes are reminiscent of those of *cry* mutants (*11*) and suggest a defect in circadian photoreception.

Using meiotic recombination and deficiency mapping strategies, we mapped the mutation to a small region containing 18 genes on the left arm of the second chromosome. One of these genes, CG8873 (Flybase), encodes an F-box protein with leucine-rich repeats (LRRs), a putative component of a Skp1/Cullin/F-box (SCF) E3 ubiquitin ligase complex. We sequenced the coding region of the gene in 13 strains, including some wild-type strains, the original mutant strain, and several other strains that did not complement the original mutation for the LL phenotype. In six of the seven mutant strains, we found a phenylalanine-to-isoleucine substitution in a conserved LRR domain. In the remaining mutant strain, there was a serine-to-leucine substitution in an adjacent LRR domain (Fig. 1, C and D). The two mutations will be referred to as *common* and *rare* (*c* and *r*), respectively. The two alleles did not complement each other, nor did they complement chromosomal deletions that remove the *jet* locus (Table 1).

The JET protein contains an N-terminal F-box domain thought to be involved in binding the Skp1 component of the SCF complex, as well as seven LRRs constituting a protein-protein interaction domain thought to be involved in target recognition (*12*) (Fig. 1C). Functions of the mammalian F-box proteins with highest similarity to JET (F-box and LRR protein 15) have yet to be determined.

Almost all (>96%) of the *jet*^{r} and *jet*^{c} flies had rhythmic behavior in LL, whereas very few of the wild-type control flies did (Table 1). In contrast, the mutants' behavior was indis-

Table 1. Activity rhythms of *jet* mutants. For each fly, the free-running period was determined with the use of χ^2 periodogram analysis. FFT, determined by fast Fourier transform analysis, is a measure of rhythm strength.

Genotype	DD			LL		
	% Rhythmic (n)	Period ± SEM (hours)	FFT ± SEM	% Rhythmic (n)	Period ± SEM (hours)	FFT ± SEM
Control-*r*	97.7 (44)	23.75 ± 0.08	0.141 ± 0.008	5.6 (18)	23.5	0.045
jet^r	95.7 (69)	23.65 ± 0.07	0.148 ± 0.008	96.9 (32)	24.29 ± 0.15	0.168 ± 0.012
Control-*c*	100 (46)	24.00 ± 0.09	0.165 ± 0.008	0 (16)		
jet^c	96.2 (42)	24.20 ± 0.07	0.143 ± 0.008	100 (15)	23.57 ± 0.13	0.200 ± 0.018
jet^r/*jet*^{c}	100 (22)	23.91 ± 0.09	0.166 ± 0.014	100 (16)	24.34 ± 0.11	0.171 ± 0.013
Df/+*	89.5 (19)	23.71 ± 0.12	0.206 ± 0.013	4.3 (23)	24.5	0.079
Df/*jet*^{r}*	100 (44)	23.74 ± 0.09	0.172 ± 0.010	93.8 (16)	23.93 ± 0.15	0.228 ± 0.017
Df1/*jet*^{c}†	100 (15)	23.70 ± 0.11	0.150 ± 0.016	100 (22)	23.31 ± 0.19	0.148 ± 0.009
Df2/*jet*^{c}†	100 (17)	23.74 ± 0.11	0.161 ± 0.014	100 (25)	22.74 ± 0.15	0.178 ± 0.012

*Comparable results were obtained with two overlapping deficiencies [*Df(2L)Exel8012* and *Df(2L)Exel7021*] that remove the *jet* locus; pooled data are presented. †One of the deficiencies [*Df2*: *Df(2L)Exel7021*] over *jet*^{c} produced a shorter period in LL than the other [*Df1*: *Df(2L)Exel8012*], and data are presented separately.

tinguishable from wild-type behavior in DD, which suggests that the mutants have a largely intact circadian system with a specific defect in the light input pathway. Consistent with its limited role in free-running rhythms, the *jet* mRNA does not cycle in a circadian fashion (*13*) (fig. S1). The reduced light sensitivity of *jet* mutants is similar to that of *cry* mutants; however, unlike *cry* mutants (*11*), *jet* mutants showed rhythmic activity of a luciferase reporter for a clock gene, *period* (*per*) (*14*), in DD, which suggests that their peripheral clocks function normally (Fig. 1E). Because luciferase is assayed in whole flies and therefore reports the activity of multiple peripheral clocks, rhythmic luciferase activity in *jet* mutants also indicates synchrony among these clocks. Peripheral clocks can be entrained to an LD cycle via CRY-independent pathways (*15*), which may account for the synchrony of peripheral clocks in *jet* mutants. Loss of *per*-luciferase cycling in *cry* mutants most likely occurs because CRY, in addition to its role as a circadian photoreceptor, has a role in the regulation of core clock components in the periphery (*16*).

To characterize the behavioral light sensitivity of *jet* mutants in more detail, we measured phase shifts in response to brief light pulses at night. *jet* mutants had significantly reduced phase shifts relative to wild-type control flies (Fig. 2A). Expression of wild-type JET from a *UAS-jet* transgene under the control of a *cry*- or *tim-Gal4* driver partially rescued the mutant phenotype (Fig. 2B). The increase in phase shifts was greater with *tim-Gal4* than with *cry-Gal4*, probably because the former is a stronger driver. Together with the sequence data described above, the rescue results provide strong evidence that the mutations in the *jet* locus are responsible for the observed mutant phenotypes.

To determine the molecular correlates of the behavioral defects, we examined the changes in TIM levels in central clock neurons after brief light pulses. Light-dependent degradation of TIM was substantially reduced in *jet* mutants (Fig. 2C) and was restored in rescued flies expressing the *UAS-jet* transgene (Fig. 2D), which suggests that the behavioral defects in the mutants are mediated by defects in TIM degradation. Light-dependent TIM degradation was also reduced in head extracts of mutants (fig. S2), implying that JET facilitates TIM degradation in the peripheral clock in the eye as well.

To further explore the role of JET in TIM degradation, we next turned to an S2R+ *Drosophila* embryonic cell line. Unlike in the fly, in S2R+ cells, TIM does not degrade in response to light (*7*) (Fig. 3A). To test whether JET is the crucial component missing in these cells, we expressed JET with the use of a constitutive promoter. The JET protein had little effect on TIM levels in the dark, but it rapidly reduced TIM levels upon light exposure (Fig. 3A and fig. S3A). This light-induced degradation of TIM required coexpression of CRY and was blocked by a proteasome inhibitor, MG132. JET did not promote degradation of another core clock protein, PER (Fig. 3B), demonstrating specificity for its target selection. In addition, light-dependent degradation of CRY did not require JET (Fig. 3A and fig. S3B), although it was facilitated by JET in the presence of TIM (Fig. 3, A and B). The JET protein itself was also not affected by light in S2R+ cells (Fig. 3A).

One of the mutant versions of the protein (the *r* allele) was significantly less effective than wild-type JET at promoting TIM degradation (Fig. 3C and fig. S3C). The *r* mutation reduced the stability of the JET protein (Fig. 3C and fig. S3D), which may explain its mutant phenotype. The other mutant allele (*c*) was also less effective than the wild-type allele, although the difference was not statistically significant. The *r* mutation is in a residue conserved among insects and mammals, but the *c* mutation is in a residue conserved only among insects (Fig. 1D), which may explain the stronger effects of the *r* allele in both behavioral and molecular assays.

Wild-type JET protein also promoted ubiquitination of TIM in cultured cells. In the presence of wild-type JET and CRY, a significant increase in TIM ubiquitination was observed after only 10 min of exposure to light (Fig. 3D and fig. S3E). Mutant proteins, especially the *r* allele, were less effective at ubiquitination of TIM (*17*). Consistent with its role as a component of an SCF complex, JET interacts with SkpA, one of several Skp1 homologs in *Drosophila* (Fig. 3E). In addition,

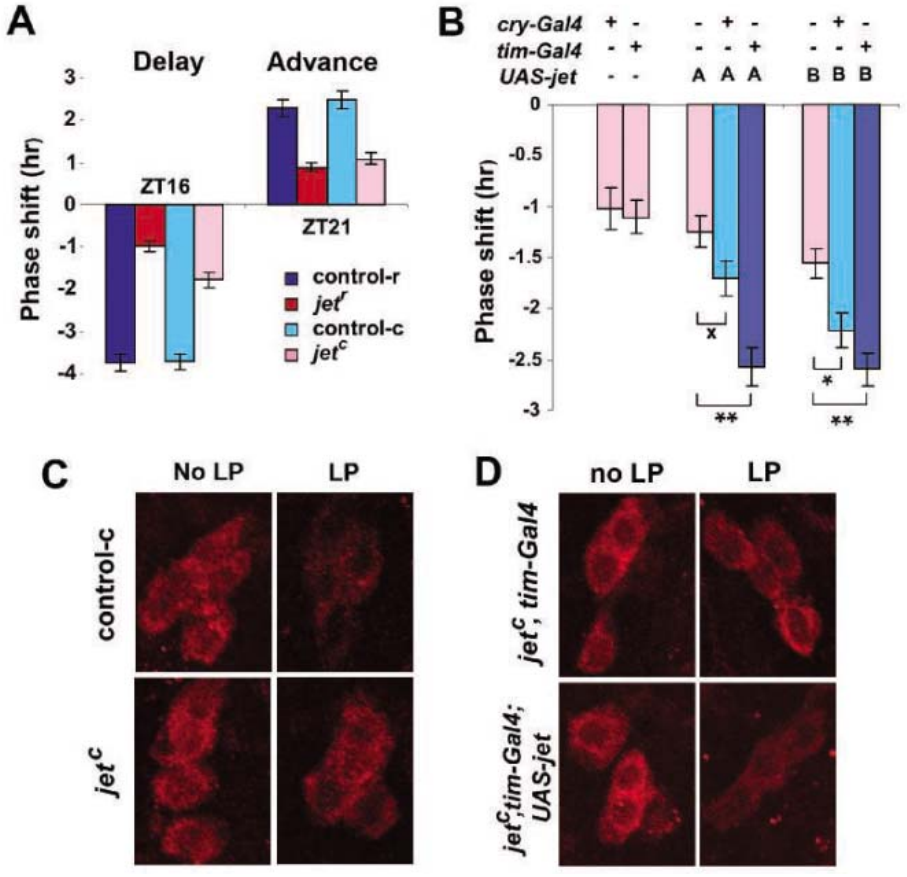

Fig. 2. Reduced responses to light pulses in *jet* mutant flies. (**A**) Behavioral response to phase-delaying and phase-advancing light pulses. All differences between control and mutant flies for both alleles and both zeitgeber times (ZTs) were significant [$P < 0.0001$ by analysis of variance (ANOVA)]. In this and subsequent figures, error bars denote SEM. (**B**) Rescue of reduced light sensitivity of *jet* mutants with a *UAS-jet* transgene. Phase delays in response to light pulses at ZT 16 in *jet*^{c} flies with a *UAS-jet* transgene and either a *cry*- or *tim-Gal*4 driver were assayed as in (A). Two independent *UAS-jet* lines, A and B, produced similar results. $^x P = 0.06$, $^* P < 0.01$, $^{**} P < 0.001$ by ANOVA. (**C**) Reduced light-dependent degradation of TIM in clock neurons of *jet*^{c} mutants. Representative TIM staining in small ventral lateral neurons is shown 1 hour after a 2-min light pulse (LP) at ZT 16. TIM staining without LP is shown for comparison; 8 to 10 fly brains were examined per condition. (**D**) Rescue of the TIM response to light in clock neurons of *jet*^{c} mutants with a *UAS-jet* transgene. *jet*^{c} mutants with a *tim-Gal4* driver alone or with a *UAS-jet* transgene and a *tim-Gal4* driver were assayed as in (C).

JET physically associates with TIM, and the association is stronger in light than in dark (Fig. 3F and fig. S3F).

Flies share many of the core clock components with mammals (*18*), but their mechanism for light-induced phase resetting appears to differ. Circadian photoreception in mammals relies on adenosine 3′,5′-monophosphate response element–binding protein (CREB)–mediated induction of mPer-1 transcription (*19*, *20*) and does not appear to involve CRY (*21*). Fly circadian photoreception resembles that of plants, where CRY functions as a circadian photoreceptor, although the mechanism is somewhat different from that of *Drosophila* CRY (*4*, *22*). Notably, the plant F-box protein ZEITLUPE mediates dark-dependent degradation of the clock protein TIMING OF CAB EXPRESSION 1 (*23*).

jet mutants did not show any detectable defects in the free-running rhythm in constant darkness. We propose that the *Drosophila* circadian system uses two separate mechanisms for controlling TIM levels: a clock-controlled one for maintaining rhythm in the dark, and a light-dependent one for entraining the clock to the photic environment. Both mechanisms use SCF complexes but with distinct F-box proteins: SLIMB for the clock-controlled mechanism (*24*, *25*) and JET for the light-dependent mechanism.

We have identified a component of the *Drosophila* light entrainment pathway that is critical for light-induced degradation of TIM. Single amino acid substitutions in JET lead to molecular and behavioral defects in light entrainment. Our results, together with those of previous studies, suggest the following model of how light resets the clock in *Drosophila*. Upon light exposure, CRY undergoes conformational change, allowing it to bind TIM (*4*–*8*). TIM is then modified by phosphorylation (*7*), which allows JET to target TIM for ubiquitination and rapid degradation by the proteasome pathway.

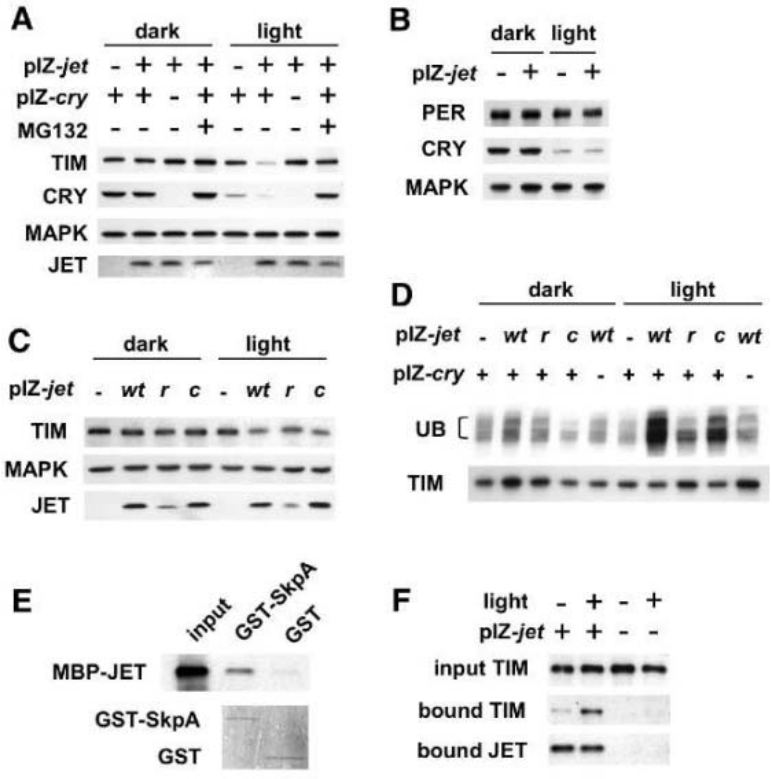

Fig. 3. Light-dependent degradation of TIM in S2R+ cells. (**A**) Light-induced degradation of TIM is mediated by CRY, TIM, and the proteasome pathway. S2R+ cells were transiently transfected with pAc-*tim* along with the pIZ vector or FLAG epitope–tagged pIZ-*jet* (pIZ-FLAG-*jet*), with or without MYC epitope–tagged pIZ-*cry* (pIZ-MYC-*cry*). MYC-CRY and FLAG-JET protein levels were determined with antibodies to MYC and JET, respectively. (**B**) JET does not promote degradation of PER. Hemagglutinin (HA)–tagged pAct-*per* and pIZ-MYC-*cry* were transfected with or without pIZ-FLAG-*jet*. (**C**) Mutant JET proteins are less effective at promoting TIM degradation than wild-type JET, and the *r* version of mutant JET is less stable than wild-type JET. Cells were transfected with pIZ or pIZ-FLAG-*jet* (wild-type or mutant) at one-fifth the concentration used in (A) along with pIZ-*tim* and pIZ-MYC-*cry*. (**D**) JET promotes light-dependent ubiquitination of TIM. S2R+ cells were transfected with HA-tagged ubiquitin (UB) under the control of a heat shock promoter along with pAc-*tim* and wild-type or mutant pIZ-FLAG-*jet*, with or without pIZ-MYC-*cry*. Transfected cells were kept at 25°C. Cell extracts were immunoprecipitated with antibody to TIM, and the relative amounts of ubiquitinated TIM were measured with antibodies to HA and TIM. (**E**) JET interacts with SkpA in vitro. Purified JET protein fused to maltose binding protein (MBP) was incubated with either glutathione S-transferase (GST) or GST-SkpA fusion protein. MBP-JET was detected with an antibody to JET (top), and GST and GST-SkpA were visualized by Coomassie staining (bottom). (**F**) JET physically associates with TIM in S2R+ cells in a light-dependent manner. Extracts from cells transfected with pAc-*tim*, pIZ-MYC-*cry*, and pIZ or pIZ-FLAG-*jet* were immunoprecipitated with antibody to FLAG, and TIM and JET levels were measured. Experiments in each panel were repeated three to five times with similar results. Data are quantified in fig. S3.

References and Notes

1. P. E. Hardin, *Curr. Biol.* **15**, R714 (2005).
2. S. Panda, J. B. Hogenesch, S. A. Kay, *Novartis Found. Symp.* **253**, 73 (2003).
3. L. J. Ashmore, A. Sehgal, *J. Biol. Rhythms* **18**, 206 (2003).
4. A. Busza, M. Emery-Le, M. Rosbash, P. Emery, *Science* **304**, 1503 (2004).
5. S. Dissel *et al.*, *Nat. Neurosci.* **7**, 834 (2004).
6. M. F. Ceriani *et al.*, *Science* **285**, 553 (1999).
7. N. Naidoo, W. Song, M. Hunter-Ensor, A. Sehgal, *Science* **285**, 1737 (1999).
8. F. J. Lin, W. Song, E. Meyer-Bernstein, N. Naidoo, A. Sehgal, *Mol. Cell. Biol.* **21**, 7287 (2001).
9. Z. Yang, M. Emerson, H. S. Su, A. Sehgal, *Neuron* **21**, 215 (1998).
10. V. Suri, Z. Qian, J. C. Hall, M. Rosbash, *Neuron* **21**, 225 (1998).
11. R. Stanewsky *et al.*, *Cell* **95**, 681 (1998).
12. T. Cardozo, M. Pagano, *Nat. Rev. Mol. Cell Biol.* **5**, 739 (2004).
13. M. F. Ceriani *et al.*, *J. Neurosci.* **22**, 9305 (2002).
14. R. Stanewsky, C. F. Jamison, J. D. Plautz, S. A. Kay, J. C. Hall, *EMBO J.* **16**, 5006 (1997).
15. M. Ivanchenko, R. Stanewsky, J. M. Giebultowicz, *J. Biol. Rhythms* **16**, 205 (2001).
16. B. Collins, E. O. Mazzoni, R. Stanewsky, J. Blau, *Curr. Biol.* **16**, 441 (2006).
17. Although light-induced TIM ubiquitination, but not degradation, was previously observed without cotransfected JET (*7*, *8*), we did not detect significant ubiquitination under these conditions. This discrepancy may arise from procedural differences (e.g., use of S2R+ cells instead of S2 cells, or the fact that we did not apply heat to induce expression of hemagglutinin-tagged ubiquitin).
18. J. C. Hendricks, A. Sehgal, *Sleep* **27**, 334 (2004).
19. S. A. Tischkau, J. W. Mitchell, S. H. Tyan, G. F. Buchanan, M. U. Gillette, *J. Biol. Chem.* **278**, 718 (2003).
20. Z. Travnickova-Bendova, N. Cermakian, S. M. Reppert, P. Sassone-Corsi, *Proc. Natl. Acad. Sci. U.S.A.* **99**, 7728 (2002).
21. A. Sancar, *Chem. Rev.* **103**, 2203 (2003).
22. H. Q. Yang *et al.*, *Cell* **103**, 815 (2000).
23. P. Mas, W. Y. Kim, D. E. Somers, S. A. Kay, *Nature* **426**, 567 (2003).
24. B. Grima *et al.*, *Nature* **420**, 178 (2002).
25. H. W. Ko, J. Jiang, I. Edery, *Nature* **420**, 673 (2002).

26. We thank P. Emery for the *cry-Gal4* strain, J. Nambu for the GST-SkpA construct; the Bloomington Stock Center for fly strains; J. Evans, Z. Yue, and D. Chen for technical assistance; S. Sathyanarayanan for help with cell culture experiments; Y. Fang for the pIZ-MYC-*cry* construct; K. Ho, N. Naidoo, and Q. Yuan for comments on the manuscript; and other members of the lab for discussions. Supported by NIH grant NS048471 (A.S.). A.S. is an Investigator of the Howard Hughes Medical Institute.

Supporting Online Material

www.sciencemag.org/cgi/content/full/312/5781/1809/DC1
Materials and Methods
Figs. S1 to S3
References

13 January 2006; accepted 17 May 2006
10.1126/science.1124951

Affinity Chromatography Media

The ProSep range of chromatography media is designed primarily for affinity purification of antibodies, other proteins, and nucleic acids. ProSep media make use of porous glass as the support, permeated by interconnecting pores of uniform size. ProSep chromatography media exhibit chemical and mechanical stability over a range of conditions such as exposure to low pH, detergents, buffers of varying ionic strengths, and many organic solvents. They permit high flow rates with low back pressure. ProSep-vA Ultra is designed to facilitate efficient purification of antibodies. ProSep-G is for the purification of antibodies that do not bind efficiently to protein A, such as rat IgGs and human IgG3. ProSep-PB is designed for the affinity chromatography of a variety of glycoproteins, nucleic acids, and other biomolecules containing 1,2 diol functionality.

Millipore For information 800-MILLIPORE www.millipore.com/bioscience

Hollow Fiber Bioreactor

The hollow fiber bioreactor is an in vitro method for producing milligram to gram quantities of monoclonal antibodies (mAbs). Traditional mAb production uses static cultures that create conditions in which waste accumulates and secreted protein production is lower. In contrast, hollow fiber is modeled after the mammalian circulatory system to create an optimal growth environment for cells to decrease large-scale production time. Although hollow fiber is an established technology, advances in fiber materials have improved productivity, allowing for denser cell growth. Other benefits include elimination of murine contaminants and the ability to adapt cells to serum-free media.

Covance For information 800-345-4114 www.CRPinc.com

Focus Feedback System

The Continuous Reflective Interface Focus Feedback (CRIFF) system substantially eliminates focus drift in high-power microscopy by sensing minute changes between the objective lens and the specimen's cover slip, and then providing a feedback signal to any of Applied Scientific Instrumentation's focus controllers. The CRIFF system provides high level focus stability for hours at a time with less than 50 nm of drift caused by temperature or mechanical variations. The CRIFF module fits on the camera port of most microscopes.

ASI/Applied Scientific Instrumentation For information 541-461-8181 www.ASIimaging.com

Experiment Design Software

Design-Expert 7.0 software for statistical design of experiments offers dozens of new features for design and analysis of experiments. Minimum-run two-level factorial designs allow users to screen for main effects with the least number of experimental runs. New analysis tools include the Pareto chart of effects, which allows users to easily see the vital few effects relative to the trivial many. Mixture-in-mixture designs are available for sophisticated experiments involving separate formulations that may interact. Additional features include design creation tools, enhanced design augmentation ability, analysis capabilities, diagnostic capabilities, improvements to the user interface, options for design evaluation, and new import/export tools.

Stat-Ease For information 612-378-9449 www.statease.com

Stem and Endothelial Cell Reagents

The CD133 unconjugated mouse monoclonal antibody, suitable for indirect protein immunoblot or immunofluorescent analysis, is a tool for the screening of CD133 antigen expression in different human tissues and cell lines. The CD133 antigen is specifically expressed on early stem cells from many cell sources, including bone marrow, umbilical cord blood, and brain tissue. The CD31 MicroBead Kit is for the isolation of human microvascular and umbilical vein epithelial cells. The kit has been developed for the magnetic isolation of CD31+ cells from human foreskin biopsies or umbilical cord vein for in vitro cultivation. Purified CD31+ cells represent a key model for cardiovascular research and endothelial dysfunction in atherosclerosis.

Miltenyi Biotech For information +49 2204-8306-0 www.MiltenyiBiotec.com

Literature

Bioinformation and Text Mining Solutions for Biomedical Discovery is a brochure that describes the AlmaKnowledgeServer (AKS) for biomedical literature mining, CodeQuest biocomputing workstation, and DeCypher enterprise informatics solutions. AKS is a text mining system that examines all abstracts added to PubMed, then applies statistics and rules-based analysis to uncover relationships in the scientific literature between genes, proteins, chemical compounds, and diseases. The CodeQuest workstation enables the user to easily compare sequence collections to major genomic databases without the frustration and expense of setting up a computer cluster. It efficiently processes a suite of powerful sequence comparison applications on its high-performance DeCypher Engine accelerator card. DeCypher is a set of software applications designed to run on powerful accelerator hardware. It outperforms computer clusters for applications like BLAST, HMM, Smith-Waterman, repeat masking, and gene modeling.

Active Motif For information 877-222-9543 www.timelogic.com

Newly offered instrumentation, apparatus, and laboratory materials of interest to researchers in all disciplines in academic, industrial, and government organizations are featured in this space. Emphasis is given to purpose, chief characteristics, and availability of products and materials. Endorsement by *Science* or AAAS of any products or materials mentioned is not implied. Additional information may be obtained from the manufacturer or supplier by visiting www.science.labvelocity.com on the Web, where you can request that the information be sent to you by e-mail, fax, mail, or telephone.

ScienceCareers.org

Classified Advertising

For full advertising details, go to **www.sciencecareers.org** and click on **For Advertisers,** or call one of our representatives.

United States & Canada

E-mail: advertise@sciencecareers.org
Fax: 202-289-6742

JILL DOWNING
(CT, DE, DC, FL, GA, MD, ME, MA, NH, NJ, NY, NC, PA, RI, SC, VT, VA)
Phone: 631-580-2445

KRISTINE VON ZEDLITZ
(AK, AZ, CA, CO, HI, ID, IA, KS, MT, NE, NV, NM, ND, OR, SD, TX, UT, WA, WY)
Phone: 415-956-2531

KATHLEEN CLARK
Employment: AR, IL, LA, MN, MO, OK, WI
Canada; Graduate Programs; Meetings & Announcements (U.S., Canada, Caribbean, Central and South America)
Phone: 510-271-8349

DARYL ANDERSON
(AL, IN, KY, MI, MS, OH, TN, WV)
Phone: 202-326-6543

GABRIELLE BOGUSLAWSKI
(U.S. Recruitment Advertising Sales Director)
Phone: 718-491-1607

Europe & International

E-mail: ads@science-int.co.uk
Fax: +44 (0) 1223-326-532

TRACY HOLMES
Phone: +44 (0) 1223-326-525

HELEN MORONEY
Phone: +44 (0) 1223-326-528

CHRISTINA HARRISON
Phone: +44 (0) 1223-326-510

SVITLANA BARNES
Phone: +44 (0) 1223-326-527

JASON HANNAFORD
Phone: +81 (0) 52-789-1860

To subscribe to *Science*:
In U.S./Canada call 202-326-6417 or 1-800-731-4939
In the rest of the world call +44 (0) 1223-326-515

Science makes every effort to screen its ads for offensive and/or discriminatory language in accordance with U.S. and non-U.S. law. Since we are an international journal, you may see ads from non-U.S. countries that request applications from specific demographic groups. Since U.S. law does not apply to other countries we try to accommodate recruiting practices of other countries. However, we encourage our readers to alert us to any ads that they feel are discriminatory or offensive.

ScienceCareers.org
We know science
AAAS

POSITIONS OPEN

UT SOUTHWESTERN MEDICAL CENTER

CENTER FOR IMMUNOLOGY POSITIONS

The Center for Immunology at the University of Texas (UT) Southwestern Medical Center at Dallas is seeking highly qualified applicants for **ASSISTANT, ASSOCIATE,** and **FULL PROFESSOR** faculty positions. Candidates with interest in the molecular mechanisms of infectious disease are encouraged to apply, but strong applicants from other areas will also be considered. Salary and startup packages are highly competitive. All applicants must have a Ph.D. and/or M.D. and have an outstanding track record in research. The appointee will be expected to either develop a competitive, independently funded research program or, if at the Associate or Full Professor level, to have a proven ability to attract external funds. Please send curriculum vitae, a three to five-page summary of proposed research interests, and the names and addresses of three references to:

Center for Immunology
c/o Renee Gugino
University of Texas Southwestern Medical Center
5323 Harry Hines Boulevard
Dallas, TX 75390-9093
E-mail: renee.gugino@utsouthwestern.edu

Review of applications will start July 15, 2006, and will continue until the positions are filled.

UT Southwestern Medical Center is an Equal Opportunity Employer.

A **POSTDOCTORAL POSITION** is available to study the mechanisms of multidrug resistance. Projects involve biochemical and structural characterizations of multidrug binding transcription regulators from pathogenic bacteria. Applicants must have significant and meaningful experience in protein purification and a strong understanding of protein structure-function relationships. Those with doctorates in biochemistry, chemistry, or macromolecular x-ray crystallography or other structure determination methodologies are most appropriate. Please send your curriculum vitae, a brief description of your research accomplishments and interests, and the names and e-mail addresses of three references to: **Dr. Richard G. Brennan, Department of Biochemistry and Molecular Biology, Unit 1000, The University of Texas M. D. Anderson Cancer Center, 1515 Holcombe Boulevard, Houston, TX 77030; e-mail: rgbrenna@mdanderson.org.**

M.D. Anderson Cancer Center is an Equal Opportunity Employer and does not discriminate on the basis of race, color, national origin, gender, sexual orientation, age, religion, disability, or veteran status except where such distinction is required by law. All positions at the University of Texas M. D. Anderson Cancer Center are security sensitive and subject to examination of criminal history record information. The University of Texas M. D. Anderson Cancer Center is a smoke-free and drug-free environment.

A **POSTDOCTORAL POSITION IN MICROBIAL GENETICS** is available to investigate gene regulation in Haemophilus ducreyi, the etiologic agent of chancroid. Emphasis will be placed on the elucidation of the regulatory mechanism(s) by which H. ducreyi controls the differential expression of the LspA1 and LspA2 proteins; these exoproteins are major virulence determinants. Position requires a Ph.D. in microbiology, biochemistry, genetics, or a related biological science and experience with recombinant DNA techniques. Position includes salary, fringe benefits, and the opportunity to work in a dynamic research environment. Send curriculum vitae and the names and telephone numbers of three references to: **Dr. Eric J. Hansen, Department of Microbiology, The University of Texas Southwestern Medical Center at Dallas, 5323 Harry Hines Boulevard, Dallas, TX 75390-9048. Fax: 214-648-5905. E-mail: eric.hansen@utsouthwestern.edu.**

University of Texas Southwestern is an Equal Opportunity/ Affirmative Action Employer.

POSITIONS OPEN

Fluidigm

PROTEIN EXPRESSION APPLICATIONS SCIENTIST (Job Code: 2006-29-SCI)

Fluidigm Corporation, a Red Herring award winner, seeks an experienced professional to develop assay formats and sample preparation methods while implementing a wide variety of immunoassays on Fluidigm's microfluidic platform. Must be an expert scientist with deep experience using and optimizing immuno assays, including antibody selection, sensitivity enhancement, background reduction, and reporter formats. Requires a Ph.D. in molecular biology, biochemistry or chemistry, or equivalent experience in a commercial setting; over seven years of experience in assay development and commercialization; a track record of success in project leadership and external collaborations; the demonstrated ability to independently run experiments, analyze data, interpret results, and modify procedures; hands-on experience developing/designing procedures for commercial customers; and knowledge of statistics. Fluidigm offers a collegial work environment, excellent salary and benefits, and pre-IPO stock options. Reference job code 2006-29-SCI and e-mail your resume and cover letter to **e-mail: jobs@fluidigm.com.** For a complete list of all our current openings, visit **website: http://www.fluidigm.com.** *Equal Opportunity Employer.*

FACULTY POSITIONS IN PHARMACEUTICS/DRUG DELIVERY
Department of Pharmaceutical and Biomedical Sciences
College of Pharmacy, University of Georgia

The Department of Pharmaceutical and Biomedical Sciences at the University of Georgia, Athens, invites applications for two full-time, tenure-track faculty positions (one **ASSISTANT PROFESSOR** and one **ASSOCIATE/FULL PROFESSOR**) in the areas of drug delivery/nanotechnology, drug targeting/drug transport. Applicants should possess a Ph.D. or Pharm.D./Ph.D. or equivalent degree with pharmaceutical sciences or a closely related area as the focus of their graduate education and research training. Excellent communication skills and the ability to teach basic pharmaceutics and drug delivery concepts at both the Pharm.D. and Ph.D. levels are required. Each successful applicant is expected to have or to develop a dynamic, extramurally funded research program in an area identified above. To be assured of full consideration, applications should be received by September 1, 2006. Interested qualified applicants should submit a letter of application, curriculum vitae, a research plan, and three confidential letters of recommendation to: **Chair, Pharmaceutics Search Committee, Department of Pharmaceutical and Biomedical Sciences, R.C. Wilson Pharmacy Building, University of Georgia, Athens, GA 30602-2352.** Applicants may also apply online to **e-mail: pbssearch@rx.uga.edu.** *The University of Georgia is an Equal Employment Opportunity/ Affirmative Action Employer. Applications from qualified women and minority candidates are encouraged.*

UNIVERSIDAD DE LOS ANDES
Faculty Positions

The Department of Chemistry at the Universidad de los Andes in Bogota D.C., Colombia (South America), invites applications for full-time **PROFESSOR** positions in the areas of biochemistry, organic chemistry, and geochemistry. Applicants should have a Ph.D. degree in the area of interest. Candidates must be committed to excellence in teaching and research. Applicants should submit detailed curriculum vitae and make arrangements to have recommendation letters sent to **e-mail: jumoreno@uniandes.edu.co.**

UT-ORNL
Governor's Chairs

The University of Tennessee in partnership with the Oak Ridge National Laboratory is recruiting leading scientists to conduct research in the Joint Institute for Computational Sciences with access to some of the most advanced scientific and computational tools available. In addition to working in an exciting atmosphere of intellectual and academic freedom, you would be living in one of the most beautiful areas in the country with easy access to miles of inland waterways, pristine state and national parks, diverse cultural opportunities, and a unique mix of convenient urban and rural living settings.

Find out more at http://www.tennessee.edu/governorschairs/

Governor's Chairs in the UT-ORNL Joint Institute for Computational Sciences

The State of Tennessee is investing in 20 exceptionally accomplished researchers who will have joint appointments as tenured professors at the University of Tennessee (UT) and distinguished research staff at the Oak Ridge National Laboratory (ORNL). This Governor's Chair (GC) program seeks to catalyze the development of leading edge research under the auspices of four joint institutes between UT and ORNL: Biological Sciences, Computational Sciences, Neutron Sciences, and Advanced Materials Sciences. The GC appointments include an ongoing discretionary research fund equal to twelve months salary.

The Joint Institute for Computational Sciences (JICS)
JICS will support both fundamental and applied research and teaching programs in computational sciences, computational mathematics, computer science, high performance computing, storage and networking, and cyber security.

UT and ORNL have strong research efforts in these areas. The research environment favors cross-disciplinary, leading-edge efforts that leverage special facilities in the physical and computational sciences. World-class research facilities include the DOE Leadership Computing Facility (LCF). LCF is planning the acquisition and deployment of a 250TF high-performance computing (HPC) system by 2007 and a 1000TF (PF) system by 2008. It is expected that JICS will focus on application and system software essential to optimal sustained performance at the petascale to enable a range of computationally challenging science and engineering applications.

The UT-ORNL environment nurtures a rich interdisciplinary community of researchers with common interests and collaborative projects. The UT-ORNL research enterprise has more than $2 billion in investments in some of the world's most advanced research facilities.

There are immediate openings for Governor's Chairs in the following areas:

Science and engineering applications – Applications are sought from candidates interested in:

- **Computational science at the petascale in the physical, biological, and environmental sciences**

Computer science applications – Applications are sought from candidates interested in developing:

- **Algorithms, methods, and libraries**
- **Component-based, petascale program development and tools**
- **Systems software that scale to hundreds-of-thousands of processors**
- **Scalable systems for moving, storing, and analyzing data**

Successful candidates will have an exceptional record of scientific productivity and accomplishment, as manifested, for example, in high-impact publications, scientific awards, or Fellow status in scientific and engineering societies. Successful candidates will also have a demonstrated record of leading cross-disciplinary teams of researchers and of developing substantial externally-funded research programs.

APPLICATIONS: Applicants should submit a letter of interest and a curriculum vita to: Dr. Thomas Zacharia, Chair, JICS-Governor's Chair Search Committee, Computing and Computational Sciences, Oak Ridge National Laboratory, P.O. Box 2008, Oak Ridge, TN 37831-6163; zachariat@ornl.gov. Screening of applications will commence on July 1, 2006, and will continue until the positions are filled. The University of Tennessee is an EEO/AA/Title VI/ Title IX/Section 504/ADA/ADEA institution in the provision of its education and employment programs and services.

Scientists and engineers at the Oak Ridge National Laboratory and the University of Tennessee conduct basic and applied research and development to create scientific knowledge and technological solutions that strengthen the nation's leadership in key areas of science; increase the availability of clean, abundant energy; restore and protect the environment; and contribute to national security. UT and ORNL provide an environment that encourages collaborative research and development. UT-Battelle manages and operates ORNL under contract DE-AC05-000R22725.

UT-BATTELLE

THE UNIVERSITY of TENNESSEE

OAK RIDGE National Laboratory

Positions @ NIH
THE NATIONAL INSTITUTES OF HEALTH

Department of Health and Human Services
National Institutes of Health
Director, National Center for Research Resources

The Office of the Director, National Institutes of Health (NIH) in Bethesda, Maryland, is seeking applications from exceptional candidates for the position of Director, National Center for Research Resources (NCRR). The Director, NCRR, will also serve as the NIH Associate Director for Clinical Research (Extramural). NCRR, with a staff of approximately 100 employees and a $1 billion budget, is the focal point at NIH for biomedical, clinical and translational research resources. The incumbent serves as a principal advisor to the Director, NIH; participates in discussions relative to the development of major policy decisions affecting biomedical, clinical and translational research resources; provides advice and consultation to NIH components, advisory councils and grantee organizations and institutions; and assures that effective administrative procedures are established so that program operations and obligations of government funds and other resources are rendered consistent with statutory and regulatory requirements and within limitations imposed by the Department of Health and Human Services (DHHS) and Executive Branch policies. Applicants must possess a Ph.D., M.D., or a comparable doctorate degree in the health sciences field plus senior level scientific experience and knowledge of biomedical, clinical and/or translational research programs in one or more health science areas. Salary is commensurate with experience and a full package of benefits (including retirement, health, life, long term care insurance, Thrift Savings Plan participation, etc.) is available. A detailed vacancy announcement, along with mandatory qualifications and application procedures, can be obtained via the NIH Home Page at: http://www.jobs.nih.gov under the Senior Job Openings section. Dr. Stephen Katz, Director, National Institute of Arthritis and Musculoskeletal and Skin Diseases, and Dr. David Schwartz, Director, National Institute of Environmental Health Sciences, will be serving as co-chairs of the search committee. Questions on application procedures may be addressed to Ms. Regina Reiter at ReiterR@od.nih.gov or discussed with Ms. Reiter by calling 301-402-1130. **Applications must be received by close of business July 31, 2006.**

Staff Scientist, Clinical Pharmacology Research Core, Medical Oncology Branch

With nation-wide responsibility for improving the health and well being of all Americans, The Department of Health and Human Services oversees the biomedical research programs of the National Institutes of Health and those of NIH's research Institutes.

A Staff Scientist position is now available in the Clinical Pharmacology Research Core (CPRC), Medical Oncology Branch (MOB) of the Center for Cancer Research (CCR), National Cancer Institute (NCI), National Institute of Health (NIH), Department of Health and Human Services (DHHS). This position will focus on pharmacological aspects of clinical trials, including pharmacokinetic and pharmacogenetic studies.
Leadership in clinical pharmacology is required. Expertise in pharmacokinetics, including bioanalytical techniques, modeling of pharmacokinetic data, data analysis and study design, and pharmacogenetics is required.

The CCR provides an environment in which interdisciplinary and multidisciplinary translational research is encouraged and supported and uses a disease-based translational research matrix to identify the intersection of research areas and particular cancers to identify programmatic efforts. These specific program areas will enhance and enable collaborations, interdisciplinary and multidisciplinary research and a dynamic translational research process in which discovery, development and delivery flow seamlessly.

The successful candidate must have a Ph.D., Pharm.D., or MD degree (or equivalent).

The NCI offers competitive salaries along with an excellent work environment.

Interested applicants should send a CV, brief description of research interests and experience, and contact information for three references by **July 31, 2006** to: **Dr. William Douglas Figg, Medical Oncology Branch, Center for Cancer Research, National Cancer Institute, Building 10, Room 5A01, 9000 Rockville Pike, Building 10, Room 5A01, Bethesda, MD, 20892**.

WWW.NIH.GOV

Director, National Institute of Diabetes and Digestive and Kidney Diseases (NIDDK)
National Institutes of Health
Department of Health and Human Services

NIDDK

The Office of the Director, National Institutes of Health (NIH) is seeking exceptional candidates for the position of Director, National Institute of Diabetes and Digestive and Kidney Diseases (NIDDK). The incumbent serves as the leader of an organization that conducts and supports biomedical and behavioral research to understand, treat, and prevent some of the most common and severe diseases affecting public health today, and disseminates these research findings and health information to the public. The Director, NIDDK provides leadership for a national program in three major disease categories: 1) diabetes, endocrinology, and metabolic diseases; 2) digestive diseases and nutrition; 3) and kidney, urologic, and hematological diseases. This position offers a unique opportunity for the right individual to provide strong and visionary leadership for the Institute and to actively promote trans-NIH initiatives in the areas that promote the NIDDK mission, especially in the areas of diabetes and obesity for which NIDDK is the agency lead. Applicants must possess an M.D., Ph.D., or a comparable doctorate degree in the health sciences field plus senior-level scientific experience and outstanding scientific knowledge of research programs in one or more scientific areas related to diabetes, digestive diseases, and kidney diseases. Salary is commensurate with experience and a full package of benefits (including retirement, health and life insurance, long-term care insurance, Thrift Savings Plan participation, etc.) A detailed vacancy announcement, along with mandatory qualifications and application procedures, can be obtained via the NIH Home Page at: http://www.jobs.nih.gov under Executive Jobs section. We are pleased to announce that Dr. Anthony Fauci, Director, National Institute of Allergy and Infectious Diseases, and Dr. Francis Collins, Director, National Human Genome Research Institute, will be serving as co-chairs of the search committee. Questions on announcement procedures may be addressed to **Ms. Kim Westervelt at westervk@od.nih.gov** or discussed with **Ms. Westervelt by calling 301-402-4607**. **Applications must be received by close of business July 31, 2006**.

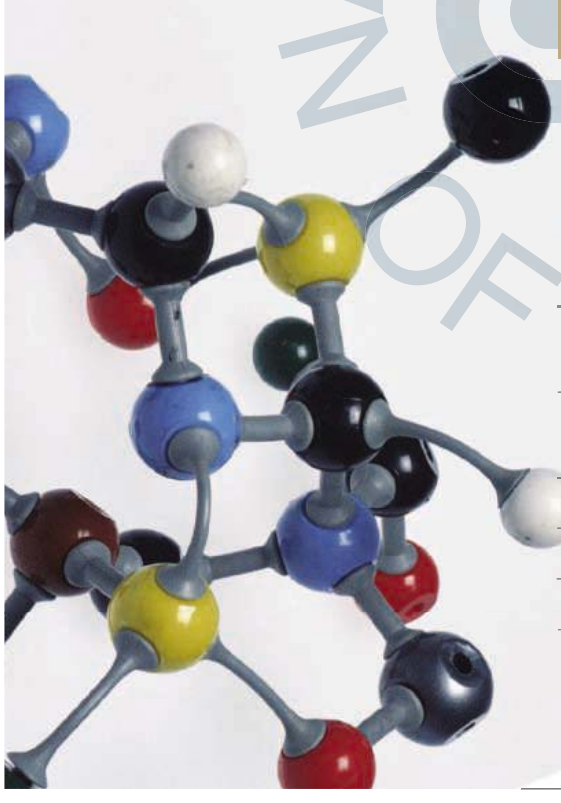

Postdoctoral Research Training at NIH

- Launch a career to improve human health
- Work in one of 1250 of the most innovative and well-equipped biomedical research laboratories in the world
- Explore new options in interdisciplinary and bench-to-bedside research
- Develop the professional skills essential for success
- Earn an excellent stipend and benefits
- Click on www.training.nih.gov

Office of Intramural Training and Education

Founded in 1807, John Wiley & Sons, Inc. is a global publisher of print and electronic products. We specialise in scientific, technical, and medical books and journals; professional and consumer books and subscription services; textbooks and other educational materials for undergraduate and graduate students as well as lifelong learners.

Due to rapid expansion plans, Wiley Asia is looking for dynamic professionals for the following challenging positions in Asia.

⇨ **Position:** **STM 3006 EDITORIAL DIRECTOR, STM INDIA (based in New Delhi)**

Reporting to the Publishing Director, Asia Pacific, you will lead and direct Wiley's Scientific, Technical, and Medical publishing activities in India, including: the recruitment of a world class editorial team; the management of existing relationships; the delivery of the targeted revenues and publishing activities for India; and the development of new business and publishing opportunities which enhance John Wiley's global STM programmes.

We're looking for:

- PhD or Masters Degree in Science or Engineering.
- Minimum 5 – 10 years experience in Publishing environment with successful track record in recruiting and leading a team.
- A proven team player with excellent interpersonal and leadership skills.
- Excellent track record in the development of new businesses.

⇨ **Positions:** **STM 3003 EXECUTIVE COMMISSIONING EDITOR (based in Beijing)**
STM 3004 COMMISSIONING EDITOR (based in Beijing)
STM 3010 COMMISSIONING EDITOR (based in New Delhi)

Reporting to the Editorial Director, STM (at the respective locations) you will be responsible for achieving the publishing activity objectives, acquiring content for books and journals for existing programs and developing new publications. You are also required to provide support and guidance to the editorial teams of other Wiley global publishing locations (USA, Europe, Asia Pacific) on their publications.

It is essential that you possess confidence and excellent communications skills in dealing with people at all levels. The key element of success in these roles is your ability to spot trends and exploit commercially viable market opportunities with energy and enthusiasm.

We're looking for:
For Position STM 3003,

- PhD or Masters in Chemistry or other physical science or engineering.
- Minimum 5 – 10 years experience in a Publishing environment.

For Position STM 3004,

- PhD or Masters in Engineering or in Technical discipline.
- Minimum 3 – 5 years experience in a commissioning role in STM Publishing environment.

For Position STM 3010,

- PhD or Masters in Scientific or in Engineering discipline.
- Minimum 3 – 5 years experience in Publishing environment. Candidates with international publishing experience will have an added advantage.

⇨ **Position:** **STM 3007 DIRECTOR OF MARKETING, STM (based in Singapore)**

This position reports to the Executive Director and will be responsible for the development and implementation of marketing strategies for Wiley's Scientific, Technical, Medical division in Asia. You will lead the marketing team in Asia to develop strategies to reach out to academic, practitioners, and scientists, for Wiley's print and online content; and work with counterparts in other global locations in Wiley to ensure strategies are aligned.

We're looking for:

- Bachelor Degree or equivalent, preferably in Science or Engineering discipline.
- Minimum 5 years experience in sales and marketing with successful track record of leading a team.
- A highly self-motivated professional with strong communications and interpersonal skills who can build and maintain relationships at all levels.
- A key element of success is your ability to inspire others to share your vision.
- Can travel extensively in Asia, North America, and the UK.

You may send your application stating your present and expected annual compensation. Please state the Job Ref No. you are applying for on the envelope and send your application to:

Director, Human Resources
John Wiley & Sons (Asia) Pte. Ltd.
2 Clementi Loop #02-01
Singapore 129809

Email : **hrasia@wiley.com.sg**
http://www.wiley.com

We would like to thank all applicants in advance and regret that only shortlisted candidates will be notified.

Application closes on 14th July 2006.

Founding Director

Health Sciences Research Institute
University of California, Riverside

The University of California, Riverside seeks an internationally recognized research scientist to become the founding Director of its Health Sciences Research Institute (HSRI). The HSRI is a new, campus-wide interdisciplinary institute whose mission is to significantly strengthen research and education in the health and biomedical sciences. More details of this campus initiative can be found at www.hsri.ucr.edu. The HSRI is also closely linked to the proposed development of a four-year MD program and research-based School of Medicine from the current UCR/UCLA joint MD program.

The Director will: provide vision and administrative leadership; identify frontier area(s) of biomedical and health sciences research and build integrated research programs in these area(s); recruit and support the development of faculty members who are national leaders in these area(s); identify new funding opportunities for interdisciplinary health sciences research; foster collaborations among UCR colleges in health sciences research; nucleate new initiatives for support of post-baccalaureate student training; represent the HSRI to state, national and international professional societies and academies; actively engage and involve the campus in the HSRI mission; report to the Vice Chancellor for Research.

The campus has committed considerable resources to the HSRI, including searches and contiguous research space for 10 core faculty, many at senior levels. Up to 25 additional searches for faculty with health and biomedical research interests are planned for the next five years. A new research facility will be linked to the planned School of Medicine, subject to University of California construction rules. The Director will hold an endowed chair as well as a tenured faculty position in an appropriate academic department. Salaries will be nationally competitive and commensurate with qualifications.

Applications should include a curriculum vitae, a vision statement regarding institute leadership, a listing of administrative experience, and names and addresses of references. Application materials (and letters of nomination) should be sent to: Chair, Health Sciences Research Institute Director Search Committee, Office of the EVC, University of California, Riverside, CA 92521.

Review of applications will begin on July 15, 2006, with appointment as early as January 1, 2007. Applications will be accepted until the position is filled. Inquiries regarding the position can be directed to the Office of the Executive Vice Chancellor.

The Riverside campus of the University of California is growing rapidly and has a strong record of success in research, teaching, and extramural funding. The campus is centrally located in Southern California, about 50 miles east of downtown Los Angeles and less than an hour's drive from the area's mountains, deserts, and beaches.

The University of California is an Equal Opportunity/Affirmative Action Employer.

Senior Faculty Member
Director, Allergic Diseases Research Laboratory

The University of South Florida's Department of Internal Medicine, Division of Allergy and Immunology is seeking a well established scientist with a PhD or MD or PhD/MD degree and considerable experience in the field of allergy research. The candidate should have an ample CV with publications in international journals with a high impact index. Experience in writing grants, as well as peer-reviewed papers is needed.

Must have experience in the following laboratory procedures: preparation of industrial scale allergen extracts for diagnosis and treatment of allergic diseases; preparation of modified extracts; classical dialysis and flat-bed diafiltration ultrafiltration techniques; chromatography technology for the purification of proteins in complex mixtures; electrophoretic techniques, including SDS-PAGE, western blots, 2-D electrophoresis, chemiluminesce technology and radio-isotope handling; molecular biology techniques destined to clone and sequence allergens; RT-PCR and expression of proteins in bacteria and *Pichia pastoris*; ELISA techniques to measure allergenic potencies and major allergen content; and be knowledgeable in micro array and Multiplex technology. The candidate should also have experience with laboratory techniques used to prepare, analyze and characterize allergen extracts and experience in the methodology used to standardize allergenic/biological materials and be able to accurately interpret the results. Experience in environmental risk assessments is also warranted.

The candidate should be able to objectively interpret data gathered from environmental surveys and make decisive decisions on how to remediate the problems. Other skills of value include language skills, previous experience as a research director, with experience in the pharmaceutical industry, writing and the probability of attracting funds from national and international government institutions as well as nonprofit and for-profit corporations. The candidate should develop a program in aerobiology and assist in developing technologies for immunotherapy to treat allergic diseases and asthma.

Previous experience in directing research projects and PhD students is desirable. The candidate should have good scientific judgment and be able to think and work independently and coordinate the research projects of the members of the Division. Appointment requires a minimum of five years of experience at the Associate Professor rank.

Position is open until filled; first reviews begin **June 23, 2006**. Salary is negotiable. Send CV, cover letter and letters of recommendation to: **Richard F. Lockey, M.D., Professor and Director, C/O Michelle Grandstaff, USF Division of Allergy and Immunology, 13801 Bruce B. Downs Blvd., Suite 505, Tampa, FL 33613.**

USF Health is committed to increasing its diversity and will give individual consideration to qualified applicants for this position with experience in ethnically diverse settings, who possess varied language skills, or who have a record of providing medical care to underserved or economically challenged communities. The University of South Florida is an EO/EA/AA Employer. For disability accommodations, contact Michelle Grandstaff at (813) 631-4024 x 201 minimum of five working days in advance. According to FL law, applications and meetings regarding them are open to the public.

100 Top Hospital expanding in Central Texas

PEDIATRIC ONCOLOGIST: Central Texas

The Section of Pediatric Hematology/Oncology at Scott and White Hospital and Clinic and the Texas A&M University System Health Science Center College of Medicine (TAMUS HSC-COM) are seeking a BE/BC pediatric oncologist for a faculty position in a rapidly growing program. This faculty appointment will be at the Assistant/Associate Professor rank contingent upon qualifications. Preference will be given to candidates with strong clinical skills and a commitment to teaching and clinical research. The Division sees the full spectrum of pediatric hematologic and oncologic disorders and is a full member of the Children's Oncology Group. Excellent opportunities for clinical, translational and basic research collaborations are available within the Department of Pediatrics, and at the new state-of-the-art Cancer Research Institute under the recently appointed Director Art Frankel. The Department of Pediatrics has a fully-accredited, free-standing Pediatric Residency Program. An outstanding start-up package includes excellent benefits and competitive salaries commensurate with academic qualifications.

Scott & White Clinic is a 500+ physician directed multi-specialty group practice that is the leading provider of cancer care in Central Texas. Scott and White Clinic and the 486 bed tertiary Scott & White Memorial Hospital is the main clinical teaching facility for TAMUS HSC-COM. Outstanding clinical practice and laboratory facilities on campus that perform state of the art molecular and cellular biology research, flow cytometry, genomics and biostatistics are in place to support the research effort.

For additional information, please call or send your CV to: **Jason Culp, Physician Recruiter, Scott & White Clinic, 2401 S. 31st, Temple, TX 76508. (800) 725-3627 jculp@swmail.sw.org** *Scott & White is an equal opportunity employer. A formal application must be completed to be considered for this position. For more information on Scott & White, please visit our web site at: www.sw.org*

SCOTT & WHITE
A WORLD OF HEALING™

TEXAS A&M HEALTH SCIENCE CENTER
COLLEGE OF MEDICINE

UNIVERSITY OF MARYLAND

CHAIR
DEPARTMENT OF ANIMAL AND AVIAN SCIENCES
COLLEGE OF AGRICULTURE AND NATURAL RESOURCES

The University of Maryland, College Park invites applications for the position of Chair, Department of Animal and Avian Sciences, College of Agriculture and Natural Resources. Candidates must have a PhD in animal sciences or related field, be internationally recognized for accomplishments in research, have a demonstrated commitment to teaching and/or extension, and be qualified for tenure as Professor. Outstanding oral and written communication skills; a demonstrated ability to work effectively with faculty, students, staff, administrators, industry and others, and to attract extramural funding are required. Responsibilities will include providing vision and leadership for the department; administering departmental finances, policies and facilities; providing proactive liaison with internal and external clientele; recruitment and retention of outstanding faculty, staff and students; and contributing directly to scholarly activities of the department. Salary will be commensurate with experience and background, and an extensive benefits package is offered. Detailed information on the department is available at **http://www.ansc.umd.edu**.

Initial screening of applications will occur on **August 30, 2006**; however, the position will remain open until a suitable candidate has been identified. Applications should include a statement of interest, curriculum vitae and contact information. References may be requested at a later date. Please send applications to: **Animal Sciences Chair Search Committee, College of Agriculture and Natural Resources, 1296 Symons Hall, University of Maryland, College Park, MD 20742-5551, Attn: Ms. Glenda Canales (gcanales@umd.edu).**

MINORITIES AND WOMEN ARE ENCOURAGED TO APPLY. THE UNIVERSITY OF MARYLAND IS AN AFFIRMATIVE ACTION/EQUAL OPPORTUNITY EMPLOYER.

University of Hawai'i at Hilo
Academic Administrative Positions at the College of Pharmacy

The Hawaii State Legislature and the Board of Regents of the University of Hawaii has authorized the launch of a new College of Pharmacy at the University of Hawaii at Hilo located on the Big Island of Hawaii. Dean John M. Pezzuto and the University of Hawaii at Hilo invite applicants to join the academic administrative team and form a core faculty to initiate the mission of providing exemplary professional pharmacy education leading to the degree of Pharm. D. A goal of the College is to advance excellence in pharmacy practice while capitalizing on translational research programs designed to enhance pharmaceutical healthcare throughout the world. Advantage will be taken of the unique and creative energies of Hawaiian, Pacific Islanders and other diverse cultures in the nexus of cultural beliefs and practices with innovations and discoveries for global health and well being.

The University of Hawaii at Hilo seeks applicants for the following academic/administrative positions, all of which are contingent upon State Legislative and BOR approval, and availability of funds.

Department Chair for Pharmaceutical Sciences: The successful applicant will oversee the scientific base of the curriculum. This Chair will lead the faculty in implementing the professional curriculum that provides the scientific underpinnings of pharmacy practice, and will manage the faculty in program delivery of teaching and research initiatives. The candidate will be a member of the Dean's administrative council. Minimum qualifications are: doctoral degree (PhD or professional doctorate such as PharmD, MD, JD); three (3) years of relevant experience; eligibility for an academic appointment (Associate Professor or higher) at the University of Hawaii at Hilo.

Department Chair for Pharmacy Practice: The successful applicant will oversee the education of professional practice in the curriculum. This Chair will lead the faculty in implementing the curriculum that forms the foundation of professional pharmacy practice as a health discipline, and organizes the faculty in program delivery of teaching and professional education initiatives. The candidate will be a member of the Dean's administrative council. Minimum qualifications are: doctoral degree (PhD or professional doctorate such as PharmD, MD, JD); licensure as a professional pharmacist and eligibility for Hawaii licensure; three (3) years of relevant experience; eligibility for an academic appointment (Associate Professor or higher) at the University of Hawaii at Hilo

Clinical Education Coordinator: The successful applicant will design and manage a clinical pharmacy training network for diverse clinical teaching-learning experiences. This coordinator will develop partnerships among the diverse health care systems throughout the state and nationwide to afford students quality clinical educational experiences in accord to national standards and benchmarks of excellence determined by the faculty. This candidate will be a member of the Dean's administrative council. Minimum qualifications are: degree in pharmacy; licensure as a professional pharmacist and eligibility for Hawaii licensure; three (3) years of relevant experience; eligibility for a clinical/academic position at the University of Hawaii at Hilo. A doctoral degree is preferable (PhD, PharmD, MD).

Librarian II or III: Successful applicants will be responsible for a wide range of academic library public services duties with emphasis in the areas of pharmacy and health sciences. This position may require work during evenings and on weekends. This is a new position in response to enrollment growth and the new College of Pharmacy. At rank of Librarian II: ALA accredited MLS or international equivalent. At rank of Librarian III: ALA accredited MLS or international equivalent; 24 post-baccalaureate credits in addition to the MLS; at least three (3) years of relevant experience. Minimum qualifications for post-baccalaureate credit and years of experience for rank are non-negotiable. Full-time, tenure-track, 11-month, general funds to begin approximately December 1, 2006, pending position clearance and availability of funds. The position will remain open until filled. However, applications received after Monday, August 7, 2006, cannot be guaranteed full consideration.

Pharm Science Faculty: Successful applicants will teach the scientific base of pharmacy as a health discipline and health profession to students entering the College of Pharmacy curriculum. As tenure track faculty in academic pharmacy, these positions entail establishing a funded research program that balances teaching and research. Minimum qualifications are: doctoral degree (PhD, PharmD, MD); relevant teaching and research experience; eligibility for appointment at the rank of Assistant Professor or higher at the University of Hawaii at Hilo. Preference will be given to candidates with postdoctoral experience.

The University of Hawaii at Hilo is one of three, 4-year institutions in the University of Hawaii system (see **http://ww.uhh.hawaii.edu**). Information about the pharmacy program can be accessed at **http://www.uhh.hawaii.edu/academics/pharmacy**. Review of applications will begin **August 1, 2006**, and continue until the positions are filled. Candidates should submit a cover letter summarizing his/her interests and qualifications for the position, a current C.V. and the names of three (3) professional references including postal, email address and telephone contact information. For a job description, specific position requirements and desirable qualifications, please go to **http://www.uhh.hawaii.edu/uhh/hr/jobs.php**. Applications should be submitted to:

Dr. Daniel Brown, Chairperson
c/o Jackie Sales-Iyo
Search Committee for (position you are applying for)
University of Hawaii at Hilo
200 W. Kawili St.
Hilo, HI 96720

The University of Hawaii at Hilo is an Equal Employment Opportunity/Affirmative Action Employer D/M/V/W.

NATIONAL INSTITUTE OF IMMUNOLOGY, INDIA

Career Opportunities in India for Scientists in Life Sciences

The National Institute of Immunology, New Delhi, India, would like to recruit scientists as independent investigators in the biomedical sciences, leading their own groups and responsible for both research projects and teaching. They should be holding Indian citizenship. A demonstrated record of scientific productivity in the form of recent peer-reviewed publications in scientific journals of high international repute and/or internationally valid and productive patents is essential, as is some indication of independence in scientific thinking, and three to four years of post-doctoral experience.

The Institute's primary goal is to gain insights into the immune system and its interplay with disease so as to facilitate the development of new approaches to disease amelioration. Of particular interest will be ideas in analysing the immune system at the level of cellular biochemistry, cell biology, developmental biology, physiology, signal transduction, apoptosis proteomics, structural, chemical and systems biology. Research areas involving host-pathogen interactions, covering the entire range of expertise and interest from the statistical and epidemiological to the cellular and molecular levels will also be welcome.

Appointments are offered as Staff Scientists in various grades, which range from those equivalent to university positions of Senior Lecturer or Assistant Professor upwards. Length of experience and the quality of the scientific productivity record will be major factors in deciding the level of appointment as well as the salary offered. Investigators will be provided shared laboratory space and adequate start-up resources. They are expected to generate extramural project based funding. Some housing can be made available for allotment.

Interested scientists may send their bio-data containing details of qualification, positions held, professional experience/distinctions and copies of notable publications, and the names, addresses, fax numbers, telephone numbers and electronic mail addresses of three potential referees, to the Director, National Institute of Immunology, Aruna Asaf Ali Marg, New Delhi –110067, India. People working in public sector Institutions within India are requested to have their applications forwarded through proper channels. Only shortlisted candidates will be contacted for further discussions.

POSTDOCTORAL POSITION IN MOLECULAR IMAGING

Biomedical Engineering, University of California – Davis

Applications are invited for a postdoctoral position to develop a hyperspectral optical tomography system for *in vivo* molecular imaging applications. Applicants must have a Ph.D. in biomedical engineering, physics, medical physics, electrical engineering or a related discipline. Specific research experience in biomedical optics or optical imaging is required and the applicant should possess documented experimental skills and a strong background in scientific computer programming.

To apply, please submit a curriculum vitae, the names of three people willing to provide letters of recommendation, and a brief statement outlining short-term research interests and long-term research goals, to:

Simon R. Cherry, Ph.D.
Department of Biomedical Engineering
UC Davis
One Shields Avenue
Davis, CA 95616

E-mail: srcherry@ucdavis.edu

The University of California is an Affirmative Action/Equal Opportunity Employer.

IOWA STATE UNIVERSITY

Where you can become your best.

Tenure-track Assistant/Associate Professor Faculty Position (9 months, Full Time) in PHARMACOLOGY

The Department of Biomedical Sciences, College of Veterinary Medicine, Iowa State University is seeking candidates to teach professional and graduate courses and establish/conduct independent research. Biomedical Sciences has research interests in cellular and molecular biology, neuropharmacology, and neuroscience and is looking for individuals who are interested in teaching veterinary pharmacology. The department is looking for energetic candidates to join the expanding BMS faculty and interact with interdisciplinary graduate programs.

- **Assistant Professor:** ***Required Qualification:*** PhD; ***Preferred Qualifications:*** DVM (or equivalent) and PhD, teaching experience with DVM students, evidence of extramural grant applications, and publication record in recognized research journals.
- **Associate Professor:** ***Required Qualifications:*** PhD, record of extramural funding and publication record in recognized research journals; ***Preferred Qualifications:*** DVM (or equivalent), PhD and ACVCP (or equivalent), teaching experience with DVM students.

To guarantee consideration, applications must be received by **October 1, 2006**. Proposed start date is January 1, 2007 and is negotiable. All applications must be submitted electronically. To apply for this position, visit **www.iastatejobs.com (Vacancy #060447)** and complete the employment application form. Be prepared to attach or enter a letter of application, curriculum vitae, teaching and research goals statement, and contact information for three references. Attach teaching and research goals statement as "other document". Inquiries regarding the position should be directed to **Walter Hsu, Search Committee Chair, whsu@iastate.edu, 515-294-6864**. For further information contact our Website: **http://www.vm.iastate.edu/departments/bms**.

Iowa State University is an Affirmative Action/ Equal Opportunity Employer.

Career matters. Life matters. Health matters.

At the heart of all that matters are people, connected in purpose by career, life, and health. Throughout the world and here at home, sanofi-aventis fights for what is essential to us all–health. Now the world's third-largest pharmaceutical company, our R&D organization has created a superior product portfolio and one of the industry's richest pipelines that will set the course for improving the health of millions worldwide.

Your expertise in your field and your passion for science and discovery will ensure we continue to improve the health of millions…because health matters.

Postdoctoral Fellow

Bridgewater, NJ • (Req S&MA3749)

The goal of this position is to develop cellular assays based on HCS (high throughput imaging) that will enable us to predict and understand the behavior of compound series in preclinical and clinical studies. We are extremely interested in differentiating compounds within series and looking for new clinical indications. We will start with series of compounds that are in preclinical or clinical trials to try to validate the strength of our assays and their ability to help us exploit the clinical potential of our compounds.

A recent PhD and a thorough knowledge of cell biology is required. You must be comfortable with cell biology and cellular signaling pathways, and be able to integrate information rapidly to discern patterns. Knowledge of neural networks, high throughput imaging and image analysis, basic pharmacology, signal transduction pathways, and skills in tissue culture of cell lines, primary and stem cells are a plus.

Driven by a pioneering spirit, a strong set of core values and a mosaic of talent worldwide, we strive for success–in health. In doing so, we strengthen careers and enrich lives. Discover your future with sanofi-aventis. Apply online.

www.careers.sanofi-aventis.us
Apply to Req S&MA3749

sanofi aventis
Because health matters

Sanofi-aventis is an **equal opportunity employer** that embraces diversity to foster positive, innovative thinking that will benefit people worldwide. Sanofi-aventis is also committed to employing qualified individuals with disabilities and, where warranted, will provide reasonable accommodation to applicants, as well as its employees.

UNIVERSITY OF MISSOURI-COLUMBIA

Director MU Informatics Institute

We seek a dynamic, nationally recognized researcher to develop the MU Informatics Institute into an internationally recognized health and bioinformatics research and education institute. The Institute provides the structure for interdisciplinary health and bioinformatics research and educational programs that link the Departments of Health Management and Informatics in the School of Medicine, and Computer Science in the College of Engineering. The Institute will offer a doctoral program in informatics starting fall 2006 that combines the faculties of these two departments. The Institute affords exceptional opportunities to develop and enhance the outstanding and internationally recognized research programs at MU in health and medical informatics, health systems engineering, computational and statistical sciences, and the life and physical sciences. Nominees and applicants should hold a terminal doctorate (PhD, MD, DO, DVM) outstanding research accomplishments, and qualifications to be appointed as a senior faculty member in the tenure track in Health Management and Informatics or Computer Science. The position demands a commitment to interdisciplinary informatics research; exceptional interpersonal and communication skills; administrative, intellectual and programmatic leadership in basic and applied research as well as in pre-doctoral and post-doctoral training; and an appreciation of the land-grant mission. The University of Missouri-Columbia is a comprehensive AAU Carnegie Doctoral-Research-Extensive, land-grant institution with more than 20,000 undergraduate and more than 6,000 graduate and professional students. MU's federal research dollars have been growing faster than any other AAU public institution. MU is one of only six American universities with a comparable breadth of academic units on one campus. Nominations and letters of intent, plus a curriculum vitae and names of 3 references, should be submitted to: **Chair, MU Informatics Institute Director Search Committee, Office of the Dean of Medicine, Ma202 Med Sciences Bldg, University of Missouri-Columbia, Columbia, MO 65211**.
Review of applications will begin on August 1 and continue until a suitable candidate is selected.

The University of Missouri-Columbia is an equal opportunity and affirmative action employer.

Visit the University of Missouri-Columbia's Web site at http://mujobs.missouri.edu

IOWA STATE UNIVERSITY

Tenure-track Assistant/Associate Professor Faculty Position in BIOMEDICAL SCIENCES

The Department of Biomedical Sciences in the College of Veterinary Medicine at Iowa State University invites applications for a faculty position at the Assistant or Associate Professor level. The successful candidate will teach and mentor professional and graduate students as well as develop and sustain a vigorous, extramurally funded research program focused on cellular/molecular biology, neuroscience, or neurotoxicology. Instruction will include participation in teaching Pharmacology/Physiology in the veterinary medical curriculum.

- **Assistant Professor:** ***Required Qualifications:*** PhD (or equivalent in a relevant discipline), research experience and a strong publication record; ***Preferred Qualifications:*** DVM or MD (or equivalent), teaching experience in a professional graduate curriculum, extramural grant applications, publication record, and two years postdoctoral training.
- **Associate Professor:** ***Required Qualifications:*** PhD (or equivalent in a relevant discipline), university teaching experience, record of extramural funding, strong publication record, and nationally/internationally recognized investigator in one of the above fields; ***Preferred Qualifications:*** DVM or MD (or equivalent) and teaching experience in a professional graduate curriculum.

The Biomedical Sciences Department has a dynamic faculty with excellent laboratory space and easy access to animal facilities. Excellent opportunities exist for collaboration with faculty across the university as well as with scientists at the USDA/ARS National Animal Disease Center and National Veterinary Service Laboratories.

To guarantee consideration, applications must be submitted electronically and received by **October 1, 2006**. Proposed start date is January 1, 2007. To apply, visit **www.iastatejobs.com (Vacancy #060481)** and complete the employment application form. Be prepared to attach a letter of application, curriculum vitae, teaching and research goals statement, and contact information for three references. Attach teaching and research goals statement as "other document". Direct inquiries regarding position to **James R. Bloedel, Search Committee Chair: jbloedel@iastate.edu, 515-294-4415**. For further information contact **http://www.vm.iastate.edu/departments/bms**.

Iowa State University is an Affirmative Action/Equal Opportunity Employer.

Stanley Cobb Professor of Psychiatry

Harvard Medical School and Beth Israel Deaconess Medical Center Department of Psychiatry, to serve at the Massachusetts Mental Health Center, Boston MA

Beth Israel Deaconess Medical Center (BIDMC) and **Harvard Medical School** are seeking an established psychiatric investigator with demonstrated excellence in mentoring, who will be responsible for developing and implementing an enhanced psychiatric research program based at the **Massachusetts Mental Health Center (MMHC)**. MMHC, whose research and academic programs have recently been integrated into the BIDMC Department of Psychiatry, has an unparalleled reputation in American Psychiatry. Through its unique and complex coordination of public, private, and academic resources, it has provided state of the art care to patients with major mental illness and severe psychosocial disadvantage and has trained generations of psychiatric leaders, in a setting of world class research, educational, and training programs. Its new affiliation with the BIDMC strengthens and advances its decades-long cooperative relationship with Harvard Medical School and the Commonwealth of Massachusetts and enhances this relationship with the clinical and academic resources of the BIDMC, which ranks third among the nation's hospitals in federal research funding. The new MMHC will be housed in a state of the art building with access to significant laboratory and other space.

The successful candidate for this position must have a record of successful independent funding, as well as demonstrated excellence and achievement in the area of mentoring students and faculty. The candidate would preferably have significant public sector experience and dedication. A major responsibility of this position will be the fostering and growth of research at all levels of the Department, including Harvard Medical Students, psychiatry and psychology trainees, and junior and more experienced faculty. Additional junior faculty are expected to be recruited as part of enhanced research growth. The Cobb Professor will have no formal departmental administrative responsibilities separate from the development of a thriving research program focused on major mental illness. **Women and minorities are actively encouraged to apply. Candidates should send a letter of interest and CV to: Dr. Mary Anne Badaracco, Chair, Department of Psychiatry, Beth Israel Deaconess Medical Center, 185 Pilgrim Road, Boston MA 02115, mbadarac@bidmc.harvard.edu**

Beth Israel Deaconess Medical Center

HARVARD MEDICAL SCHOOL

Faculty Position
University of California, San Diego
The Division of Biological Sciences
Section of Molecular Biology
http://biology.ucsd.edu/

The Molecular Biology Section of the Division of Biological Sciences at the University of California, San Diego is seeking qualified (Ph.D. or M.D.) applicants for the position of Assistant or Associate Professor. The area of research interest may relate to immunology, immunopathology, or host-pathogen interactions. The successful applicant should have postdoctoral and academic experience commensurate with the level of the appointment, and in particular have demonstrated the potential to be a leader in his or her chosen field. Women and minorities are encouraged to apply.

Resources will be made available to provide for laboratory start-up and operation until extramural funding has been obtained. In addition to carrying out outstanding research, the successful candidate will be expected to participate in undergraduate and graduate education in his or her area of expertise. The level of appointment will be commensurate with qualifications and experience, with salary based on University of California pay scale.

Complete applications received by **September 1, 2006** will be assured of consideration. Applicants should send a curriculum vitae, publication list, synopsis of research interests and professional goals, and three letters of reference (forwarded separately) to:

Molecular Biology /
Immunology Search Committee
c/o Andrea Schnitz – Mail Code 0377-A
University of California, San Diego
9500 Gilman Drive
La Jolla, CA 92093-0377

UCSD is an Equal Opportunity-Affirmative Action Employer with a strong institutional commitment to the achievement of diversity among its faculty and staff.

Scientific Curator
University of Oregon

ZFIN, the zebrafish model organism database, seeks scientific curators to join our dynamic, interactive team of biologists and computer scientists at the University of Oregon in Eugene, OR.

ZFIN curators acquire, analyze and index information about zebrafish gene structures, expression patterns and mutant phenotypes. Successful candidates will be primarily responsible for the curation of zebrafish phenotype data. Particular attention will be given to phenotypes that serve as models of human disease. Zebrafish phenotypes and their human orthologs will be annotated using common terms and methods when possible. Curators also participate in database, web interface and ontology design by providing biological perspectives for new content and display.

A Ph.D. in Life Sciences or M.S. with appropriate experience is required. Applicants should have backgrounds in developmental genetics, comparative genomics or phenotype evaluation, preferably in zebrafish. Complete position description available at **http://zfin.org/zf_info/news/ZFIN_jobs.html**.

Send curriculum vitae and references to: **Dala Ramsey, Institute of Neuroscience, University of Oregon, Eugene, OR 97403-1254 USA.; Fax: 541-346-4548; Email: dala@uoregon.edu.**

Affirmative Action/Equal Opportunity/ADA Institution committed to cultural diversity.

Director of Biotechnology Institute
College of Biological Sciences and Institute of Technology
University of Minnesota

The University of Minnesota seeks an internationally recognized scientist/engineer for the position of Director of the BioTechnology Institute (BTI). The University is strongly committed to research in biotechnology, and the new director is expected to provide a strong vision that will form the basis for developing and coordinating biotechnology research involving life science and engineering disciplines at the University. The BTI has a twenty year history at the University of Minnesota (see **http://www.bti.umn.edu/index.html** for details), and has recently been named home to the Presidential initiative on Biocatalysis (see **http://www.bti.umn.edu/biocatalysis**). The new Director of BTI will take a leadership role in the President's Biocatalysis Initiative and substantial, recurring, resources will be provided for this purpose. The new Director will also provide leadership in leveraging existing resources such as the Biotechnology Resource Center, the NIH Biotechnology training grant (see **http://www.bti.umn.edu/btitraining.html**), and interfacing with related initiatives, such as the University's Institute for Renewable Energy and the Environment (**http://www1.umn.edu/iree/**).

The successful candidate for this position must have Ph.D. (or equivalent) in biological, chemical or physical sciences, or engineering, and have recognized accomplishments in inter/multi-disciplinary research. The director will hold a tenured position in an appropriate department in either the College of Biological Sciences, the Institute of Technology, or the Medical School. He or she will be expected to maintain an active, externally funded research program and will have a laboratory in the BTI. The appointee will have a substantial record of research accomplishment and be a recognized intellectual leader in their chosen area of research. Individuals working in academia, industry, or government are encouraged to apply.

Applicants must include a cover letter, current CV, and the names and contact information for three references. Applications and inquiries should be addressed to:

Michael J. Sadowsky
Chair, Search Committee
BioTechnology Institute
140 Gortner Labs
University of Minnesota
St. Paul, MN 55108
Phone: 612-624-2706

Applicants are encouraged to send application materials by email to: **Sadowsky@umn.edu**. Evaluation of applications by the search committee will begin on **July 15, 2006** and will continue until the position is filled.

The University of Minnesota is an Equal Opportunity Educator and Employer.

IOWA STATE UNIVERSITY

Where you can become your best.

Tenure-track Assistant/Associate Professor
Faculty Position (12 months, Full Time)
in Microscopic and Macroscopic ANATOMY

The Department of Biomedical Sciences, College of Veterinary Medicine, Iowa State University is seeking candidates to teach professional, graduate and undergraduate students and conduct independent research. Primary responsibilities will be to teach anatomy (gross anatomy and/or histology) to DVM students. BMS has focused its main research interests in molecular biology, neurotoxicology, and neuroscience. However, applicants in other fields are encouraged to apply. The department is looking for energetic candidates to join the expanding BMS faculty and interact with interdisciplinary graduate programs.

- **Assistant Professor:** ***Required Qualification:*** PhD; **Preferred Qualifications:** DVM (or equivalent) and PhD, teaching experience with DVM students, record of extramural grant application, and publication record in recognized journals.
- **Associate Professor:** ***Required Qualifications:*** PhD, teaching experience at university level, record of extramural funding, publication record in recognized journals; ***Preferred Qualifications:*** DVM (or equivalent) and PhD, teaching experience with DVM students, and extramural grant support.

To guarantee consideration, applications must be received by **October 1, 2006**. Proposed start date is January 1, 2007 and is negotiable. All applications must be submitted electronically. Send application letter, curriculum vitae, teaching and research goals statement, and contact information for three references to **Linda Erickson** at **lericks@iastate.edu**. Direct inquiries regarding position to **Etsuro Uemura, Search Committee Chair, euemura@iastate.edu, 515-294-7328**. For further information contact our Website: **http://www.vm.iastate.edu/departments/bms**.

Iowa State University is an Affirmative Action/ Equal Opportunity Employer.

Department of Health and Human Services
National Institutes of Health
Office of the Director
Office of Extramural Research (OER)

The National Institutes of Health (NIH), in Bethesda, Maryland, the world's largest medical research facility, is seeking applications from exceptional candidates for a challenging position in the Office of Laboratory Animal Welfare, which is located in the Office of Extramural Research. The NIH, a component of the Department of Health and Human Services, is the principal health research agency of the Federal Government. The NIH Extramural Program is the largest single source of funding for biomedical and behavioral research in the United States. Extramural research represents approximately 85% of the NIH budget.

The Director, Office of Laboratory Animal Welfare (OLAW) provides executive leadership and direction to the Office of Laboratory Animal Welfare, which is responsible for developing and coordinating appropriate Public Health Service (PHS) regulations, policies, and procedures on the humane care and use of laboratory animals involved in research conducted or supported by any component of the PHS. The Director, OLAW reports directly to the NIH Deputy Director for Extramural Research.

For full information concerning the duties and responsibilities of this position, salary and benefits available, required qualifications, and mandatory application procedures, interested candidates should visit the OER website at **http://grants.nih.gov/grants/oer_vacancies.htm**

Applications for this position must be postmarked or received by **July 13, 2006.**

DHHS and NIH are Equal Opportunity Employers

2 Great Career Events

Science Career Fair

Make your next career move easier. *Science* Careers is hosting our annual Boston career fair in conjunction with the upcoming DDT meeting. Come meet recruiters face to face and explore career opportunities for all levels of scientists.

Science is hosting this career fair in conjunction with **Drug Discovery Technology™ 2006**

Event ..... *Science* Career Fair
Date..... 10 August 2006
Time ..... 11:00 am – 4:00 pm
Location..... Seaport Hotel, Plaza ballroom, Boston, MA

For information on exhibiting, please contact Daryl Anderson at (202) 326-6543.
Exhibitors receive free access to *Science*'s Resume/CV Database through 31 August.

Making the Most of Your Career Fair

If you are planning on attending the career fair, be sure to attend our Making the Most of Your Career Fair seminar, and learn how to promote yourself quickly and professionally.

Event ..... Making the Most of Your Career Fair
Date..... 8 August 2006
Time ..... 6:00 pm – 7:00 pm, with reception to follow
Location..... The Conference Center at Harvard Medical

For more information on both of these events, please visit www.sciencecareers.org and click on career fairs

ScienceCareers.org
We know science AAAS

In a joint appointment of the Medical Faculty of the **Ruhr-University Bochum** and the **ISAS – Institute for Analytical Sciences in Dortmund** the position of a

ISAS Institute for Analytical Sciences

Full Professor (W3) for "Applied Proteomics & Bioanalytics"

will be filled as soon as possible. After appointment as a **full professor (W3)** the successful candidate will be granted unpaid leave to take over the position of a

department chair of the division for development of methods and instruments in proteome research

at the ISAS in Dortmund.

ISAS - Institute for Analytical Sciences, jointly supported by the German Federal and States' Governments is a scientific research establishment for analytical research using physical, chemical and biological methods (see: www.ansci.de).

The successful candidate should have a proven record in developing and realizing innovative research concepts. He/she will be responsible for the new department of applied proteomics. He/she is expected to design new research concepts in the field of applied proteomics and bioanalytics with a strong focus on methods and instrument development. Therefore, profound expertise, experimental experience and an independent portfolio in applied research, methods and instrument development for proteomics, bioinformatics for proteomics and related fields are expected; i.e. mass spectrometry, protein biochip technology or multidimensional electrophoresis or chromatography.

The candidate must be able to provide strong leadership and promote a powerful vision for advancement of the department's mission and goals. A successful record is required in fund raising from national and international research programs as well as from industry. Tight collaboration is expected with the Medical Faculty of the Ruhr-University Bochum, especially with the Medical Proteom-Center and the relevant departments and faculties of neighbour universities as well as with the other research institutes in Dortmund and Bochum. We offer a position which allows independent scientific research in an interdisciplinary environment and teaching at the Ruhr-University Bochum including biochemistry as well as basics in proteomics and bioanalytics.

Habilitation or equivalent achievements are mandatory. The requirements for the position comply with § 46 of the University Law of the state NRW.

Applications from women are strongly encouraged, and priority will be given to women with equal qualifications. Priority will also be given to physically disabled persons with equivalent qualifications. Because of our international orientation, we encourage candidates from abroad to apply for the position.

Interested candidates should send respective documents in double version including the http://www.ruhr-uni-bochum.de/medizin/dekanat/ServiceDekanat/Allgemeines/Bewerbungsbogen.pdf (PDF version) or http://www.ruhr-uni-bochum.de/medizin/dekanat/ServiceDekanat/Allgemeines/Bewerbungsbogen.rtf (RTF version) until 6 weeks after publication of this advertisement to the

Dean of Medical Faculty
Ruhr-University
D-44780 Bochum, Germany

Further details are available upon request [+49 231 1392 103 (Prof. Manz)].

www.cam.ac.uk/jobs/

The Professorship of Botany

The Board of Electors to the Professorship of Botany invite applications for this Professorship from persons whose work falls within the general field of plant and microbial biology to take up appointment by 1 October 2007.

Further information may be obtained from the Academic Secretary, University Offices, The Old Schools, Cambridge CB2 1TT, (e-mail: ibise@admin.cam.ac.uk), to whom a letter of application should be sent, together with details of current and future research plans, a curriculum vitae, a publications list and form PD18 with details of two referees, so as to reach him no later than Monday 31 July 2006.

Informal enquiries may be made to Professor John Gray, Head of the Department of Plant Sciences, telephone: (01223) 333925 or 333958. E-mail: john.gray@plantsci.cam.ac.uk

UNIVERSITY OF CAMBRIDGE

The University offers a range of benefits including attractive pension schemes, professional development, family friendly policies, health and welfare provision, and staff discounts. The University is committed to equality of opportunity.

THE ROYAL SOCIETY

Royal Society Research Professorships

The Royal Society is seeking applications for four Royal Society Research Professorships. These posts are designed to enable individuals of the highest ability and achievement to undertake independent, original research at a UK university or not-for-profit organisation into any of the natural and applied sciences including medical and engineering science.

Research Professorships provide long-term support for world-class scientists of outstanding achievement and promise, allowing them to focus on research and collaboration. Previous holders include five Nobel Laureates.

Applications are particularly welcomed from scientists currently resident outside the UK. The Professorships are available for scientists of any nationality.

The Royal Society is the independent scientific academy of the UK. It is dedicated to promoting excellence in science, by supporting many of the UK's top scientists, engineers and technologists, by influencing science policy and by debating scientific issues with the public.

Further information is available from the Royal Society website: **www.royalsoc.ac.uk** and by email from: **ukgrants@royalsoc.ac.uk**

The closing date for applications is Friday 8 September.

British Columbia Leadership Chair In Macular Research

The University of British Columbia
Department of Ophthalmology and Visual Sciences
and The Centre for Macular Research

The Government of British Columbia has established a Leading Edge Endowment Fund of $45 million, matched equally by private donors, as part of its New Era commitments. The Leading Edge Endowment Fund will support 20 permanent BC Leadership Chairs to attract to the province key, internationally renowned individuals in the fields of medical, social, environmental and technological research.

The University of British Columbia Department of Ophthalmology and Visual Sciences and the Centre for Macular Research invite applications for the British Columbia Leadership Chair in Macular Research. Applicants should hold a PhD and/or M.D. and head a successful, independent research program in areas related to the retina and/or retinal degenerative disease.

British Columbia Leadership Chairs are designed to attract world-class faculty, strengthen the province's capacity for innovative research, promote British Columbia as a centre for cutting-edge research, enhance economic development and position the province as a leader in the knowledge-based economy. Each British Columbia Leadership Chair will be endowed with up to $4.5 million.

The successful applicant will be recommended for appointment at the Full Professor level. This is a full time tenure position. Salary and rank will be commensurate with qualifications and experiences. UBC hires on the basis of merit and is committed to employment equity. We encourage all qualified applicants to apply; however, Canadians and permanent residents of Canada will be given priority.

The anticipated start date is January 2008. Further information is available at www.cmr.ubc.ca. Interested individuals should send their updated CV and a list of publications to: **Dr. Robert S. Molday, Centre for Macular Research, Department of Biochemistry and Molecular Biology, Life Sciences Centre, 2350 Health Sciences Mall, University of British Columbia, Vancouver, B.C. V6T 1Z3 Canada; Tel No. 604-822-6173; Fax No. 604-822-5227; Email: molday@interchange.ubc.ca.**

AWARDS

Boehringer Ingelheim (Canada) Ltd.

Canadian Young Investigator Award

The recipient of the 2006 Boehringer Ingelheim Canadian Young Investigator Award in Biological Sciences is:

Dr. Hao Ding
Department of Biochemistry and Medical Genetics, University of Manitoba

Prof. Ding's research program involves the application of mouse transgenic technologies to address gene function in normal development and in tumorigenesis. He currently focuses on understanding the role of a newly identified platelet-derived growth factor, PDGF-C, in the development of medulloblastoma.

The R&D division of Boehringer Ingelheim Canada Ltd. is one of Canada's largest pharmaceutical research centres. One of our important corporate policies is to support and encourage basic research in Canadian universities. To this end, we have established the Boehringer Ingelheim Young Investigator Award in Biological Sciences. The award is made annually to a new faculty member conducting biological research in a Canadian university, and consists of an unrestricted three-year research grant.

Previous recipients

2005 **Dr. John H. Brumell**, University of Toronto
2004 **Dr. Shun-Cheng Li**, University of Western Ontario
2003 **Dr. Michele Barry**, University of Alberta
2002 **Dr. Chantal Autexier**, McGill University

Boehringer Ingelheim

IBC's 11th Annual World Congress

Drug Discovery Technology® & Development

Science Subscribers Register Early and Save

See website for details

Conference: August 7-10, 2006 • Exhibition: August 8-10, 2006 • World Trade Center Boston/Seaport Hotel • Boston, MA

Keynote Speakers

Andrew C. von Eschenbach, M.D.
Acting Commissioner, **FDA**
and Director, **National Cancer Institute**

Steven M. Paul, M.D.
Executive Vice President, Science and Technology, President, Lilly Research Laboratories, **Eli Lilly and Company**

Peter B. Corr, Ph.D.
Senior Vice President, Science & Technology
Pfizer Inc

Susan Hockfield, Ph.D.
President
Massachusetts Institute of Technology

Providing Coverage of the Most Vital Topics in Drug Discovery and Development

More *Sessions than Ever Before ... Six Dedicated Conferences*

- Targeting Disease and Evaluating Disease-Relevant Targets
- Lead Discovery and Lead Optimization
- Discovery to Development: *Case Studies, Safety, PK/PD and Pharmacogenomics*
- Biomarkers: *Utility, Validation and Applications from Discovery to Clinic*
- R&D Strategies and Business Alliances
- The Interface between Drug Discovery and Informatics

Plus! 7 In-Depth, Focused Pre-Conference Workshops

200+ Speakers

Plus! *The Top Ten Reasons You Can't Afford to Miss this Event*

1. **Discover new approaches for targeting disease** and next generation target prioritization techniques including the re-emergence of genetics approaches
2. **Gain insights** to reduce cost and attrition, improve innovation, implement new R&D models and develop productive alliances **from the perspective of 60+ thought leaders**
3. **Improve your lead discovery and optimization efforts** by attending 14 case studies, and hear about innovative chemistry techniques, compound collection strategies and the latest in fragment-based approaches from 30+ speakers
4. **Hear cutting-edge biomarker applications** from 35+ leading voices and get the latest updates on the FDA's pharmacogenomics guidance and biomarker validation
5. **Find out which approaches to safety and PK/PD are adding value** and how pharmacogenomics and personalized medicine are being applied from discovery to clinic
6. **Bridge the gap between Science and Informatics** in your company and learn how to put your scientific data to use. Attend the informatics sessions featuring 40+ speakers, 5 interactive panel discussions and new exciting debates
7. **Evaluate over 300 exhibit booths** showcasing the latest technologies, products and services in drug discovery and development....all under one roof
8. **Participate in 16 thought provoking panels** on cost reduction, the role of Asia & Eastern Europe, VC funding, strategic alliances dos and don'ts and more....
9. **Network with 4000+ attendees** by taking advantage of DDT Event Connect...the on-line networking tool that lets you set up meetings before the event
10. **Learn from 200+ speakers, 150+ poster presentations** covering all facets of drug discovery and development

VIP CODE: 3200SADM

Presidential Sponsor ELSEVIER MDL

Executive Sponsors CCS Caliper LifeSciences

Executive Support Sponsors Roche GENE LOGIC

Sponsoring Publication Science AAAS

Association Sponsor MBC Massachusetts Biotechnology Council

Organized by ibc Life Sciences

To Register: Call (800) 390-4078 • Fax: (941) 365-0104 • Email: reg@ibcusa.com

www.drugdisc.com

POSITIONS OPEN

ASSOCIATE DIRECTOR FOR RESEARCH

Indiana University School of Medicine, Medical Sciences Program in Bloomington, Indiana, is seeking a leading Ph.D., M.D., or M.D./Ph.D. in cancer biology to become the Associate Director for Research; this is a tenure-track position. The Medical Sciences Program is presently expanding its research efforts by recruiting several basic/translational scientists. The successful applicant will have a well-established federally funded research program and will be expected to develop and direct an active cancer biology program that builds on existing collaborations between medical sciences faculty and others from the College of Arts and Sciences (biology, biochemistry, chemistry, neurosciences, physics) in Bloomington and with the established cancer researchers of the Indiana University School of Medicine in Indianapolis as outlined in the Indiana University Life Sciences Strategic Plan **(website: http://lifesciences.iu.edu).** The Associate Director for Research will be expected to maintain a federally funded research program, lead and coordinate new faculty recruitment, assist existing programs in expanding their funding base, and develop new research programs relevant to cancer biology. The Associate Director is also expected to strengthen existing ties with the NCI-designated Cancer Research Institute, the Indiana Genomics Initiative, and the Indiana Metabolomics and Cytomics (METACyt) Initiative. Outstanding scholarly achievements, a deep commitment to academic excellence, strong leadership and administrative skills, proven teaching skills, and a vision for basic science and translational research in an academic setting are expected. Additional information may be obtained from **website: http://medsci.indiana.edu.** A full review of applications will commence July 2006, and continue until the position is filled. Applicants should send their curriculum vitae, a statement of current and future research activities and training philosophy, and the names of four references as a single PDF file to **e-mail: bevhill@indiana.edu.** Additional materials may be mailed to: **Associate Director Search Committee, Indiana University School of Medicine, Medical Sciences Program, Jordan Hall 105, 1001 East 3rd Street, Bloomington, IN 47405.**

Equal Employment Opportunity/Affirmative Action Employer, Minorities/Females/Persons with Disabilities.

Two **POSTDOCTORAL POSITIONS** are open to study the biochemical mechanism of ubiquitylation in the control of cell cycle and stem cell self-renewal/differentiation. Collaborations with proteomic facilities, oncologists and stem cell core laboratory at the newly opened Hillman Cancer Center will be involved. Candidates with strong background in biochemistry, molecular biology, and stem cell biology are encouraged to send their curriculum vitae and three references to: **Dr. Yong Wan Ph. D., University of Pittsburgh Cancer Institute, Hillman Cancer Center, 5117 Centre Avenue, Room 2.6C, Pittsburgh, PA 15213. E-mail: yow4@pitt.edu.** Laboratory **website: http://www.cbp.pitt.edu/faculty/yong_wan.** *The University of Pittsburgh is an Affirmative Action, Equal Opportunity Institution.*

CHIEF MEDICAL OFFICER

Highly intelligent individual with exceptional communication skills sought by prominent Manhattan family to research and coordinate family medical and healthcare issues. Act as liaison with leading medical researchers and consultants in academia and industry, with full responsibility for technical, financial, and administrative functions. Considerable weight given to evidence of unusual academic or other intellectual distinction. Ph.D. or M.D. required, clinical experience a plus but not essential. Possible entrepreneurial opportunities involving delivery of ultrahigh-end medical care to other, similar families. Full-time position. Excellent compensation with significant upside potential and management possibilities. Resume to **e-mail: fmc4@spsfind.com.**

POSITIONS OPEN

Advocate Health Care

RESEARCH ASSOCIATE

Advocate Illinois Masonic Medical Center, located in Chicago, Illinois, is currently seeking a full-time Postdoctorall Research Fellow to investigate cardiovascular pathophysiology in chronically-instrumented animal models. Experience in surgery and cardiovascular monitoring is desirable. This position is eligible for benefits and works out of the University of Illinois at Chicago campus. For more information, please contact **Nidia Daniel** at **telephone: 773-296-7572** or via **e-mail: nidia.daniel@advocatehealth.com.**

TENURE-TRACK FACULTY POSITION
Immunology

The Department of Pathology, Microbiology and Immunology, School of Medicine, University of South Carolina, Columbia, is undergoing major expansion. Applications are invited for a tenure-track **ASSISTANT/ASSOCIATE/FULL PROFESSOR** position in immunology. Research experience related to cancer immunology preferred. Candidates for the Assistant Professor position must have a Ph.D. or M.D. or equivalent with postdoctoral research experience. Candidates for **ASSOCIATE/FULL PROFESSOR** positions should have current extramural funding. Competitive salary and startup funds are available. Candidates are expected to develop a strong, extramurally funded research program and participate in the teaching mission of the Department. Apply with curriculum vitae, statement of research plans, and three letters of recommendation to: **Dr. Mitzi Nagarkatti, Chair, Department of Pathology, Microbiology and Immunology, University of South Carolina School of Medicine, Columbia, SC 29208** or **e-mail: pathmicroimads@gw.med.sc.edu.** The search will start immediately and continue till the position is filled. *University of South Carolina, Columbia, is an Equal Opportunity Affirmative Action Employer and encourages applications from women and minorities.*

PHYSICIAN SCIENTIST

The Department of Medicine/Division of Infectious Diseases at the University of Pennsylvania's School of Medicine seeks candidates for an **ASSISTANT, ASSOCIATE** and/or **FULL PROFESSOR** position in the tenure track. Rank will be commensurate with experience. Applicants must have an M.D. or Ph.D. degree and have demonstrated excellent qualifications in education. If M.D., must be Board-eligible or Board-certified in infectious disease.

We are seeking an individual with strong background in laboratory-based research. We are particularly interested in candidates performing research with agents important for biodefense and emerging infectious diseases, although applicants are encouraged to apply in all areas of basic research related to infectious diseases.

Please submit curriculum vitae, a letter of interest, and references to: **Harvey Friedman, M.D., Chief, Infectious Diseases, University of Pennsylvania School of Medicine, 502 Johnson Pavilion, Philadelphia, PA 19104 – 6073. Telephone: 215-662-6417; fax: 215- 662-2473; e-mail: hfriedma@mail.med.upenn.edu.**

The University of Pennsylvania is an Equal Opportunity, Affirmative Action Employer. Women and minority candidates are strongly encouraged to apply.

POSTDOCTORAL POSITION
University of Maryland, College Park

A Postdoctoral Position is immediately available to study the biology of host-pathogen interaction. Ph.D. in biology or related field required and experience in molecular biology or biochemistry desirable. Knowledge in microbial pathogenesis or arthropod biology a plus. E-mail curriculum vitae to: **Utpal Pal, Ph.D., Assistant Professor, Department of Veterinary Medicine, University of Maryland, College Park, MD 20742 (e-mail: upal@umd.edu).**

POSITIONS OPEN

TWO RESEARCH ASSOCIATE POSITIONS

are available at the University of Oregon. The researchers will participate in two projects focused on microbial community ecology. The first project is an ongoing study of the response of soil bacteria to simulated global change. The second project is a recently funded study of the biogeography of soil bacteria. Both positions require extensive experience in molecular microbial community analyses and biogeochemistry, and a strong interest in ecological theory and statistical modeling. Ph.D. in microbiology, ecology or related field required. Salary commensurate with education and experience. See **website: http://jobs.uoregon.edu/unclassified/academic/** and reference Post 6113AB for full description.

Please send curriculum vitae, a statement of relevant research experience, and three names of references to: **Postdoctoral Research Position, Dr. Brendan Bohannan, Center for Ecology and Evolutionary Biology, 5289 University of Oregon, Eugene, OR 97403-5289,** or **e-mail: sara@uoregon.edu.** Review of applications will begin immediately and continue until the position is filled; applications must be received by July 15, 2006, to be assured full consideration. *The University of Oregon is an Equal Opportunity/Affirmative Action Institution committed to cultural diversity and compliance with the Americans with Disabilities Act. Women and minorities encouraged to apply. We invite applications from qualified candidates who share our commitment to diversity.*

CONFERENCE

THE LEGACY OF RAMÓN Y CAJAL
An Interdisciplinary Conference
at Chestnut Hill College
Philadelphia, Pennsylvania
United States of America
October 5 to 7, 2006

On the centenary of Santiago Ramón y Cajal's Nobel Prize, this multidisciplinary gathering will consider his contributions to neuroscience and beyond. Proposals in English or Spanish for papers (20 minutes in length), posters, and artwork that consider any aspect of Cajal's legacy: in science, letters, and educational reform and the work of those influenced by him are due by August 1, 2006. Contact **e-mail: cajal@chc.edu.**

MARKETPLACE

Watch Your Tissue MELT™ Into High Quality RNA

MELT™

Multi-Enzymatic Liquefaction of Tissue

Learn more at
www.ambion.com/prod/melt

MELT™
Total Nucleic Acid Isolation System

Physical dissociation of tissue is cumbersome, low throughput, and potentially hazardous when samples are disrupted in open tubes. Ambion's MELT™ Total Nucleic Acid Isolation System (patent pending) is a simpler and safer alternative to traditional isolation procedures that also allows high throughput tissue processing.

- Ensures reliable gene expression and gene profiling
- Hands-free tissue digestion in minutes – convenient, multi-enzymatic liquefaction of tissue eliminates need for polytron or grinding
- Faster and easier multi-sample processing
- Be confident that your RNA is intact and stable – potent enzymes and RNase inhibitors protect and preserve RNA in tissue lysates for days at room temperature

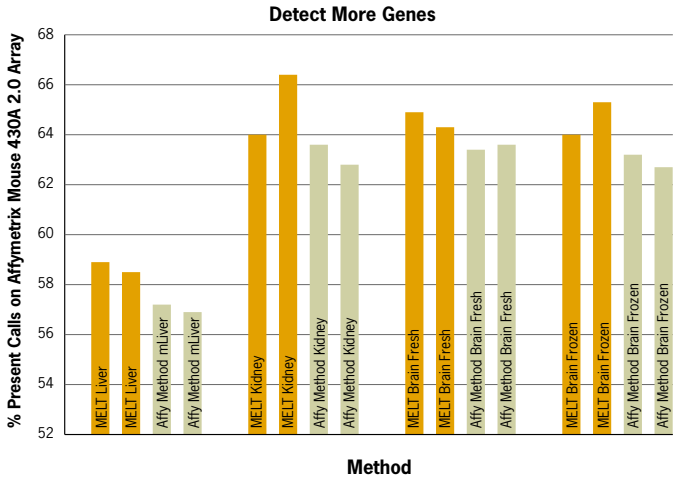

Achieve Higher Percent Present Calls. Results obtained using either the MELT or Affymetrix recommended isolation method from the indicated fresh and frozen mouse tissues. Compared to the recommended method, the MELT System produces an additional 1-2% percent present calls, which corresponds to as many as 145 to 290 genes.

Ambion®
THE RNA COMPANY®
An Applied Biosystems Business

Ambion, Inc.
U.S. 800-888-8804 • Canada 800-445-1161
U.S. tel +1-512-651-0200 • fax +1-512-651-0201

Ambion (Europe) Ltd
tel +44 (0)1480-373-020
fax +44 (0)1480-373-010

Ambion K.K. (Japan)
tel +81 (0)3-5638-2181
fax +81 (0)3-5638-2182

Direct free phone numbers, distributors:
www.ambion.com/contact